

The Mars Gravity Biosatellite as an Innovative Partial Gravity Research Platform

by

Thaddeus R. F. Fulford-Jones

A.B., Engineering Sciences, Harvard University, 2004
S.M., Electrical Engineering and Computer Science, Harvard University, 2004

Submitted to the Department of Aeronautics and Astronautics
in partial fulfilment of the requirements for the degree of

Doctor of Philosophy

in Aerospace Biomedical Engineering at the
Massachusetts Institute of Technology

August 2008

[September]

© 2008 Massachusetts Institute of Technology. All rights reserved.

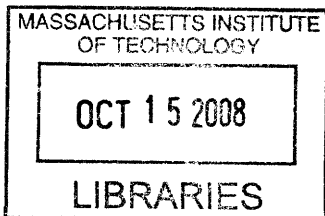
Author
Department of Aeronautics and Astronautics
Harvard-MIT, Division of Health Sciences and Technology

Certified by
Jeffrey A. Hoffman, Professor of the Practice of Aerospace Engineering
MIT Man-Vehicle Laboratory, Thesis Supervisor

Certified by
Mark T. Whary, Associate Director of the Division of Comparative Medicine
Thesis Committee Member

Certified by
Laurence R. Young, Apollo Program Professor of Aeronautics and
Professor of Health Sciences and Technology
Thesis Committee Member

Accepted by
David L. Darmofal, Associate Professor, Associate Department Head
Chair, Committee on Graduate Students



ARCHIVES

Dedication

For my father, Dr. Richard F. F. Fulford-Jones (1939-1989).

(A very different sort of Doctor ... but one who would have been quite fascinated by Aerospace Biomedical Engineering.)

Acknowledgements

To my advisers and mentors – thank you. Jeff Hoffman, thank you so much for your enthusiasm, guidance, inspiration and support during my time at MIT. I could not have hoped for a better adviser. Mark Whary and Larry Young: thank you for your vision, input and encouragement. John Keesee and Dava Newman: your excellent feedback was instrumental in shaping the final version of this dissertation. Alan Natapoff, the hours spent in your office have given me a deeper appreciation of statistics. Thank you for your patience and insight.

The Mars Gravity Biosatellite Project has been intertwined with my time at MIT in so many different ways. Erika Wagner, colleague and erstwhile officemate, thank you for your knowledge, boundless energy, perceptiveness and sense of humour. Rosie Combs-Bachmann, thank you for teaching me how to craft a budget – and for being supportive in countless other ways. Alex Cosmas, thanks for your friendship and for your amazing leadership.

Stavros Kotsiaros, test engineer extraordinaire, I appreciate all that you did during your time at MIT. Assembling and disassembling that centrifuge got a lot more difficult after your departure! Charlie Flugel, thank you. You single-handedly taught me more than anyone else about how world-class ECLSS engineers create world-class designs. Andrew Heafitz, thank you for your collaboration – you are the best mechanical designer I have ever met and one of the most talented people I know.

David Fair, Joanne Vining, and Joe Zapetis: I am grateful for your remarkable efforts on the SBIR and in building extra ASMs on tight timelines and even tighter budgets. Your genuine enthusiasm, sense of humour and support of my work was humbling and is greatly appreciated.

Mars Gravity would not be where it is today without the talent of so many past and present students who have given so much to the project. At the risk of forgetting many, I will mention a few whose contributions and dedication to the payload team were truly remarkable. Daniel Blustein, Theresa Dixon, Greg Durrett, Jeremy Franklin, Adam Fuhrmann, Emily Grosse, Arthur Huang, Jillian James, Richard Li, Jesse Marsh, Anna Massie, David Newell, Joao Ricardo, Jerry Richard, Stephanie Schmit, Mark Scott, Noelle Steber, Kendra Toole, Nathan Wang, Paul Yang. Students like you leave me with so many great memories from my time as Payload Lead.

Jim MacArthur, thank you for letting me use your lab – and more importantly thank you for your sense of humour, guidance and expert advice. “But USB 2.0 barely works at 0 rpm, let alone 31.6!”

My thanks to the staff of the MIT Committee on Animal Care and to the veterinary technicians and supervisors who work in the sub-basement of Building 68 South. Those mice are in good hands . . .

Financial support for my studies and research at MIT came from the Mars Gravity Program Office. I was also supported by NASA SBIR Phase II Grant NNA05CP01C, NSBRI Education Grant EO00004, and the NASA Space Grant Consortium of Massachusetts. I would like to acknowledge the 2007 Hugh Hampton Young Jr. Memorial Fund and the YourNameIntoSpace.org public outreach programme. The Howard Hughes Medical Institute supported me as an HST GEMS Scholar.

Thank you to all my colleagues and friends in the Man-Vehicle Lab. I could not have hoped for a better lab to belong to during my time at MIT, nor a more engaging group of people to work with.

To my three longest-suffering flatmates – John Hart, Alec Robertson and Eric Weiss – thank you for putting up with me and for keeping me sane. Erin Aylward, Hansen Bow, Christian Ekholm-Jacobson, Henryk Faas, John Henson, Eric Jones, Roxie Myhrum, Ryan Tam, Geoff Werner-Allen: thanks for everything . . . and thank goodness for biking, dancing, rowing, running and the great outdoors.

And finally, the greatest thanks of all go to my family, who are so much more wonderful than perhaps they often realise. “You only get to do a PhD once, and if you do it right, once is enough.”

CONTENTS

Abstract	11
Chapter One: Introduction.....	12
1.1 Motivation.....	12
1.1.1 Sensorimotor Challenges of Spaceflight.....	13
1.1.2 Broader Physiological Issues Associated with Microgravity	15
1.1.3 Rotating Artificial Gravity Solutions	18
1.1.4 Prior Rodent Research in Space	19
1.1.5 Sensorimotor Targets for the Mars Gravity Biosatellite.....	26
1.1.6 Rodent Care on Board the Mars Gravity Biosatellite.....	27
1.2 Research Aims and Hypotheses.....	27
1.2.1 Chronic Rodent Centrifugation Hypothesis	27
1.2.2 Environmental Control System Design Hypothesis.....	28
1.3 Thesis Outline	28
1.4 Contributions	29
Chapter Two: Payload Module Design as Presented at PDR.....	30
2.1 Overview	30
2.2 Requirement Flowdown Principles	30
2.2.1 Overview of Level 0 Requirements	31
2.2.2 The Science Requirements Documents.....	32
2.3 Interface Control	33
2.3.1 Interfaces to Spacecraft Bus.....	35
2.3.2 Interfaces to Entry, Descent and Landing System	36
2.4 Robustness and Control	36
2.4.1 Payload Computing Architecture.....	37
2.5 Habitat Modules.....	41
2.5.1 Requirements.....	41
2.5.2 Design Overview	42
2.5.3 Habitat Structure.....	43
2.5.4 Waste Management	45
2.5.5 Provision of Food and Water.....	47
2.5.6 Lighting and Video	50
2.5.7 Body Mass Monitoring	53
2.5.8 Habitat Control Electronics	54
2.6 ECLSS Sensors	57
2.6.1 Whole-Payload Sensor Suite Software and Electronics.....	57
2.6.2 Sensor Suite Data Acquisition	59
2.6.3 Distributed Atmospheric Sensors.....	63
2.7 ECLSS Actuators	63
2.7.1 Carbon Dioxide Removal Subsystem.....	66
2.7.2 Humidity Removal Subsystem.....	67
2.7.3 Ammonia Removal Subsystem.....	68
2.7.4 Oxygen and Nitrogen Delivery.....	69
2.7.5 Canisters.....	70
2.7.6 Compressors, Blowers, Valves and Fans	71
2.7.7 Algorithmic ECLSS Decision-Making.....	72
2.8 Thermal Control.....	73

2.9	Structures	73
2.9.1	Payload Hardware Layout.....	74
2.10	Electrical Systems and Sensors	74
2.10.1	Power Conditioning	74
2.10.2	Additional Sensors	75
	Chapter Three: On-Orbit Operations	76
3.1	Overview	76
3.2	Phase E0: Pre-launch	76
3.3	Phase E1: Launch.....	77
3.4	Phase E2: Transition.....	79
3.5	Phase E3: Orbital.....	79
3.5.1	ECLSS Algorithmic Operations	80
3.5.2	ECLSS Data Collection Operations.....	90
3.5.3	Sensor Data Acquisition	92
3.5.4	Responding to Ground Commands.....	93
3.5.5	Preparing for E4	94
3.6	Phase E4: Deorbit	95
3.7	Phase E5 to E7: EDL, Recovery and Post-Flight.....	95
	Chapter Four: Engineering Design of a Prototype Rotational Payload Test Apparatus	97
4.1	Motivation.....	97
4.2	Mechanical Structures	98
4.2.1	Design of the Central Shaft, Centrifuge Arms and ASM Holders.....	100
4.2.2	Design of the Centrifuge Base, Bearings and Motor Mounting Bracket.....	103
4.2.3	Design of the Outer Frame, Barrier Membrane and Portal Door	105
4.2.4	Lessons Learnt through the Mechanical Design Process.....	107
4.3	Centrifuge Electronics and Software.....	107
4.3.1	Habitat Control Module	109
4.3.2	Lighting and Video Board.....	110
4.3.3	Multiplexing Aggregator.....	110
4.3.4	Baseboard	112
4.3.5	Interfaces and Cabling.....	112
4.4	Environmental Control and Life Support	114
4.4.1	Design Overview	114
4.4.2	Implementation	115
4.5	Lessons Learnt from Systems Integration.....	122
	Chapter Five: Results of a Chronic 5-Week Rotation Experiment ..	126
5.1	Motivation.....	126
5.1.1	Justification for Choice of Discrete Behavioural Tests	127
5.1.2	Justification for Use of In-Habitat Video	127
5.2	Apparatus.....	127
5.2.1	Video Analysis of Mouse Behaviour	128
5.3	Methods.....	128
5.3.1	Mouse Ages	130
5.3.2	Atmospheric Environment	130
5.3.3	Procedural Details.....	130
5.4	Results and Discussion	137
5.4.1	Body Mass and General Appearance.....	137
5.4.2	Water Consumption.....	140

5.4.3	Nightly Video-Derived Behavioural Metrics	141
5.4.4	Discrete Behavioural Trials.....	151
5.5	Conclusions.....	160
5.5.1	Limitations and Future Work.....	161
Chapter Six: Results from a Closed-Loop ECLSS Test.....		162
6.1	Motivation.....	162
6.2	Procedures.....	162
6.2.1	Preparation of ECLSS Consumables	162
6.2.2	Installation of ASMs and Rodent Consumables	163
6.2.3	Acceptance and Verification Testing.....	163
6.2.4	Test Commencement	168
6.3	Control Algorithms.....	168
6.4	Results and Discussion	170
6.5	Conclusions.....	174
6.5.1	ECLSS Limitations	175
6.5.2	Future Recommendations.....	176
Chapter Seven: The Biosatellite as a Research Platform		177
7.1	Motivation.....	177
7.2	Group Housing Options.....	178
7.3	Other Animal Models of Interest.....	179
7.3.1	Rats.....	181
7.3.2	Newts and Geckos.....	182
7.4	Alternative Gravity Setpoints	183
7.5	Alternative ECLSS Setpoints	184
7.6	Exploration-Relevant Radiation Studies.....	185
7.7	Summary	187
Chapter Eight: Conclusions		188
8.1	Summary of Major Findings.....	188
8.1.1	Chronic Rotation of Rodents	189
8.1.2	ECLSS Performance	190
8.2	Future Work	190
Appendix A: Abbreviations.....		192
Appendix B: Payload Autonomy		194
Appendix C: Food Bar Experiments.....		198
Appendix D: Condensing Heat Exchanger Design.....		201
Appendix E: Ammonia Production Experiment.....		208
Appendix F: Thermal Design.....		212
Appendix G: Payload Structural Design		227
Appendix H: Circuit Diagrams		231
Appendix I: CAC Protocols		245
Appendix J: Statistical Analyses		266
Appendix K: References		269

TABLES AND FIGURES

Table 1: Cosmos biosatellite flights involving rodents.....	19
Table 2: Definitions of Mars Gravity mission phases.....	31
Table 3: Level 0 requirements for the Mars Gravity Biosatellite.....	32
Table 4: Interfaces between payload module and spacecraft bus.....	36
Table 5: Interfaces between payload module and EDL system.....	36
Table 6: Payload autonomy and data storage requirements.....	37
Table 7: Partial specimen chamber mechanical requirements.....	41
Table 8: Waste collection, sampling and preservation requirements.....	45
Table 9: Consumables requirements.....	47
Table 10: Lighting and video hardware requirements.....	50
Table 11: Body mass monitoring requirements.....	53
Table 12: Body mass data aggregation requirements.....	55
Table 13: Water consumption measurement requirements.....	55
Table 14: Sensor Suite atmospheric monitoring components.....	57
Table 15: Temperature and humidity sensing requirements.....	59
Table 16: Carbon dioxide monitoring requirements.....	60
Table 17: Ammonia monitoring requirements.....	61
Table 18: Oxygen monitoring requirements.....	61
Table 19: Air flow rate monitoring requirements.....	62
Table 20: Air pressure monitoring requirements.....	62
Table 21: ECLSS atmospheric requirements.....	64
Table 22: Payload structural requirements.....	73
Table 23: Sensor operations during Phase E1.....	78
Table 24: Sensor operations during Phase E2.....	79
Table 25: Overview of algorithmic ECLSS controls.....	81
Table 26: Atmospheric sensors within the payload module.....	90
Table 27: Sensor operations during Phase E3.....	92
Table 28: Sensor operations during Phase E4.....	95
Table 29: Mechanical requirements for the IGTA.....	99
Table 30: Centrifuge stoppages.....	129
Table 31: Rotarod pretraining schedule.....	134
Table 32: Balance beam pretraining schedule.....	134
Table 33: Enumeration of test order for air righting and balance beam.....	137
Table 34: Balance beam step categorisation criteria.....	156
Table 35: Balance beam performance differences.....	159
Table 36: Extract of the verification checklist for power.....	164
Table 37: Extract of the verification checklist for sensors.....	164
Table 38: Extract of the verification checklist for actuators.....	165
Table 39: Extract of the verification checklist for software.....	166
Table 40: Extract of the verification checklist for rodent care.....	167
Table 41: Extract of the verification checklist for IGTA preparation.....	167
Table 42: Oxygen control algorithms.....	169
Table 43: Magnitude of weight gain for both test animals.....	170
Table 44: Modifications for group housing.....	179
Table 45: Animals in space (embryos, eggs and larvae excluded).....	180
Table 46: Modifications for rats.....	182
Table 47: Modifications to house newts and geckos.....	183
Table 48: Modifications for weightlessness.....	184
Table 49: Modifications for ECLSS contaminant buildup studies.....	185
Table 50: Performance envelopes for each configuration.....	186
Table 51: Fan inlet air flow velocity for fan/TEC/heatsink modules.....	217

Table 52: Anemometry for crossflow configuration fans in location 1	218
Table 53: Impacts of artificial gravity on convection.....	218
Table 54: Computed required minimum air flow velocities	219
Table 55: Performance envelopes for each configuration	222
Table 56: Performance envelopes given Figure 107.....	224
Table 57: Thermodynamics of CHE operation	225

Figure 1: The Mars Gravity Biosatellite in low Earth orbit (CAD: David Newell)	13
Figure 2: Structure of the vestibular system (after Costanzo 2006)	14
Figure 3: The rodent cages of Cosmos biosatellites (from NASA 1990)	20
Figure 4: Five cages in the Cosmos-936 mockup (from Gurovsky, Gazenko <i>et al.</i> 1980)	20
Figure 5: Group mating chamber for Cosmos-1129 (from NASA 1990)	21
Figure 6: Outer appearance of the Cosmos biosatellites (from NASA 1990)	23
Figure 7: Design of the Cosmos-936 1-g centrifuge (from NASA 1990).....	24
Figure 8: ECLSS on board Cosmos-936 (from Gurovsky, Gazenko <i>et al.</i> 1980)	25
Figure 9: Spacecraft interfaces prior to launch.....	33
Figure 10: Spacecraft interfaces while in orbit	34
Figure 11: Spacecraft interfaces for reentry and aerocapture.....	35
Figure 12: Payload computing hardware architecture	39
Figure 13: The Animal Support Module (CAD: Adam Fuhrmann)	42
Figure 14: ASM disassembly diagram	43
Figure 15: Upper structure of the ASM, viewed from beneath	44
Figure 16: Habitat base, viewed from above and from beneath	44
Figure 17: Waste Collection System (CAD: Adam Fuhrmann).....	46
Figure 18: WCS tensioning mechanism and scraper (CAD: Adam Fuhrmann).....	47
Figure 19: Water delivery hardware (CAD: Edison Guerra).....	49
Figure 20: Water delivery	50
Figure 21: Lighting board layout.....	52
Figure 22: Video camera view angle (CAD: David Newell).....	53
Figure 23: Body mass sensor hardware (CAD: Edison Guerra)	54
Figure 24: HCM block diagram	54
Figure 25: Sensor Suite microcontroller interfaces	58
Figure 26: Sensirion combined temperature/humidity sensor	60
Figure 27: ECLSS atmospheric actuators	65
Figure 28: Cross-sectional view of LiOH/carbon canister air flow	70
Figure 29: Payload configuration (CAD: Emily Grosse).....	74
Figure 30: The Mars Gravity Biosatellite during Phase E3 (CAD: David Newell)	80
Figure 31: Total pressure and oxygen partial pressure algorithms	84
Figure 32: Relative humidity and temperature algorithms.....	86
Figure 33: Carbon dioxide and ammonia algorithms	88
Figure 34: Air flow rate algorithms	89
Figure 35: G-vectors for space and ground configurations	98
Figure 36: Upper part of the IGTA centrifuge (CAD: Kendra Toole)	100
Figure 37: Holding bracket for a single ASM (CAD: Kendra Toole).....	101
Figure 38: ASM holder attachments (CAD: Kendra Toole).....	102
Figure 39: ASM with lightshields (CAD: Adam Fuhrmann).....	103
Figure 40: Lower part of centrifuge without motor (CAD: Kendra Toole)	104
Figure 41: Motor, mounting block and belt (CAD: Kendra Toole)	105
Figure 42: IGTA outer frame (CAD: Kendra Toole).....	106
Figure 43: IGTA centrifuge electronics	108
Figure 44: The 8-lead rotating electrical connector (manufacturer image)	109
Figure 45: CAD rendering of the Multiplexing Aggregator board (front)	111
Figure 46: CAD rendering of the Multiplexing Aggregator board (back)	111
Figure 47: CAD rendering of the Baseboard PCB	112
Figure 48: IGTA wiring for lower electrical connector (partial image content from Mercotac.com) ...	113

Figure 49: IGTA ECLSS design	115
Figure 50: The IGTA ECLSS canister for LiOH and activated carbon.....	116
Figure 51: The air distribution manifold (fitted for 4 ASMs)	117
Figure 52: The USP oxygen cylinder, regulator and Parker valve.....	118
Figure 53: The CHE and pumping system as installed in the IGTA.....	119
Figure 54: IGTA ECLSS implementation	120
Figure 55: CAD rendering of the ECLSS Actuator Interfacing PCB	121
Figure 56: The datalogger within the IGTA (CAD: Kendra Toole).....	122
Figure 57: Fully integrated IGTA (CAD: Kendra Toole)	122
Figure 58: The rightmost lead fractured due to compressor vibration	124
Figure 59: A representative video frame from early pilot studies	131
Figure 60: The four open field enclosures configured for video capture.....	132
Figure 61: Representative video frame from open field testing	132
Figure 62: Rotarod testing	133
Figure 63: Beam balance / walking.....	135
Figure 64: Air righting	136
Figure 65: Body mass during non-rotational control experiment.....	138
Figure 66: Body mass during rotational experiment	139
Figure 67: Rodent water consumption in 18-day increments	141
Figure 68: ASM central zones as defined in Ethovision XT	142
Figure 69: Head direction (adapted from Noldus product manual)	143
Figure 70: Movement states (adapted from Noldus product manual)	144
Figure 71: Mean angular velocity per night during entire experiment	147
Figure 72: Total distance travelled per night during entire experiment.....	148
Figure 73: Time spent moving each night during entire experiment	149
Figure 74: Time spent in central zone during entire experiment	150
Figure 75: Box plot of rotarod performance over time	152
Figure 76: Box plot of mobility duration over time	153
Figure 77: Box plot of number of immobility episodes over time	154
Figure 78: Sample video frames showing footfaults of increasing severity.....	155
Figure 79: Box plot showing percentage of faultless footsteps	157
Figure 80: Box plot showing percentage of “major” footfaults	158
Figure 81: Box plot showing percentage of “very major” footfaults.....	159
Figure 82: Control algorithm for condensing heat exchangers	168
Figure 83: Control of ammonia and carbon dioxide.....	169
Figure 84: Water consumption data for both rodents.....	170
Figure 85: Oxygen concentration.....	171
Figure 86: Ammonia concentration	172
Figure 87: Carbon dioxide concentration	173
Figure 88: Relative humidity	174
Figure 89: RAX architecture for DS-1 (after Rayman <i>et al.</i> 1999)	195
Figure 90: CASPER architecture for EO-1 (after Chien <i>et al.</i> 2003).....	197
Figure 91: Results of food bar dehydration test	199
Figure 92: The condensing heat exchanger	202
Figure 93: Condensation rate for one CHE unit at 70% RH.....	203
Figure 94: Effects on condensation of temperature and humidity	204
Figure 95: CHE performance characterisation.....	205
Figure 96: CHE tilt testing to model 0.38-g operation	206
Figure 97: Aggregated rodent body mass from all six specimens.....	209
Figure 98: Ammonia production rates from all six specimens.....	210
Figure 99: Key elements of the thermal control system.....	212
Figure 100: Cross-section of the payload module and heatshield (CAD: David Newell).....	214
Figure 101: Cross-sectional layout of the air flow testing mockup.....	215
Figure 102: The crossflow configuration of cooling unit	216
Figure 103: The impingement configuration of cooling unit.....	216
Figure 104: Impingement configuration units installed in the mockup.....	217

Figure 105: Simplified payload thermal mockup in test configuration	221
Figure 106: Configuration A at various TEC power levels and four fan speeds	223
Figure 107: Performance summary for all three configurations at varying power	223
Figure 108: Finite element analysis of aft fairing design (CAD: Joao Ricardo).....	228
Figure 109: Life support bucket design (CAD: Emily Grosse)	228
Figure 110: Parker Stratoflex Slide-Lok™ (manufacturer image)	229
Figure 111: Central Utilities Truss (CAD: Emily Grosse).....	230

Abstract

The Mars Gravity Biosatellite is an unprecedented independent spaceflight platform for gravitational biology research. With a projected first launch after 2010, the low Earth orbit satellite will support a cohort of fifteen 14.5- to 25.5-week-old female BALB/cByJ mice for up to five weeks. During this time, the spacecraft will rotate at a rate of 31.6 rpm to generate Mars-equivalent artificial gravity of magnitude 0.38-g. Reentry capability will permit the return of live specimens to the Earth's surface at the culmination of the study. The proposed first mission aims to explore the physiological impacts on mice of 0.38-g.

On board the Mars Gravity Biosatellite, a video acquisition and digitisation system will enhance in-flight collection of data on sensorimotor adaptation. As part of this thesis, a rotational ground control system has been designed and constructed at MIT. The apparatus incorporates a video processing module similar to that baselined for the mission. It also features the first custom-designed gondola centrifuge that accommodates up to four singly-housed rodents in flight-equivalent habitat modules. At a rotation rate of 31.6 rpm, the centripetal acceleration experienced by each animal is less than 1.07-g. The 0.34 m radius of rotation is equivalent to that of the orbital vehicle. A behavioural study with four BALB/cByJ mice explores the effects of chronic rotation alone and confirms that they can be quantified and therefore decoupled from the anticipated on-orbit effects of rotation-induced Mars-equivalent gravity. The results provide justification for the scientific validity of the Mars Gravity Biosatellite as a rotating spaceflight platform.

In addition, details are presented on the design, implementation, test and operation of a two-mouse closed-loop environmental control and life support system (ECLSS). The ground-based assembly is colocated with the centrifuge, and the entire apparatus is enclosed within a sealed zero-pressure urethane/polyethylene membrane. It incorporates scaled-down versions of a subset of flight-equivalent atmospheric reconditioning subassemblies together with sensors, actuators and a computer to perform autonomous feedback-driven supervisory control. Data is presented that validates a system that includes oxygen replenishment, carbon dioxide scrubbing via reaction with lithium hydroxide, ammonia removal using acid-treated activated charcoal, and humidity control with a custom-designed condensing heat exchanger. Results of a multi-week test represent an experimental proof-of-concept for the Mars Gravity Biosatellite's ECLSS strategy, showing good control of environmental parameters within specified ranges.

The work presented in this thesis offers four primary contributions to aerospace biomedical engineering and rodent behavioural science:

1. Preliminary design and operations plans for the Mars Gravity payload. This thesis claims specific contributions in the areas of electronics, instrumentation, software and systems-level design of the payload module.
2. The first direct measurement of the influence of chronic rotation on mice in flight-like habitats at 31.6 rpm. The first in-centrifuge use of video-based behavioural analysis.
3. Proof-of-concept justification for the Mars Gravity Biosatellite ECLSS strategy.
4. The conception, design, implementation and operation of the first integrated ground test apparatus to combine chronic rotation capability with an ECLSS testbed.

Chapter One: Introduction

Would it be of any use, now, to speak to this mouse? Everything is so out-of-the-way down here, that I should think very likely it can talk: at any rate there's no harm in trying.

-Alice¹

1.1 Motivation

The scientific community has long contemplated the effects of Earth's gravity (1-g) on mammalian physiology. Over the past four decades, the abundance of 1-g data has been supplemented and contextualised through investigations conducted in the weightless environment of space. At the simplest level, scientists have learnt that adaptation to one gravitational environment is typically ill-suited for performance in another. For example, all terrestrial species have evolved under the constant pull of Earth's gravitational force. But with the 1-g vector suddenly replaced by microgravity, serious physiological problems develop – some of which persist long after a specimen returns to the planet's surface. Despite these research discoveries, there has been scarcely any exploration of the realm between weightless and 1-g; the physiological challenges of “partial gravity” remain almost wholly unknown.

Initiated in 2001, the Mars Gravity Biosatellite Program is currently led by MIT and the Georgia Institute of Technology. Previous participants include the University of Washington and the University of Queensland. With a projected first space launch after 2010, the university-led project aims to provide an unprecedented independent research platform for gravitational biology research. In its baseline configuration, the low Earth orbit satellite will support a cohort of fifteen 14.5- to 25.5-week-old female BALB/cByJ mice for periods of up to five weeks (Figure 1). Reentry capability will permit the return of live animals to the Earth's surface at the culmination of the study.

The biosatellite's proposed first flight will be dedicated to studying the effects of simulated Mars-level gravity (0.38-g) on mammalian physiology. The spacecraft will rotate at 31.6 rpm throughout the mission to generate centripetal accelerations of 3.73 m/sec^2 within each of the 15 specimen chambers.

This thesis is motivated by the need to provide a scientific justification for the Mars Gravity Biosatellite's proposed mission profile. Specifically, this work seeks to confirm in 1-g that a spin rate of 31.6 rpm with rotation radius 0.34 m has no adverse impacts on rodent health in terms of body mass, hydration and general well-being. In addition, it seeks to explore and quantify the nature of any behavioural changes under this rate of chronic centrifugation, both as a measure of vestibular function and to serve as an index of potential stress.

¹ *Alice's Adventures in Wonderland*, Lewis Carroll.

Concurrently, the design element of this research is driven by the need to provide proof of concept justification for the environmental control and life support strategies of the Mars Gravity Biosatellite. The penultimate chapter is motivated by a desire to position the biosatellite as a multipurpose research platform that offers broader capabilities for work with other species and at different gravity setpoints.

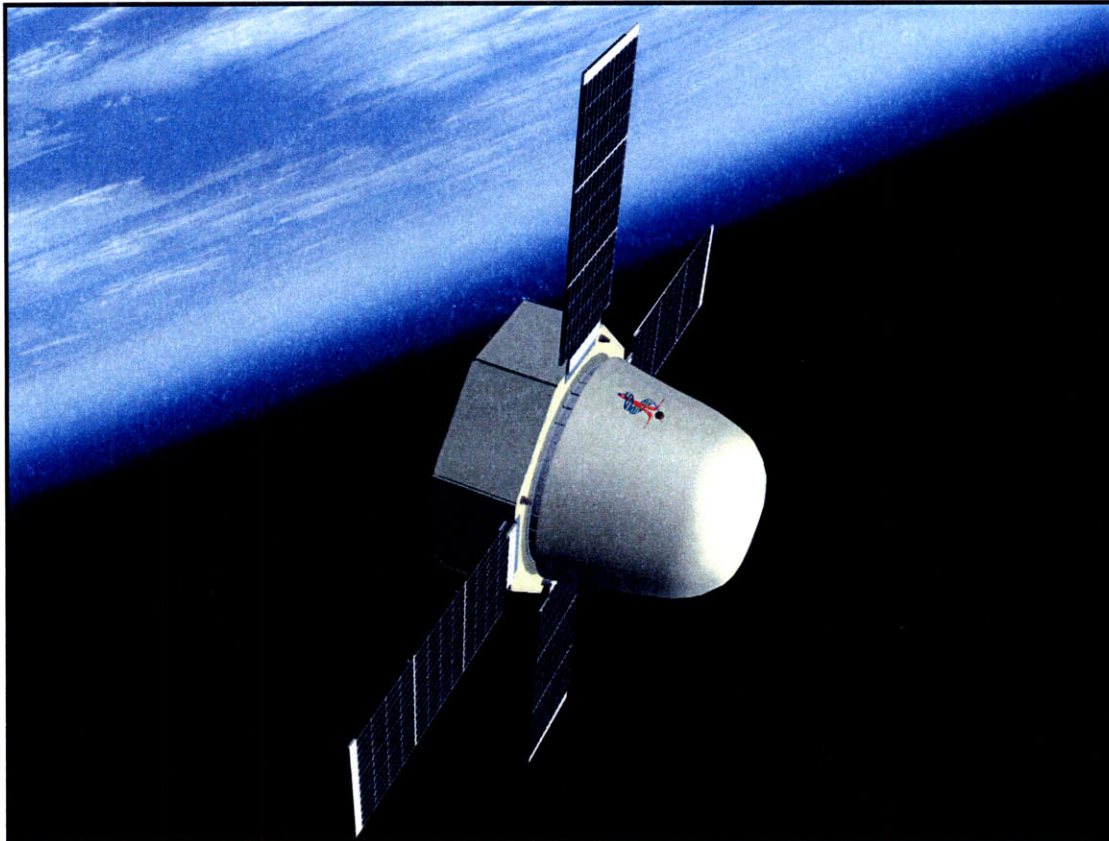


Figure 1: The Mars Gravity Biosatellite in low Earth orbit (CAD: David Newell)

1.1.1 Sensorimotor Challenges of Spaceflight

Sensorimotor adaptation to a microgravity environment raises a number of questions of immediate operational relevance to the field of astronautics. In vertebrates, the *vestibular organ* determines orientation and provides information critical for maintaining sense of balance. It consists of a membranous labyrinth within a bony encasement as shown in Figure 2. The organ comprises three mutually orthogonal semicircular canals (horizontal, superior and posterior) together with two otolith organs (utricle and saccule). Each of these elements is filled with endolymph and surrounded by perilymph.

The otolith organs are responsible for sensing linear accelerations, including those due to gravity. The signal transducer within the utricle and the saccule is known as the *otolith mass*. Comprised of mucopolysaccharides and calcium carbonate crystals, this pinhead-sized sphere lies atop a bed of highly sensitive mechanoreceptors known as the vestibular hair cells. When the subject is exposed to a linear acceleration, the otolith mass moves very slightly across the hair cells, each of which is covered with a carpet of tiny apical cilia and one particularly tall element known as the kinocilium. Together, these cilia sense movement of the otolith mass. The resulting activation of certain hair cells and deactivation of others

translates to the sensation felt upon tilting one's head. This feeling allows the subject to determine both the direction and the magnitude of an external acceleration.

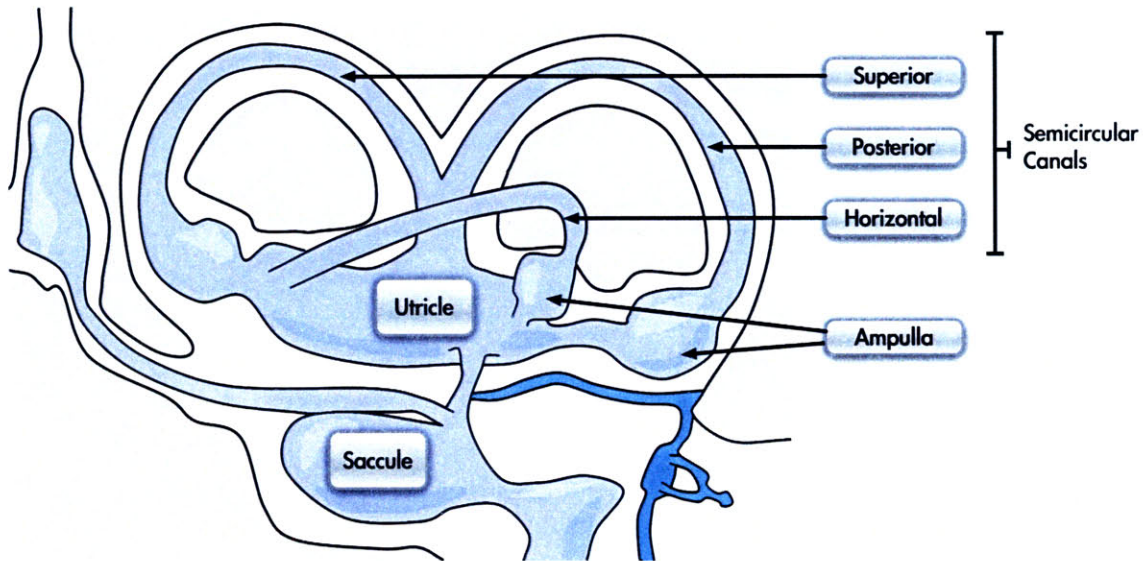


Figure 2: Structure of the vestibular system (after Costanzo 2006)

In microgravity, the otoliths are no longer presented with the constant downward input that is characteristic of Earth's gravity. As a consequence, the otolith mass literally floats above (but remains connected to) the bed of hair cells, and the vestibular nerve receives a flatline signal. This is one reason why astronauts commonly feel disorientated and unsure of their surroundings, particularly during the first few days of spaceflight. In a given orientation, their optical and auditory systems may provide inputs that suggest the subject is (for example) standing "upright" with respect to the spacecraft interior. However, with the vestibular system providing no meaningful information to reinforce this conclusion, the astronaut is said to experience an *intralabyrinthine sensory conflict* (Nikolaev and Ilyin 1981). In severe cases, this may result in space motion sickness, motor control difficulties, and a number of disorientating perceptual illusions (Kozlovsaya, Grigoriev *et al.* 1995).

Of greater concern, however, is the fact that the vestibular system undergoes marked histological adaptation while the subject is in the spaceflight environment. When a lifetime's worth of gravity-derived stimulation is suddenly removed, the body attempts to remodel its vestibular systems to compensate for the absence of a stimulus that ostensibly should still be present. Remarkably, rat studies have shown that there is a profound change in the distribution of hair cell types and in the innervation of cell bodies (Ross 1993; Ross 2000). As articulated by Wade (2005), investigators recorded a startling increase of 100% in the number of synapses on type II hair cells. These results and others support the current research consensus that mature utricular hair cells maintain some degree of synaptic plasticity.

The ability of the vestibular system to adapt is in some sense a double-edged sword. On the one hand, adaptation to a microgravity environment permits the subject to function effectively in space and therefore carries with it a significant survival value. On the other hand, hypersensitized hair cells provide unhelpful and problematic cues when the subject returns to a gravitational environment. The result is that astronauts returning to Earth

often encounter sensations of sensory conflict which persist until readaptation to 1-g is complete.

Symptoms presented by postflight astronauts include postural instability, locomotion difficulties, oscillopsia, misinterpretation of the tilt-translation ambiguity, and increased dependence on visual orientation cues (Young 1993; Young and Sinha 1998). It has been argued that these are nothing more than minor inconveniences. However, such issues could become critical in the event of an emergency egress or strenuous post-flight activity – such as may be required following a six-month journey to Mars. This reality motivates and inspires researchers to better understand and explore the data generated to date. The Mars Gravity Biosatellite represents an achievable “next step” in bolstering and contextualizing the historical results from microgravity experiments.

1.1.2 Broader Physiological Issues Associated with Microgravity

Sensorimotor organs are only one of many body systems that are negatively impacted by microgravity-induced deconditioning. In his seminal review, Wade (2005) provides a comprehensive appraisal of the effects of spaceflight on both humans and rodents. His work and that of other gravitational biologists is summarised in this section.

1.1.2.1 Body Mass and Plasma Volume

Spaceflight-induced changes in body mass have been well-documented. In 1-g, a human standing upright will exhibit a noticeable gravity-induced pooling of blood within the legs. However, upon exposure to microgravity, fluid shifts away from the lower body and redistributes toward the torso and arms. The physiological reality is that the baroreceptors are situated in the upper body, within the carotid sinuses and the aortic arch (Costanzo 2006). The fluid shift associated with weightlessness is consequently interpreted as an overall increase in blood plasma volume. Sensing of this input causes activation of homeostatic mechanisms for diuresis, with the result that astronauts will void more frequently until the baroreceptors register an Earth-normal reading once again. The attendant reduction in plasma volume leads to a well-documented set of cardiovascular changes including modulation of cardiac output and baroreflex sensitivity, together with reduced aerobic capacity (Pavy-Le Traon, Heer *et al.* 2007). Fortunately, however, the voiding-induced reduction in body mass is reversible. Upon return to Earth, astronauts exhibit orthostatic hypotension and swiftly regain plasma volume through normal fluid intake.

Aside from changes in wet mass as a consequence of volume reduction, there is some evidence that a true change in dry mass may occasionally occur in microgravity. However, studies with rodents have yielded contradictory results. Wade explains that the great majority of these experiments have suggested no significant differences between controls and spaceflight specimens. However, two studies did show a significant change; the first suggested a 12% mass reduction in space, while the second indicated a 9% increase in spaceflight animals when compared with ground controls (Wade, Ortiz *et al.* 2000). Wade indicates that perhaps operational/engineering issues can account for one or more of these results. For example, it is known that small temperature differences between ground and space hardware can cause body mass changes on the order of those observed.

1.1.2.2 Growth Rates and Body Composition

The data on growth rates and body composition in space is confounded for reasons similar to those already discussed. Again, the number of available studies is minimal. As reported

by Wade, no change in body composition was observed in either young or old rats flown for a period of seven days on board Spacelab 3 (Fast, Grindeland *et al.* 1985). However, from the 18.5-day Cosmos-1129 flight researchers concluded that rats exhibited a significant increase in body fat (Ushakov, Smirnova *et al.* 1980). Consequently, it is hypothesised that spaceflight duration may impact body composition via physiological mechanisms that are currently not well understood.

1.1.2.3 Nutrition

There exists extensive literature covering the impacts of space flight on nutrition. Astronauts frequently suffer from a negative energy balance on account of a gross reduction in food intake. This also appears to be true for primates. However, to date this finding has not been replicated in rodents. By pooling data from 15 different spaceflight experiments, researchers concluded that there was no significant difference in either caloric intake or fluid consumption between rats in space and on the ground (Wade, Miller *et al.* 2002). To ensure the validity of inter-group comparisons, ground specimens were kept under the same conditions and provided the same diet.

1.1.2.4 Muscle

Wade reports that muscular changes have been evaluated in over 100 rodent spaceflight studies to date. Importantly, the data suggests significant muscle atrophy in mice and rats across a range of different strains, ages and genders. The overall mass reduction in weight-bearing muscle is attributed to a reduction in cross-sectional area and changes in fibre type. These histological changes are mirrored behaviourally in terms of decreased contraction strength and duration. Rats flown on board the Cosmos biosatellites were reported to be inert during the first few days following return to Earth (Nikolaev and Ilyin 1981). Their motor activity and general muscle tone was decreased. In addition, gait was strongly altered and the rodents did not exhibit normal movements or postures in self-righting reaction tests. Static endurance was also reduced.

Astronauts encounter similar problems associated with muscular degeneration. Following flight, they report symptoms of skeletal muscle weakness and fatigue, and experience a delayed onset muscle soreness.

An examination by electron and light microscopy of hindlimb muscles of rats flown in microgravity suggested that the effects of spaceflight on skeletal muscle are multifaceted (Riley 1998). Tissues were obtained both inflight (sampled by astronauts on board Spacelab Shuttle missions) and postflight following the return of Cosmos biosatellites 1887 and 2044. This allowed a direct exploration of primary microgravity-induced changes and secondary reentry- and reloading-induced alterations.

Riley reports that changes observed from inflight tissue sampling included muscle atrophy, increased percentage of fibres expressing fast myosin-heavy chains, a reduction in subsarcolemmal mitochondria and an increase in glycogen. Observed fibre atrophy accounted for a 20-40% decrease in cross-sectional area; such changes are now believed to be the primary cause of muscular weakness. Fatigue reported by astronauts can be partially attributed to the shift from slow oxidative toward fast glycolytic fibre types.

Secondary alterations induced by the stresses of reentry and return to 1-g were also explored by Riley's group. As early as two hours post landing, the slow antigravity adductor longus muscle exhibited a doubling of interstitial area, consistent with severe oedema in this region.

By 8-12 hours following return, further oedema was observed together with degranulation of mast cells and thrombosis in postcapillary venules. By two days postflight there was evidence for ischaemia and attendant anoxia that resulted in widespread necrosis of muscle fibres and degeneration of motor nerve terminals. Taken together, these cellular changes contribute to gross muscle weakness, fatigue and faculty disruption. By two weeks postflight, the oedema had subsided, muscle fibres had been rebuilt and nerve terminals had regrown.

Muscular soreness is attributed to segmental tearing of muscle fibres that presents in rats approximately 5 hours postflight. This is most likely due to the high G-forces associated with reentry. The resulting lesions are accompanied by breakage of contractile filaments and localised disruption of muscle cell membranes, leading to segmental necrosis. However, tissue repair is rapid and within 48 hours the lesion sites have been filled with parenchyma similar to sarcomeric Z line material. 9 days later, lesions are no longer detectable, indicating that the healing process has reached completion.

1.1.2.5 Bone

Loss of bone mass has been widely recognised as a major problem associated with long-term spaceflight. However, unlike other physiological changes, there is evidence that bone never reaches a homeostatic setpoint in microgravity. Instead of adaptation, researchers have observed involution (Nikolaev and Ilyin 1981). In general, calcium excretion is increased from day one in microgravity and a sustained negative calcium balance continues indefinitely thereafter (Pavy-Le Traon, Heer *et al.* 2007). Calcium absorption is impaired, and both density and stiffness of weight-bearing bones is reduced.

The three Skylab flights of 1973 and 1974 were the first metabolic studies to specifically investigate bone density changes in humans. Bones were imaged in-flight and calcium excretion was recorded. Test data showed an 81% increase in urinary calcium excretion and a slightly elevated faecal calcium output. Importantly, the daily excretion rates increased progressively from a pre-flight baseline until reaching a plateau approximately one month into each flight (Whedon and Rambaut 2006). Net calcium uptake, as measured by taking the difference between calcium ingested and calcium excreted, was unaffected during the first (and shortest) Skylab mission. However, astronauts on the subsequent two flights encountered a progressive decline in intestinal calcium absorption, which ultimately fell to barely one-fifth of the Earth-normal rate by the end of the final mission. Densitometry showed significant bone loss in the lower (weightbearing) extremities of three of the nine Skylab astronauts. Increased bone resorption was confirmed by elevated urinary hydroxyproline and hydroxylysine content (respectively 134% and 140% of normal). However, there was substantial inter-subject variation and some researchers believe that certain astronauts will not suffer any significantly increased risk of fracture following microgravity exposure (Scheuring 2007).

The Cosmos-1667 biosatellite exposed ten male rats to seven days of weightlessness in 1985. Seven of these specimens were used in post-flight bone studies. In the proximal tibial metaphysis, the trabecular bone volume was markedly reduced (Vico, Chappard *et al.* 1988). Bone formation activity at the cellular level was decreased while resorption was increased. These findings have been replicated in ground-based hindlimb suspension studies (Schultheis, Ruff *et al.* 2000).

More recent work has focused on astronauts on board the Space Shuttle and International Space Station (ISS). Cortical and trabecular bone loss was measured in the spine and hip of 14 crewmembers who underwent 4- to 6-month stays in microgravity (Lang, LeBlanc *et al.*

2004). Importantly, results recorded using the latest bone imaging techniques provided insight into the actual mechanisms of mineral loss in space. Although researchers found no compartment-specific loss of bone in the spine, mineral loss in the hip was evident and occurred by means of endocortical thinning. These changes occurred in ISS astronauts at a rate similar to that reported in earlier Mir studies. Future work will involve investigations into the beneficial effects of biphosphonates, powerful anti-osteoporosis drugs that have been successfully used in ground studies with immobile patients (Shapiro, Smith *et al.* 2007).

1.1.2.6 Immune System

Spaceflight data on immune system changes is mixed. It remains unclear to what extent the response is related to general stress as opposed to weightlessness specifically. Nonetheless, there is some evidence that mission length and suboptimal performance of ECLSS apparatus may directly correlate with immune system weakness (Wade 2005). Specific changes include alterations in the makeup of leukocytes, resistance of bone marrow cells to chemical stimuli that would normally promote leukocyte formation, and a decrease in modulating factors such as interferon and cytokines. However, some scientists argue that all the aforementioned changes can be explained by a combination of radiation exposure and the increased carbon dioxide concentrations commonly associated with closed-loop atmospheric systems (Sonnenfeld, Koebel *et al.* 1995).

1.1.2.7 Cardiovascular System

Bipedal species such as humans generally have a much taller hydrostatic column than do quadrupeds. As a consequence, it remains unclear to what extent rodent data can shed light on cardiovascular problems encountered by astronauts. Humans experience a reduction in cardiac tissue mass and a lower stroke volume consistent with gravitational unloading of the vasculature. Dogs and rodents exhibit a decreased heart rate during spaceflight and an alteration in vascular responsiveness upon return to Earth (Nikolaev and Ilyin 1981; Wade 2005). However, a recent review of evidence from multiple missions suggests that the human response varies among individuals but that spaceflight does not significantly impact vascular function. The apparently lower peripheral vascular resistance among astronauts who experience presyncopal episodes on landing day can simply be attributed to microgravity-induced reductions in total blood volume (Convertino and Cooke 2007).

1.1.3 Rotating Artificial Gravity Solutions

Centrifugation has long been proposed as a countermeasure to the problems of microgravity (Clement and Pavy-Le Traon 2004). Rotating artificial gravity systems have the potential to alleviate the myriad of musculoskeletal and cardiovascular problems encountered during spaceflight. In some configurations they may also provide the tonic otolith input needed to counter the symptoms of sensory conflict previously discussed. However, high rates of rotation typically induce other problems, including motion sickness, inappropriate eye movements, and illusory sensations of self-motion.

Recent work indicates that, at least in the case of intermittent centrifugation in a 1-g environment, adaptation can lessen these disorientating and nauseating effects over time (Brown, Hecht *et al.* 2002; Young, Sienko *et al.* 2003). However, it is unclear whether such results also apply to continuous centrifugation in space. Consequently, concerns surrounding the sensorimotor effects of chronic rotation still present a barrier to its use as a countermeasure.

In considering both spacecraft-generated artificial gravity and reduced gravity environments such as on Mars, there exists very little prior research on which to build hypotheses regarding sensorimotor adaptation to partial gravity. Experimental heritage includes ground-based unloading studies (PavyLeTraon, Allevard *et al.* 1997; Schultheis, Ruff *et al.* 2000), small low earth orbit research centrifuges (Hemmersbach, Voormanns *et al.* 1996), the Soviet Cosmos-782 and Cosmos-936 biosatellites (NASA 2007), and limited data from the six lunar landings (Johnston, Dietlein *et al.* 1975; Rambaut, Leach *et al.* 1975). However, these studies provide insufficient evidence to answer the fundamental Mars-relevant questions: “Is 0.38-g sufficient to prevent deconditioning?” and “How will extended exposure to partial gravity affect basic physiological processes?” Anecdotal reports from Apollo noted that lunar 0.17-g resulted in “no disorientation or vestibular disturbances” (Johnston, Dietlein *et al.* 1975), suggesting that 0.38-g should likewise preserve critical vestibular function. The Mars Gravity Biosatellite’s proposed first mission aims to provide more rigorous, quantitative information to answer these outstanding questions.

1.1.4 Prior Rodent Research in Space

Since the earliest days of spaceflight, scientists have used both mice and rats for gravitational biology research. The first mouse in space was launched on board a U.S. Air Force Aeromedical Laboratory V2 rocket in August 1950 (Gray 1998). Over the subsequent decade, multiple missions (some successful, many not) were launched to test engineering systems and explore the feasibility of human spaceflight.

Table 1: Cosmos biosatellite flights involving rodents

Name	Year	Duration	Nature of rodent experiments
Cosmos-605	1973	21.5 days	45 rats of unknown gender and strain – general exploration of microgravity
Cosmos-690	1974	20.5 days	35 male Wistar – microgravity and ionising radiation
Cosmos-782	1975	19.5 days	25 male SPF Wistar rats – core temperature, motor and immune systems, bone, retina, readaptation
Cosmos-936	1977	18.5 days	30 male SPF Wistar rats, of which 20 were in microgravity, 10 in continuous 1-g centrifugation
Cosmos-1129	1979	18.5 days	Singly-housed: 30 male SPF Wistar rats. Group-housed: 2 males and 5 females. No births following flight and return to Earth.
Cosmos-1514	1983	5 days	10 group-housed pregnant SPF Wistar rats
Cosmos-1667	1985	7 days	10 male SPF Wistar rats
Cosmos-1887	1987	13 days	10 group-housed male SPF Wistar rats
Cosmos-2044	1989	14 days	10 group-housed male SPF Wistar rats, 50% with surgical wounds to investigate tissue healing

The earliest rodent missions served simply to demonstrate survival of biological payloads and to explore the capabilities and limitations of closed-loop life support systems. The Soviet Cosmos/Bion series of spacecraft were the first flights intended primarily to study the mechanisms and processes of mammalian responses to weightlessness. The very first flights of the mid-1960s flew dogs, but rats soon became the species of choice for subsequent missions. These rodent studies focused on physiological, morphological and biochemical changes, as shown in Table 1 (from Nikolaev and Ilyin 1981; Lange, Andrews *et al.* 1987; NASA 1990).

On most flights, rats were housed individually in small cages as shown in Figure 3. The zone marked (a) represents the specimen chamber while (b) indicates the waste collection trap. Each specimen holding cylinder was about 20.8cm long and had a diameter of 9.5cm. The rat had sufficient volume that it could just barely turn around within the habitat.

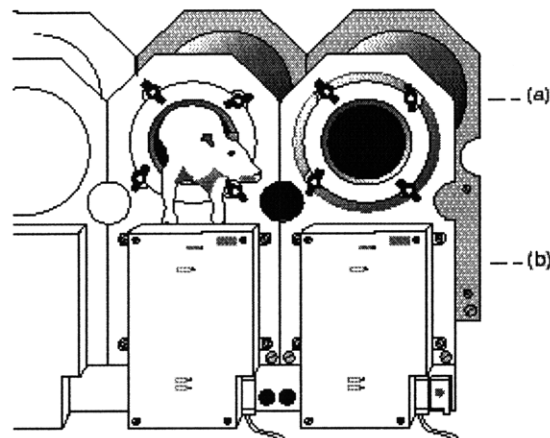


Figure 3: The rodent cages of Cosmos biosatellites (from NASA 1990)

Figure 4 illustrates the standard five-cage Cosmos arrangement for microgravity experiments. Cabin air circulated through the specimen cylinder before being returned, via the waste collection trap, through an activated charcoal filter (NASA 1990). Twelve hour day/night lighting was provided to each cage.

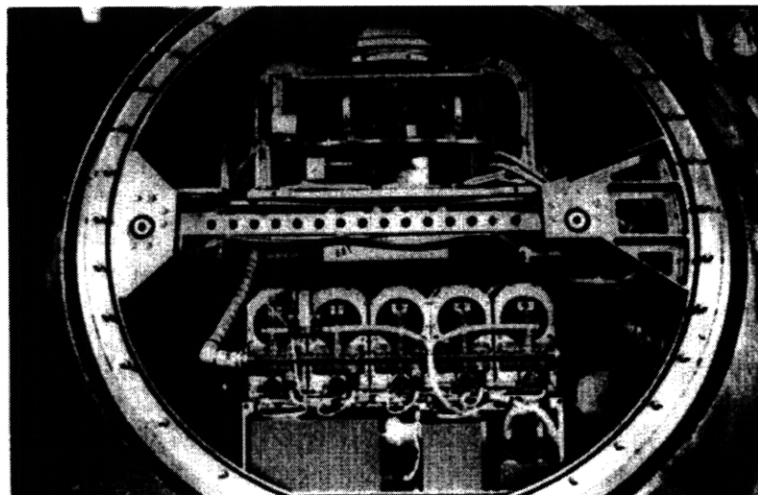


Figure 4: Five cages in the Cosmos-936 mockup (from Gurovsky, Gazenko *et al.* 1980)

An automated water delivery system provided *ad libitum* access to each animal, while a feeder nozzle dispensed 10 grams of paste every 6 hours. Each group of five cages was supplied by a common food and water reservoir, the ductwork of which is clearly visible in Figure 4.

Cosmos-1129 was the first mission to group-house a subset of the rodents. The mating chamber shown in Figure 5 included the partition marked (c) to separate the male chamber, (d), from the females in zone (a). This partition was mechanically removed two days into the mission in order that the specimens could mingle and mate. Feeding stations at the rear of the chamber are labelled (b). Missions following Cosmos-1129 used the same design as Figure 5 but with the partition omitted.

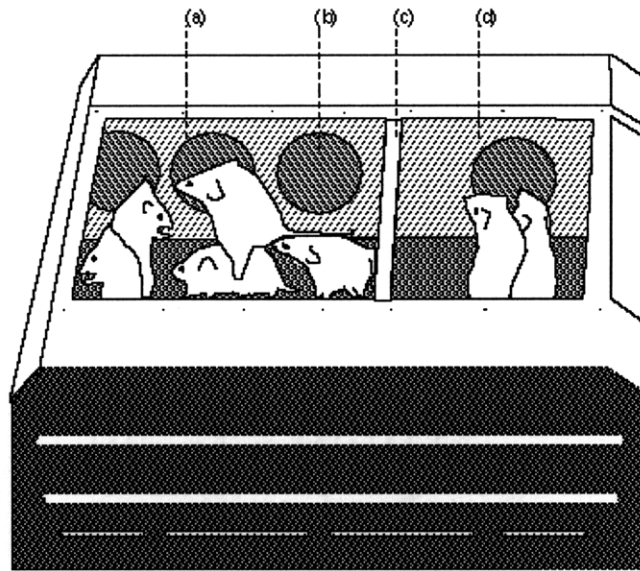


Figure 5: Group mating chamber for Cosmos-1129 (from NASA 1990)

Extensive preflight testing was employed to select the cohort of rodents for each mission. Scientists emphasised the need for the rats to exhibit uniform clinical data and appropriate, predictable behavioural reactions (Nikolaev and Ilyin 1981). After selection, the healthy rats were divided into flight, general control and ground synchronous groups. The latter cohort was installed within a biosatellite mockup similar to that shown in Figure 4. Environmental conditions were matched to those recorded inflight, with a delay of a few days. This group was also subjected to dynamic loading intended to simulate the forces and vibrations of launch and recovery.

Following landing, the flight animals were examined as swiftly as possible. In the case of Cosmos-605 and Cosmos-690 this was within 1-2 days, while subsequent missions achieved a tighter 5-11 hour schedule. Morphological and biochemical investigations were subsequently conducted at multiple time intervals in order to assess readaptation and recovery.

Animals that experienced microgravity conditions were generally inactive during the first few days postflight. Their motor activity and muscle tone was significantly reduced, and they either crawled or exhibited a very different gait. Endurance was also diminished. Disorientation was observed and general stress-related symptoms were evident. An array of post-flight behavioural testing was conducted, including maze performance, air-righting

reaction tests, balance beam studies, lifting reflex investigations, and possibly some basic gait analysis. Many of the animals were euthanised following flight, and tissue/organ samples led to findings consistent with those already described in sections 1.1.1 and 1.1.2.

1.1.4.1 Predecessors to Cosmos

In general, Soviet attitudes to biological spaceflight in the 1970s were very different to those of NASA and ESA researchers today. The design teams were highly flexible and routinely deployed experiments at short notice and with minimal funding. Soviet engineers were seemingly more willing to use spaceflight as a testbed to develop new technology and to accept possible failure as a necessary first step on the path to eventual success. Attention to the scientific method was also sometimes incomplete. It is known, for example, that a number of the dogs flown on early Soviet missions were in fact stray animals that had been caught in and around the space biomedical research facility. There are multiple reports of dogs escaping from their enclosures prior to missions and of substitute specimens being found at short notice.

The NASA Life in Space archive reports an interview with Rodney Ballard that provides a colourful illustration. In 1970, Oleg Gazenko, then Director of the Institute of Biomedical Problems in Moscow, contacted Eugeny Ilyin, Director of the Cosmos Biosatellite Program, with an urgent request. Georges Pompidou, the president of France, was on a tour of the U.S.S.R. and Leonid Brezhnev, General Secretary of the Communist Party, had invited him to attend a satellite launch. The available satellite had substantial empty space and Ilyin was invited to quickly prepare some biological experiments for the flight. He developed a mission scenario within two hours and was given eight days thereafter to deliver the experiments. Fruit flies, cell cultures, mice, and rats were selected for the microgravity flight.

The mission lasted just three days, and both Brezhnev and Pompidou attended the launch. Unfortunately, not all the rats survived, but the other specimens did. This hastily-arranged flight was the first major step in developing the rodent life support systems that flew for 21 days on Cosmos 605 three years later.

1.1.4.2 Early Rodent ECLSS: the Cosmos-605 Biosatellite

Cosmos-605 was the very first of the Bion series to fly rodents. It was similar in appearance to Figure 6, which shows a group of five rodent cages through the cutaway window. The ECLSS apparatus was not robust and encountered multiple failures. The system was supposed to maintain oxygen in the 17% to 33% range (considered scientifically inadvisable by today's standards). In reality, oxygen reached as high as 51% during the final stage of the flight (Ilyin, Serova *et al.* 1975). Temperature remained between 20°C and 24°C while the relative humidity was controlled in the 65% to 75% range. Carbon dioxide and trace contaminant levels were not monitored.

Six animals died between the twelfth and twentieth days of flight. Two more rats died immediately following recovery. All of these deaths were attributed to prolonged starvation on account of failures in the feeding systems. In addition, a ninth animal died fifteen days postflight after struggling with a bout of pneumonia.

The average weight gain of flight animals was 20 g, as compared with an 80 g average increase exhibited by ground control specimens.

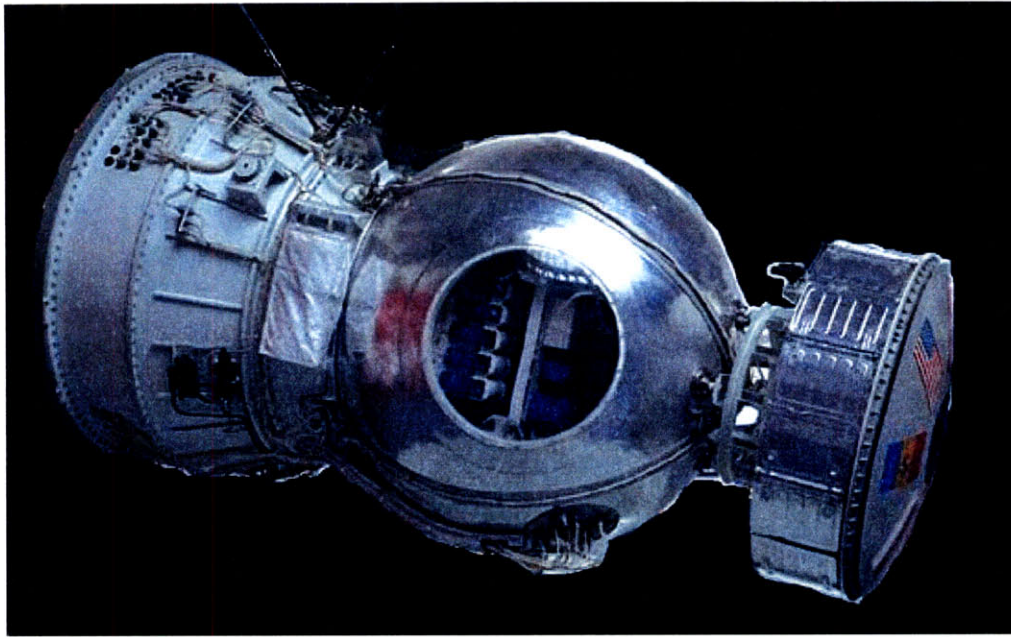


Figure 6: Outer appearance of the Cosmos biosatellites (from NASA 1990)

1.1.4.3 Cosmos-690: Studies of Ionising Radiation

The second Soviet attempt at rodent-compatible life support was substantially more successful. Cosmos-690 flew 35 Wistar rats in 1974. Its ECLSS assembly maintained air pressure to within -1.5% and +7% of 1 atm. The temperature ranged from 20°C to 22°C and relative humidity was 60-70% at all times (Gazenko, Adamovich *et al.* 1978). Oxygen was maintained in the range 18.5% to 28%.

A gamma radiation exposure unit was designed to dose all animals between days 10 and 11 of the mission. Ten of the rats received an average of 220 rad, while a further 21 animals received 800 rad. During the 20.5-day flight, two of the high-exposure rodents died, while a third specimen expired on account of a severe intestinal infection 24 days after landing. A series of pathological and biochemical studies postflight led Soviet scientists to conclude that mammals are no more susceptible to the effects of radiation damage in microgravity than in 1-g (Gurovsky and Ilyin 1978).

1.1.4.4 Artificial Gravity: the Cosmos-936 Biosatellite

The mission of the greatest relevance to the Mars Gravity Biosatellite is undoubtedly Cosmos-936, the first and only mission to date to provide artificial gravity for a cohort of mammals (Gurovsky, Gazenko *et al.* 1980). 30 male SPF Wistar rats were sourced from the colony at the Institute of Experimental Endocrinology, Slovakian Academy of Sciences, for this 18.5-day spaceflight. Ten of the animals received body temperature transmitters that were implanted in the peritoneal cavity (NASA 1990). Certain rodents were given surgical labyrinthectomies to resect the vestibular organs.

Each rat received a series of injections. These included 2-¹⁴C-glycine that was presumably used to estimate protein serum synthesis. The antibiotic declomycin was injected as a label to permit postflight assessment of bone growth. A 10% sheep erythrocyte suspension was also injected for the purpose of monitoring erythrocyte survival times. Final selection of the

flight animals occurred a few days before launch. The rodents were just barely under 9 weeks of age upon liftoff.

20 of the specimens were exposed to microgravity while the remaining 10 were installed on two counter-rotating centrifuges that generated the artificial gravity vector of $1\text{-g} \pm 11\%$. In all cases, the rats were housed in the same cylindrical chambers that had become standard on prior Cosmos flights. Each rat received 40g of paste diet per day on orbit, and 45g per day during postflight readaptation. Figure 7 illustrates the centrifuge design, with each cylindrical habitat orientated longitudinally at the periphery of the spacecraft.

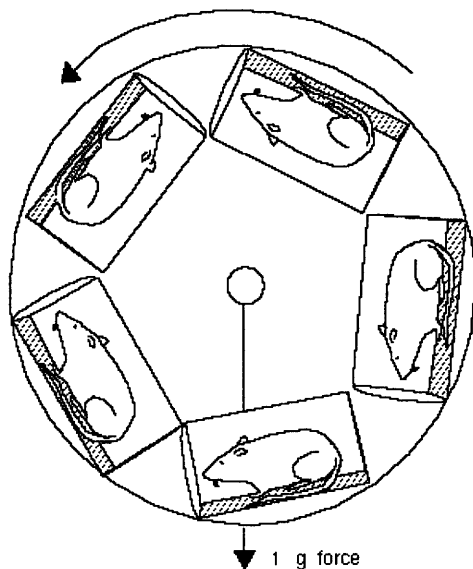


Figure 7: Design of the Cosmos-936 1-g centrifuge (from NASA 1990)

Centrifuge rotation commenced immediately after insertion of the spacecraft into orbit. Rotation ceased prior to deorbit burn, approximately 2 hours before landing. The rotation rate was nominally 53.5 rpm and each animal was situated at a radius of 320 mm from the central axis.

During the mission, oxygen was maintained between 19% and 27.5% and carbon dioxide was controlled to below 18,000 ppm. Temperatures ranged between 21.5°C and 24.0°C with a relative humidity of 80%-90%. Ammonia concentrations were not measured during the flight. As noted previously, the environmental conditions on board would not be considered acceptable under today's rodent care standards.

Environmental parameters recorded from the biosatellite are shown in Figure 8. The horizontal axis shows day of mission. Oxygen and carbon dioxide concentrations are shown in mmHg while relative humidity is expressed as a percentage and temperature is reported in Celsius. It is clear that simple on/off control algorithms were used to replenish oxygen and to scrub carbon dioxide. The oxygen valve appears to have activated on seven separate occasions, each separated by a few days. The carbon dioxide controller was triggered on perhaps three or four instances. The mechanisms by which temperature and humidity were controlled in this flight are unclear.

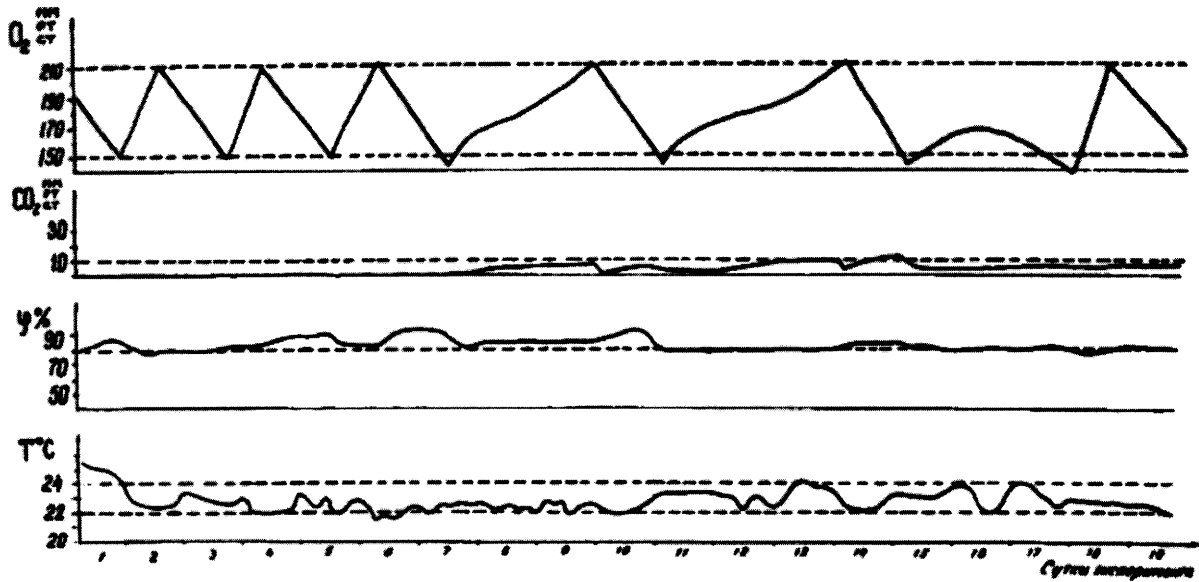


Figure 8: ECLSS on board Cosmos-936 (from Gurovsky, Gazenko *et al.* 1980)

Similar to other Cosmos flights, the ground control experiments included both synchronous specimens housed in a flight-equivalent biosatellite mockup and control rats in group-housed laboratory vivaria. On day 16 of the synchronous control experiment, one of the centrifuges in the spacecraft mockup malfunctioned, with the result that the five animals on it had to be removed from the study.

1.1.4.5 Cosmos-936 Findings

The health of animals on orbit was deemed acceptable as evidenced by the total motor activity and body temperature. Importantly, the motor activity of the weightless rats was significantly higher than that of the centrifuged animals. Average core temperature of the microgravity specimens was reported to be significantly lower than that of the rotating cohort.

Immediately after flight, Gurovsky *et al.* report that all the weightless animals were inactive and failed to exhibit normal exploratory activity such as rearing, climbing over obstacles and peering out of their cages. By contrast, the centrifuged animals were active and qualitative observation suggested their gait was very nearly normal.

Recovery of the specimens was measured in part by static endurance testing (methodology not documented). Although all the rats were sluggish following flight, the centrifuged animals regained normal performance within a five-day period while the weightless rats needed sixteen days to fully recover. In addition, the centrifuged rodents were shown to perform significantly better in maze tests than their weightless counterparts.

Weight gain was similar for both spaceflight groups; on average, the centrifuged rats exhibited a 64.4 g body mass increase while the weightless animals averaged 71.4 g. However, postflight weight gain of the centrifuged group was substantially faster than that of the microgravity cohort. In the 24 days following flight, the weightless group increased 57.4 g on average while the centrifuged specimens gained 81.2 g.

In terms of vestibular effects, researchers reported that animals exposed to rotation (both in orbit and on ground control hardware) exhibited slower nystagmus. Experimental details are unknown, but in general both the duration of each nystagmic event and the frequency of nystagmus was generally reduced in postflight testing. By contrast, the weightless animals were unaltered in terms of nystagmic response. This suggests a down-regulation of responsiveness involving the semicircular canals.

Both centrifuged and weightless rats had greater difficulty righting themselves postflight than prior to the mission. The degree of performance degradation was similar for both the microgravity and the rotated 1-g specimens.

Finally, the otolith function was measured by means of the rodent lifting test. A delayed response was found in those animals that had experienced weightlessness, while the response of the artificial gravity group remained essentially unchanged.

Histological and other studies showed that the 1-g artificial gravity vector largely eliminated the adverse vestibular, musculoskeletal and cardiac effects evidenced in the weightless animals.

1.1.5 Sensorimotor Targets for the Mars Gravity Biosatellite

To date, gravitational biology research has examined (i) changes in end organ structure, (ii) synaptic patterns in the vestibular nucleus and related areas, (iii) basic reflexes driven by combined sensory inputs, and (iv) complex behavioural changes that reflect collective sensorimotor function. Due to in-flight constraints, the bulk of the Mars Gravity Biosatellite mission science will be conducted during pre- and post-flight investigations. Test batteries will be broad and will include behavioural, histological, morphological, and gene expression/proteomics components. The overarching goal of sensorimotor investigations will be to examine changes in the vestibular system, its associated neural structures, and integrated functional responses. The intent will be to explain these results in terms of adaptation to a 0.38-g environment and chronic rotation.

Otolith adaptation is projected to be similar to that found in analogous microgravity work, albeit less severe. Reduction of the tonic gravitational input may cause reorganisation of otolith arborisation and changes in neural connectivity as described in section 1.1.1. This may result in increased sensitisation, such that signals generated at rest in 0.38-g begin to approach those previously experienced in 1-g. Following return to Earth, intensified reactions to linear accelerations are expected (Aizikov, Markin *et al.* 1992; Walton, Heffernan *et al.* 1997; Ronca and Alberts 2000).

While semicircular canal morphology is not expected to change under the Mars Gravity Biosatellite's mission conditions, studies in chronically rotating environments have shown a down-regulation of the response to angular accelerations (see section 1.1.4.5). This is likely a result of decreased synapsing between the canals and the vestibular nucleus (Gurovsky, Gazenko *et al.* 1980; Shipov and Ovechkin 1980; Wubbels and de Jong 2001). With a spacecraft or ground control rotating at 31.6 rpm, similar changes are certainly expected. Therefore, responses to angular stimulation may be reduced in both flight and rotational ground control animals, compared to non-rotational controls.

Complex reflexes and behaviours that rely on some combination of vestibular, visual, somatosensory, and other sensory inputs are expected to change in complex ways consistent with the changes in their respective inputs. Animals raised in 1-g will likely have some

initial difficulty adjusting to the lower gravity environment and to the chronic rotational stimulus. This may be evidenced by changes in food consumption, water intake, and video-derived behavioural parameters. However, it is hypothesised that the effects of chronic rotation can be quantified during ground studies and therefore decoupled from those associated with the 0.38-g artificial gravity vector. As explained in section 1.1, a desire to confirm this hypothesis is one of the major motivating factors behind this thesis research.

1.1.6 Rodent Care on Board the Mars Gravity Biosatellite

Throughout the 35-day flight, onboard life support systems will provide the animals with a comfortable and healthy environment. Radio downlink capability will permit daily animal monitoring, paving the way for the first significant assessment of the effects of chronic 0.38-g exposure. Each mouse will have unrestricted access to food and water while living in a controlled Earth-like atmosphere. An underfloor unit will collect and preserve mouse waste products for post-flight analysis. Each chamber will be equipped with an array of sensors for scientific data and system telemetry, while in-habitat video cameras and advanced computer software will detect rearing, activity levels and other characteristic rodent behaviours.

At the culmination of the mission, the live specimens will be returned safely to Earth, enabling extensive post-flight investigation of physiological function and readaptation. The data generated during and after the mission will provide new insight into the continuum of biological response to gravitational stimuli. Consequently, this program represents a major first step in preparing for human missions to Mars. The flight is unique in its simultaneous provision of chronic rotation and chronic hypogravity exposure.

1.2 Research Aims and Hypotheses

The aims of this thesis are as follows:

1. To translate scientific mission requirements into a set of core design features for the Mars Gravity Biosatellite's payload module.
2. To propose an on-orbit payload operations plan for the 35-day mission.
3. To scientifically evaluate the effects of chronic centrifugation using habitat modules and instrumentation identical to that proposed for the Mars Gravity Biosatellite.
4. To thereby explore the effects of chronic centrifugation (if any) and to confirm that they can be quantified and hence decoupled from the anticipated effects of chronic hypogravity exposure.
5. To provide proof of concept validation of the Mars Gravity Biosatellite's proposed environmental control and life support systems strategy.
6. To position the biosatellite as a multipurpose research platform that offers broader capabilities for work with other species and at different gravity setpoints.

1.2.1 Chronic Rodent Centrifugation Hypothesis

Female BALB/cByJ mice will be chronically rotated for 5 weeks at 31.6 rpm on a gondola centrifuge with effective radius 0.34 metres (distance from rotating spindle to centre of habitat floor). The mice will be aged 14.5-25.5 weeks at the start of both the control and the rotational studies. Behavioural metrics derived from automated top-down video

observation will include activity, time spent at habitat centre versus periphery, turn angle and meander trajectories. It is hypothesised that mice will survive while maintaining normal body mass and will exhibit behaviour that indicates vestibular adaptation to this rate of rotation. Specifically, it is hypothesised that:

- Hypothesis 1. Body mass at the end of a 5-week period will be no less than at the start of the experiment.
- Hypothesis 2. Mean water consumption will normalise to within 15% of that exhibited by non-rotating animals.
- Hypothesis 3. Video-derived behavioural metrics will normalise to within one standard deviation of those exhibited by non-rotating animals.
- Hypothesis 4. Performance in open field testing, rotarod running, balance beam walking and air-righting will normalise to within one standard deviation of those exhibited by non-rotating animals.

1.2.2 Environmental Control System Design Hypothesis

It is proposed that a closed-loop life support system comprising humidity control, oxygen replenishment, lithium hydroxide-based carbon dioxide scrubbing and activated carbon for the removal of ammonia/trace contaminants can support female BALB/cByJ mice for a period of 3.5 weeks. Specifically, it is hypothesised that body mass at the end of a 3.5-week period will be consistent with published growth curves for this strain, and that eating and drinking behaviours will be consistent with available data on NASA's Nutrient Upgrade 12D Rodent Food Bar.

1.3 Thesis Outline

Chapter 2 focuses on the process of translating scientific and other requirements into engineering solutions for the Mars Gravity payload module. This chapter discusses the design of the entire payload, including the habitat modules, environmental control hardware, structures and avionics.

Chapter 3 proposes an on-orbit operations plan for the payload. This chapter describes each of the mission phases from pre-launch to aerocapture and recovery. It details hardware and software performance within the payload module during these periods.

Chapter 4 highlights the ground control system. This section outlines the engineering design of a prototype integrated ground test apparatus, including a custom life support and environmental control apparatus. The chapter details the design of mechanical structures, electronics and software. It also includes an assessment of key lessons learnt during the process.

Chapter 5 focuses on experimental results from 5-week centrifugation of mice within the ground control system. The study methods are described in detail, and conclusions are drawn from the body mass, water consumption, in-habitat video and discrete behavioural tests.

Chapter 6 reports experimental findings from a 3.5-week closed-loop environmental control test with two mice. Procedures for preparing and testing the apparatus are described, and

the control algorithms are outlined. Results and conclusions are discussed for each of the atmospheric parameters that were monitored.

Chapter 7 proposes and evaluates modifications to the payload module that would allow it to support different species, gravity levels and environmental conditions. Individual subsections focus on group-housed animals, exploration-relevant radiation studies and alternative animal models, including rats and geckos.

Chapter 8 summarises the major findings and key contributions of this thesis. It also makes recommendations for future work.

1.4 Contributions

The work presented in this thesis offers four unique contributions to aerospace biomedical engineering and rodent behavioural science. In so doing, it provides scientific and engineering validation for the Mars Gravity Biosatellite's proposed first mission and its future deployment as a multipurpose research platform for space life sciences.

1. This thesis showcases the most comprehensive design and operations plans to date for the payload module of the Mars Gravity Biosatellite. Specific elements which the author claims as unique contributions include the electronics, software and systems-level design of the payload module.
2. The centrifugation experiment was the first direct measurement of the influence of chronic rotation on mice in flight-like habitats rotated at 31.6 rpm. It was the first use of video-based behavioural analysis software to monitor specimens undergoing continuous centrifugation.
3. The closed-loop environmental control test characterised the performance of a subset of life support hardware and software proposed for the Mars Gravity mission. It provided proof-of-concept justification for the environmental control and life support systems design strategy.
4. A sophisticated hardware and software platform was conceived, designed, implemented and operated. The integrated Mars Gravity ground test apparatus is the first system to incorporate high-fidelity flight-like habitat modules on a centrifuge matched to on-orbit radius and rate of rotation. It is the first to additionally provide a closed-loop life support test platform for ongoing refinement of environmental management hardware and control algorithms.

Chapter Two: Payload Module Design as Presented at PDR

It was much pleasanter at home, when one wasn't always growing larger and smaller, and being ordered about by mice ...

-Alice²

2.1 Overview

The design, prototyping and iteration of the Mars Gravity payload module was a team effort which involved the participation of multiple graduate students, undergraduates, advisers and industry professionals. For completeness, this chapter showcases the entire payload module design as arrived at during the author's time as Payload Engineering Lead from June 2004 until June 2008. The responsibility of the Payload Engineering Lead is to assign, supervise and manage all work related to the payload module. The author claims primary responsibility for the following specific contributions:

- Systems-level design and integration of the payload module, including verification of interfaces with the spacecraft bus and reentry vehicle.
- Design of the payload computer architecture including functionality breakdown between embedded and integrated computing solutions (section 2.4.1).
- Selection of electronic components and design of electronics circuitry and instrumentation for the habitat modules discussed in section 2.5. This includes the lighting, video, and habitat control module. It also includes the design of the water and food delivery systems, but does not include the body mass sensor.
- Design and implementation of the ECLSS sensor suite and distributed air quality monitoring systems as discussed in section 2.6.
- Design and iteration of the ECLSS atmospheric hardware described in section 2.7, excluding the condensing heat exchanger which was developed collaboratively.

2.2 Requirement Flowdown Principles

The payload module comprises four core subassemblies: the habitat modules, ECLSS apparatus, structures and avionics. The design process used a systems engineering approach by which high-level mission science and system interface requirements were flowed down into

² *Alice's Adventures in Wonderland*, Lewis Carroll.

justifiable and traceable design decisions. Many requirements apply only to certain Mars Gravity mission phases, which are defined in Table 2 (Bethke, Wagner *et al.* 2008).

Table 2: Definitions of Mars Gravity mission phases

Phase	Definition
E0: Pre-launch	From integration of rodents into the payload module until launch.
E1: Launch	From ignition of the launch vehicle to orbital insertion.
E2: Transition	From orbital insertion through spin-up to nominal cruise.
E3: Orbital	Nominal cruise phase until just prior to reentry manoeuvres.
E4: Deorbit	All manoeuvres leading to reentry, including spin-down, reorientation, spin-up and reentry burn, until the instant of bus and reentry vehicle (RV) separation.
E5: Entry, Descent and Landing	From completion of bus-RV separation until aerocapture.
E6: Recovery	From aerocapture until delivery of specimens to science facilities.
E7: Post-flight	All operations after specimens have been delivered to science facilities, including post-flight science collection and dissections, data and sample distribution, and completion of asynchronous ground control experiments.

2.2.1 Overview of Level 0 Requirements

The high-level mission requirements are shown in Table 3. Each Level 0 element spawned several dozen Level 1 requirements. Over 200 Level 2 scientific requirements ultimately flowed down into Level 3 requirements directly applicable to payload design efforts.

Of particular note is the second requirement in Table 3. This requirement states that the appropriate flight environment is to be maintained only during nominal operations, i.e. the payload module is not required to be fail-operational or fail-safe. While this design approach has generally been followed, it has been an engineering-level decision of the author (as Payload Engineering Lead) to eliminate single-point failure modes where feasible in certain elements critical to life support. In such cases, redundant and/or alternative backup systems have been incorporated to reduce risk and bolster the mission success profile.

Table 3: Level 0 requirements for the Mars Gravity Biosatellite

ID Number	Short Name	Requirement Text
1	Regulations Compliance	Mission design and operations shall abide by all government, university, and contractor regulations for mission operation.
2	Flight Environment	The Mars Gravity system (spacecraft and launch vehicle) shall be designed to keep the mice alive and enable desired science during nominal launch, orbit, reentry and extraction from the spacecraft.
3	Data Collection	The spacecraft shall collect and store data of sufficient quality in type, precision, and accuracy through phases E0-E7 to achieve science, engineering, and fundraising goals.
4	Operations	Engineering and science operations shall be designed such that the nominal mission objectives can be met.

2.2.2 The Science Requirements Documents

The Mars Gravity Level 2 Science Requirements Document (Bethke, Wagner *et al.* 2008) served as the starting point for payload module design activities. This internal document was developed and revised over the course of several years with the guidance of expert reviewers and experienced researchers from industry and academia. It sets out requirements for the mission itself, for ground control experiments, and for postflight specimen experimentation and tissue harvesting. Where possible, the stipulations are aligned with NIH-recommended best practises for care of animals in research settings. The document is consistent with requirements for the (now cancelled) Advanced Animal Habitat–Centrifuge (AAH-C), originally envisioned as a gravitational biology research platform for the International Space Station. The science requirements also reference multiple NASA standards, particularly those pertaining to air quality control and offgassing specifications.

In general, the requirements flowdown process was iterative and involved the following phases:

- *Assessment of feasibility.* An initial attempt was made to translate each scientific requirement into one or more engineering specifications. If a conceivable approach was deemed not acceptable, it was categorised as either too costly, too complex, too risky or a combination thereof.
- *Pushback against science requirements.* In the event that the feasibility assessment returned a “no practical solution” verdict, attempts at negotiation usually resulted in a relaxation of scientific requirements or in an acceptable compromise. Requirement modifications were recorded in the Mars Gravity internal requirements database. Any requirements already under Configuration Control were modified through a management-mediated Engineering Change Order process.

- *Preliminary Design.* Once each science requirement had been finalised, the preliminary design was drawn up, prototyped, iterated and refined. Where appropriate, such testing was conducted with live mice in order to ensure operational relevance. The Mars Gravity Biosatellite payload module successfully passed Preliminary Design Review in June 2007.
- *Critical Design.* At the time of writing (2008), the payload module is entering Critical Design phase. During this period, preliminary designs will be proven out and translated into high-fidelity prototypes and flight-ready hardware.

At all steps of the process, efforts were made to build upon existing biological spaceflight heritage. Reference was made to hardware, software, programmatic philosophies and anecdotal reports from the NASA Animal Enclosure Module, the Soviet Bion missions (discussed in section 1.1.4) and AAH-C. Commercial off-the-shelf (COTS) solutions were baselined whenever possible.

2.3 Interface Control

Figure 9 summarises the spacecraft interfaces while the vehicle is on the launch pad undergoing safety checks during preparation for lift-off. Colours in each block are consistent with those in the miniature spacecraft cross-section at top left. Linkages are non-directional except in the case of power (regular dashed line) where a single destination arrowhead indicates supply/receive orientation. Where linkages pass over blocks, this indicates a physical pass-through routing. The payload module is entirely encapsulated by the heatshield (above) and by the aft fairing (below); accordingly, all connections either link to or pass through the EDL (Entry, Descent and Landing) system.

Immediately prior to launch, the ground support equipment will disconnect and the vehicle will begin operating under power drawn from the launch vehicle. Upon delivery into the appropriate orbit, the bus will manoeuvre the vehicle into a sun-pointing position and the spacecraft will spin up to a rate of 31.6 rpm. The solar panels will unfurl and the bus will begin recharging the batteries and powering all spacecraft systems. On-orbit subassembly checkouts and startup sequences will activate in the bus, payload module and EDL system.

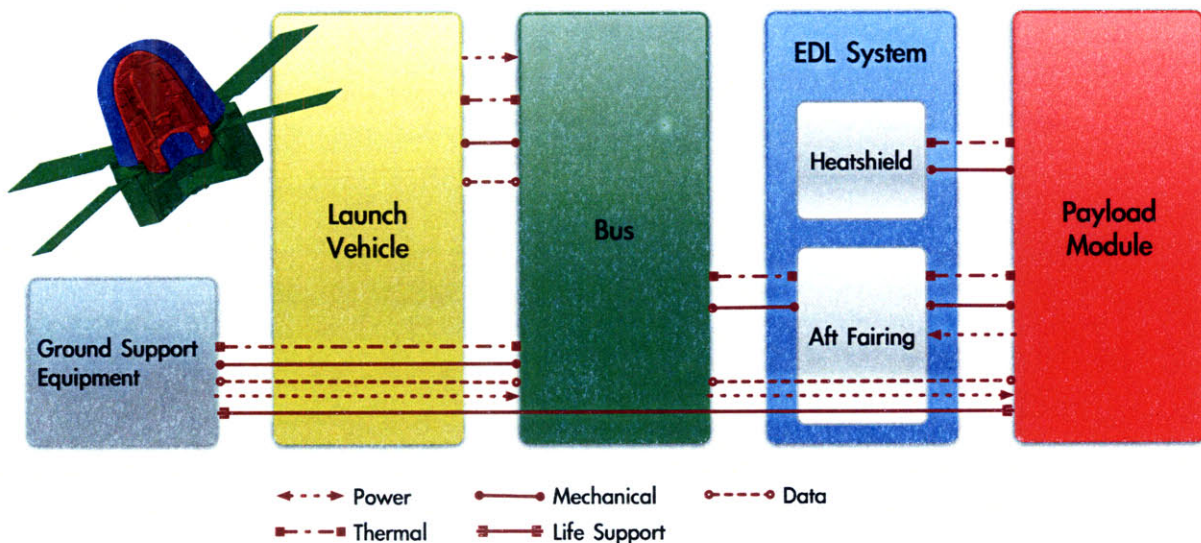


Figure 9: Spacecraft interfaces prior to launch

During the orbital phase, communication with the ground will be via radio equipment as a service of the spacecraft bus (Figure 10). Communications requires line-of-sight connectivity and is limited by the number and location of ground stations. Funding constraints mean that the spacecraft will have only a few minutes of communication per 24-hour period. Accordingly, autonomous operation and software fault tolerance/recovery is essential (see Appendix B: Payload Autonomy). The payload module will provide life support, data aggregation, science analysis and system health monitoring services during this period.

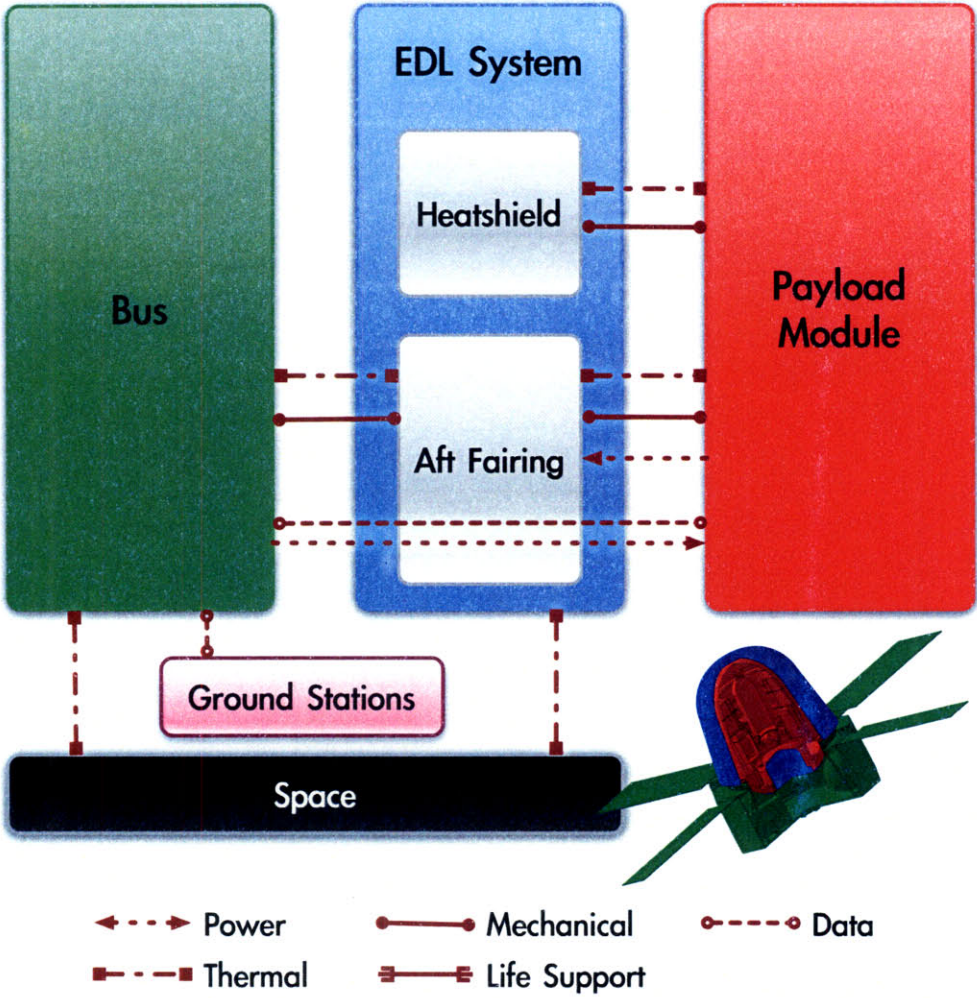


Figure 10: Spacecraft interfaces while in orbit

After five weeks of continuous rotation, the spacecraft will despin and reorientate. The propulsion system will subsequently start the vehicle on a reentry trajectory. Just minutes before entry, the spacecraft bus will be jettisoned into space by means of a pyrotechnic quick-disconnect separation ring. With power no longer supplied by the bus, the payload module will automatically transition to battery operation. The heatshield will protect the vehicle as it plummets into the Earth’s atmosphere and descends toward Utah Test and Training Range. A parachute will deploy to slow the rate of descent and a self-locating beacon will begin transmitting the spacecraft’s coordinates to local ground stations.

A specially-equipped helicopter will capture the vehicle at an altitude of several thousand metres. The helicopter will immediately carry the spacecraft to the ground so that technicians may connect life support hoses and power/data lines in order to verify spacecraft health. Thereafter, the spacecraft will be taken on the final and shortest leg of its journey, arriving at the scientific analysis centre a maximum of two hours after first touchdown. A team of Principal Investigators will subsequently perform various experiments on the fifteen rodents in order to augment and contextualise the data generated on orbit.

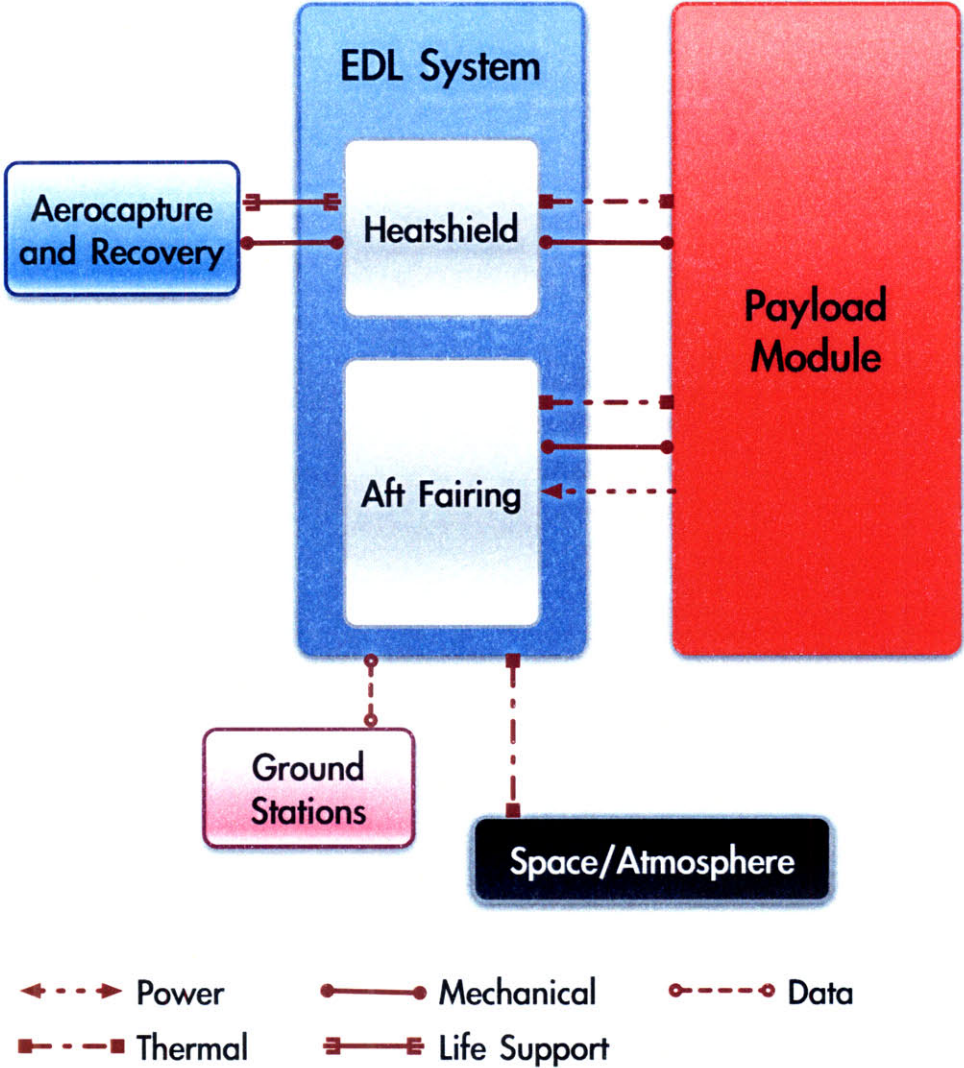


Figure 11: Spacecraft interfaces for reentry and aerocapture

Figure 11 shows spacecraft interfaces during atmospheric entry, aerocapture and recovery. The reentry vehicle comprises the EDL system and the payload module.

2.3.1 Interfaces to Spacecraft Bus

Table 4 highlights key interfaces with the spacecraft bus, taken from program Interface Control Documents (McLinko 2008).

Table 4: Interfaces between payload module and spacecraft bus

Domain	Interface Requirement
Power	The bus provides unregulated DC power in the range $27\text{ V} \pm 5\text{ V}$. Average power provision is 53.1 W with peak capability of 262 W. Power is routed through the separation ring and EDL aft fairing.
Thermal	Capable of rejecting 80 W steady-state and up to 100 W peak from the payload module to space via the EDL aft fairing, separation ring and spacecraft bus.
Data	Data destined for ground stations will be transferred from the payload module to the spacecraft bus via the separation ring for subsequent radio downlink. Uplinked commands from the ground destined for the payload module will use the same pathway. Data formats and communication protocols will match MIL-STD-1553B.

2.3.2 Interfaces to Entry, Descent and Landing System

Table 5 describes interfaces between the payload module and EDL system (Korzun 2008).

Table 5: Interfaces between payload module and EDL system

Domain	Interface Requirement
Power	The payload module provides power to the EDL system only during deorbit and descent. During this period, TBD Watts are required from the payload module batteries.
Thermal	There will be negligible thermal soakback from the heatshield to the payload module during entry. Although the properties of the heatshield material are known, they cannot be published for reasons of Export Control.
Data	The payload module must transmit accelerometer, gyroscope and timing data to the EDL system during the deorbit and descent phase only.
Mechanical	The EDL system fully encapsulates the payload module with a pressurised aeroshell. At the bus side of this aeroshell is the aft fairing, while the heatshield is opposite. O-rings seal the system.

2.4 Robustness and Control

Human-rated spacecraft often feature systems that are a combination of fail-operational and fail-safe. Due to cost constraints and the perceived lower risk associated with a five-week rodent mission, these requirements have been relaxed for the Mars Gravity Biosatellite. Fail-operational fault tolerance has been left open to be implemented by individual subsystems on an as-needed basis. However, the spacecraft does require operational autonomy as a consequence of limited communications and the need to rapidly respond to developing off-nominal mission scenarios. Under current projections, the spacecraft will have ground

communication opportunities (both downlink and uplink) for only a few minutes every six hours. Appendix B: Payload Autonomy discusses some of the historical approaches to autonomous spacecraft and outlines the key alternatives that were considered in arriving at the payload design.

2.4.1 Payload Computing Architecture

The requirements of relevance to the payload computing infrastructure are listed in Table 6. The acronym C&DH refers to Command and Data Handling. 4.1.1 and 4.2.1 are considered foundational requirements. The Mars Gravity mission would be partially successful even if no on-orbit data were acquired, so long as all the specimens were returned safely to Earth for post-flight analysis. Accordingly, requirement 4.1.1 is highly mission-critical and failure-intolerant, while requirement 4.2.1 falls into the “desirable if practical” category. Accordingly, the design calls for two hardware/software solutions to meet the needs of the payload module. A robust, radiation-hardened CPU with modest performance parameters and an autonomous planning agent will meet requirement 4.1.1. A state-of-the-art high-speed module optimised for video processing, data analysis and result storage will address 4.2.1.

Table 6: Payload autonomy and data storage requirements

Requirement ID	Detail
4.1.1	The Payload C&DH subsystem shall be able to control all ECLSS functions without ground control input for 37 days.
4.1.2	The Payload C&DH subsystem shall be able to prepare the Payload for deorbit within 36 hours of ground command.
4.1.3	The Payload C&DH subsystem shall be capable of triggering the deorbit in such a way that the vehicle lands in a safe area.
4.1.4	The C&DH subsystem shall identify pre-specified emergency situations and activate the associated emergency procedures.
4.1.5	The C&DH subsystem shall be capable of detecting a hardware failure and recovering from the failure if possible.
4.2.1	The data storage system shall store all science data (except video imagery) until confirmed receipt by ground station.

2.4.1.1 Software

The Mars Gravity payload will not need to perform “science opportunity identification” of the type often required for Earth observing spacecraft and scientific monitoring satellites. However, it will need to perform “power opportunity identification,” involving dynamic tracking of power usage to appropriately allocate time windows for events with substantial power requirements. Available electrical resources must be balanced against the need for ECLSS performance and regular scientific data aggregation and analysis. Critically, the software must account for the fact that additional power usage will necessarily result in a greater thermal load within the payload module. This will be evidenced by an increase in

atmospheric temperature and a reduction in relative humidity, one or both of which may be problematic in the context of ECLSS functionality.

The chosen on-board remote agent for the payload module utilises a dynamic real-time decision making engine (see discussion in Appendix B: Payload Autonomy). It comprises the following core elements:

- A planner/scheduler to map out system activations in a manner that treats as resources the available power, maximum thermal load and communications downlink. Critically, this element is able to rapidly and dynamically replan in light of new information and performs incremental plan updates rather than waiting for event horizons.
- An executive to manage communications both within and to/from the remote agent, and to carry out the plans created by the planner/scheduler.
- A fault detection/identification/recovery system that will monitor the payload and compare it with operational models in order to determine the system state. In the event of a failure such as an over-power condition or a reduction in communication bandwidth due to electric storms, the agent would lay out plans to return the spacecraft to a normal mode of operation. This may be achieved through judicious scheduling of subsystem shutdowns or through the selective transmission of representative off-nominal datapoints.

Payload software operation is discussed in detail in chapter 3.

2.4.1.2 Hardware

Much of the processing load within the payload module will be handled by a distributed computing architecture. Each of the primary payload subassemblies will have its own dedicated microcontroller. These will be supervised by one or more iNode processing modules. iNode is a product of Microsat Systems Inc. and its specifications are protected under Export Control laws. Figure 12 shows the payload hardware architecture, focusing on the processing units and interconnections within the payload module.

In Figure 12, microcontroller-governed elements are green while central processing units are blue. Each microcontroller is part of the Microchip PIC family of products, a collection of low-power, low-mass COTS units that have good spaceflight heritage (Day 1999; Galysh, Doherty *et al.* 2000). Black lines indicate bidirectional communication pathways. Data storage units are yellow. Black oblongs identify other spacecraft systems.

Functionality is as follows:

- Governing iNode CPUs provide supervisory control of all payload functions with the exception of video processing and analysis. They interface with 1GB of solid state NOR EEPROM memory manufactured by Intel, Inc.
 - The fifteen Habitat Control Modules (HCMs) monitor the system health of each specimen chamber and communicate with associated habitat-level sensors and actuators. These are discussed further in section 2.5.8 on page 54.

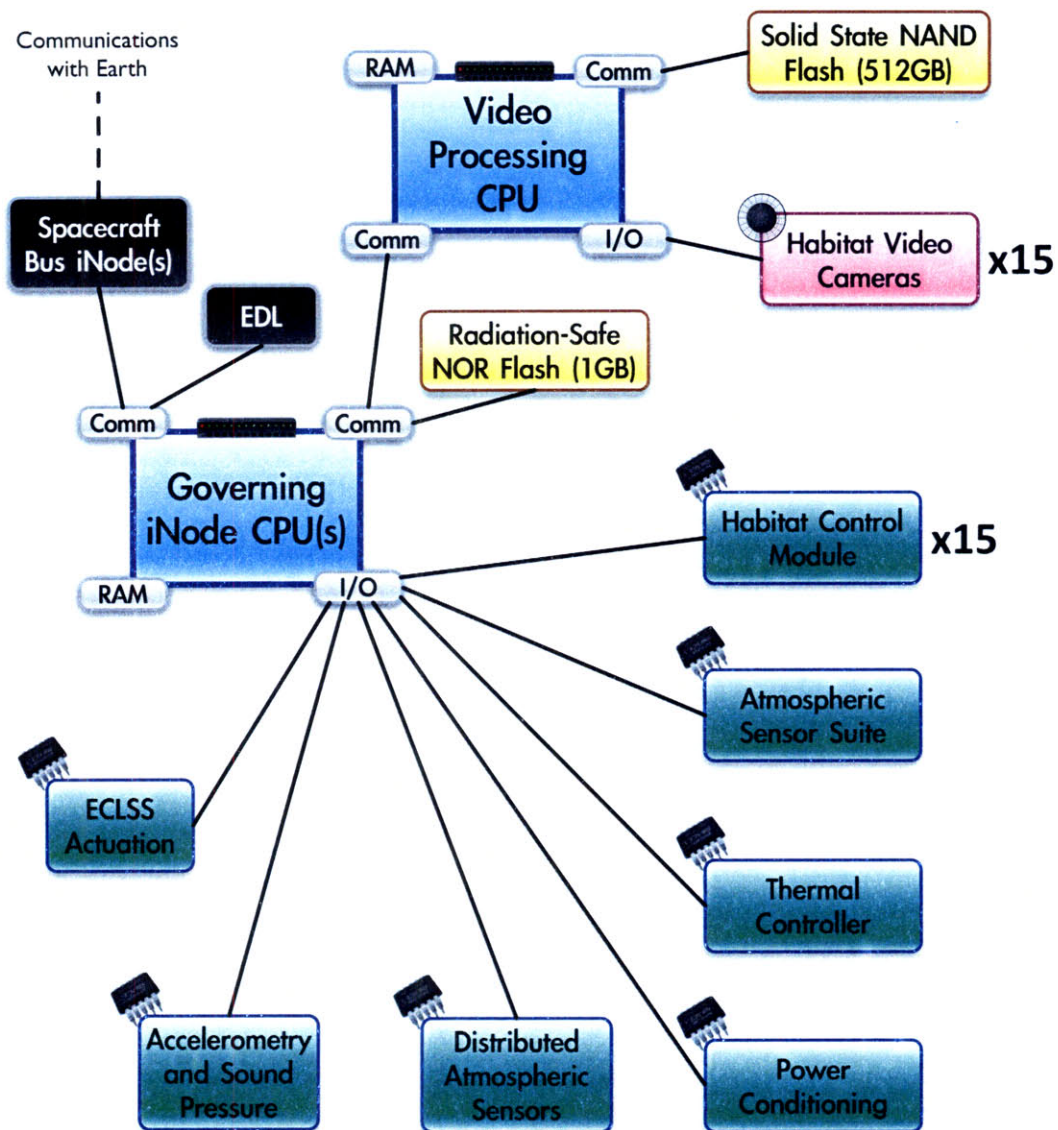


Figure 12: Payload computing hardware architecture

- The Atmospheric Sensor Suite is a triply-redundant collection of sensors that continuously monitors relevant environmental parameters at the level of the entire payload module. The supervisory microcontroller acquires, error-checks, packages and transmits this data to the iNode CPUs for the purpose of ECLSS decision-making. Sensor Suite details are in section 0 on page 57.
- The PIC-based Thermal Controller interfaces with the condensing heat exchange units and provides low-level control of thermoelectric coolers, circulatory fans and reservoir micropumps. See section 2.8 on page 73.
- The Power Conditioning module is electrically connected to the spacecraft bus and directs power to each of the various payload subassemblies. The governing PIC microcontroller can receive commands from the iNode CPUs

to electrically isolate any given subsystem in the event of an overpower condition. Further information is on page 74 in section 2.10.1.

- The distributed atmospheric sensors block in Figure 12 includes all monitoring equipment not in the HCMs or centralised Sensor Suite. Judiciously placed throughout the payload module, these are primarily temperature, humidity and air flow rate detectors (detail in section 2.6.3 on page 63). Their data is aggregated by a microcontroller that can be polled by the iNode as necessary.
- Accelerometer and sound pressure data is recorded only for scientific record-keeping. A governing microcontroller processes data from these sensors and reports it to the iNode CPUs as explained on page 75 in section 2.10.2.
- The ECLSS actuation microcontroller manages low-level interactions with compressors, valves and other atmospheric reconditioning equipment. It actualises control decisions made at the level of the iNode CPUs, detailed in section 2.7.7 (page 72).
- The video processing CPU is baselined as an Intel Core 2 Duo processor. Although this unit is not radiation-tolerant, it is a high-performance computing module that can efficiently handle all operations related to video acquisition and processing. A 512GB solid-state STEC Inc. Zeus-IOPS drive will store acquired video files, still images, and the results of rodent tracking/analysis operations.
- Connections to the spacecraft bus have not been specified at time of writing, due to concerns about the current level of bus design maturity. Similarly, EDL hardware has not been specified to a level of detail sufficient to write code and design electronics to support that interface.

2.4.1.3 The Radiation Environment

Multiple university-based small satellite design teams have had to address issues associated with space radiation. Various strategies have been employed. Certain programs have chosen to use radiation-hardened components, while others have combined non-hardened COTS alternatives with appropriate risk mitigation software and electronics (Heidt, Puig-Suari *et al.* 2000; Lovellette, Wood *et al.* 2002).

The Mars Gravity payload module uses a hybrid approach that takes into account the mission-criticality of different subassemblies. The iNode CPUs will be radiation-hardened, while the video processing module will be a COTS unit with no specific radiation protection. Solid-state non-volatile EEPROM (“Flash”) storage media will be used throughout the spacecraft because it has no moving parts, is tolerant of vibrations and offers a very favourable mass-per-Gigabyte ratio. NOR solid-state memory is known to be significantly more radiation-tolerant than the higher-density NAND drives found in most consumer electronics products. Accordingly, a NOR drive has been selected to support the iNode CPUs while a substantially higher capacity NAND media disk will meet video processing needs.

Semiconductors in space are at risk of single event errors on account of radiation-induced charge deposition or current dispersion. There are two broad categories of error: single event upset (SEU) and single event latchup (SEL). SEU anomalies are known as “soft errors” since they rarely cause hardware damage and instead only result in flipped bits or other localised

data corruption. SEL is far more problematic, since it causes semiconductor short-circuiting and consequent high current draw, which can destabilise satellite systems. SEU problems can be addressed through software checksum routines or by treating one bit in each byte as a parity flag to allow algorithmic self-correction of corrupted data. The SEL risk has been addressed in the payload module with the dedicated power conditioning controller (section 2.4.1.2). This microcontroller-managed hardware can isolate any subsystem the instant its current consumption exceeds a pre-defined upper limit.

The Microchip PIC family of microcontrollers is known to be robust to radiation-induced SEU and SEL events. For this reason, and for ease of programming, a PIC device is used wherever low-level microcontroller functionality is required.

2.5 Habitat Modules

2.5.1 Requirements

The requirements affecting the specimen chamber structures are listed in Table 7. The habitat module passed CDR independently of the rest of the payload module as a consequence of accelerated development through a NASA Phase II SBIR grant (Ames Research Center). The SBIR effort was a collaboration between the Mars Gravity Biosatellite team and Aurora Flight Sciences, Inc. (formerly Payload Systems, Inc.). In subsequent sections, it is explicitly noted where Aurora employees took primary responsibility for a segment of the design effort. Contributions claimed by the author are similarly flagged at the start of each section.

Table 7: Partial specimen chamber mechanical requirements

Req. ID	Detail
5.2.1	All chambers have dimensions within 0.5 cm of one another.
5.2.2	Each chamber shall have a minimum floor area in E3 of at least 200 cm ² .
5.2.3	Each chamber shall have minimum floor length of 13 cm in Phase E3.
5.2.4	Each chamber shall have a minimum height of 12.7 cm for Phases E0-E6, where the height is defined in the direction of the local gravity vector.
5.2.5	The design of each specimen chamber during Phases E0 and E6 shall not induce a statistically significant loss in body mass.
5.3.1	Specimen chamber interior structures shall be constructed so as to prevent escape, injury, or entrapment of mice or parts of their bodies.
5.3.2	No specimen chamber surfaces exposed to mice or handlers shall be abrasive or sharp to the touch, in accordance with Section 6.33 of NASA-STD-3000.
5.3.3	All materials used in cage construction shall resist corrosion and rusting.
5.3.4	All materials shall withstand normal handling without chipping or cracking.
5.3.5	All materials used in cage construction shall be non-reactive with by-products of the mice or life-support systems.

5.3.6	All materials that come in contact with the mice shall be non-toxic to them.
5.3.7	Materials used in specimen chambers or air handling systems shall comply with offgassing and odour mandates in accordance with NASA STD 6001.
5.3.8	Specimen chamber components that come into contact with the mice shall be able to be sterilised to no more than 3 Colony-Forming Units per cm ² .
5.3.9	Mouse-accessible hardware shall resist damage by chewing and gnawing.
5.3.10	The specimen chambers shall be designed to limit and control odour production. The concentration of any odour-producing agent shall not cause a significant rise in stress hormones, as determined by pre-flight testing.
5.3.11	The specimen chambers and associated life support systems shall be designed to limit and control microbial growth.

2.5.2 Design Overview

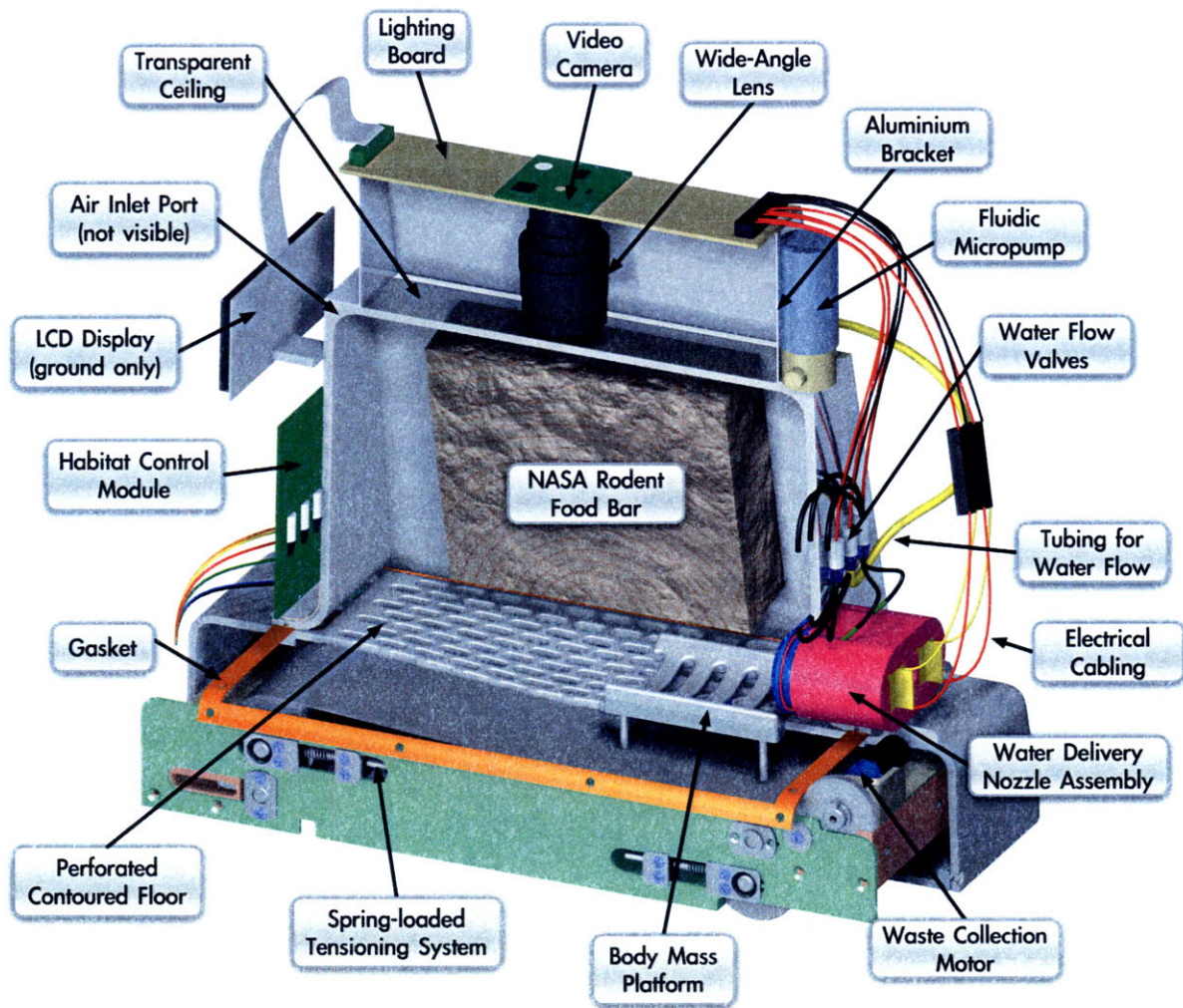


Figure 13: The Animal Support Module (CAD: Adam Fuhrmann)

Figure 13 shows an annotated diagram of a single Mars Gravity Animal Support Module (ASM).

2.5.3 Habitat Structure

The habitat structure (outer shell) was designed by employees of Aurora Flight Sciences. The shell of the habitat is fabricated using a cold-pour urethane casting method. The resulting structure is then coated with rodent-safe Krylon matte black spray-on paint. It was designed to meet all the requirements previously listed in Table 7. A mouse may be loaded into the structure by removing the joining screws before separating the upper shell (specimen chamber) from the lower Waste Collection System (WCS) enclosure, as shown in Figure 14.

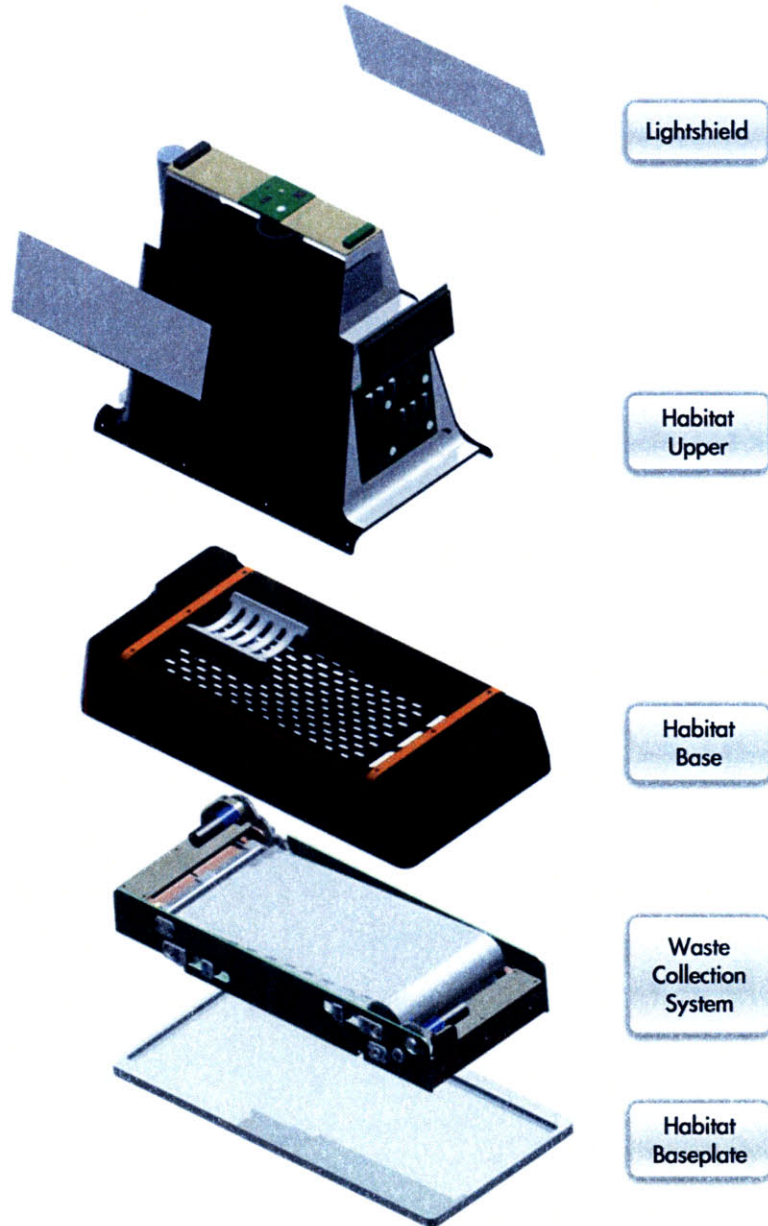


Figure 14: ASM disassembly diagram

2.5.3.1 Habitat Upper

The cold pour urethane casting method produces parts similar in quality to injection moulded units. The habitat upper serves as the point of attachment for the aluminium side brackets that support the Habitat Control Module (HCM), water delivery system and lighting/video assembly. A rubber flange gasket serves to hermetically seal the junction between the upper and lower halves of the ASM. The ceiling is the only part left unpainted in order to ensure an appropriate window for light to enter the specimen chamber and for the video camera to capture footage.

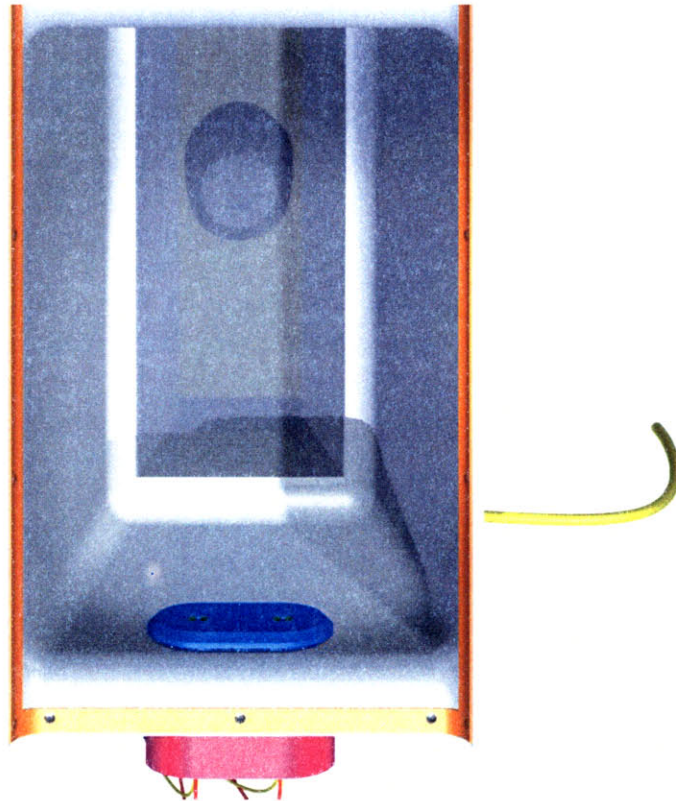


Figure 15: Upper structure of the ASM, viewed from beneath

2.5.3.2 Habitat Base:

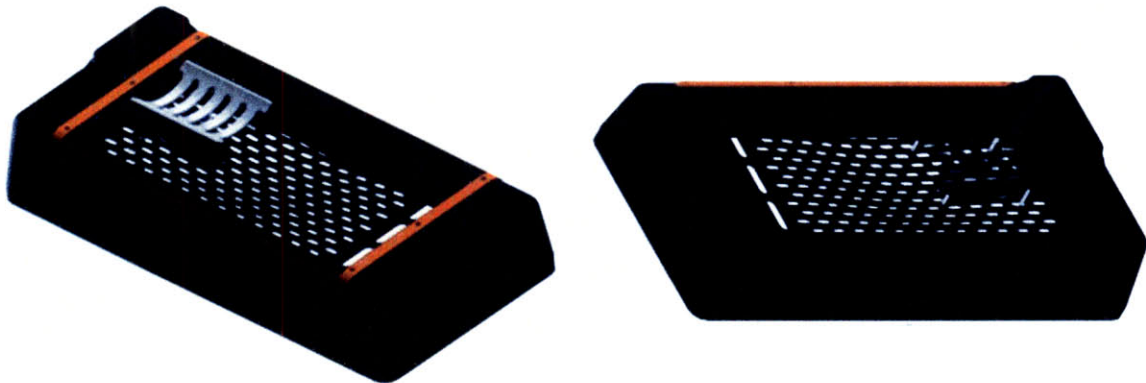


Figure 16: Habitat base, viewed from above and from beneath

The base provides a perforated floor for the rodent while also enclosing the Waste Collection System. The floor is contoured to promote channelling of urine toward the centre of the waste collection substrate. The base also serves as the attachment point for the body mass sensor, which is further discussed in section 2.5.7.

2.5.4 Waste Management

Waste collection requirements are outlined in Table 8. The Waste Collection System (WCS) was designed by employees of Aurora Flight Sciences.

Table 8: Waste collection, sampling and preservation requirements

Requirement ID	Detail
3.1.1	The waste management system shall contain mouse waste products from the specimen chamber throughout all Phases.
3.1.2	While under containment, mouse waste products shall be inaccessible by mice.
3.1.3	The waste management system shall collect mouse waste products during Phase E3.
3.1.4	Less than 5% by volume of collected mouse waste products shall re-enter the specimen living area.
3.1.5	Waste accumulation in the specimen chamber shall remain below levels that would affect mice behaviourally or physiologically.
3.2.1-3.2.4	(Abbreviated) Solids shall be segregated from liquids and liquid samples shall be collected at least once weekly. The system shall handle up to 25 ml of liquid waste and 25 g of solids per week.
3.3.1-3.3.2	(Abbreviated) Urine samples shall be preserved for 7 weeks through mould and/or microbial growth retardation.

2.5.4.1 Features of the WCS

On Earth, rodent care facilities will normally exchange bedding and provide clean cages on a weekly basis. This may be extended to fortnightly if there is a need to avoid disturbing pregnant or rearing mothers. The five-week Mars Gravity mission will require the removal of animal wastes from the specimen chamber in order to maintain proper sanitation. Both solid and liquid wastes can be detrimental to animal health, most dangerously as a result of gaseous ammonia, which is produced as a side effect of microbial breakdown and fermentation processes. Since moisture and humidity are both catalysts of ammonia production, waste must be dried, inactivated, or sealed in order to maintain a rodent-safe environment.

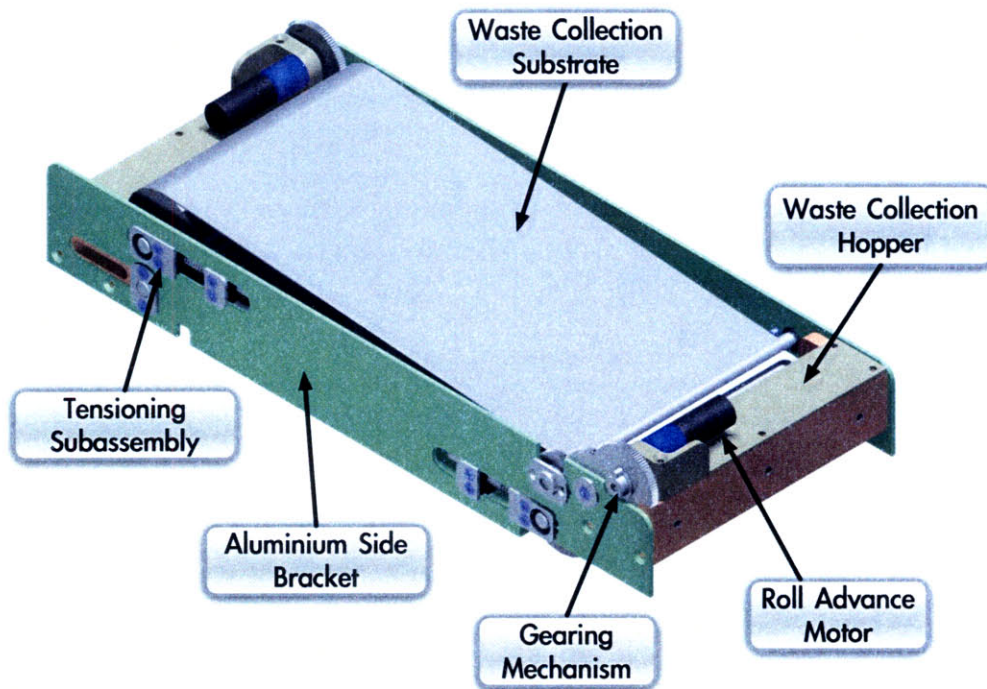


Figure 17: Waste Collection System (CAD: Adam Fuhrmann)

2.5.4.2 Waste Collection and Preservation Hardware

The proposed waste management system is designed to permit laboratory analysis of mouse urine throughout the five-week mission. The hardware design of the system depends on artificial gravity causing a directional flow of waste, assisted by air flow through the specimen chamber from top to bottom. Solid waste from the specimen chamber falls through the perforated plastic floor, while liquid flows toward the centre, assisted by the contoured flooring design. Beneath the floor is a plastic-backed, ultra-absorbent paper impregnated with urine preservative. In order to conduct a time-dependent study, the attached motor will periodically advance the rollers in order to provide clean paper absorbent beneath the floor of the specimen chamber. Testing suggested that advancement every three or four days was appropriate to ensure non-adhesion of the substrate and free movement of the motors throughout the study.

The scientific justification for this design is that differing amounts of urinary chemicals indicate changes in physiological parameters. There exist markers that indicate bone turnover, bone density loss, muscle wasting, and stress. Analysis of the changes in these chemicals over the duration of the mission will give insight into the nature of adaptation processes in the mammalian skeletal and muscular systems.

A notable feature of the WCS is a spring-loaded self-tensioning mechanism that prevents the substrate from sagging. The waste collection material comprises a hydrophobic microfibre woven nylon barrier over a blotting paper-like 3M Durapore™ membrane. The Durapore™ is impregnated with the chemical urine preservatives Chlorhexidine and N-Propyl-Gallate. The nylon barrier is sealed against a plastic backing layer using spray-on adhesive. Six individual packets of membrane are separated from one another to ensure no cross-seepage of urine from one week to the next. The barrier funnels on each side of the waste collection frame prevent liquid waste from collecting on the sides of channel.

The automated roll advancement system features a motor that pulls the roll toward a scraper bar. The scraper bar causes solids to travel into a collection trough at one end of the WCS. The substrate manufacturing process includes a step whereby small aluminium indexing strips are glued into the material. An optical switch senses the presence of each strip, thereby detecting the length of paper that has travelled past since the most recent motor actuation.

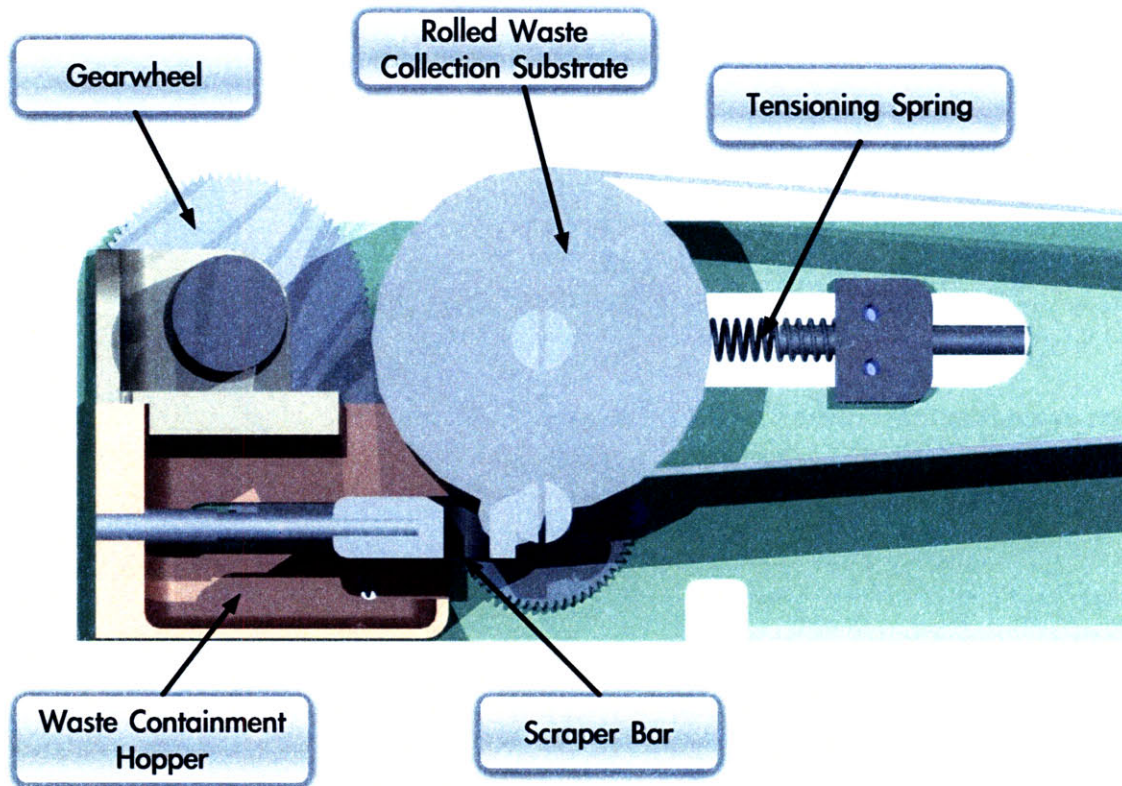


Figure 18: WCS tensioning mechanism and scraper (CAD: Adam Fuhrmann)

2.5.5 Provision of Food and Water

Consumables requirements are outlined in Table 9. Each of the fifteen BALB/cByJ mice on board will have *ad libitum* access to food throughout the duration of the flight. The food substrate will be affixed to one wall of the specimen chamber as previously shown in Figure 13. Water will be continuously available during phases E0 and E3 via two delivery nozzles.

Table 9: Consumables requirements

Requirement ID	Detail
6.1.1, 6.2.1	The amount of food and drinking water available to each specimen chamber shall be sufficient to sustain a mouse for at least 42 days.
6.1.2	The diet shall consist of palatable, nutritionally adequate food as defined in <i>Nutrient Requirements of Laboratory Animals</i> (4e, 1995).

6.1.3, 6.2.5	The food shall be able to withstand sterilisation. Drinking water shall be low in contaminants as specified in 7.2.2.3.2 of NASA-STD-3000.
6.1.4, 6.2.3	During all Phases, mice shall have access to food at least once every 12 hours. During E0-E2 and E4-E6, mice shall have water access at least once every 12 hours.
6.1.5, 6.2.2	During Phases E0, E3 and E6, mice shall have continuous food access. During E3, mice shall have continuous access to drinking water.
6.1.6, 6.2.4	No more than 17 g of food and 12 ml of water may escape the specimen chamber per week.
6.2.7, 6.2.8	The system shall provide for the introduction of a predefined volume between 10 and 100 microlitres of bone formation labelling chemical into each specimen chamber water supply on at least two predefined occasions during Phase E3. The predefined volume of label shall be delivered to the mouse such that at least 95% is ingested within 24 hours of administration.

2.5.5.1 Food Delivery

NASA's Nutrient Upgrade 12D Rodent Food Bar has been baselined as the preferred food substrate for this extended-duration mission. This textured hydrated solid has the consistency of hard confectionery and has significant spaceflight heritage with both mice and rats (Tou, Grindeland *et al.* 2003). Previous crewed NASA missions have required that astronauts provide fresh food bars approximately once every seven days. It was initially hypothesised that a 5-week mission may require additional treatment of the food substrate in order to ensure environmental stability and nutritional adequacy. In order to explore this question, the author conducted a series of experiments in 2005. Measures explored included coating the bars with edible wax to prevent dehydration and reduce fungal/bacterial contamination (Fulford-Jones, Steber *et al.* 2005). This approach was of limited benefit owing to the rodents' tendency to strip off the wax within 48 hours of food bar presentation. Results demonstrated that standard untreated food bars remain edible and free from pathogenic bacteria when presented to mice for over five weeks. Specimens that consumed these bars over a mission-equivalent duration showed good maintenance of body weight when compared with control animals. A detailed summary of these results can be found in Appendix C: Food Bar Experiments.

2.5.5.2 Volumetric Delivery of Drinking Water

The author claims primary responsibility for the design of the water delivery system.

In the ASM, water is supplied through two nozzles that protrude through the wall of the specimen chamber. From a mouse-side perspective, operation of the system mimics that of the "lixit" watering assembly used in some Earth-based rodent care facilities. Each nozzle houses a central mouse-safe steel rod that is displaced as the mouse positions her jaws around the outer tube and performs a toggling action with her tongue. Each rod toggle results in the closure of a circuit as the distal end of the rod (electrically grounded) makes

contact with a circumferential ring that is held at +5 Volts DC (Figure 19). This trigger event is recorded by the Habitat Control Module that increments a volumetric counter and causes an 8-microlitre sip of water to dispense from the reservoir via a fluidic micropump.

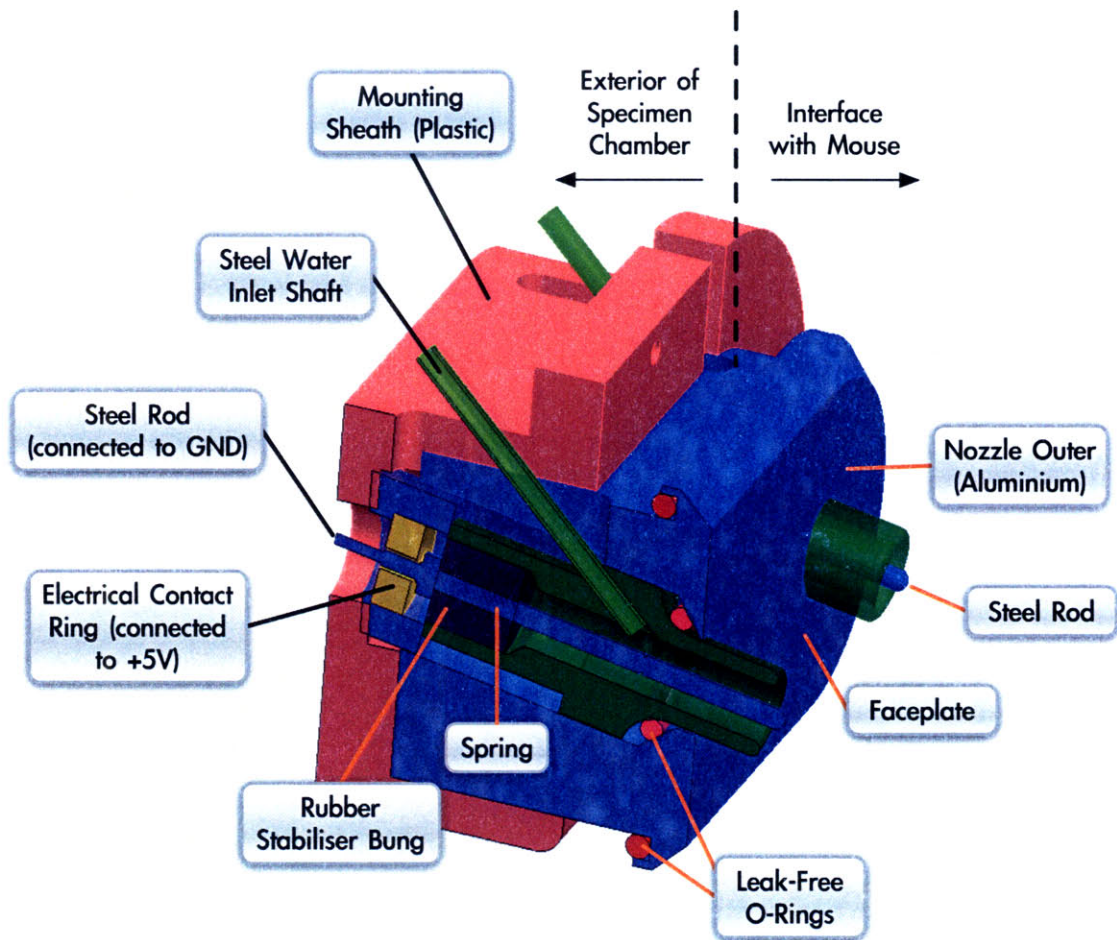


Figure 19: Water delivery hardware (CAD: Edison Guerra)

A feature of this system is the ability to infuse into the water supply a chemical additive that marks bone growth (necessary for post-flight scientific data analysis). This additive is offered to the animals on two pre-programmed occasions during the mission. Figure 20 outlines the design of the entire system. Blue tubes indicate paths of water flow, representing rubber hoses of 1 mm internal diameter. The yellow check valves ensure that any bacterial or fungal colonies within the specimen chamber cannot travel upstream and risk contaminating the water reservoir. Each red numeral indicates an element that is electrically connected to the Habitat Control Module. Operation is as follows:

- A mouse activates one of the water nozzles (5) by moving the control rod.
- The HCM sets the two-way valve (4) so that fluid will be channelled to the appropriate water nozzle (left or right).
- The HCM sets the valves (2) and (3) to cause water either to flow through or to bypass one of the additive reservoirs.

- Once all valves have been appropriately set, the habitat control module causes the fluidic micropump to activate for 350 milliseconds in order to force 8 microlitres of water from the reservoir through the system.

Flight-like prototypes of the entire system have been tested extensively. The habitat software is coded such that a nozzle will be automatically disabled in the event its rod becomes jammed in the “on” position or malfunctions in some other way. Since the habitat microcontroller governs operation of the pump, the entire system can be deactivated during periods of high vibration such as launch and aerocapture.

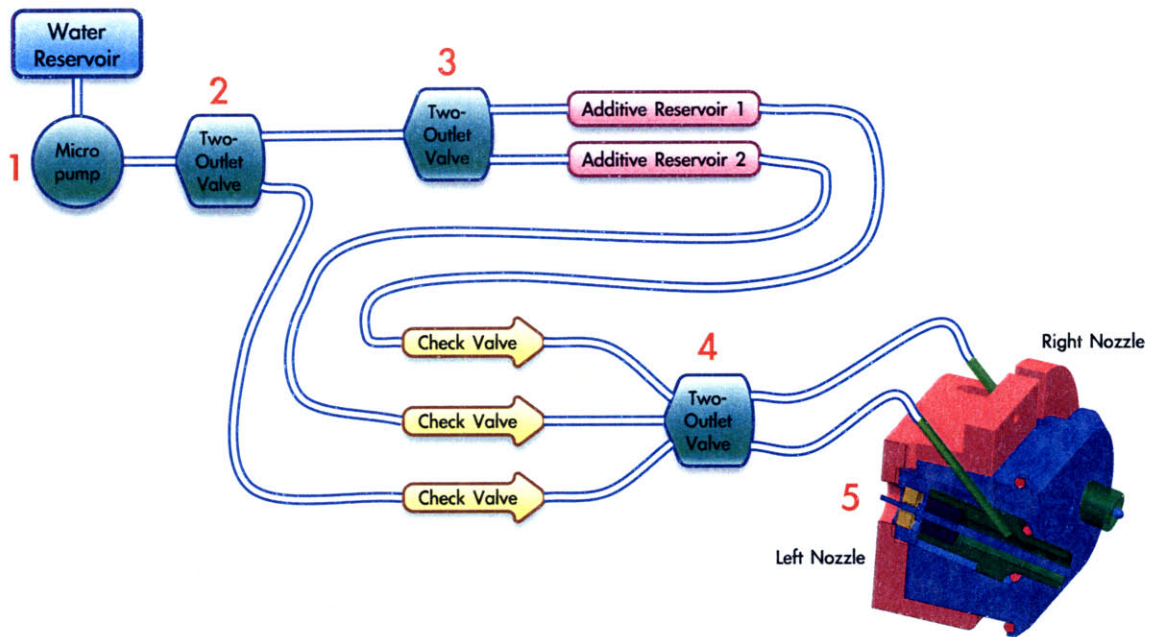


Figure 20: Water delivery

2.5.6 Lighting and Video

Requirements of relevance appear in Table 10. The author claims primary responsibility for the design of the lighting and video system.

Table 10: Lighting and video hardware requirements

Requirement ID	Detail
2.8.1	The lighting system shall allow for observation at all times.
2.8.2, 2.8.3	The lighting system shall provide 12 hours \pm 1 minute of continuous light conditions (the “light period”), and 12 hours \pm 1 minute of continuous dark conditions (the “dark period”) every 24 hours.
2.8.4	The lighting system shall be able to provide 24 hr/day lighting.

2.8.5	Lighting used for dark phase observation shall remain on throughout the entire mission.
2.9.1	During the light period, the lighting system shall illuminate the centre of the specimen chamber between 34 and 46 lux.
2.9.2	During the light period, the lighting system shall maintain the lighting in all parts of the specimen chamber at a minimum of 5 lux.
2.9.3	During the dark period, irradiance throughout the specimen chamber shall be under $0.001 \mu\text{W}/\text{cm}^2$ for all wavelengths below 640 nm.
2.9.4	During the dark period, irradiance in all parts of the specimen chamber shall be under $0.2 \mu\text{W}/\text{cm}^2$ for wavelengths above 640 nm.
2.9.5	Lighting shall be diffused throughout the specimen chamber so that the maximum apparent brightness does not exceed 170 lux anywhere.
2.9.6	During transition to a new lighting level set point, the lighting level overshoot shall be less than 20%.
7.14.2/10/11	Each specimen chamber shall have an imaging system that can record 8-bit greyscale video of the inside of the chamber at 240x320 pixels.
7.14.4	The field of view of the greyscale video during phases E0, E1, E3 and E6 shall include at least 90% of the specimen chamber volume.

2.5.6.1 LED-based Lighting Design

In order to meet the requirements above, the HCM governs two sets of light-emitting diodes (LEDs). These LEDs are installed on the video/lighting board that is positioned above the transparent ceiling of each habitat module. A set of 18 bright white LEDs turn on at 7am and off at 7pm, time zone matched to that of the projected reentry area. These white LEDs illuminate the ASM brightly during the daytime period. 16 low-intensity red LEDs remain constantly powered to provide illumination sufficient to support night-cycle camera operation. BALB/cByJ specimens are albino animals that are unable to sense red light of the chosen wavelength.

In order to minimise losses due to light absorption, the printed circuit board (PCB) carrying the LEDs is manufactured as a non-standard mask-free product. Instead of being coated with the green soldermask substrate commonly seen on production-level PCBs, the board is removed from the manufacturing line before the last step of the process. The result is that the top and bottom copper pour layers are exposed. Since these metallic layers are reflective, there is substantially less light absorption and therefore increased net power efficiency. Compliance with the requirements for lighting intensity and wavelength was confirmed through experimental measurements and with reference to manufacturer datasheets. The lighting duration accuracy requirement is met through software. A 0.8 mm thick translucent silicone rubber sheet placed immediately beneath the lighting board serves to diffuse the illumination in order to meet requirement 2.9.5.

At the centre of the lighting board is a square cut-out to accommodate the video camera. The PCB features two connectors, one at either end, to interface with the Habitat Control Module PCB and with the water delivery systems. The cabling layout was previously shown in Figure 13. Figure 21 shows digital views of an unpopulated lighting PCB (further detail in Appendix H: Circuit Diagrams).

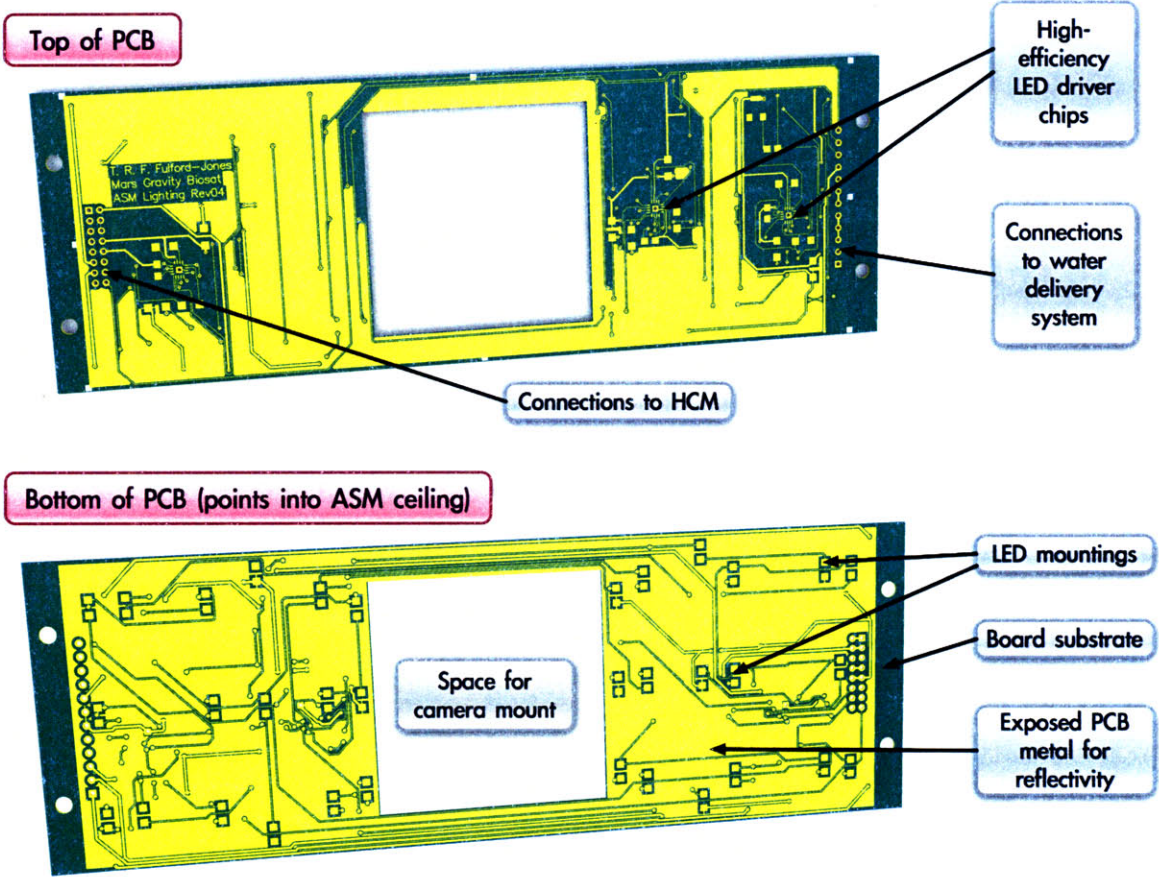


Figure 21: Lighting board layout

2.5.6.2 A Standards-Compliant COTS Camera for Video Monitoring

Figure 22 illustrates the field of view of the video camera when mounted to the selected wide-angle (120°) lens. The green dot represents the Charge Coupled Device (CCD) element of the chosen analogue video camera. The unit is compliant with the North American National TV Standards Committee (NTSC) standard. The video stream from each of the fifteen cameras connects via a multiplexer to a dual-feed acquisition/digitisation board colocated with the video processing CPU.

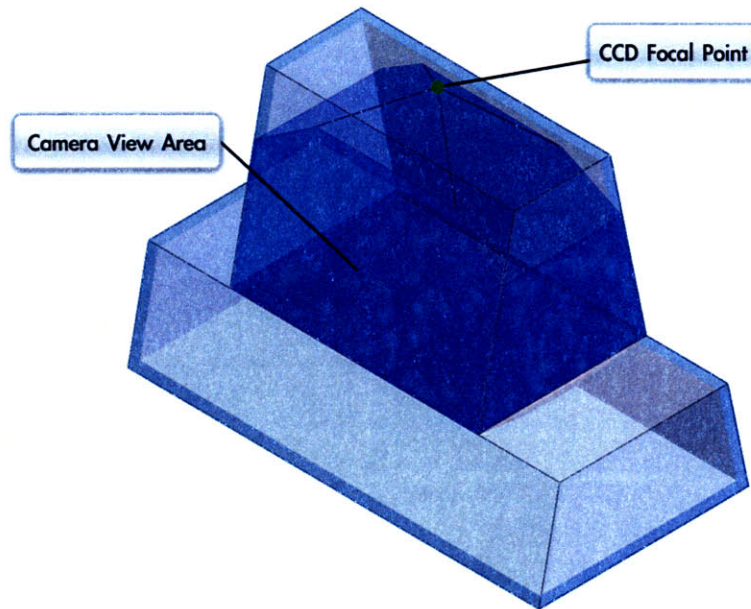


Figure 22: Video camera view angle (CAD: David Newell)

2.5.7 Body Mass Monitoring

Body mass monitoring requirements are outlined in Table 11. The apparatus was designed by employees of Aurora Flight Sciences.

Table 11: Body mass monitoring requirements

Requirement ID	Detail
7.1.1	There shall be a body mass sensor in each specimen chamber.
7.1.2	The body mass sensors shall be capable of measuring the mass of the mouse in the range from 15 grams to 35 grams.
7.1.3	The body mass sensors shall be capable of taking measurements at least once every 6 hours during Phase E3.
7.1.4	The body mass sensors shall have an accuracy of at least ± 0.05 g.

The body mass monitor comprises a vertically moveable platform attached to a load cell together with signal conditioning electronics. The platform is intentionally positioned adjacent to the water nozzles since the rodent must periodically traverse that region in order to drink. Figure 23 shows the hardware as viewed from beneath the floor of the specimen chamber.

Unfortunately the current implementation of the body mass hardware fails to meet requirement 7.1.4. This is due to sub-optimal load cell model selection and to limitations of the HCM's on-board analogue-to-digital converter. In practise, the body mass sensing apparatus rarely provides meaningful output data, and even with known masses, the test data is at best within 2 grams of the actual mass.

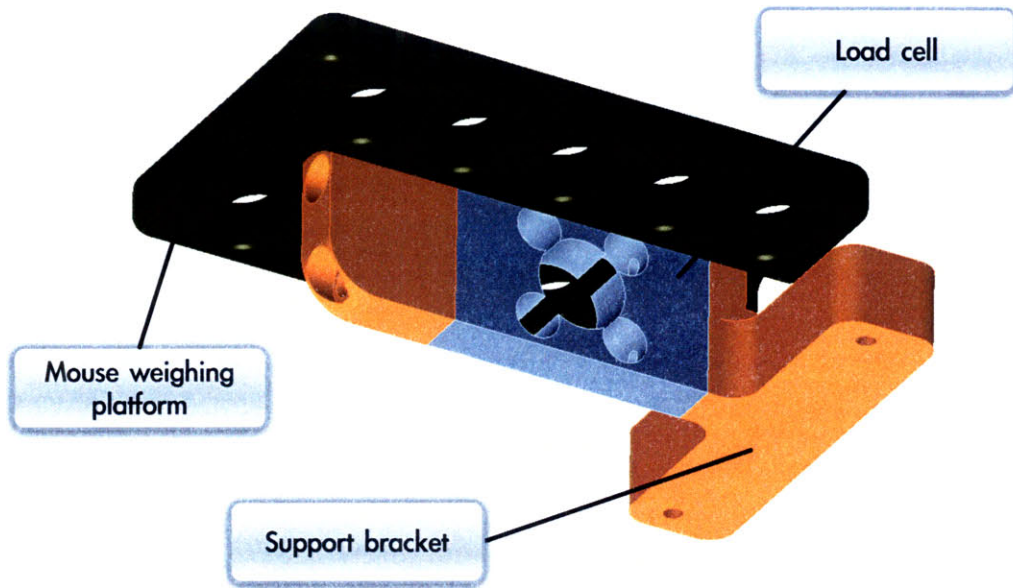


Figure 23: Body mass sensor hardware (CAD: Edison Guerra)

A partial redesign of the assembly will be required during Phase C. The next iteration of the system should include a standalone higher-specification analogue-to-digital converter and a load cell which is tuned to the 0-15 g range (for 0.38-g operation). Further testing should be conducted to achieve smoother motion of the platform and a more sensitive output.

2.5.8 Habitat Control Electronics

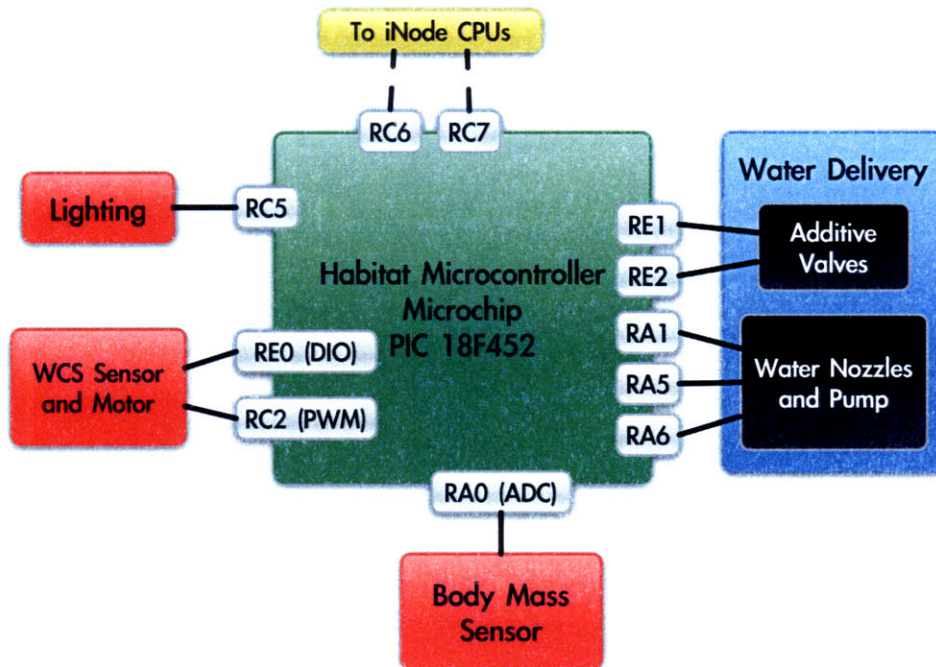


Figure 24: HCM block diagram

Each ASM features a microcontroller and associated electronics collectively known as the Habitat Control Module (HCM). The block diagram is shown in Figure 24. The author claims primary responsibility for the design of the HCM hardware.

The HCM is responsible for commanding habitat module actuators and for monitoring all attached sensors. Its functions include periodically recording mouse body mass, activating the water pumps/valves, maintaining a log of rodent drinking activity, actuating the waste collection roller, commanding the lighting system, and transmitting collected data to the governing iNode CPU when appropriate. The HCM software was designed at MIT and subsequently modified by employees of Aurora Flight Sciences for compatibility with the Aurora-implemented body mass sensor and WCS.

2.5.8.1 Recording Body Mass Data

Table 12 lists requirements for acquiring data from the body mass sensors.

Table 12: Body mass data aggregation requirements

Requirement ID	Detail
7.1.2	The body mass sensors shall be capable of measuring the mass of the mouse in the range from 15 grams to 35 grams.
7.1.3	The body mass sensors shall be capable of taking measurements at least once every 6 hours during Phase E3.
7.1.4	The body mass sensors shall be accurate to at least ± 0.05 grams.

Body mass data is automatically acquired at regular intervals. A high-reliability flag marks those readings that coincide with mouse activation of the water delivery system. Ground experiments confirm that the mice regularly step onto and off the body mass platform in the course of their normal daily activity. Readings are taken by sampling the Analogue-to-Digital Converter (ADC) channel on pin RA0 at a high frequency over a period of a few seconds. The resulting readings are averaged and a tare value is subtracted from the raw data. Multiplication by a scaling factor yields the result in grams. The tare value is calculated by averaging readings while the mouse is away from the body mass platform. This generates a raw data value that corresponds to the weight of the platform together with any accumulated food/waste debris. The scaling factor must be hard-coded into the firmware since it is intrinsic to the sensor and to the operating g-level. The highest available data value from the previous 6 hours is transmitted when requested by the iNode CPUs.

2.5.8.2 Tracking Volumetric Water Consumption

Table 13: Water consumption measurement requirements

Requirement ID	Detail
7.2.1	There shall be a water consumption sensor in each specimen chamber.
7.2.2	The water consumption sensors shall be capable of determining the cumulative water consumption throughout a 6-hour period.

7.2.3	The water consumption sensors shall be capable of measuring cumulative water consumption in the range from 0 to 6.00 ml for every 6-hour period.
7.2.4	The water consumption sensors shall have an accuracy of at least ± 0.025 ml.

Each of the two water nozzles are enabled as external high priority interrupts on pin RB1. This ensures that the micropump can be triggered synchronously (see Appendix H: Circuit Diagrams). Each activation is recorded using a bucket counter, with one bucket for every hour of the day. Total water consumption is calculated through a simple addition over all buckets stored in memory. The HCM software also features a timeout which triggers in the event a nozzle rod should become stuck in the activated position. The software can also check that the nozzle is functioning by attempting to power down and reactivate before querying its status again.

Water consumption data is stored as a count of lick activations during a given period. Since each nozzle activation results in a dispense event that provides the mouse with 8 microlitres of water, accuracy requirement 7.2.4 in Table 13 is substantially exceeded.

2.5.8.3 Augmenting the Waste Collection Roller

Motor speed is controlled using the PIC's built-in pulse-width modulation (PWM) capability. To measure how far the roller has advanced, the optical sensor is enabled as a high priority interrupt on pin RB0. The sensor increments a counter variable every time it is obstructed by one of the aluminium strips that is adhered into the waste collection substrate. When the variable increases, the HCM software halts the motor immediately.

2.5.8.4 Transmitting Data and Responding to Commands

Data is transmitted from the HCM PIC to the iNode CPU by means of serial communication on the PIC's built-in Universal Synchronous and Asynchronous Receiver/Transmitter (USART). Every thirty seconds, a low priority interrupt is generated that causes the system to transmit a telemetry string. To generate the telemetry string, the system first queries the real-time clock (see Appendix H: Circuit Diagrams) for year, month, day, hour, minute, and second data, and generates an ASCII text string to encapsulate this. Body mass data, including mass readings and the current tare value, and water count data are then appended to this string, which is transmitted via the USART.

The HCM software also recognises several different commands. Body mass, water count, and current week count can be requested off-cycle by transmitting one of several pre-defined strings to the HCM over the USART. In addition, a command from the iNode CPU can reset a deactivated water nozzle. Because data reception on the USART constitutes a high priority interrupt, the system will immediately postpone any ongoing process to handle the incoming request. A USART transmission can also be used to automatically tare the body mass sensor, which would normally be done on the launch pad before the mouse is introduced into the ASM.

2.5.8.5 Priority

The HCM software operates under an interrupt-driven paradigm that ensures responsiveness and a clean command hierarchy. Priority levels are as follows:

- High priority interrupts: Reception on the USART, water count updates, optical switch monitoring.
- Low priority interrupts: Real-time clock (second counter) and USART transmissions.

This hierarchy can be justified in terms of ASM functionality. Receiving messages from an external source is a process that should never be interrupted, and one which is essential to allow the iNode to properly manage the system and request data. Of similar importance are water counter updates – data on drinking activity could be lost if the PIC were unable to handle a nozzle activation event. It is also critical to move the WCS substrate a precise distance during each advancement. If monitoring the optical sensor were lower priority, the motors might remain active while the PIC handled a higher priority interrupt, thereby wasting unused collection substrate.

The only non-critical function that requires an interrupt involves updating the second counter. Although accurate timekeeping is of the utmost importance, the real-time clock always maintains the correct time regardless of the PIC's activity profile. Accordingly, even if the PIC were to miss multiple updates, this would not present a problem since the HCM would later resynchronise with the clock in any case.

2.6 ECLSS Sensors

The author claims primary responsibility for all material which appears in this section.

2.6.1 Whole-Payload Sensor Suite Software and Electronics

In order to make ECLSS decisions at the level of the entire payload module, the design includes a centralised sensor array to generate reliable and actionable air quality data.

Table 14: Sensor Suite atmospheric monitoring components

Sensor	Pin(s)	Data Range	Units
SensoriC A7AM (Ammonia)	RA0, RA1 (AN0, AN1)	0-50	ppm ammonia
Vaisala GMM111 (CO ₂)	RA2 (AN2)	0-50,000	ppm CO ₂
Omega PX138-030A5V (Pressure)	RA3 (AN3)	0-2	Bar
SensoriC MOX-9 (Oxygen)	RA5 (AN4)	0-100	Percent
Honeywell AWM5104 (Flow rate)	RE0 (AN5)	0-20	SLPM
Figaro TGS2611 (Methane)	RE1 (AN6)	500-10,000	Ppm
Sensirion SHT15 (Temp)	RB4, RB5	-40-123.8	degrees C
Sensirion SHT15 (Humidity)	RB4, RB5	0-100	Percent

Table 14 lists requirements for the Sensor Suite while Figure 25 shows a high-level block diagram of the design. At the core of the system is a data aggregation and management module based on the PIC 18F452 microcontroller.

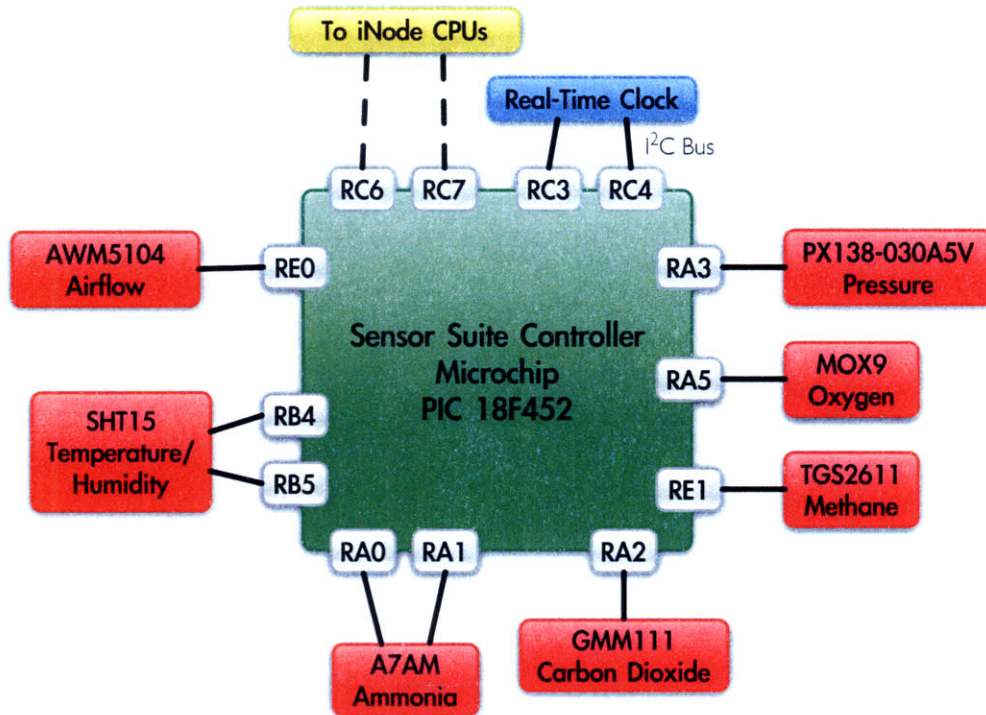


Figure 25: Sensor Suite microcontroller interfaces

The sensor suite software aggregates data from the temperature, humidity, air flow rate, oxygen, pressure, carbon dioxide, methane and ammonia sensors. The PIC samples each sensor and transmits the averaged data on command. Key requirements include acquiring data from each sensor, managing the storage of this data given limited memory, and transmitting the data using a robust and fault-tolerant protocol.

The first six sensors in Table 14 are connected to pins designated by ANx, which is consistent with data acquisition using the PIC's built-in 10-bit ADC. Each reading is averaged over a multi-second period for accuracy. The 10-bit integer result is readily stored in a two-byte array. The A7AM ammonia sensor requires that two lines of data be sampled, so 4 bytes are used to store this result.

The SHT15 temperature/humidity sensor is not read via the ADC pins, but both types of data are ultimately also stored as 10-bit integers. Accordingly, with nine different data lines and two bytes of storage per line, a total of 18 bytes is generated in each sampling round. In addition, a timestamp is recorded to specify the hour, minute, and second when the reading was taken. Therefore, every reading cycle generates 22 bytes of data.

The sensor suite comprises three units of each sensor and three PIC18F452 chips as a means of increasing system reliability through triple-mode redundancy.

2.6.1.1 Data Output

Since the PIC cannot store large datasets, regular transmission to the iNode CPUs is necessary to allow memory reuse. Payload requirements dictate that atmospheric sensor data must be made available to ground personnel at least once every 8.5 hours. The Sensor Suite is designed such the PIC will transmit all new data to the iNodes on command. If the iNode CPUs receive this data correctly, they will respond with a confirmation string. If the PIC does not receive this string, it will assume a transmission error and will attempt retransmission. Once transmission succeeds, the copied data will be flagged for overwriting so that the microcontroller can continue storing new data.

2.6.1.2 Priority

Since the PIC microcontroller does not have library support for multi-threading, it is important to establish a priority order for the different tasks. The scheme for the Sensor Suite models that previously described for the HCM:

- High-priority interrupt: reception/transmission of data via the USART.
- Low-priority interrupt: real-time clock updates.

2.6.2 Sensor Suite Data Acquisition

This section details the operation of each of the sensors previously listed in Table 14.

2.6.2.1 Temperature and Relative Humidity

Humidity and temperature monitoring requirements are listed in Table 15.

Table 15: Temperature and humidity sensing requirements

Requirement ID	Detail
7.5.1	Temperature shall be recorded from at least one payload location.
7.5.2	The temperature sensors shall be able to detect temperatures in the range from 5 to 45°C.
7.5.3	The temperature sensors shall be capable of taking measurements at least once every 4 minutes throughout all Phases.
7.5.4	The temperature sensors shall have an accuracy of at least $\pm 0.5^{\circ}\text{C}$ for temperatures between 18 to 28°C.
7.5.5	The temperature sensors shall have an accuracy of at least $\pm 5^{\circ}\text{C}$ for temperatures in the ranges 5-18°C and 28-45°C.
7.7.1	Relative humidity shall be collected from each specimen chamber.
7.7.2	The relative humidity sensors shall detect relative humidity in the range from 0 to 100%.
7.7.3	The relative humidity sensors shall be capable of taking measurements at least once every 4 minutes throughout all Phases.

7.7.4	The relative humidity sensors shall have an accuracy of at least $\pm 2\%$ for humidity between 40% to 70%.
7.7.5	The relative humidity sensors shall have an accuracy of $\pm 5\%$ for humidities between 0%-40% and 70%-100%.

The sensor selected to meet these requirements is the SHT15 Humidity and Temperature Sensor, manufactured by Sensirion. This device is a single chip relative humidity and temperature sensor that features a calibrated digital output. It is highly compact, low power and lightweight (Figure 26).

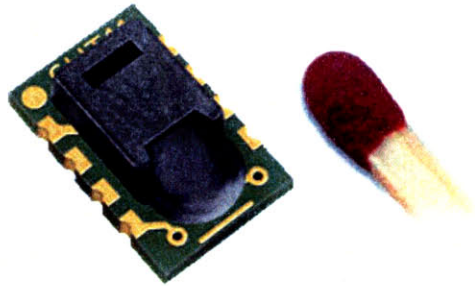


Figure 26: Sensirion combined temperature/humidity sensor

Manufacturer product literature confirms that the sensor measures temperature over a range of -40°C to $+120^{\circ}\text{C}$, which substantially exceeds the required range. Between 0°C and $+50^{\circ}\text{C}$, the accuracy is better than $\pm 0.5^{\circ}\text{C}$, which more than meets requirement 7.5.4. The temperature sensor has a response time ranging from 5 to 30 seconds, which means it is possible to take readings every 4 minutes.

The sensor measures relative humidity between 0 and 100% RH, and thereby complies with requirement 7.7.2. Sensor accuracy between 10% and 90% RH is $\pm 2\%$, and the accuracy is better than $\pm 4\%$ over the remainder of the measurable range. The sensor has a typical response time of 4 seconds, which meets requirement 7.7.3. Design strategy to meet requirement 7.7.1 is discussed in section 2.6.3 on page 63.

2.6.2.2 Carbon Dioxide

Table 16: Carbon dioxide monitoring requirements

Req.	Detail
7.9.1	CO ₂ concentration shall be recorded from at least one payload location.
7.9.2	The CO ₂ sensors shall be able to detect CO ₂ concentrations in the range from 1,000 to 20,000 ppm.
7.9.3	The CO ₂ sensors shall be capable of measuring the concentration of CO ₂ at least once every 4 minutes throughout all Phases.
7.9.4, 7.9.5	The CO ₂ sensors shall have an accuracy of at least ± 1000 ppm for concentrations between 1,000 and 20,000 ppm.

Table 16 summarises requirements for monitoring carbon dioxide.

The selected sensor is the GMM111 infra-red carbon dioxide monitor, manufactured by Vaisala. Inaccuracy can be quantified from factors that include repeatability, non-linearity and calibration uncertainty. Manufacturer literature states that the accuracy ranges from 750 ppm to 1300 ppm over the measured carbon dioxide range of 0-20,000 ppm. This confirms compliance with requirements 7.9.2, 7.9.4 and 7.9.5. With a response time of one minute, requirement 7.9.3 is also satisfied. This sensor is attractive owing to its low mass (47 g) and the provision of both analogue and digital outputs.

2.6.2.3 Ammonia

Gaseous ammonia buildup is of great concern due to the potential for adverse rodent health effects from this contaminant.

Table 17: Ammonia monitoring requirements

Requirement ID	Detail
7.10.1	NH ₃ concentration shall be recorded from at least one Payload sensor.
7.10.2	The NH ₃ sensors shall be able to detect a range of 0 to 15 ppm.
7.10.3	The NH ₃ sensors shall be capable of measuring the concentration of NH ₃ at least once every 4 minutes throughout all Phases.
7.10.4	The NH ₃ sensors will have ± 0.5 ppm accuracy for 0-10 ppm NH ₃ .
7.10.5	The NH ₃ sensors will have ± 1 ppm accuracy for 10-15 ppm NH ₃ .

The baseline sensor is the A7AM Citicel, manufactured by SensoriC. With a response time of 180 seconds, a measurement resolution of 0.5 ppm and a nominal range of 0-50 ppm, all relevant requirements are satisfied. A low mass of 17 g and minimal cross-sensitivity to other gases makes the A7AM an excellent choice.

2.6.2.4 Oxygen

Table 18: Oxygen monitoring requirements

Requirement ID	Detail
7.8.1	O ₂ data shall be collected from at least one payload location.
7.8.2	The O ₂ sensor detection range shall be 10% to 70% oxygen.
7.8.3	O ₂ shall be measured at least once every 4 minutes during all Phases.
7.8.4	The O ₂ sensors shall have an accuracy of at least $\pm 0.1\%$ for O ₂ concentrations between 19% and 23%.
7.8.5	The O ₂ sensors shall have an accuracy of at least $\pm 1\%$ for O ₂ concentrations in the ranges 10%-17% and 23%-70%.

Requirements for oxygen monitoring are listed in Table 18.

The chosen sensor is the MOX-9 Medical, manufactured by SensoriC. This oxygen sensor requires no power; it is essentially an oxygen-powered battery. A chemical reaction within the sensor consumes minute volumes of oxygen to generate an output that varies linearly with ambient oxygen over the range 0-100%. The analogue output can subsequently be recorded with a COTS preamplifier and an ADC. Assuming atmospheric pressure of 1032 mbar, the resolution of 1 mbar O₂ substantially exceeds requirements 7.8.4 and 7.8.5. Response time for this sensor is better than 15 seconds.

2.6.2.5 Air Flow Rate

Table 19 shows requirements relevant to air flow monitoring.

Table 19: Air flow rate monitoring requirements

Requirement ID	Detail
7.11.1	Air flow rate shall be collected from at least one payload location.
7.11.2	The air flow rate sensors shall measure the specimen chamber air flow rate in the range from 5 to 160 ACH (air changes per hour).
7.11.3	The air flow rate sensors shall record at least once every 6 hours.
7.11.4, 7.11.5	The air flow rate sensors be accurate to ± 2 ACH on a range of 5-160 ACH.

The sensor selected to meet these requirements is model AWM5104, manufactured by Honeywell. The unit will be connected in line with the blower that circulates air through the fifteen specimen chambers. The sensor features a venturi type flow housing together with internal circuitry to perform amplification, linearisation, temperature compensation and flow rate calibration.

The volume of each ASM is 5.34 litres. The flow rate range of 0 to 20 standard litres per minute (SLPM) corresponds to a range of 0-225 ACH, which meets the requirements. With a linearity error of 3% of the reading, the maximum error is 1.6 ACH. In addition, the small mass (60 g) and low power consumption (100 mW maximum) make this sensor an attractive choice for the payload module.

2.6.2.6 Air Pressure

Ambient pressure requirements are listed in Table 20.

Table 20: Air pressure monitoring requirements

Requirement ID	Detail
7.6.1	Air pressure shall be recorded from at least one payload location.
7.6.2	The air pressure sensors shall be able to measure pressures in a range from 300 to 1560 millibars.

7.6.3	The air pressure sensors shall record at least once every 4 minutes.
7.6.4	The air pressure sensors shall have an accuracy of at least ± 5 mbar for pressures between 970 mbar and 1040 mbar.
7.6.5	The air pressure sensors shall have an accuracy of at least ± 50 mbar for pressures between 300-970 mbar and 1040-1560 mbar.

The chosen product is Omega PX138-030A5V, a micromachined silicon-based temperature-compensated sensor. This unit outputs an analogue voltage which varies linearly with ambient pressure over the absolute range 0 to 2100 mbar. With a typical nonlinearity of 0.5% of the full-scale range, this equates to an accuracy of ± 2.1 mbar, in full compliance with requirements 7.6.4 and 7.6.5.

2.6.3 Distributed Atmospheric Sensors

In order to provide more comprehensive monitoring and control of the payload environment, additional sensors will be distributed throughout the pressurised volume.

2.6.3.1 Sensors at the Level of Each Habitat Module

Importantly, temperature/humidity sensors and ammonia detectors will be placed at the air outflow port of each specimen chamber. It is desirable to know the ammonia concentrations at the level of each habitat module because this contaminant can severely impact rodent health if it should exceed certain limits. Data from habitat humidity sensors is expected to be useful because microbial ammonia production rates are known to increase in warm, damp conditions. An increase in humidity could indicate a water leak or an unusually high rodent metabolic rate. ECLSS hardware and control strategies are discussed in section 2.7.

The SHT15 and A7AM products previously discussed in section 2.6.2 will also be deployed to monitor each of the fifteen specimen chambers.

2.6.3.2 Distributed Thermal Monitoring

The rodents on board represent only a very minor source of thermal energy. Most heat is generated outside the habitat modules, by electrical equipment such as computer processors, blowers, compressors and fluidic pumps. To ensure proper fan-driven mixing of the payload air volume, the design calls for thirty SHT15 sensors to be distributed throughout the atmospheric pressure vessel. These will be under the control of a single PIC 18F452 device that will monitor temperature gradients and adjust fan speeds accordingly. Data from the microcontroller will be uploaded to the iNode CPUs on demand.

2.7 ECLSS Actuators

The payload ECLSS assemblies must create an atmospheric environment similar to that found in Earth-based animal facilities. Table 21 lists relevant requirements. The author claims primary responsibility for the design and iteration of ECLSS hardware described in this section, with the exception of the condensing heat exchanger which was developed collaboratively.

Table 21: ECLSS atmospheric requirements

Requirement ID	Detail
2.2.1	The atmospheric system shall maintain air pressure in the specimen chambers during Phases E1 through E6 between 970 and 1040 mbar.
2.2.2	The atmospheric system shall prevent the air pressure within the specimen chamber from changing faster than 70 mbar/min.
2.3.1	The atmospheric system shall maintain the concentration of oxygen within the specimen chamber between 19% and 23%.
2.3.2	The atmospheric system shall maintain the concentration of nitrogen within the specimen chamber between 76% and 80%.
2.3.3	The atmospheric system shall maintain the concentration of all other gases besides oxygen and nitrogen below a total of 2%.
2.3.4	The atmospheric system shall ensure the concentration of ammonia within the specimen chamber is generally below 10 ppm and never exceeds 25 ppm.
2.3.5	The atmospheric system shall ensure the concentration of carbon dioxide within the specimen chamber does not exceed 7,000 ppm.
2.3.6	The atmospheric system shall ensure the concentration of methane within the specimen chamber does not exceed 5,300 ppm.
2.3.7	The atmospheric system shall ensure the concentration of other atmospheric contaminants in the specimen chamber shall not exceed NASA Spacecraft Maximum Allowable Concentrations (JSC 20584).
2.4.1	The atmospheric system shall maintain the relative humidity within the specimen chamber between 40% and 70%.
2.5.1	The atmospheric system shall restrict the concentration of airborne particles with diameters greater than 0.5 microns within the specimen chamber to below 3,500,000 particles/m ³ .
2.6.1	The atmospheric system shall exchange the air within the specimen chamber at a rate between 10 and 80 times per hour.

The ECLSS atmospheric subsystem is responsible for regulating air quality within the payload volume. To the extent possible, the payload must meet environmental standards equivalent to those of Earth-based animal facilities. Such a requirement ensures operational validity and will also be applied to ground control systems to guarantee scientific integrity. Specifically, the module will be pressurised to within 4.3% of one atmosphere and the temperature will be maintained between +18°C and +28°C, in accordance with laboratory animal care and use guidelines. Temperature control is achieved through a separate system, the thermal control subassembly, discussed in section 2.8.

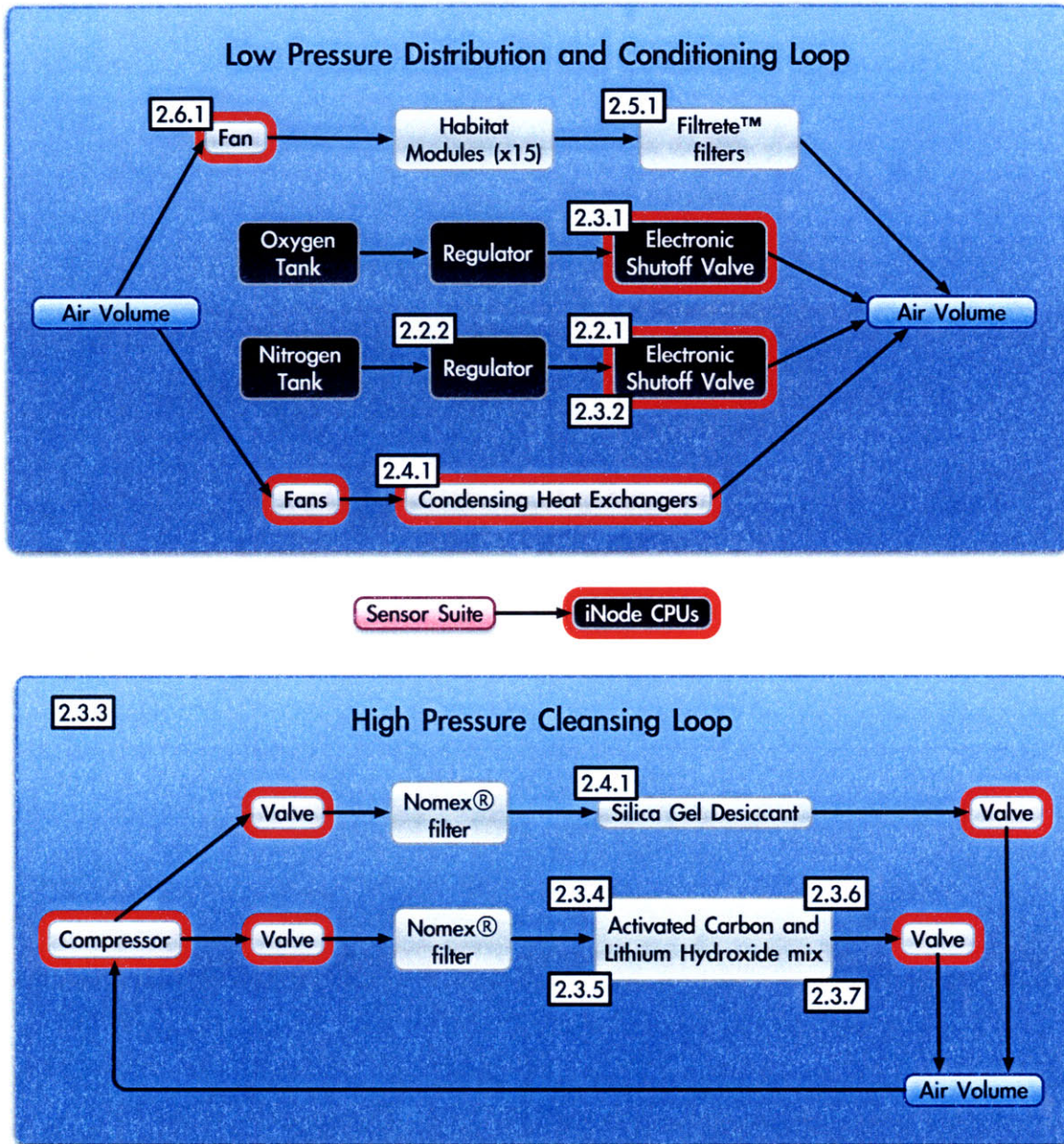


Figure 27: ECLSS atmospheric actuators

The five-week Mars Gravity mission will be the longest-ever rodent spaceflight in low Earth orbit, and the first to study the physiological effects of partial gravity. As such, the atmospheric processing unit must overcome unique challenges. First and foremost, the system must control and largely eliminate contaminants produced by the mice including water vapour, carbon dioxide and gases such as methane and ammonia which derive from microbial decomposition of rodent waste products. Dust, hair, food and faecal particulates must be continuously filtered out. The system is also designed to replenish oxygen while maintaining near-constant pressure within the payload module. Carbon dioxide and ammonia shall not exceed 7000 ppm and 10 ppm respectively, while oxygen must remain in the range 19-23%. Carbon dioxide is a product of rodent respiration and is toxic to mice in high concentrations. Ammonia buildup is a common cause of rodent health problems in

Earth-based laboratories. Specifically, chronic ammonia exposure can lead to mucosal irritation, lung damage and mycoplasmosis in both mice and rats (Broderson, Lindsey *et al.* 1976). In recent years, increasing recognition of such issues has been one of the core drivers for higher air exchange rates in animal care facilities.

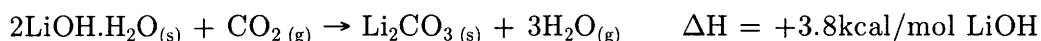
The baseline design calls for a lithium hydroxide (LiOH) canister to remove carbon dioxide, an active carbon bed to eliminate trace gases such as ammonia and methane, and a condensing heat exchanger to control humidity. Lithium hydroxide scrubs carbon dioxide from the air by means of a chemical reaction, while the activated carbon removes gaseous contaminants via adsorption. The condensing heat exchanger entraps and sequesters water vapour via thermodynamic processes. A silica gel desiccant bed serves as a backup system for more aggressive control of humidity if necessary.

The ECLSS atmospheric design calls for two separate air circulation loops that are linked through the common air volume within the payload module (Figure 27). The low-pressure loop (top) is driven by fans and performs air distribution, contaminant sensing, oxygen replenishment, and thermal control. The high-pressure loop (bottom) cleanses the air. In Figure 27, numbers adjacent to each element refer to requirements previously listed in Table 21. Blocks outlined in red are part of the iNode-powered supervisory control loop.

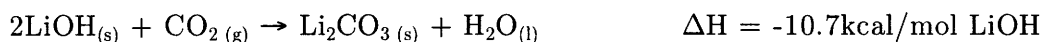
2.7.1 Carbon Dioxide Removal Subsystem

One of the requirements of the atmospheric system is to limit the level of carbon dioxide within the payload volume to 7,000 ppm, which is equivalent to 12,600 mg/m³.

Lithium hydroxide is an appropriate choice because of its extensive spaceflight heritage and its exceptional performance even when tested alongside modern alternatives (Hoehn, Clawson *et al.* 2005). The chemical formulae for its chemisorption of carbon dioxide are as follows (Boryta and Maas 1982):



The net reaction is as follows:



As is shown by the above equations, the reaction is exothermic (generates heat) and requires some initial amount of water vapour to form lithium monohydrate as an intermediate chemical. The net reaction produces water that can remain in the bed if the flow rate is too low. This phenomenon was found to be problematic on missions such as the 1969 U.S. Biosatellite 3 that used lithium hydroxide canisters for upwards of 15 days (Flugel 2007). The water eventually glazed the crystals and left them unable to react with incoming carbon dioxide, thereby severely shortening the life of the canister. In general, predicting performance of LiOH beds during long-term deployments is considered highly challenging due to the long dwell times and varying humidity levels. The effective utilisation of such chemical beds is dependent upon a number of variables, not all of which have been adequately characterised (Davis and Kissinger 1982).

The LiOH bed will be 100% efficient at the start of its life and will remove virtually all the carbon dioxide from the incoming air stream. However, research has shown that toward the

end of the canister's operational life this efficiency drops markedly (Balinskas 2007). This effect can be modelled by use of the Mass Transfer Zone (MTZ) method. This assumes the existence of a reactive zone within the canister that moves down the length of the bed as it becomes expended.

The average adult female BALB/cByJ mouse produces 3747 ± 433 ml/kg/hr of carbon dioxide through respiration (Bethke, Wagner *et al.* 2008). The spacecraft will house 15 mice, each of which will weigh approximately 30g (a conservative estimate). With the mission scheduled to last up to 37 days (888 hours), the atmospheric system must filter between 1324 and 1670 litres of carbon dioxide over the course of the mission. At standard temperature and pressure (STP), this is between 2.6 and 3.3 kg of CO₂. If a safety margin of two standard deviations is added to this total, then the maximum mass of CO₂ produced will be 4 kg.

Based on stoichiometric calculations, lithium hydroxide can adsorb 0.92 kg of CO₂ per kilogram of chemical. Accordingly, a maximum of 4.3 kg of LiOH would be used for adsorption, assuming 100% of the LiOH reacts with the incoming carbon dioxide. MTZ theory confirms that the latter assumption is realistic up until the very end of the bed's operating life. The density of chemical lithium hydroxide is 1.46 g/cm³, but a realistic packing density given granules of 4-14 mesh is closer to 0.5 g/cm³ (Flugel 2007). 4.3 kg LiOH would therefore occupy a volume of 8.6 litres.

As previously noted, the average adult female mouse produces 3747 ± 433 ml/kg/hr of carbon dioxide. This results in an hourly production rate for the entire spacecraft of 1.68 ± 0.195 litres. This is equivalent to 3.33 ± 0.385 grams of carbon dioxide produced every hour, or a worst-case of 4.1 g if two standard deviations are added to the mean. Accordingly, it will be necessary to bring at least this mass of carbon dioxide into the LiOH canister every hour in order to scrub sufficient carbon dioxide. Assuming that carbon dioxide concentrations within the payload are kept at or below the maximum allowable threshold of 12.6 g/m³, the minimum flow rate is calculated as 0.33 m³/hr. This is equivalent to 330 litres per hour or 5.5 SLPM if the compressor were to run continuously.

2.7.2 Humidity Removal Subsystem

Water is produced from several different sources within the payload module:

- Water that each mouse consumes from its specimen chamber drinking reservoir (excreted as liquid wastes that subsequently evaporate).
- Wasted water that exits the reservoir but is not consumed by the animal (experiments have shown that this is near-negligible).
- Moisture from the rodent food substrate after consumption and excretion.
- Humidity generated by mouse metabolic processes.
- Water molecules that are liberated by the LiOH carbon dioxide scrubbing process previously described.

All of the above sources result in approximately 6.7 ml/hr of water production within the payload module. If silica gel desiccant were to serve as the humidity control solution, approximately 30 kg of the chemical would be needed. This would represent an unacceptably high fraction of the spacecraft mass and would occupy a significant volume of

the payload module. The preferred solution is to significantly reduce the size of the desiccant bed and supplement its operation with condensing heat exchangers that extract vapour from the air in the form of liquid water droplets (Fulford-Jones, Grosse *et al.* 2007).

The baselined condensing heat exchanger (CHE) for artificial gravity applications comprises a cold plate that is kept at a temperature below the dew point. The heat exchanger was designed by Andrew Heafitz, formerly a staff instructor at the MIT Edgerton Center, with collaborative feedback from the author. Air from the payload is circulated over the CHE plate, and the resulting condensate drips into a holding reservoir. The thermal flux into the cold plate is expelled to the cold vacuum of space via a thermo-electric cooler (TEC) and a transfer pathway through the spacecraft bus.

Experiments have validated the design and have shown that the custom CHE effectively removes water from the air under a range of environmental conditions. Extrapolation from this data suggests that a set of three condensing heat exchangers could remove the moisture from the air as quickly as it is produced. The current design calls for the condensing system to serve as the primary dehumidification actuator. A small desiccant bed will increase control authority. A detailed discussion of the CHE can be found in Appendix D: Condensing Heat Exchanger. The testing, analysis and conclusions described in that appendix were a joint effort of Andrew Heafitz and the author.

2.7.3 Ammonia Removal Subsystem

Ammonia production is known to result from soiled bedding in part as a result of urea breakdown processes in the reaction between solid and liquid wastes. Buildup can increase the severity of rhinitis, otitis media, tracheitis and pneumonia associated with murine respiratory mycoplasmosis (Riskowski, Harrison *et al.* 2006). Requirement 2.3.4 in Table 21 mandates that specimen chamber ammonia concentration not exceed 25 ppm at any time.

An experiment was conducted to determine the rate of ammonia production within flight-equivalent habitat modules. The design and results from this experiment are reported in Appendix E: Ammonia Production . The testing, analysis and conclusions described in that appendix are the responsibility of the author. MIT UROPs Emily Grosse and Richard Li provided assistance with experiment implementation.

2.7.3.1 Impacts of Experimental Results on Charcoal Bed Design

There exists a substantial body of prior research that confirms activated charcoal adsorbs atmospheric ammonia under certain conditions. Various formulations have been tested, including:

- Carbon from a variety of different source materials, such as palm shells, wood or coal.
- Thermally activated carbon.
- Chemically activated carbon, which involves impregnation with sulphuric, phosphoric or other acids (Guo, Xu *et al.* 2005).
- Carbon inoculated with ammonia-consuming bacteria (Chung, Lin *et al.* 2005).
- Activated carbon fibre (non-granular) (Mangun, Braatz *et al.* 1999).

Carbon alone has minimal capacity for ammonia adsorption due to the low molecular weight and high vapour pressure of gaseous NH_3 . One paper suggests that thermally activated carbon of approximately 1.3 mm particle size can adsorb only 0.4 mg ammonia per gram of carbon. This result was recorded with an extremely high inflow ammonia concentration of 600 ppm and a high temperature of $+40^\circ\text{C}$ (Rodrigues, de Moraes *et al.* 2007).

However, when activated carbon is chemically impregnated with phosphoric acid, it can achieve ammonia adsorption capacities on the order of 10% by mass (Flugel 2007-2008). The selected speciality carbon product for the Mars Gravity Biosatellite is Ammonasorb II (Barnebey Sutcliffe / Calgon Carbon). This coconut shell based carbon is impregnated with 17% phosphoric acid to provide an adsorption capacity for ammonia of between 7% and 16% by weight, depending on operating conditions. The product requires no pre-baking before use and is manufactured in pellets of 4-8 US Mesh sieve size. The bulk density is 0.55 g/cm^3 , similar to that of LiOH.

Assuming a 35-day mission duration and using 10% as the adsorption capacity of Ammonasorb II, approximately 1.67 kg of activated charcoal would be required. Because insufficient data is available to calculate a standard deviation, the standard factor of safety of 1.7 is used together with a 40-day extended mission assumption. This results in a total of 3.25 kg of Ammonasorb II. Since this is to be mixed with 4.3 kg of lithium hydroxide as previously discussed, the resulting mixture will be 43% Ammonasorb II by mass. The chemical will occupy a volume of 5.9 litres.

2.7.4 Oxygen and Nitrogen Delivery

The oxygen and nitrogen valves are controlled by the iNode CPUs in order to maintain total pressure and meet oxygen partial pressure requirements. The oxygen tank will hold the equivalent of 1470 litres of gas at standard temperature and pressure. Oxygen will be consumed through mouse metabolic processes and will be lost through anticipated payload module o-ring leakage. The maximum permissible leak rate is 1% of the total payload air volume per 24 hours in space. Because humidity and other gases are also removed from the atmosphere by ECLSS systems, a small nitrogen gas canister will be used to maintain total pressure.

A trade study was performed to assess COTS oxygen tank options on the basis of mass, strength-to-weight ratio and approximate price range. Tanks are commonly made of steel, aluminium or composite materials. The latter are generally considered most appropriate for higher pressure oxygen containment scenarios (Heafitz 2005).

The factor of safety for the Mars Gravity Biosatellite is lower than that used by oxygen tank manufacturers for terrestrial human-rated applications. Accordingly, the payload design calls for the oxygen tank to be filled to a service pressure that is slightly closer to the designed burst pressure than would ordinarily be the case. This allows the use of a marginally undersized tank and saves both mass and volume within the payload. Luxfer Medical's full-wrap carbon range of oxygen tanks has been baselined for the satellite. The recommended service pressure is 227.5 Bar for the 3.4 kg Luxfer T50A model, which provides a human-rated safety factor of 3. The payload module structures are designed to a factor of safety of 1.4, and the required tank overpressurisation of less than 4% (236.6 bar) therefore still leaves substantial margin. The nitrogen tank will have a mass of approximately 1.0 kg and will hold a commensurately smaller volume of gas. Each tank will

feature a regulator set to 500 mbar above atmospheric. This in turn will connect to a DC solenoid valve that allows on/off flow control via the ECLSS software.

2.7.5 Canisters

Following the protocol adopted for multiple human crewed missions, the Mars Gravity Biosatellite ECLSS design will feature a single canister containing commingled lithium hydroxide and activated carbon. A separate canister will hold the silica gel desiccant pellets. Both canisters will be situated toward the nose of the spacecraft in order to promote a favourable centre of mass that is compatible with reentry dynamics.

The ideal canister design is squat, with a large cross-section to depth ratio. This design results in a reduced pressure drop, thereby increasing air flow and avoiding the need for power-hungry compressors (Flugel 2007). The high-vibration launch environment can cause individual pellets to impact one another, resulting in pulverisation and the production of fine dust. These particles can subsequently clog filters or cause animal health problems if they should reach the ASMs downstream. In addition, the pulverised pellets create openings within the packed canister bed, allowing channelling of air and therefore reducing the efficiency of the chemical reaction. All these issues can be avoided through the use of Nomex[®] meta-aramid felt pads that will line the interior walls of the canisters. The pads “preload” the pellets by applying pressure to keep them in place as soon as the canister is sealed. This minimises the adverse effects of vibration because the pellets are simply unable to move with the amplitude required for dust generation. Any particles that do become airborne will be trapped by the fibrous Nomex[®] substrate that also prevents channelling along the inner walls of the canister.

2.7.5.1 Design Overview

The payload module canisters are designed such that air is drawn in at the centre of a cylindrical canister before being expelled toward the periphery. Figure 28 shows a top-down cross-sectional view of the air flow pathways.

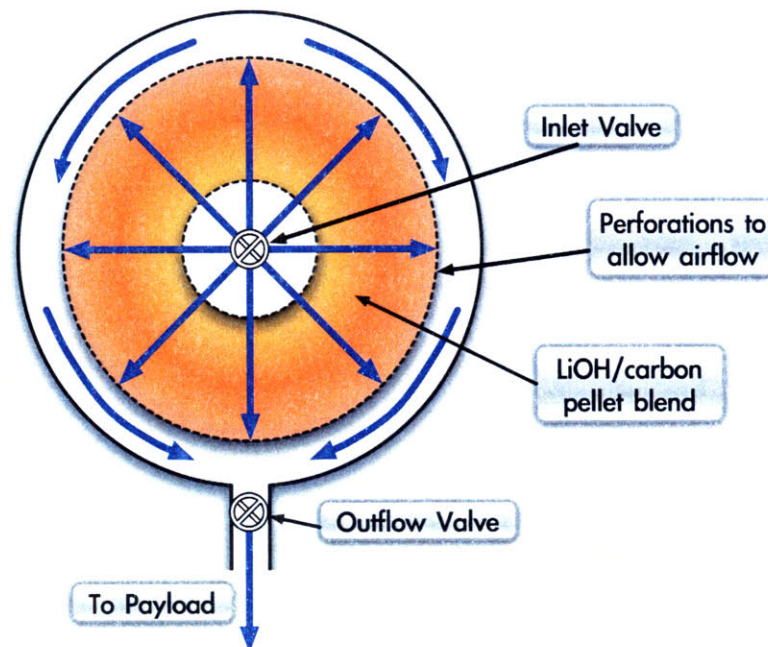


Figure 28: Cross-sectional view of LiOH/carbon canister air flow

The innermost circle represents the air inlet, which is gated by an electronically activated valve. The inlet will have a diameter of 10 cm. After entering via the valve, air from the payload module will pass through a perforated aluminium mesh featuring a rectangular array of 2 mm diameter holes at a 4 mm pitch. A Nomex® felt layer will line all surfaces which are exposed to the LiOH/activated carbon pellets. This layer will be 6 mm thick on the base and on the lid and 3 mm thick on the perforated air inlet/outflow mesh zones.

Once the air has moved radially outward through the chemical bed, it will pass through another aluminium mesh and enter the peripheral outlet channel. It will funnel toward the outlet valve (lowermost part of Figure 28) before re-entering the payload module.

All parts of the canister with the exception of the perforated mesh will be constructed from fibreglass. This material has good flight heritage for space ECLSS applications. The mesh must be constructed from aluminium because perforations would weaken the fibreglass, risking shatter or collapse.

The silica gel canister will occupy the volume immediately above the LiOH/activated carbon assembly. Its design will be essentially identical to that shown in Figure 28, but the volume will be smaller.

2.7.5.2 Canister Sizing

As previously discussed in sections 2.7.1 and 2.7.3, the lower canister must contain 8.6 litres of LiOH and 5.9 litres of Ammonasorb II activated charcoal. The upper canister must accommodate 3.75 litres of silica gel. The constraints that impact the canister dimensions are mainly associated with the outer boundary of the payload pressure vessel. It is desirable to make the canisters as tall as possible in order to increase the cross-sectional area to which incoming air is exposed.

2.7.6 Compressors, Blowers, Valves and Fans

As shown previously in Figure 27 on page 65, the ECLSS system design calls for the following air movement systems within the payload module:

- Compressors to force air through the silica gel canister and/or through the bed of lithium hydroxide and activated carbon.
- Fans to circulate the air within the payload module and ensure satisfactory mixing.
- A fan to circulate air through the fifteen ASMs.
- Fans to move air across the condensing heat exchangers.

In addition, there exists a requirement to environmentally isolate any of the habitat modules upon ground command if an animal should expire during the mission. This requirement is met with two valves, one on the inlet and one on the outflow of each ASM.

2.7.6.1 Redundancy and Reliability

The aforementioned forced air movement systems are critical to ECLSS function and rodent health. No specific science or engineering requirements mandate fail-safe or fail-operational performance. However, due to the mission-critical nature of ECLSS performance, efforts have been made to avoid single-point failure possibilities wherever feasible. A dual-compressor

design will ensure that scrubbing can continue even if one unit should fail. Over 10 fans are used to continuously mix air within the payload module. Double redundancy is evidenced in the use of two blowers to circulate air through the ASMs. The condensing heat exchangers will be triply redundant by design since three separate units will be installed within the payload module to meet performance requirements (see section 2.8).

2.7.6.2 Compressor Selection

The use of two compressors permits both functional redundancy and increased power efficiency. When both compressors are operational, each runs at half-capacity and thereby achieves a more favourable current-per-flow-rate efficiency ratio.

Two units of product BTC-IIs model D737-23-01 from Hargraves Fluidics have been selected to meet the flow rate requirements previously discussed in section 2.7.1. This low-noise, long stack brushless dual head compressor incorporates a diaphragm motor for reliable performance and efficient power consumption. Each unit can independently achieve a flow of 11 SLPM assuming zero pressure obstructions at inlet or outflow. In practise, there will be a pressure drop from the presence of the Nomex[®] substrate and (to a lesser extent) from the canister pellets beyond. Accordingly, the projected flow rate of under 6 SLPM per device is very realistic and consistent with a per-unit power consumption of under 7W. This performance has been experimentally verified (see Chapter 6) but it will be necessary to confirm the reliability of this product during the Phase C Design period.

2.7.6.3 Valve Selection

Product 075T fluidic diaphragm valve by Bio-Chem Valve has been selected to meet the canister isolation requirements. This latching solenoid model features a small orifice and power-efficient operation. Two units of this valve will also be used for each ASM in order to meet the habitat isolation requirement previously described.

2.7.6.4 Circulation to the ASMs

Requirement 2.6.1 in Table 21 mandates that the air flow rate within each specimen chamber shall be between 10 and 80 air changes per hour. With an ASM volume of 5.34 litres, the maximum air flow rate to all fifteen habitats would be 6.4 m³/hr or equivalently 106 SLPM. To meet this requirement, two units of Mechatronics product B5015H have been selected. This variable flow rate impeller-type module operates from a 5V DC supply and draws barely 2W when running at full speed (6.6 m³/hr). Both units will operate in parallel for increased current draw efficiency.

2.7.6.5 Air Mixing within the Payload Module

Ten units of Mechatronics fan product MB3006M will be positioned throughout the payload module to distribute air and ensure good mixing of the atmospheric volume. Where possible, units will be placed adjacent to heat-generating equipment such as computers, compressors, fluidic pumps and heatsinks.

2.7.7 Algorithmic ECLSS Decision-Making

The ECLSS systems are expected to have time constants on the order of hours. Accordingly, the software will command ECLSS actuation on the basis of real-time sensor readings and feedback-driven algorithms will largely implement an on/off control structure. On-orbit

ECLSS operations are covered in Chapter 3. Algorithmic operation of a prototype ECLSS testbed for the Mars Gravity ground control experiments is discussed in detail in Chapter 6.

2.8 Thermal Control

The thermal challenge is one of heat rejection (Fulford-Jones, Heafitz *et al.* 2007). 80 W of electricity from the solar panels is piped to the payload module where it is used to power life support systems and computer equipment. If allowed to accumulate, the resulting heat energy would ultimately drive the temperature of the payload above the scientifically permissible limit of +28°C. How to eliminate this excess energy? Minimal flux will pass through the nose of the payload module, which is enclosed by a heatshield of extremely high thermal resistivity. Instead, the design calls for heat to be rejected through the underside of the payload and into the spacecraft bus, which always faces away from the sun. No heat pipes or louvres are required since the thermal energy will travel through the metal connection band that serves as the interface between the payload and the bus. Thereafter, thermal energy will be transferred to the outer shell by conduction through existing bus structures. The heat energy can readily dissipate into the cold vacuum of space as soon as it reaches the outer bus panels.

Functionally separate from the thermal subassemblies, the air quality control system previously described serves only to maintain an Earth-like atmosphere within the payload module. However, there exists one element of the atmospheric reconditioning system that directly impacts thermal control: the condensing heat exchanger that both dehumidifies and cools air within the payload module. Consequently, there are two heat rejection pathways on board the Mars Gravity Biosatellite. They will ultimately operate in concert, dynamically managed by real-time control algorithms.

Detailed discussion of the thermal systems can be found in Appendix F: Thermal Design. The testing, analysis and conclusions described in that appendix were conducted by Andrew Heafitz together with MIT UROPs Arthur Huang, Jerry Richard, Anna Massie, Jesse Marsh and Harvard undergraduate intern Esther Lofgren. As Payload Lead, the author assumed a supervisory role for this work.

2.9 Structures

Global payload structural requirements are as follows:

Table 22: Payload structural requirements

Requirement ID	Detail
1.1.1	All components in the Payload volume shall be able to withstand the accelerations (G-loads) of all phases with a factor of safety of 1.4.
1.1.2, 1.1.3, 1.1.4	All components in the Payload volume shall be able to withstand the Payload thermal, vibration and acoustic environment throughout all phases.
1.1.5	All components in the Payload volume shall be able to meet the Payload EMI/EMF regulations throughout all phases.

Detailed discussion of the baseline Mars Gravity mechanical structures can be found in Appendix G: Payload Structural Design. The finite element analysis and conclusions described in that appendix were the responsibility of Joao Ricardo, a Mars Gravity international intern. He was assisted by MIT UROP Emily Grosse. As Payload Lead, the author assumed a supervisory role for this work.

2.9.1 Payload Hardware Layout

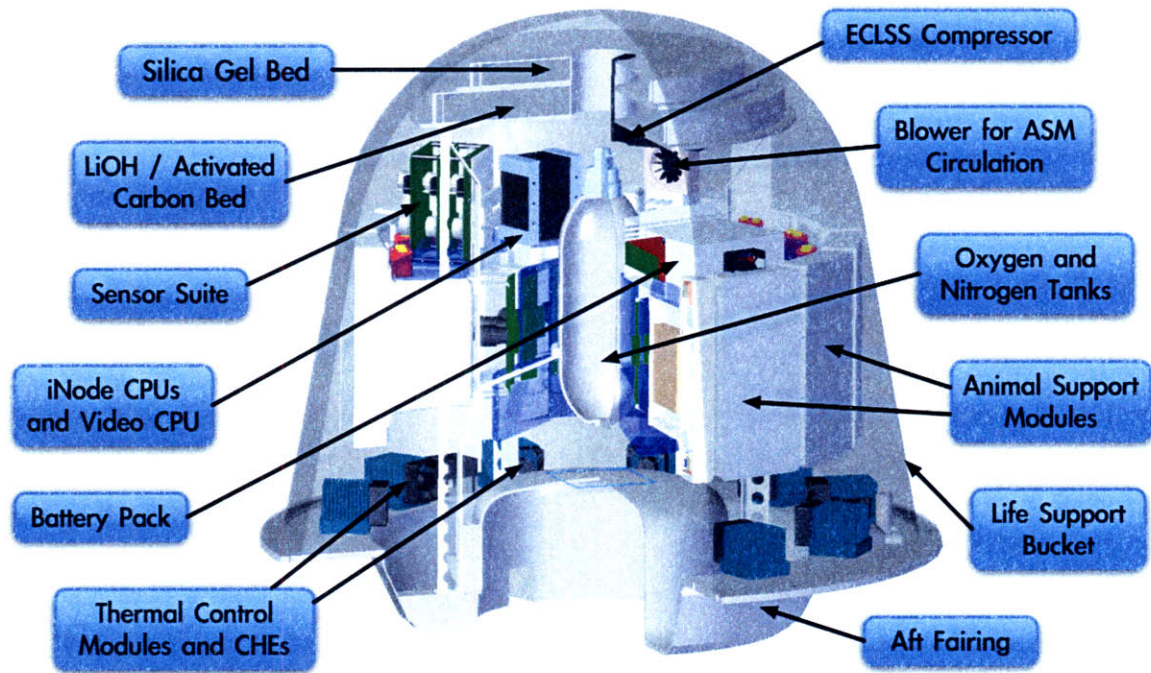


Figure 29: Payload configuration (CAD: Emily Grosse)

Figure 29 shows the location of key payload module subassemblies. The only components not attached to the truss are the thermal control modules and CHEs, each of which will be secured to the aft fairing with screws and bolts.

Two of the heaviest components within the payload module are the computer and the battery pack. In order to preserve cylindrical symmetry and to maintain axial mass balance, these two elements are placed on opposite sides of the truss.

2.10 Electrical Systems and Sensors

This section covers the design of electrical and electronic systems not discussed elsewhere in this chapter.

2.10.1 Power Conditioning

The bus provides 29 ± 5 V DC routed from the solar panels through the separation ring. It provides an average power of 53 W and a peak of 262 W. Batteries internal to the spacecraft bus ensure continuous provision of power. The payload module batteries will be used only during the final phase of the mission, following separation of the reentry vehicle

from the spacecraft bus. In both cases, the power supply needs to be regulated and stepped down. Many of the baselined digital electronics systems operate from +5 V, while fluidic micropumps, blowers and compressors require either +12 V or +24 V. Accordingly, the power conditioning board will feature an array of low dropout linear regulators that will condition the voltage and ensure that its accuracy tolerance is compatible with all payload subassemblies.

A supervisory microcontroller on the power conditioning board will continually monitor the current draw of individual electronics subassemblies from each of the different voltage lines. In the event of an over-current condition, the microcontroller can safely shut down the supply to the device that may be causing the problem. Fault metrics are subsequently reported to the iNode CPUs where automated failure mitigation can take place and direction from ground control can be used to resurrect the system if necessary.

2.10.2 Additional Sensors

A small number of sensors fall into the category of “additional scientific data” and have not been discussed elsewhere. Their selection falls outside the scope of the Preliminary Design effort and will be addressed during Phase C.

A sound pressure sensor is required for the purpose of detecting noise levels within the payload module. Characterisation of the payload sound environment is important because noise levels will be replicated in ground control experiments. Not all the requirements for this sensor are fully specified; importantly, the measurable amplitude range is currently unknown.

Accelerometers will be required to measure both linear accelerations and multi-axis vibrations. It is unclear to what extent sensors within the spacecraft bus will record such measurements and accordingly no devices have been selected for the payload module to date.

The radiation sensor is required to provide cumulative radiation dose information only at the culmination of the mission. Accordingly, the conceptual design calls for use of an unpowered radiation badge device similar to those worn by operators of radiation imaging equipment in hospitals. These badges can be read out by specialised equipment following exposure.

Chapter Three: On-Orbit Operations

Speak English! I don't know the meaning of half those long words, and I don't believe you do either!

-Alice³

3.1 Overview

This chapter focuses on the payload module's hardware, software and connectivity operations throughout the Mars Gravity mission. Each of the subsequent sections details an individual mission phase, starting with pre-launch assembly and continuing through to landing, recovery and mouse extraction.

3.2 Phase E0: Pre-launch

Assembly of the payload module will be conducted off-site. All elements except the ASMs, life support bucket and heatshield will be integrated, and the resulting assembly will be placed atop the spacecraft bus following transport to the launch preparation facility.

The ASMs will be the final payload module element to be loaded into the fully-assembled system. At this point the payload will receive power from the Ground Support Equipment (GSE). All subassemblies will have undergone comprehensive mechanical, electrical and data fidelity testing prior to ASM integration.

The payload module's operational timelines begin once the rodents are loaded into each of their habitats, which commences after the habitat circulatory blower has been confirmed as operational. With the payload module open, ASM connections will then be made (air, data/power lines, video feed) and the habitats will be latched into place on the central utilities truss. Following securement, each Habitat Control Module will be retested by the supervisory iNode CPUs to confirm proper connectivity and nominal operations.

Thereafter the payload software will perform verification of water delivery operation, WCS motor roll-through to start, and proper response of all ASM atmospheric and other sensors. The video cameras will be powered on and sample recordings will be taken to ensure data availability and correct camera view alignment. Any ASMs that fail testing at this point will be immediately switched out and full-up replacement units will be installed in their place. Following successful testing, two peripheral metal retention straps will be tightly ratcheted to secure all the ASMs in their final configuration.

³ *Alice's Adventures in Wonderland*, Lewis Carroll.

After installation of mice into the system and proper testing, checks of the whole-payload air flow management subassembly will occur via the supervisory microcontroller. In addition, the distributed atmospheric sensors will be checked for consistency and reliability. Connections from the iNode to each different microcontroller cluster will have been verified prior to mouse insertion, but their consistency will be reconfirmed at this point. In addition, checks of the ECLSS atmospheric and thermal subassemblies will occur and proper operation of compressors, fans and thermoelectric coolers will be verified through visual inspection and by instrumentation.

The payload module will then be closed, with the o-ring seals seated in place and the life support bucket mounted atop the aft fairing. The connection bolts will be secured in order to create a pressure seal. At this time, all ECLSS sensors will commence data collection. The GSE air inlet and outflow hoses will be temporarily plugged. The entire payload module will be placed within a local thermal vacuum chamber and the external pressure will be reduced to approach 0 atm. Maintenance of payload internal pressure for a period of 2 hours with ECLSS actuators deactivated will verify proper sealing. The payload module pressure sensors described in section 2.6.2.6 have an accuracy of 0.01 atmosphere or about 10 millibar, which is insufficiently high accuracy to confirm sealing. The worst-case undetectable leak rate must ensure that the payload module would lose less than 1% of its atmosphere per 24 hours in space. In two hours this is equivalent to approximately 1 millibar. A sensor with this level of accuracy will be placed within the vacuum chamber and monitored for any increase in pressure as a consequence of payload module leakage. Design verification testing during Phase C will confirm that it is possible to reliably perform leak-checking using this procedure.

It is anticipated (though not yet confirmed) that oxygen and carbon dioxide concentrations will remain within safe ranges over a two-hour time period. Phase C design and testing will determine whether or not an enriched oxygen environment may be necessary during this pressurised test. In the event a leak is detected, the o-rings will be first reseated and subsequently replaced if necessary. After the 2-hour test period, the system will be removed from the vacuum chamber, the air outflow hose will be reopened and the payload module will be flushed with clean air from the GSE via the air inlet port. The GSE will assume responsibility for providing a continuous flow of clean, conditioned air to the payload module thereafter. Because of this, no on-board air cleansing will be required and payload ECLSS consumables will be preserved. Only fans, valves and air circulatory systems will need to operate within the pressure vessel.

Once the life support bucket is sealed and verified, final connections can be made to the Lightband™ and to the spacecraft bus. The heatshield will also be seated and secured at this point.

The payload module is designed to accommodate mice on the ground for up to seven days before liftoff. During this period, GSE connections to power and to continuous air flow are required. If any mice should present signs of non-acclimation to the habitat or should exhibit illness, distress or abnormal behaviours, they will be replaced with specimens from a local backup cohort. Whole-system testing will be performed again following a procedure identical to that previously outlined.

3.3 Phase E1: Launch

Immediately prior to launch, the payload module will be filled with cool, clean air at 1 atmosphere. The temperature will be set to 17°C, slightly below the allowable range,

because the ECLSS thermal subassembly will not operate during the first hours of the mission. The mission autonomy module previously described in section 2.4.1 on page 37 will also activate at this time in order to perform dynamic scheduling of power allocations and conditional subsystem activation/deactivation.

A few minutes prior to launch, the air hoses and power/data lines will detach from the underside of the aft fairing and the quick-disconnect ports will self-seal. To guard against damage from vibrations and accelerations, any components that have moving parts (motors, compressors, fans, fluidic micropumps, etc.) will be powered down. They will remain deactivated until after the spacecraft has been released from the launch vehicle. The one exception to this rule is the ASM circulatory blowers that will be continuously operational.

After the GSE power/data lines disconnect, the payload module will draw power from its on-board battery pack. In general, the guiding operational philosophy is to minimise power draw during this period so as to prevent battery drainage. The only subassemblies that will remain powered in the payload module are the following:

- iNode CPUs and associated Flash memory.
- Habitat Control Modules, but only to monitor habitat-level atmospheric sensors and to maintain lighting performance.
- ASM circulatory blower.
- Atmospheric sensor suite.
- Power conditioning microcontroller.
- Distributed sensors and their associated microcontrollers.

Table 23 summarises those sensors that will operate during E1. In general, only the most scientifically essential are active. Importantly, elements such as the condensing heat exchangers and water delivery micropumps remain entirely unpowered. This is driven by a need to minimise the volume of free liquid present in the payload module in anticipation of weightlessness during phase E2. Weightless fluid has a tendency to rapidly disperse throughout the payload module, leading to aggregation and to pooling in undesirable locations upon spin-up.

Table 23: Sensor operations during Phase E1

Requirement ID	Sensor	Detail
4.3.8 onwards	Atmospheric monitoring (multiple sensors)	Once every 4 minutes
4.3.17	Sound pressure volume	Continuous
7.3.4	Vibration	Average and maximum once every ten seconds
7.4.2	Linear acceleration	Magnitude and duration of all accelerations between 0.01-g and 50-g with duration above 0.01 s

3.4 Phase E2: Transition

Table 24: Sensor operations during Phase E2

Requirement ID	Sensor	Detail
4.3.8 onwards	Atmospheric monitoring	Once every 4 minutes
4.3.17	Sound pressure volume	Continuous
7.3.4	Vibration	Average, maximum once every ten seconds
7.4.2	Linear acceleration	Magnitude and duration of all accelerations between 0.01-g and 50-g with duration above 0.01 s
7.14.4	Video	Four 15-second greyscale clips per ASM

The transition phase covers the period from the spacecraft's release from the launch vehicle until spin-up and unfurling of the solar panels. This will be a time of weightlessness for the payload module. In order to ensure adequate air circulation and guard against the buildup of carbon dioxide air pockets, all circulatory fans will shift to maximum at this time. Air will be forced through the ASMs at the highest permissible rate in order to promote the movement of floating waste toward the underfloor WCS. However, all other components with moving parts will remain deactivated until the spin-up has completed and the spacecraft has reached its stable cruise mode.

As shown in Table 24, sensor operations are largely identical to Phase E1. The only addition is the recording of one minute of video footage of the floating rodents from each of the ASMs. To support this, the cameras, video processing CPU and associated solid-state memory will receive power from the start of phase E2.

3.5 Phase E3: Orbital

The 35-day orbital phase is the longest segment of the mission. During this time, the spacecraft will spin at 31.6 rpm to generate a stable 0.38-g acceleration vector. With the solar panels unfurled, power will be continuously routed to the payload via the Lightband™ separation ring. At this point the power conditioning microcontroller will automatically disconnect the payload batteries and all subassemblies will come fully online. The water delivery micropumps will activate to support mouse drinking activity, and the WCS rollers will move to transfer deposited waste into the underfloor hopper. ECLSS atmospheric and thermal control will commence. The supervisory autonomy agents will actively manage and schedule both scientific data collection events and power-heavy component activations.

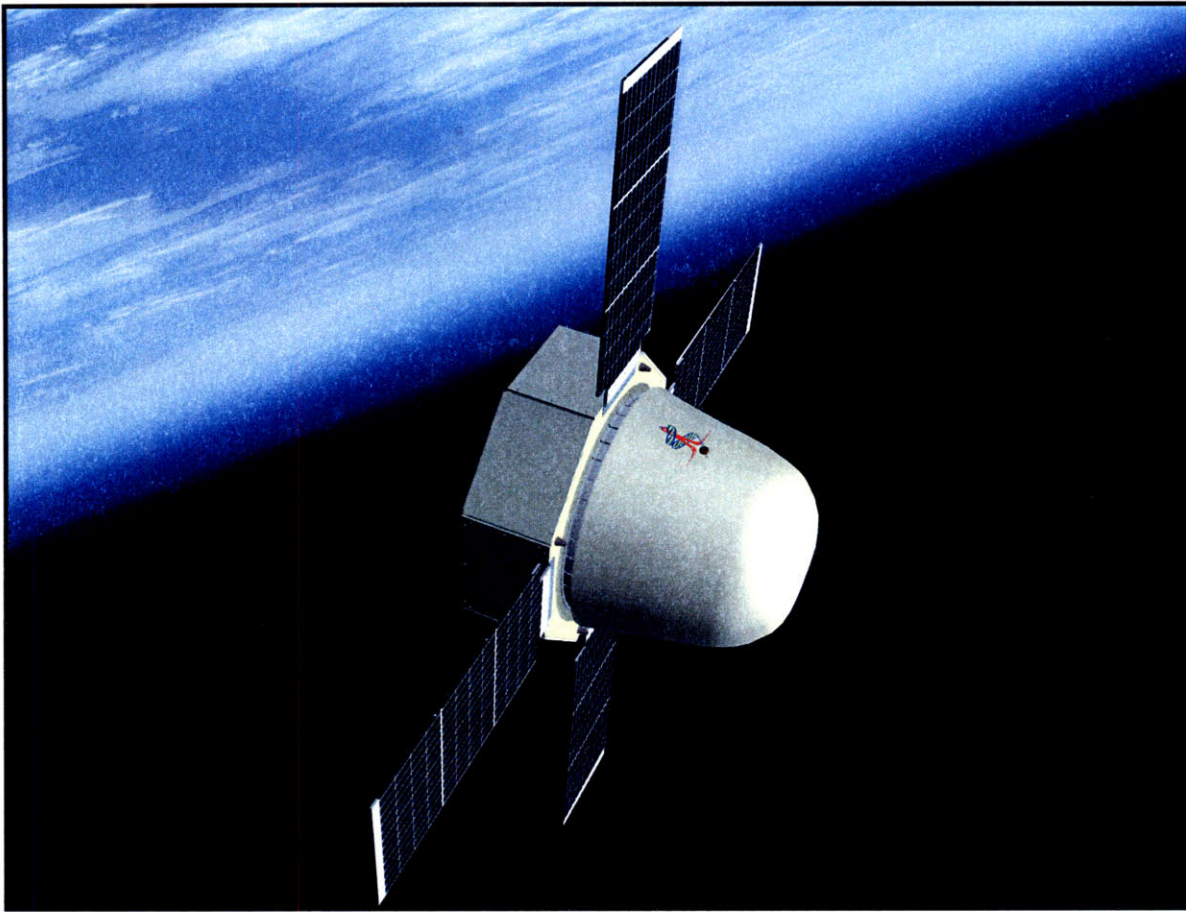


Figure 30: The Mars Gravity Biosatellite during Phase E3 (CAD: David Newell)

The first operational requirement for the iNode CPUs will be to conduct a comprehensive subsystem health check to ensure that all components are functioning correctly and reliably. Following confirmation of nominal payload operation, the iNode CPUs will communicate with other iNode modules in the spacecraft bus. Data concerning payload health will be transmitted together with sensor readings and video captured during E2.

Shortly after entering science cruise mode, one or more ground stations will initiate contact with the spacecraft bus through a handshaking and uplink/downlink procedure. At this point, data generated during E1 and E2 will be transmitted to the ground.

3.5.1 ECLSS Algorithmic Operations

Atmospheric operation is controlled almost entirely at the level of the iNode CPUs. The lower-level microcontrollers serve only to manage bit-level interactions with the sensors and actuators. The CPUs accept microcontroller-aggregated data from the various environmental sensors distributed throughout the payload module. Custom algorithms on the iNodes determine which ECLSS actuators are subsequently activated in order to maintain parameters within the ranges mandated by the science-derived requirements.

A significant element of operational robustness derives from the ability of the algorithms to determine the reliability of incoming sensor data and treat that data accordingly. In addition, ECLSS ground software will datamine readings from the spacecraft to detect

whether or not any given actuator is functioning correctly. In order to achieve this, the ground software will include built-in performance models that allow for cause-and-effect prediction. For example, one element of the model may provide a projection of the expected rate of change of payload oxygen concentration if the valve on the O₂ cylinder were set to 50% flow. Another element may describe the rate of water extraction by a condensing heat exchanger operating at 100% power in 55% relative humidity. The model will also include a characterisation of startup times together with system hysteresis and phase lags. In every case, performance deviations (differences between observed and projected) would cause flagging of datapoints. The ground software would suggest to mission managers a set of compensatory mitigation patches for upload to the spacecraft. In some cases, the software may also recommend that the spacecraft be sent additional response guidance or performance model updates.

3.5.1.1 General ECLSS Control Requirements

The general algorithmic approach to atmospheric and thermal control is simple on/off activation of the ECLSS actuators consistent with predefined setpoints. For control authority, these setpoints are generally at least 30% below the maximum and at least 30% above the minimum requirements previously shown in Table 21 on page 64. Table 25 lists the baseline control setpoints in the rightmost column.

A few elements of Table 25 merit particular discussion. Firstly, the concept of on/off operation requires further elaboration because many of the actuators can function across a range of different power levels. For example, the two redundant compressors attached to the ECLSS canisters can function with a voltage anywhere between +6 V and +12 V DC. The higher the voltage, the higher the pressure and the velocity at which air is forced through the chemical beds. The three condensing heat exchangers have been shown to operate most efficiently when each receives 5 W of power (Appendix D: Condensing Heat Exchanger Design). However, greater control authority can be gained with power levels as high as 10 W per unit.

Table 25: Overview of algorithmic ECLSS controls

Parameter	Actuator	Required Range	Algorithmic Response
Oxygen	O ₂ tank valve	19%-23%	Open valve below 20.2%, close valve above 21.8%.
Pressure	N ₂ tank valve	970-1040 mbar, 76%-80% N ₂	Open valve below 990 mbar, close valve above 1010 mbar.
Carbon Dioxide	Compressor and valve to LiOH/carbon bed	Below 7000 ppm	Activate above 5000 ppm CO ₂ or above 7ppm NH ₃ or if silica gel has been active over 30 minutes. Deactivate once trigger has been controlled, i.e. below 2500 ppm CO ₂ , below 3 ppm NH ₃ , or silica gel deactivated.
Ammonia	Compressor and valve to LiOH/carbon bed	Below 10 ppm, brief transient to 25 ppm is acceptable	

Humidity	CHEs	40%-70% RH	Activate above 50%, deactivate below 45% or if temperature is below 21°C.
Humidity	Compressor and valve to silica gel bed	40%-70% RH	Activate after 30 minutes continuously above 55% or after 1 minute above 70%. Deactivate below 50%.
Temperature	CHEs, thermal units	18°C-28°C	Activate cooling units above 25°C, deactivate below 21°C.
Temperature	Circulatory fans distributed around the payload	18°C-28°C	Increase local fan speeds stepwise when hotspots develop above 25°C, reduce fan speed below 21°C.
Air flow to ASMs	Circulatory blower	60-200 ACH	Various complex criteria.

The payload ECLSS algorithms are tuned such that components will nominally activate to a voltage level consistent with the most power-efficient setting, i.e. optimal performance per Watt as determined during the design phase. The only situation in which this may be modulated is through ground override. This may be prompted if the autonomous agent detects an inconsistency between projected and actual performance and informs ground control accordingly. For example, the mission operations team may receive notification that the rate of carbon dioxide absorption by the chemical bed at the very end of the mission is substantially lower than projected. This may indicate that the bed is approaching the end of its life. An appropriate course of action would be to issue a power setpoint change command to the payload computer. This would cause more power to be routed to the compressor with each actuation. The resulting faster air flow rate would ensure a more rapid turnover of air in the payload module and thereby maintain good atmospheric quality.

Algorithmic strategies are described in more detail in the following subsections.

3.5.1.2 Oxygen, Nitrogen and Partial/Total Pressures

Total pressure must be kept within $\pm 3.5\%$ of 1005 millibar. The oxygen requirement was calculated with this setpoint in mind. A 19-23% range corresponds to a partial pressure of oxygen between 191 millibar and 231 millibar. The algorithmic control range of 20.2-21.8% is therefore equivalent to 203-219 mb. The partial pressure is the physiologically relevant parameter since it is this metric that ensures adequate inflation of the lungs and diffusion of oxygen into the red blood cells.

Oxygen, nitrogen and pressure control are tightly interlinked. Keeping oxygen in range is of highest importance. The decision tree is shown in Figure 31. Arrows show control pathways and rectangular elements indicate operational events. Green decision diamonds denote instances where the flow of control is conditioned on an algorithmic state assessment. Purple

ovals indicate causal lead-ins by which the ECLSS control software may enter this decision tree. The system remains within the algorithm until reaching the completion star at the very bottom of the diagram. The left side of the illustration (magenta) applies when oxygen partial pressure falls below the trigger minimum of 203 millibar. The right side (turquoise) activates when oxygen is either in range or too high.

The purpose of the 3-minute delay boxes is to allow the payload module air to become fully mixed so that the oxygen sensors may adequately monitor the environmental response. The 3-minute time constant has been projected from environmental experiments that used a mockup of the Mars Gravity ECLSS design (see chapter 6 for detail).

There exist ECLSS states that fall outside the realm of nominal operations. As previously discussed, the payload module is not required to be fail-safe or fail-operational, although redundancy and fault recovery may be designed into certain systems to improve the mission risk profile. In cases where the system reaches an off-nominal ECLSS state it will be the responsibility of the payload computer only to stabilise the system (if possible) and then to await further instructions from ground control. Figure 31 shows one such example, toward the centre of the illustration, denoted “off-nominal error condition.” Essentially, the system reaches this box when an attempt to add oxygen results in the total pressure being too high. This could indicate an error condition such as a slow nitrogen valve leak or possibly the oxygen valve being stuck in the open position. The latter is highly unlikely because entry into this part of the algorithm would have been initially prompted by a low oxygen reading. The computer’s response to this off-nominal overpressure condition is to attempt to reduce total pressure by scrubbing out any remaining carbon dioxide in the atmosphere and by removing humidity. Importantly, the flow chart severely reduces the frequency of attempted oxygen replenishment events because these will serve only to further aggravate the overpressure condition.

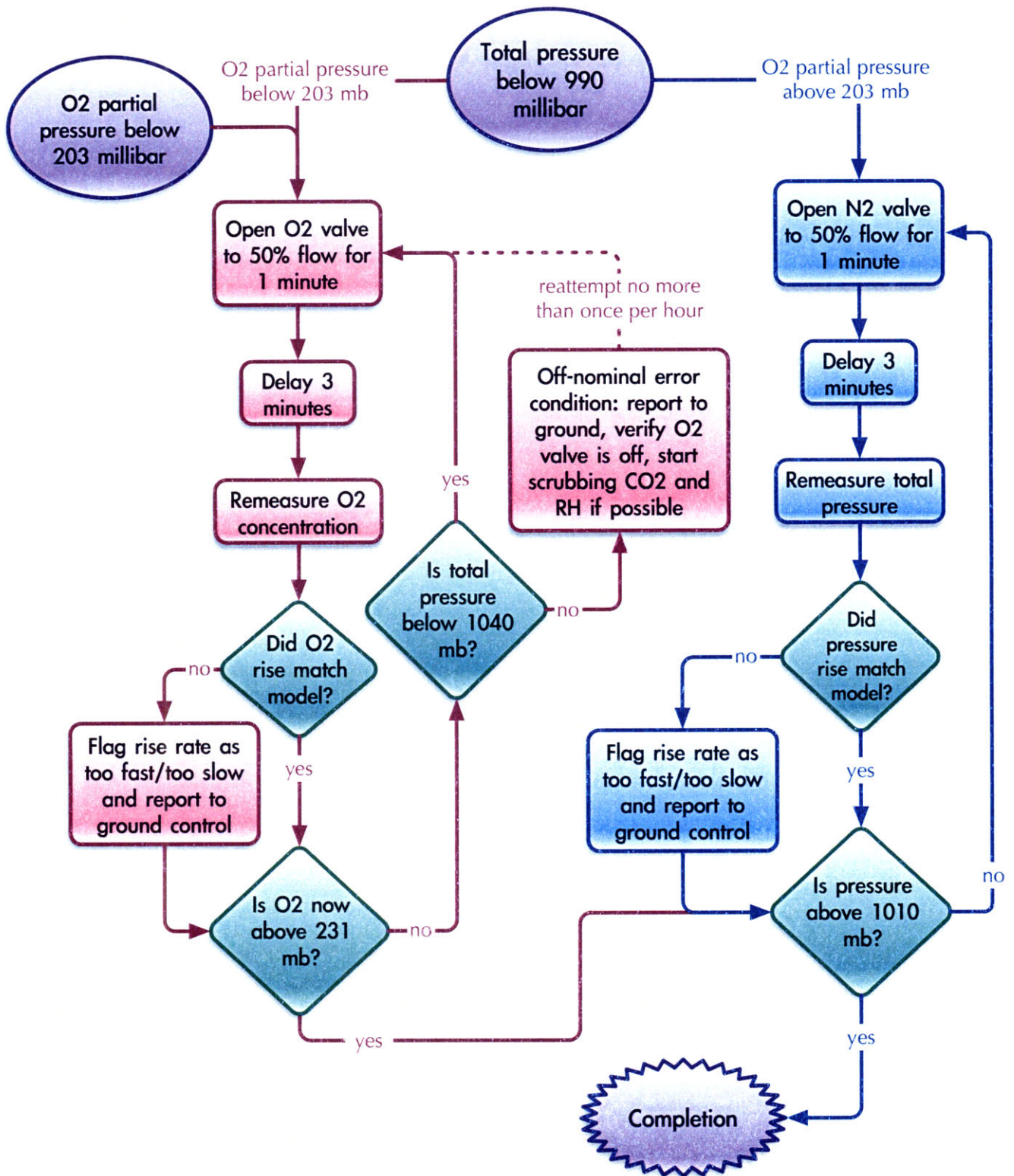


Figure 31: Total pressure and oxygen partial pressure algorithms

3.5.1.3 Relative Humidity and Temperature

Relative humidity control and maintenance of the correct temperature are tightly linked. According to psychrometric theory, a rise in temperature will increase the water capacity of a given volume of air. Accordingly, for a system to which no water is added, the relative humidity will be reduced as the temperature rises and will increase as the temperature falls.

In the ranges projected for the payload module, relative humidity is highly sensitive to temperature changes. For example, a change in temperature from 24°C to 22°C would cause a relative humidity of 45% (within the target control range) to increase to 50.7% (at which point humidity control systems would activate). This assumes constant total pressure and that the dew point remains at 11.3°C.

The interlinked nature of these systems must be taken into account for the ECLSS subassembly to have sufficient control authority. Two scenarios are of note:

- Activation of the thermal system may cause the relative humidity to increase, at which point it might need to be addressed by the condensing heat exchangers.
- If the cooling effects of the condensing heat exchangers are not adequately balanced by heat generation from electronic components, the humidity control system may pull the payload module below 21°C.

In the case of the second bullet point, the preferred control strategy would in fact be to do nothing. Ceasing control actuations and allowing the temperature to rise would be doubly beneficial; such a strategy would reduce relative humidity while also allowing the payload to warm up to a more comfortable temperature. The complex combined flow of control is illustrated in Figure 32. To address the scenario just discussed, the purple humidity control activation bubble triggers only if the temperature is above 21°C.

In Figure 32, magenta elements indicate the silica gel activation pathway that addresses very high humidity levels. Turquoise blocks are to do with activation of the condensing heat exchangers while yellow rectangles denote temperature control. From a rodent health perspective, humidity values that exceed the 70% scientific requirement are much more problematic than humidity readings below the 40% lower limit. In recognition of this fact, the general strategy is for the temperature loop to hand over control to the humidity algorithms whenever humidity should significantly increase as a consequence of cooling activity. Critically, the thermal cooling units (which tend to increase relative humidity) can never operate at the same time as the humidity control loops. This ensures that the two subassemblies will never be operational antagonists. It also guarantees that the pre-programmed algorithmic control models for system humidity response will be valid and therefore allows the ECLSS algorithms to accurately project the effects of CHE activations.

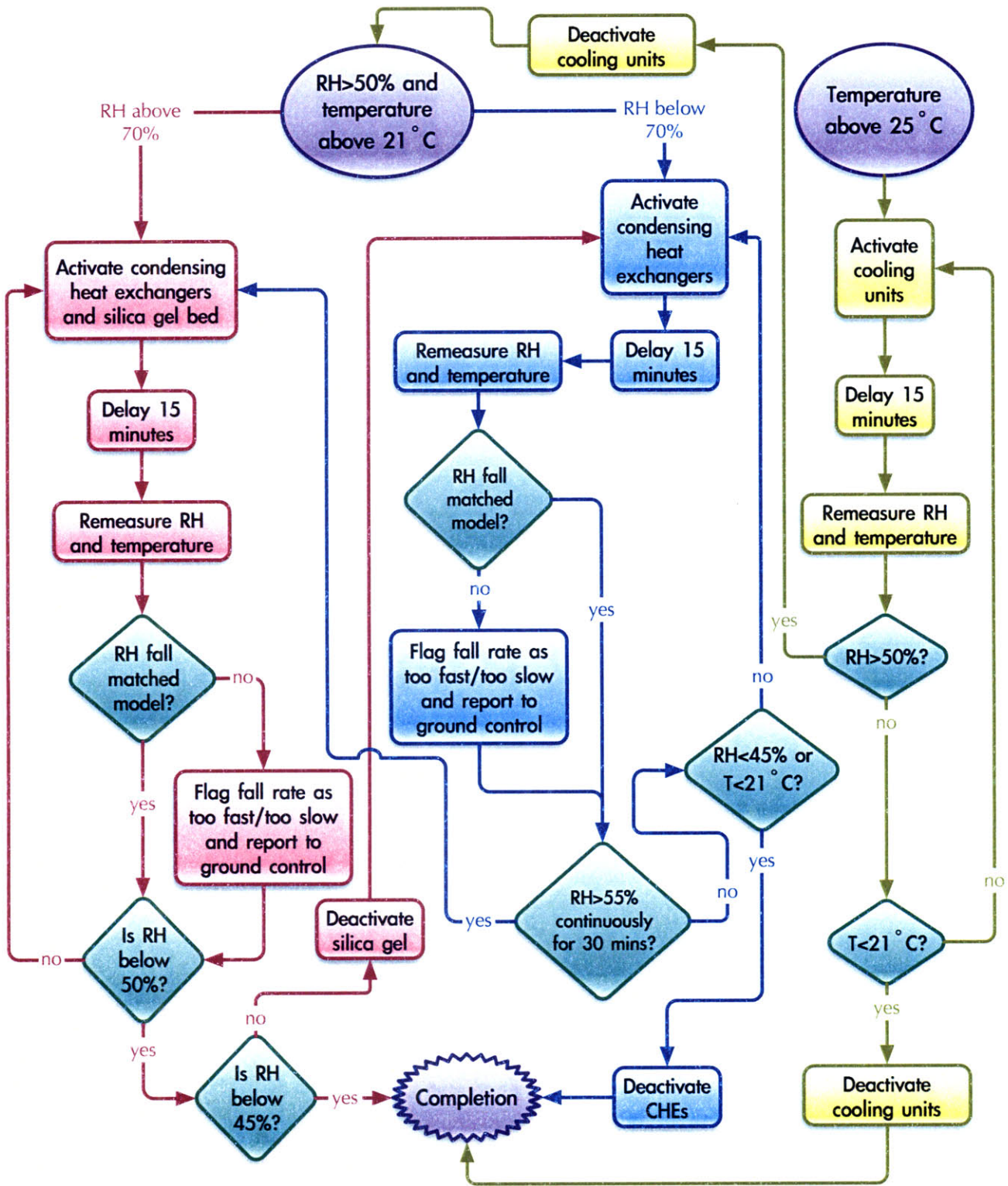


Figure 32: Relative humidity and temperature algorithms

Importantly, Figure 32 has no “report-to-ground” block for off-nominal temperature fall rates. This is intentional because it is challenging to define “off-nominal” in this case. The model for system response to temperature control actuations is non-linear and stochastic because of strong dependencies on instantaneous payload power draw and on atmospheric composition. The following three examples illustrate concrete scenarios:

- A heavy power draw will increase the temperature of the payload consistent with the rates of electric-to-thermal energy conversion in the various active components. This cannot readily be modelled since components may draw more or less power according to their age, start-up state, temperature, and other unpredictable factors.
- A high humidity level will tend to buffer temperature changes and will modulate both the cooling effects of the thermal control system and the heating effects of the electronics.
- Significant activation of the oxygen or nitrogen valves may cause a cooling of the payload since compressed gas becomes chilled when expelled through a small orifice.

3.5.1.4 Carbon Dioxide and Ammonia

The algorithmic response pathways for carbon dioxide and ammonia control are shown in Figure 33. The valves to the LiOH/carbon bed will open if control of either contaminant is mandated, or if the silica gel bed has been active for over thirty minutes. The latter scenario may initially seem counterintuitive, but results to support this strategy are described in chapter 6. Briefly, experiments with a prototype Mars Gravity ECLSS design demonstrated that a chemical bed with a high concentration of activated carbon has significant water adsorption capacity. The intention is to take advantage of this property in the event that the silica gel bed is unable to rapidly bring down a high humidity level.

The 15-minute time constants shown in Figure 33 are in accordance with projected ECLSS response times as observed in ground experiments to date.

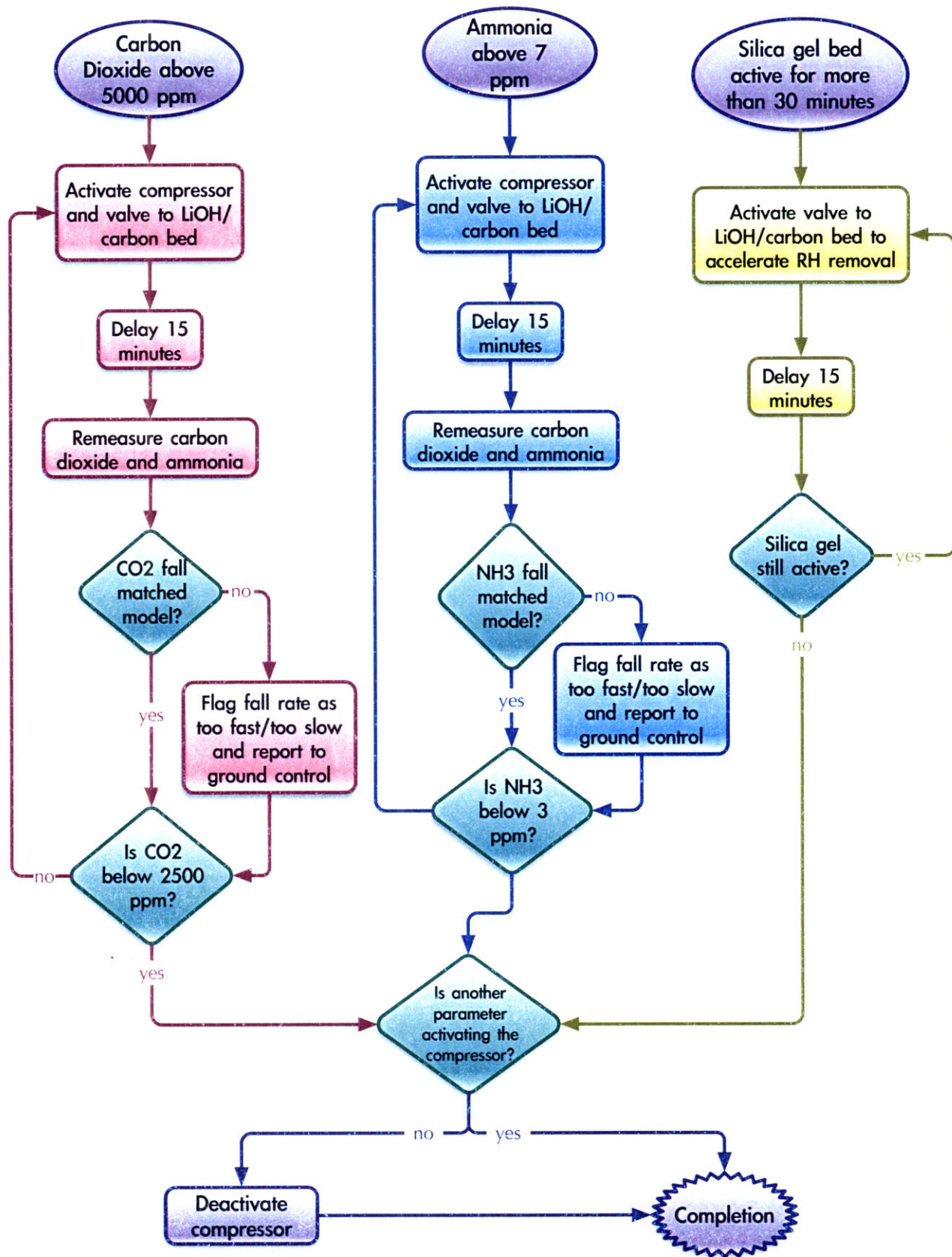


Figure 33: Carbon dioxide and ammonia algorithms

3.5.1.5 Air Flow Rates

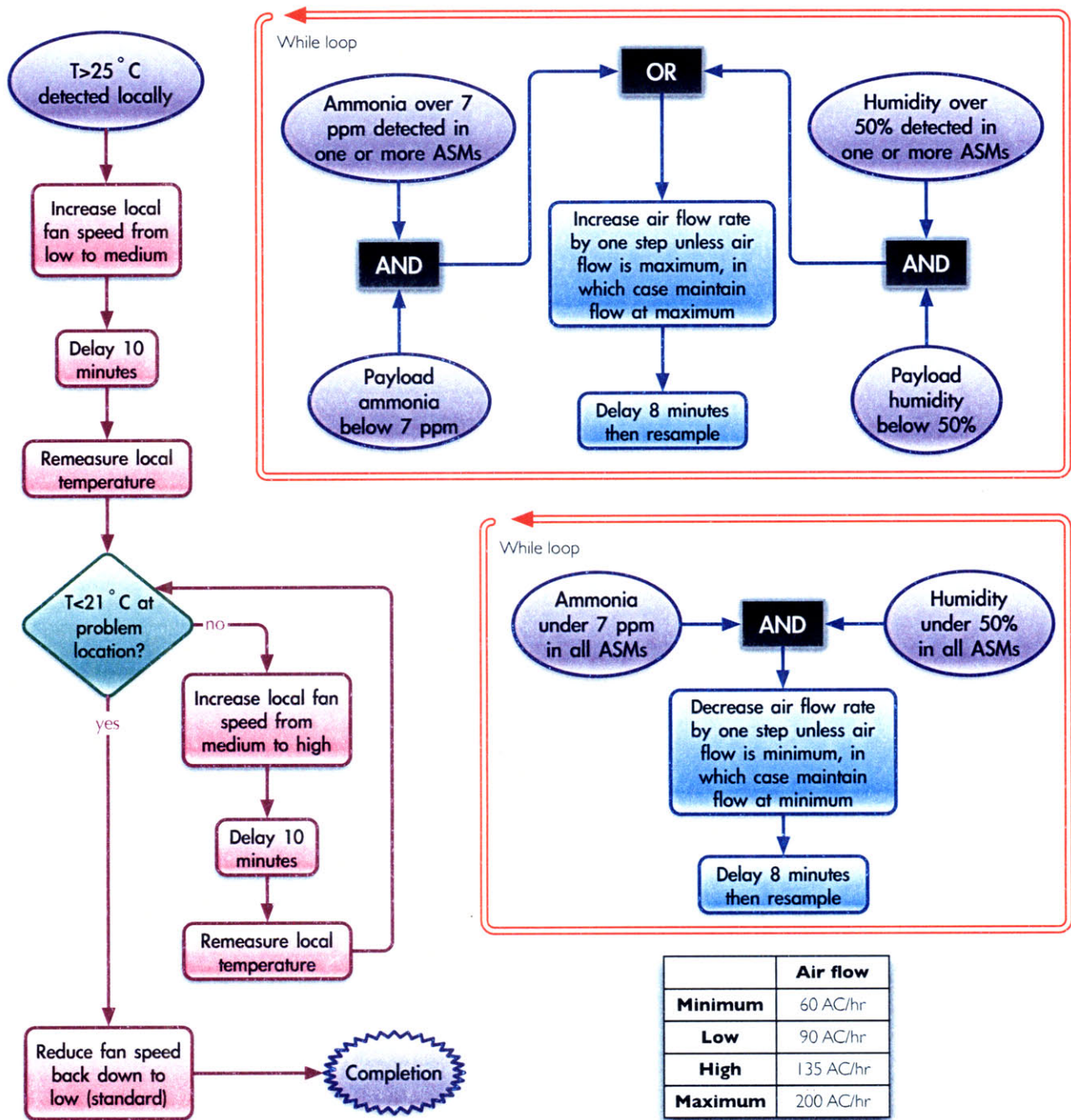


Figure 34: Air flow rate algorithms

A number of fans and blowers will be installed within the payload module, consistent with the designs previously discussed in section 2.7.6. The blower that circulates air through the fifteen ASMs can be thought of in algorithmic terms as an “equilibrator.” In general, the faster the blower runs, the more closely conditions within the habitat modules will match the global conditions measured at the level of the entire payload. Separately, the circulatory fans distributed throughout the life support bucket are intended primarily for thermal

control, to eliminate temperature hotspots. Flow rate control is depicted in Figure 34, where maroon elements denote distributed fans and turquoise boxes relate to the ASM blower.

The local temperature control fans are typically situated in areas of higher anticipated thermal flux, such as near the payload computing nodes or adjacent to the compressor and power regulation subsystems. As depicted in Figure 34, the temperature control fans have three speed settings: low, medium and high. Even in the absence of an over-temperature trigger, the fans will be continuously operational at the lowest speed setting in order to promote good mixing of the payload cabin air. The ASM circulatory blower has four power settings, and it too must operate continuously in order to meet the minimum science requirement of 60 air exchanges per hour. The general algorithmic principle calls for the ASM circulatory blower to increase its speed when the air inside the habitat modules seems insufficiently well-mixed with the air in the payload. Blower power can reduce back down once the habitats have equilibrated once more.

3.5.2 ECLSS Data Collection Operations

For the most part, the previous diagrams and control algorithms treated only global environmental changes within the payload. However, there exists the potential for significant cross-payload variation. For redundancy and reliability, there are generally at least three identical sensors to measure each atmospheric parameter. Table 26 summarises the configuration.

Table 26: Atmospheric sensors within the payload module

Sensor	Total count (# units)	On Sensor Suite PCB	Off Sensor Suite PCB
SensoriC A7AM (Ammonia)	18	3	1 per ASM, i.e. 15
Vaisala GMM111 (CO ₂)	3	3	Nil
Omega PX138-030A5V (Pressure)	3	3	Nil
SensoriC MOX-9 (Oxygen)	3	3	Nil
Honeywell AWM5104 (Flow rate)	2	1 for compressor	1 for ASM blower
Figaro TGS2611 (Methane)	3	3	Nil
Sensirion SHT15 (Temperature & Humidity)	48	3	1 per ASM, i.e. 15, plus 30 distributed for local temperature data

The question arises: how should the supervisory iNode modules determine the “actual” global value when presented with conflicting data from two or more sensors? Sections 3.5.1.2 to 3.5.1.4 assumed that this was a solved problem and that it would always be possible to unambiguously determine the correct global reading. Section 3.5.1.5 is distinct in the sense that the algorithms for air flow rate directly address and respond to cross-payload differences.

The phase E3 sampling requirements call for sensor data acquisition a minimum of once every four minutes. In reality, sampling rates will be substantially higher in order to provide enhanced data reliability. Data validation strategies are discussed in detail in the remainder of section 3.5.2.

3.5.2.1 Oxygen, Carbon Dioxide, Pressure and Ammonia Monitoring

The sensor suite features three units of each of the sensors for oxygen, carbon dioxide, pressure and ammonia monitoring. In this section, the phrase “the three sensors” should be taken to refer to the sensor set for monitoring any one of these four parameters.

The payload software requirements call for the acquisition of one datapoint from each of the three sensors every 20 seconds. Every 4 minutes, the software will calculate the median reading for each of the three sensors using the previous 4 minutes’ worth of data.

Importantly, the software provides mechanisms for ground controllers to disable or enable any of the three sensors.

The following requirements are for enabled sensors only:

- The software shall use a three-way voting algorithm to assess the validity of each sensor’s 4-minute reading. The software shall consider invalid any oxygen reading that deviates by more than 20 millibar (approximately equivalent to 2% oxygen) from either of the other two sensors, provided the other two sensors are within 20 millibar of one another. In this way, the two sensors that are in agreement will “vote out” the third sensor. The software will consider invalid any carbon dioxide reading that deviates by more than 2000 ppm from the other two. It shall consider invalid any air pressure reading that is more than 30 millibar different from the other readings. An ammonia reading more than 3 ppm different shall also be considered invalid.
- The software shall flag the readings of any sensors that are considered invalid, both for the purpose of ECLSS algorithmic decision-making and for transmission to ground.
- The software shall generate an “actionable 4-minute value” for each payload parameter by calculating the mean of the values obtained from the valid sensors, if at least two sensors are valid. The resulting value shall be considered a reliable feed-in reading for any of the ECLSS control algorithms.
- If fewer than two sensors are valid, the software shall generate an “actionable 4-minute value” for the parameter in question by taking the highest 4-minute reading, regardless of whether that sensor is valid or invalid. This is a justifiable approach because it is impossible under this error condition to ascertain which sensor has failed. Consequently:
 - For oxygen and pressure, a conservative approach that results in the least amount of oxygen/nitrogen being added to the system is preferred. Such a strategy minimises the risk of overpressurising the payload and causing a system leak. If necessary, this decision can be overridden by ground control at the next communications opportunity.

- For ammonia and carbon dioxide, a conservative approach that results in the most contaminant being eliminated from the system is preferred. Such a strategy errs on the side of providing the best air quality and therefore maximising mission science return.

3.5.2.2 Temperature and Humidity Monitoring

Since there are 48 temperature/humidity sensors on board the biosatellite, determining the global payload temperature and relative humidity is non-trivial. On the one hand, it can be argued that the fifteen ASM-based SHT sensors are of primary importance because the science requirements are written with mouse-relevant parameters in mind. On the other hand, since temperature and humidity are controlled only at the level of the entire payload, it may be more appropriate to measure these parameters outside the habitat modules.

In practise, the chosen operational approach is to use a weighted average of all the sensor readings. The software shall collect a datapoint from each of the SHT sensors once every 20 seconds. The software shall then store the median readings from each of the sensors every 4 minutes in a manner similar to that previously described for other atmospheric sensors. The mean of the fifteen ASM sensors will subsequently be calculated. The mean of the 30 distributed SHT sensors will also be derived, as will the mean of the three SHT sensors that are mounted on the Sensor Suite PCB. The final “actionable 4-minute value” for temperature will be calculated using a weighted mean whereby the ASM averaged reading has 60% weighting, the distributed devices have a 25% weighting and the Sensor Suite units contribute the remaining 15%. The “actionable 4-minute value” for payload humidity will be calculated in exactly the same way. This is appropriate because expected local temperature fluctuations will certainly impact local relative humidity readings and should therefore be averaged out using the same weighting.

Mechanisms will be provided by which mission control may enable or disable any of the 48 SHT sensors. Due to the large number of available sensors, the supervisory iNode will not attempt to determine the validity (or otherwise) of any of the sensor readings. It is assumed that the averaging approach will minimise the adverse impacts of any outliers.

3.5.3 Sensor Data Acquisition

During phase E3, acquisition of data from non-environmental sensors will stabilise to the frequencies shown below.

Table 27: Sensor operations during Phase E3

Requirement ID	Data	Detail
4.3.1	Blockage of ASM air flow	Inferred by ground control from ASM ammonia/humidity readings.
4.3.2	Body mass	Record every platform movement; aggregate every 6 hours.
4.3.3	Water consumption	Record every lick; aggregate every 6 hours.

4.3.4, 4.3.5	Vibration	Sampled once every 10 seconds over a five-minute period during every night cycle, and for one second during every day cycle.
4.3.17	Sound pressure	30-second duration clip recorded once every 96 hours.
4.3.18	Still images	10 snapshots from the video feed during each 24-hour period.
4.3.19	Health status video	Four 15-second clips each day.
4.3.20	Troubleshooting video	Up to 5 minutes per week for one ASM.
4.3.22	Video for behavioural analysis	Two 45-minute clips per ASM per day.

3.5.4 Responding to Ground Commands

The payload module is a complex system. Multiple unforeseeable failure modes could arise over the course of the mission. Significant emphasis is therefore placed on allowing ground controllers to upload commands that can help the payload computers better manage off-nominal situations. Specifically, the payload software is required to accept and respond to the following instructions as a means of increasing mission robustness during phase E3:

- Requests for additional snapshots or longer video clips of specimen chambers as delineated in Table 27. The request would specify the number of snapshots required, ASM identifiers, duration of video clips needed, and time window over which video clips and snapshots should be acquired. A numerical priority would be assigned to each data file in the event that not all imagery can be transmitted during the subsequent communications window.
- Requests for higher-resolution images following the downlink of low-resolution thumbnails. The request would specify the ID numbers of the thumbnails of interest and would assign a numerical priority to each thumbnail in the event that not all data can be transmitted during the subsequent communications window.
- Commands to activate 24-hour daytime lighting in order to provide additional well-lit video footage of an animal that is injured or in distress. The command would specify the ID of the ASM in question and the duration for which 24-hour lighting is mandated.
- Commands to atmospherically seal any animal support module following rodent death or severe injury. The command would specify the ID of the ASM and the time window within which atmospheric sealing should occur.
- Commands to rapidly eject water through a drinking nozzle to dislodge a suspected blockage. The command would specify the ID of the ASM and whether it is the right

nozzle or the left nozzle within the specimen chamber. It would normally be accompanied by a request to record video during the discharge event.

- Commands to redefine any of the “control-low” and “control-high” values previously discussed in section 3.5.1. The command would specify which value is to be reassigned, the new value for that setpoint, and the duration for which the change is to take effect. For example, if the mission were to be extended by three days owing to inclement weather in the landing zone it may be desirable to relax environmental cleansing requirements. Increasing the “control-high” trigger points for ammonia and carbon dioxide to 10 ppm and 7000 ppm respectively may ensure that life support expendables will not be depleted prior to the end of the mission. As another example, if atmospheric reentry were to be performed in an unusual manner, it may be desirable to intensively pre-cool the interior of the biosatellite in anticipation of higher than normal heating loads during descent.
- Commands to enable or disable any of the sensors as previously discussed. The command would include an identifier for the sensor, a declaration of whether this sensor should be enabled or disabled, and the duration over which this change will remain valid.
- Commands to modify the power setpoints of any of the ECLSS actuators that normally operate in an on/off modality. The command would include an identifier for the ECLSS actuator being addressed together with new voltage assignments for both the on state and the off state. In some cases, multiple voltages assignments may be required. For example, each condensing heat exchanger has distinct on/off voltage requirements for the fan, the thermo-electric cooler and the fluidic micropump that moves condensate into the collection reservoir.
- Commands to modify the power setpoints of any of the ECLSS actuators that can operate in multiple states. The command would include an identifier for the ECLSS actuator being addressed together with new voltage assignments as necessary. In the case of the variable-voltage fans that distribute air around the payload module, the command would specify new “low,” “mid” and “high” voltage targets. For the ASM air distribution blower, the command would include minimum, low, high and maximum voltage levels to correspond to the 60, 90, 135 and 200 ACH target setpoints previously discussed.
- The above requirements also encompass the situation where one unit of a double-redundant pair may have failed and can subsequently be deactivated from the ground. This may happen in the case of the dual-compressor subassembly. If one compressor were to fail, its on-voltage and its off-voltage would both be set equal to zero. The remaining operational unit would be assigned a commensurately higher on-voltage in order to compensate for the load left uncovered.
- Commands to safely reset the on-board computers if necessary. The command would include the time at which a reset attempt should occur, which in many cases will not be until after the communications session has ended.

3.5.5 Preparing for E4

During the final hours of phase E3, the supervisory iNodes will begin preparing the payload for spin-down. Following confirmation from mission control of an impending transition to

E4, the ECLSS subassemblies will begin to cool the payload to a crisp 18°C, at the lowermost point of the scientifically allowable range. Relative humidity will be aggressively transitioned into a 40%-50% zone, using the last of the silica gel desiccant adsorption capacity if necessary. Both carbon dioxide and ammonia will be scrubbed to below the lowest available control setpoint. In anticipation of a period of weightlessness, the fluidic micropumps attached to each condensing heat exchanger will remove all free condensate and sequester it in the central reservoir. Waste collection motors will activate one last time to shunt any deposited solids into the collection hopper.

3.6 Phase E4: Deorbit

The deorbit phase covers all manoeuvres leading to reentry and is projected to last less than 30 minutes. It includes spin-down, reorientation, spin-up and reentry burn, until the instant of bus and RV separation. As shown in Table 28, sensor operations are largely identical to Phase E2.

Table 28: Sensor operations during Phase E4

Requirement ID	Sensor	Detail
4.3.8 onwards	Atmospheric monitoring	Once every 4 minutes.
4.3.17	Sound pressure volume	Continuous.
7.3.4	Vibration	Average and maximum once every ten seconds.
7.4.2	Linear acceleration	Magnitude and duration of all accelerations between 0.01-g and 50-g with duration above 0.01 s.
7.14.4	Video	4 greyscale clips of 15-second duration from each ASM.

Phase E4 will include a period of weightlessness. All ECLSS systems will deactivate, with the exception of circulatory fans and blowers. In order to ensure adequate air mixing and guard against the buildup of carbon dioxide air pockets, all temperature control fans will transition to “medium” flow rate performance at the beginning of E4. All ASM water pumps and specimen body mass sensors will be deactivated. Air will be forced through the ASMs at the maximum rate of 200AC/hr in order to promote the entrapment of floating waste and debris within the underfloor WCS. All other components with moving parts will remain off. Sensors, lighting, video and avionics equipment will remain powered.

3.7 Phase E5 to E7: EDL, Recovery and Post-Flight

During the final three phases of the mission, payload operations are lightweight and focus primarily on subsystem maintenance and status checks. Phases E5 and E6 will last only a few minutes in total, while E7 is expected to be less than one hour.

EDL begins once the spacecraft bus has been jettisoned. At this time, the payload module batteries will power the entire reentry vehicle. Payload operations will continue identical to

phase E4, but where possible the fan speeds will be reduced in order to conserve power. Following on-board analysis of accelerometer data, the payload module will command the EDL controller to deploy the parachute at the appropriate moment. It will also communicate with the EDL GPS beacon during descent in order to acquire time and location data.

Recovery occurs when the helicopter's hook latches onto the aerocapture loop that is secured to the top of the reentry vehicle adjacent to the parachute cords. At this point, the payload module will continue sensor operations and will prepare a package of data concerning overall RV health ready to transmit during E7.

Once the helicopter has lowered the reentry vehicle to the ground, phase E7 will commence with the attachment of a power/data line. The payload power conditioning hardware will sense an impedance change upon connection of external electricity. At this point the vehicle will exit power conservation mode and will electrically disconnect from the internal batteries. The iNodes will transmit vehicle health information (including recent mouse video) in order for technicians to assess the state of the payload module. Thereafter, the ground operations team will determine the best and most time-efficient procedures to safe the satellite, extract the specimens and make valuable science swiftly available to investigators.

Chapter Four: Engineering Design of a Prototype Rotational Payload Test Apparatus

4.1 Motivation

The payload Integrated Ground Test Apparatus (IGTA) was designed to meet the following high-level objectives:

- Accommodate up to four mice in high fidelity prototype ASMs on a gondola centrifuge. Incorporate flight-like food and water delivery, waste collection, lighting and video, and air distribution systems. Design the centrifuge such that the rate and radius of rotation is equivalent to that projected for the mission. This configuration will permit assessment of the impacts of chronic extended-duration centrifugation on flight-age female BALB/cByJ mice. It will also permit an exploration of the capabilities and limitations of Ethovision XT with the ASM configuration. (Ethovision is an industry-standard video-based rodent behavioural analysis software suite.)
- Install the centrifuge within an enclosed vessel and incorporate a subset of ECLSS hardware similar to that baselined for the Mars Gravity Biosatellite mission. Use the resulting system to demonstrate proof-of-concept operation and confirm the feasibility of the proposed ECLSS strategy.

Figure 35 illustrates the orientation and effective gravitational vector of a single ASM in the Mars Gravity Biosatellite and on the IGTA centrifuge. While in the non-rotational configuration, the ASM experiences only the 1-g force of Earth's gravity. When spinning on the ground, this 1-g downward vector is supplemented by the 0.38-g radial vector outward. At 1.07-g, the resulting acceleration vector is not perceptibly greater than Earth's normal gravitational pull. Critically, Figure 35 confirms that in all three cases the net vector is normal to the floor. Accordingly, the mouse will always feel as if it is on a "horizontal" surface; from the perspective of the subject, the specimen chamber floor will be "down" and the ceiling will be "up" in every configuration.

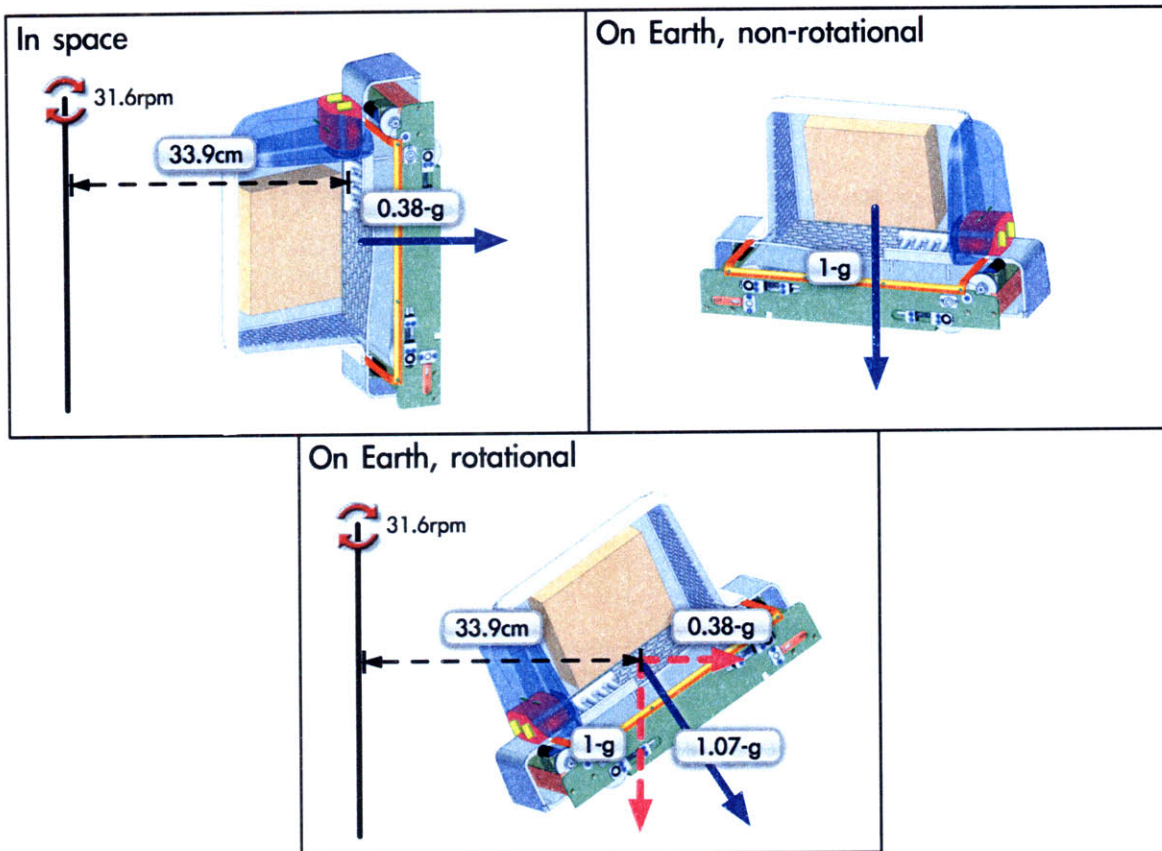


Figure 35: G-vectors for space and ground configurations

A further motivation for the IGTA was to explore design options for a first prototype of the Mars Gravity rotational ground control experiment. Such a system will be substantially more complex than the IGTA. It will be used during the mission to provide a scientific context against which to interpret results from the Mars Gravity Biosatellite. The final design will house fifteen mice in flight-equivalent ASMs on a multi-level gondola centrifuge. The entire apparatus will exist within a pressurised, sealed enclosure. Air inflow and outlet ports will connect to a complex custom ECLSS system capable of both adding and removing contaminants and other gases. A supervisory control computer will accept input parameters as transmitted to Earth by the Mars Gravity spacecraft. After a certain fixed time delay, the rotational ground control hardware will recreate the recorded on-orbit ECLSS parameters. This approach ensures that the only difference between the ground control and the spacecraft experiment will be the gravity vector: 1.07-g against 0.38-g. To the extent possible, all other measurable parameters will be matched between ground experiment and on-orbit mission.

4.2 Mechanical Structures

The mechanical design and fabrication of the IGTA was a collaboration with Andrew Heafitz, formerly a staff instructor at the MIT Edgerton Center. The mechanical requirements for the system are listed in Table 29.

Table 29: Mechanical requirements for the IGTA

Requirement	Detail
Anti-topple	The base of the IGTA shall serve as a sufficiently strong foundation that inadvertent impacts between the centrifuge arms and lab personnel shall not cause the system to topple, shatter or become unstable.
Durability	The IGTA shall be capable of supporting continuous rotation for periods of up to six weeks without the need for maintenance, component replacement or other procedures requiring stoppage.
ECLSS compatibility	The IGTA enclosure shall serve as an impermeable barrier to water vapour, ammonia, carbon dioxide and oxygen. It shall be non-rigid. It is not required to hold pressure and it may freely inflate and deflate.
Enclosure dimensions	The IGTA enclosure shall be sufficiently large that two small undergraduates each less than 165 cm tall can sit inside to assemble or disassemble systems and conduct maintenance. Every dimension shall be under 115 cm in order to fit within a single animal facility cubicle.
Gondola operation	A gondola-style tilt system shall ensure that the net acceleration vector during rotation will be perpendicular to each specimen chamber floor.
Materials selection	All IGTA materials and tooling shall be rodent-safe, non-absorbent, non-flammable and compatible with MIT animal facility cleaning regimens.
Mechanical stability	The instantaneous axis of rotation may not deviate from the theoretical axis by more than 1cm in any vertical or horizontal direction (“no wobble” and “no bounce”).
Ports	A maximum of three ports shall be present: these shall be for power supply (via connection to a wall outlet), data (a single USB cable) and air sampling (via a closable valve). Ports shall be hermetically sealed in order to preserve IGTA environmental integrity.
Rapid access in emergencies	The IGTA shall feature a solid impermeable portal door with an opening sufficiently large for one small undergraduate to climb into and out of the IGTA. The portal door shall be secured with no more than ten screws and/or nuts in order to permit speedy access in the event of an ECLSS systems failure that requires swift extraction of rodents.
Rodent accommodations	The IGTA shall accommodate up to four ASMs, each of which will house a single rodent. Each ASM shall be mechanically supported on at least its four base corners in both rotational and non-rotational configurations. It shall not be possible for any rodent to see out of its habitat module and thereby to visually detect its rotation.
Rotation	The IGTA shall support a continuous 31.6 ± 1 rpm rate of rotation. At this angular velocity, the horizontal distance from the central shaft to the centre of each specimen chamber floor shall be $34 \text{ cm} \pm 1 \text{ cm}$.

4.2.1 Design of the Central Shaft, Centrifuge Arms and ASM Holders

For mechanical strength and rigidity, Aluminium Alloy 6061 was selected for all weightbearing elements of the structure. Since power and data connections were to pass through the central shaft, a hollow round tube was selected for this part of the design. The chosen tube is a 91.4 cm aluminium cylinder with an outer diameter of 3.8 cm. The wall thickness is 6 mm, giving an inner diameter of 2.5 cm – more than adequate to accommodate several bundled wires and cables.

For centrifuge arms, two 91.4 cm long tubes of square cross-section were selected. The horizontal centre of each tube was collocated with the centre of the main centrifuge shaft. The outer cross sectional area measures 5.1 cm by 5.1 cm, with a wall thickness of just 3 mm because each arm need only carry the weight of two ASMs (while withstanding torsional effects). Two brackets were fitted to the upper arm in order to accommodate an electronics enclosure together with a central blower and manifold to circulate air to the ASMs.

The rectangular tubes were secured to the central shaft using two extended screws. The lower of the two rectangular tubes is affixed to the central shaft with a single screw that passes through both the tube and the shaft. That screw in turn secures a mounting bracket onto which is affixed the upper rectangular tube. By this approach, the first (horizontal) screw supports the weight of the centrifuge arms, while the second (vertical) screw ensures that the two rectangular tubes remain at 90° to one another.

Figure 36 illustrates how the uppermost segments fit together.

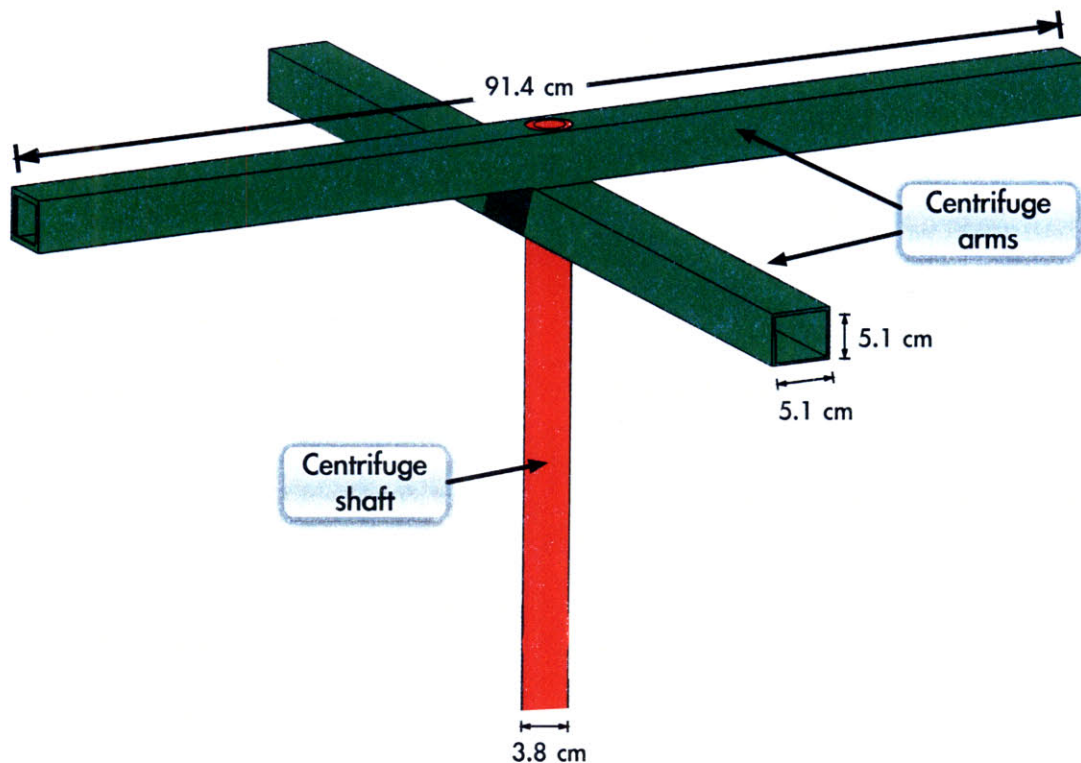


Figure 36: Upper part of the IGTA centrifuge (CAD: Kendra Toole)

Each gondola-tilting Animal Support Module is secured to the underside of a centrifuge arm via a set of aluminium sheet metal pieces that together form a holding bracket. The bracket dimensions have tight tolerances so that each ASM is secured within its holder as a press-to-fit part. Figure 37 shows relevant design detail. Each piece is a 1.5 mm thick, 2.5 cm wide Aluminium 6061 bar. The lowermost four pieces were each bent into 90° configurations using a sheet metal press brake. Thereafter, a hand-operated punch was used to create downward-facing holes of 3 mm diameter at both ends of each metal bar. Pop rivets were employed to secure all four bars to one another, and four additional holes were punched to affix the resulting ASM holder onto the attachment posts. The posts and other elements are labelled in Figure 37.

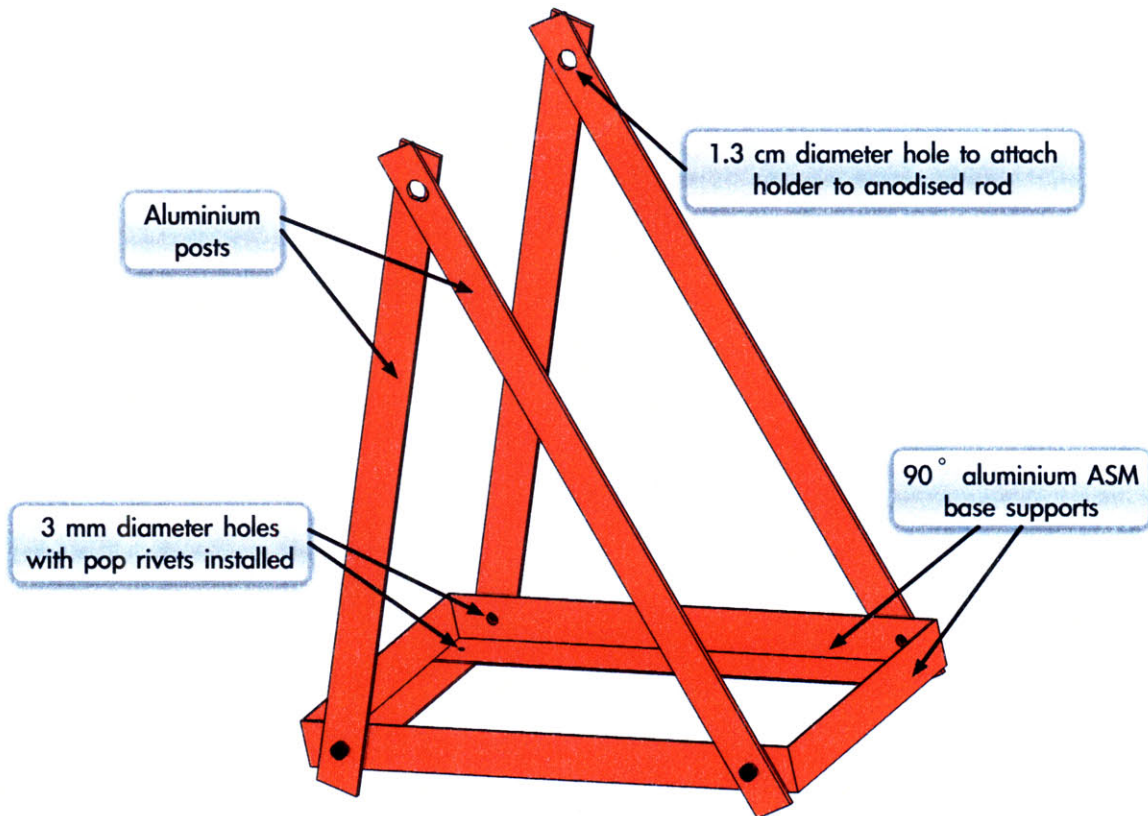


Figure 37: Holding bracket for a single ASM (CAD: Kendra Toole)

Each attachment post is a 1.5 mm thick, 2.5 cm wide aluminium bar. At the lowermost end of each post was punched a 3 mm diameter hole through which a pop rivet secured the ASM holding bracket. A 1.3 cm punch was used to create a hole in the upper end of each post. This allowed the post to slide onto a solid precision anodised aluminium rod of length 30.5 cm. The rod in turn was secured to the centrifuge arm by means of two 1.6 cm diameter holes on either side of the rectangular tube. These were fitted with polytetrafluoroethylene (PTFE) flanged sleeve bearings of 1.3 cm internal diameter to allow the anodised aluminium rod to freely rotate consistent with the gondola concept of operation. Six aluminium set screw shaft collars of bore size 1.3 cm and outer diameter 2.5 cm were used to laterally secure the anodised rod to the centrifuge arm and the attachment posts to the anodised rod. The configuration is shown in Figure 38.

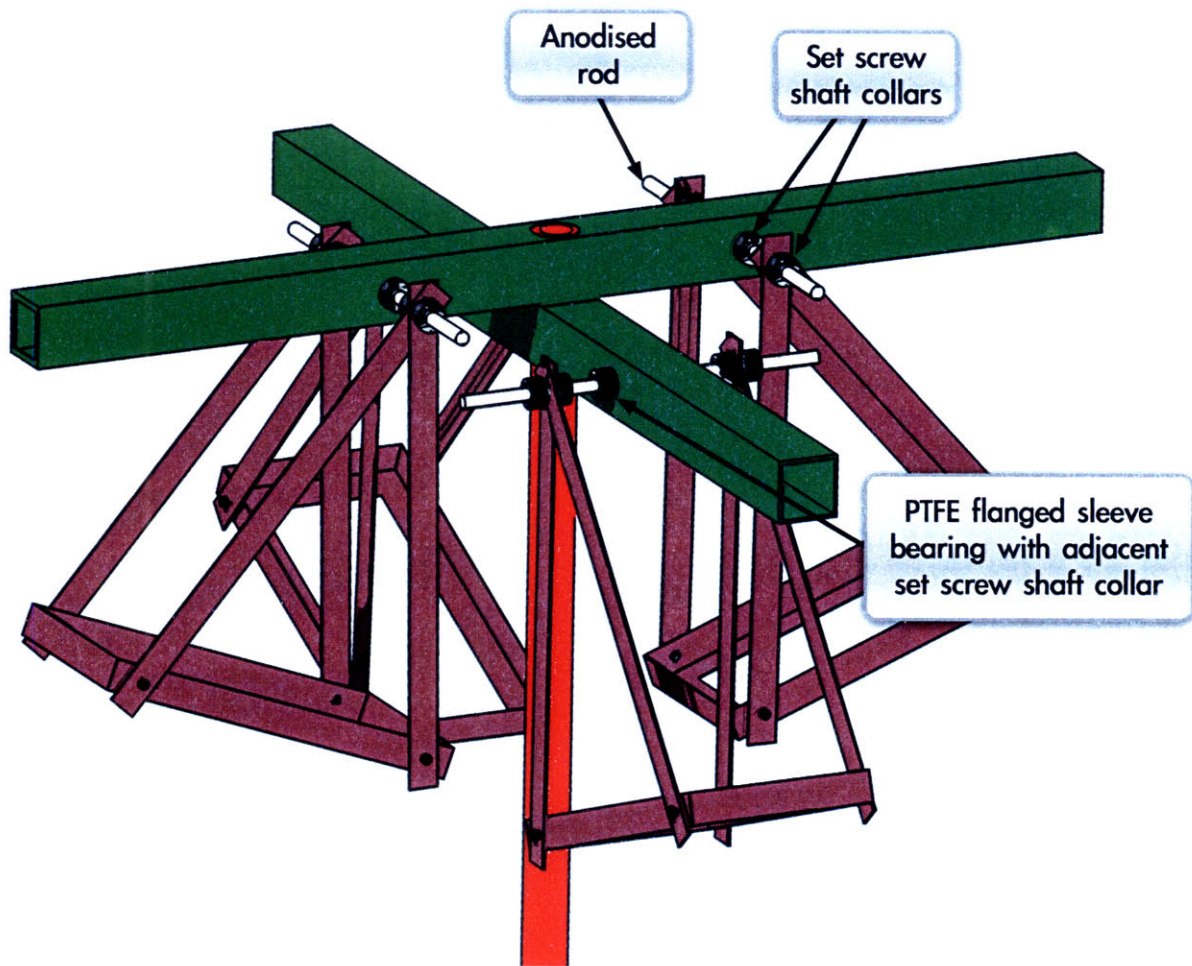


Figure 38: ASM holder attachments (CAD: Kendra Toole)

The ASMs installed within the IGTA were high-fidelity prototypes. Their functionality was flight-like except for the fact that none of the ASMs featured working body mass sensors. In order to meet the requirement that animals not be able to visually sense rotation, black cardboard lightshields were installed on the side of each ASM as shown in Figure 39. These elements were fitted adjacent to the lighting boards and ensured that no light would seep out of the habitat module to affect adjacent ASMs or other rodent cubicles.

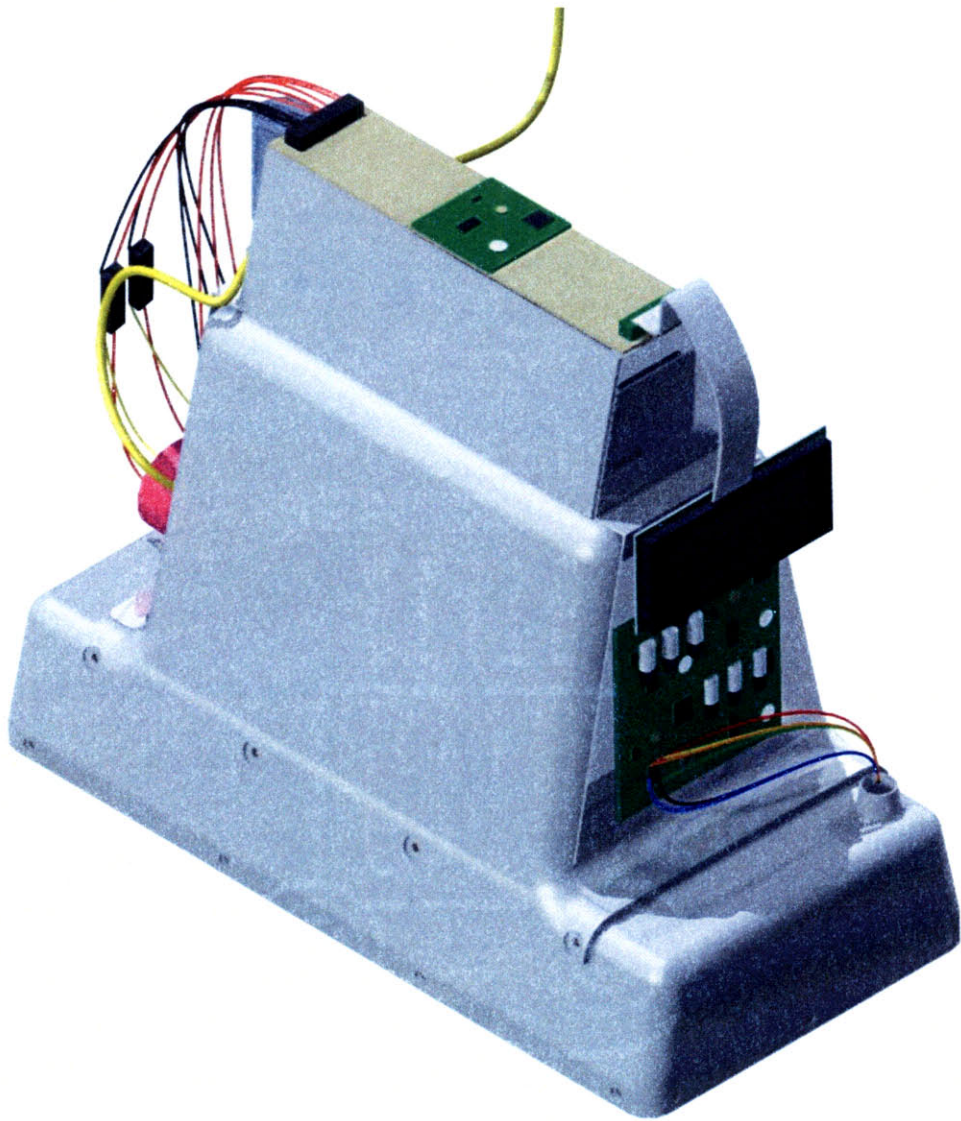


Figure 39: ASM with lightshields (CAD: Adam Fuhrmann)

4.2.2 Design of the Centrifuge Base, Bearings and Motor Mounting Bracket

Two cast iron Y-bearing plummer block units with grub screw locking mechanisms were selected to secure the centrifuge shaft and permit smooth rotation of the entire assembly. These bearing units were placed one above the other at a vertical separation of approximately 15 cm. The shaft was inserted into the two bearing units that were subsequently mounted to a solid 6 mm thick aluminium block as shown in Figure 40.

Two shelf mounting brackets each of 25 cm length were used to secure the vertical aluminium block to a horizontal baseplate foundation that was also constructed of 6 mm thick aluminium. Care was taken to ensure several centimetres of clearance between the base of the centrifuge shaft and the 7.6 cm diameter access hole in the centre of the baseplate. This clearance ensured there would be sufficient space to subsequently install cabling and electrical connectors.

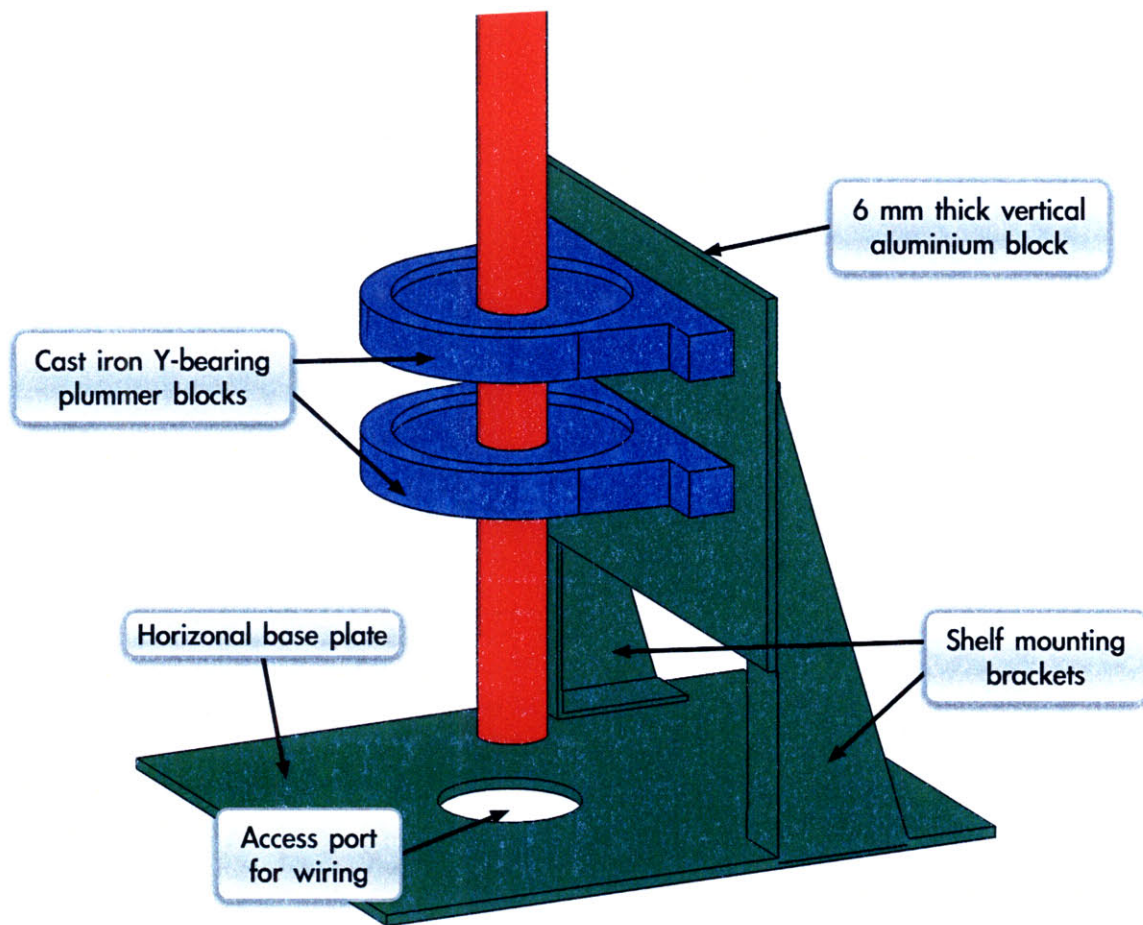


Figure 40: Lower part of centrifuge without motor (CAD: Kendra Toole)

Once the system had been assembled as shown in Figure 40, a 1.2 A 115 V AC gearmotor was incorporated into the apparatus. The selected model featured a nominal speed of 35 rpm and generated a torque of 1.7 Nm, more than sufficient to accelerate the fully-loaded centrifuge to the nominal rotation rate within a couple of seconds. The motor was bolted onto a mounting plate that in turn connected to the vertical aluminium block by means of a stainless steel surface-mountable hinge. The motor spindle and centrifuge shaft were each fitted with a trapezoidal tooth timing belt pulley that was secured in place using a quick-disconnect bushing. The pulleys were sized such that the 35 rpm motor rate would be stepped down to 31.6 rpm on the centrifuge.

A 1.3 cm wide urethane timing belt served to link the two pulleys together in order to drive torque from the motor to the centrifuge. In order to tension the timing belt, a screw was tightened to offset the motor mounting plate from the vertical aluminium block. The resulting spin rate of 31.6 ± 1 rpm was experimentally confirmed. Figure 41 illustrates the design.

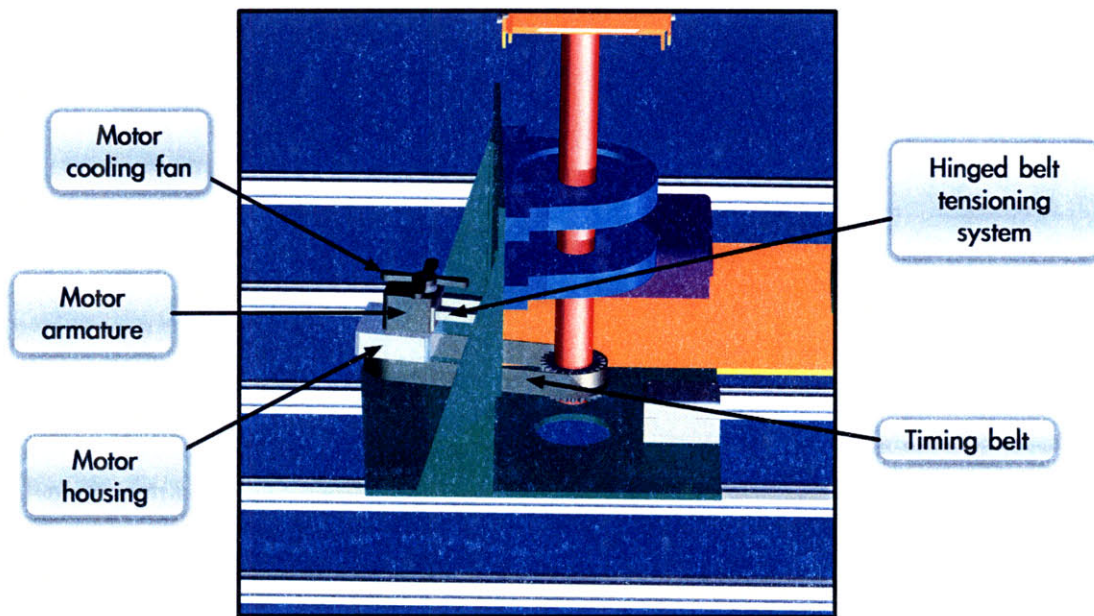


Figure 41: Motor, mounting block and belt (CAD: Kendra Toole)

4.2.3 Design of the Outer Frame, Barrier Membrane and Portal Door

A dual-layer plastic sheeting design was selected for the barrier membrane. The inner layer was an optically clear 85 Shore A polyether polyurethane of less than 1 mm thickness. Its outgassing parameters were considered acceptable since this product is commonly used in medical and food packaging applications. Thin polyurethane sheets are known to be permeable to water vapour and gaseous ammonia. Accordingly, a layer of translucent high strength low-density polyethylene (LDPE) film was incorporated as a second (outer) layer of the barrier membrane. The LDPE film was tear-resistant and had a thickness of 1.5 mm.

Both polyurethane and LDPE are heat-sealable. A commercial double-sided heat sealer similar to those commonly used in industrial packaging plants was purchased and its effectiveness confirmed with a selection of test samples.

Multiple configurations were considered for the outer frame, including spherical, cuboidal and octagonal prism designs. Ultimately the simplest possible approach was favoured. A cube configuration was deemed most suitable because it would require the fewest seals and would therefore present the lowest leak risk. 2.5 cm square cross-section aluminium fractional T-slotted framing elements were chosen for the outer structure. These commercial products are part of an extensive McMaster-Carr range that include bars of multiple lengths, corner connectors, extrusions and screw-on plates that can be used for securing other hardware onto the structure.

The T-slotted framing system is easy to assemble/disassemble and is commonly employed to erect temporary outdoor staging and for indoor product marketing displays at tradeshows and conventions. Each of the 12 sides to the IGTA cube comprised a 122 cm T-slotted framing bar. Additional bars were arrayed at the bottom of the structure to serve as mounting platforms for the centrifuge base, ECLSS apparatus and other electronic/computer hardware. Two bars were mounted a few centimetres above the top of the centrifuge to serve as a harnessing/routing framework for data cabling. The wires exit the top of the

central shaft, track laterally and route down the side of the IGTA before connecting to the supervisory PC. The resulting design is shown in Figure 42. The volume inside the IGTA is approximately four times that baselined for the spacecraft payload module.

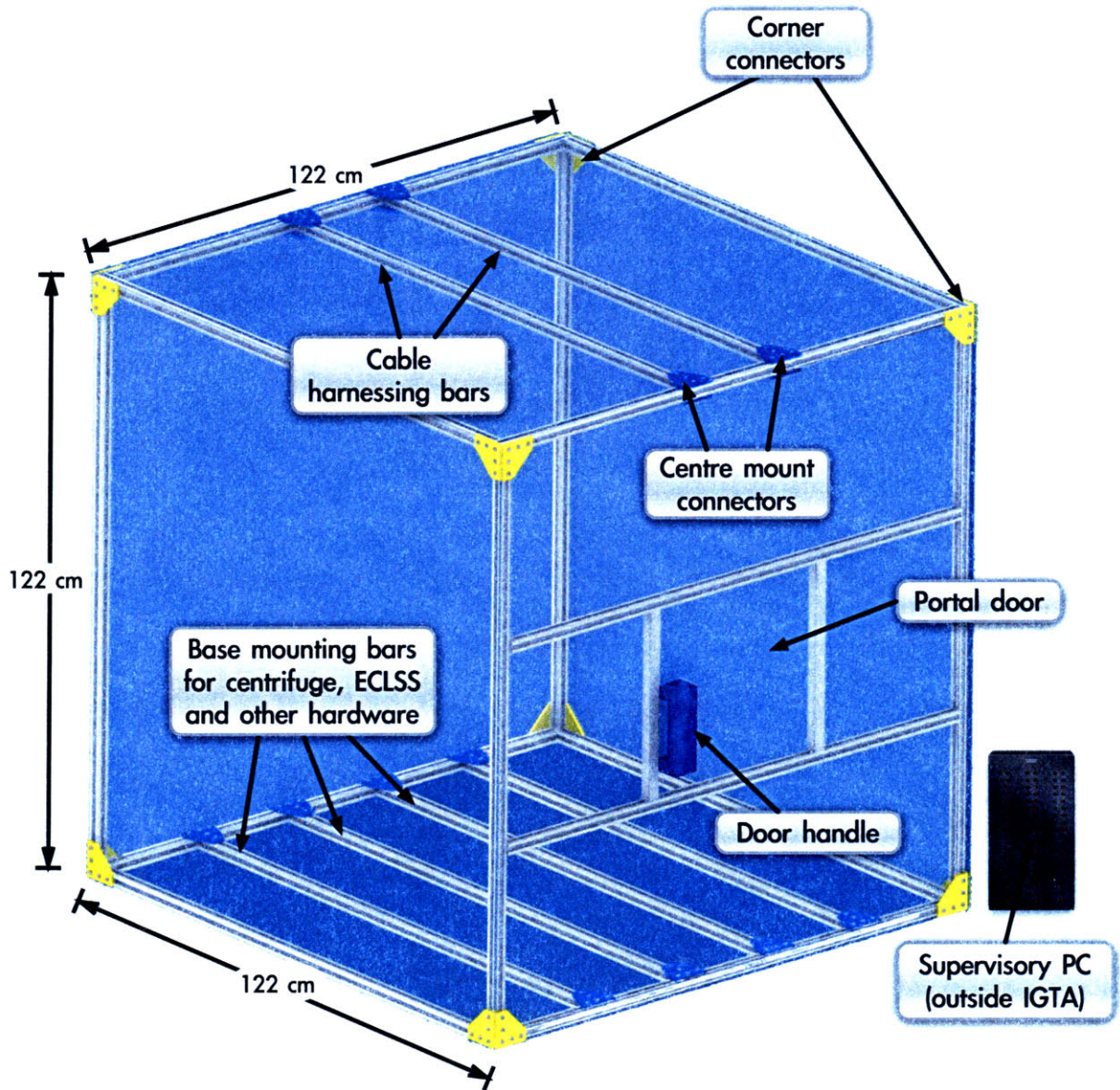


Figure 42: IGTA outer frame (CAD: Kendra Toole)

A frame for the portal door was created through the use of additional shorter T-slotted framing bars. A clear cast acrylic sheet of dimensions 61 cm by 61 cm by 1.2 cm was fitted with a thermoplastic rectangular pull handle for easy manoeuvrability. The inner polyurethane barrier membrane was first cut to shape, heat sealed and pulled taut around the outer frame. It was forced into the channel provided by the T-slotted framing bars for the portal door and a length of flexible rubber tubing was overlaid in order to create an o-ring type seal. When the portal door was seated in place and locked down onto the ten mounting screws, the entire IGTA was hermetically sealed.

Once the IGTA outer structure had been assembled, the centrifuge was lifted through the portal door and secured to the base of the structure with screws and bolts. The LDPE barrier membrane was subsequently pulled over the outside and its seams were aligned with one another in preparation for final sealing and system closure.

To meet the requirements for data, power and an air sampling port, holes were cut in the barrier membrane and cables/tubing were sealed in place using a specialised urethane glue.

4.2.4 Lessons Learnt through the Mechanical Design Process

The mechanical design previously described was arrived at through an extended process of testing and refinement. A number of key lessons were learnt:

- Initially, incorrect information was provided about the permeability of polyurethane film. Experimental observations prompted the realisation that polyurethane is not resistant to water vapour. The LDPE membrane was added to the system in response to the need to better seal the IGTA.
- An initial design called for glovebox-style arm access portals in one side of the IGTA membrane. This would have allowed access to the centrifuge for scheduled maintenance operations without breaking the ECLSS seal. Practical difficulties were encountered when constructing prototype arm access portals and attempting to seal the resulting enclosure. In addition, the limited dexterity afforded by the arm-length gloves was deemed insufficient to perform useful manipulations within the IGTA.
- To meet the data and power port requirements, hermetically sealed waterproof connectors were initially selected. These were considered desirable for reasons including easy connect/disconnect operation and compliance with a more modular design philosophy. Ultimately it became clear that waterproof connectors are rarely certifiably airtight. It was also impractical to create a dependable polyurethane/LDPE seal around a rectangular connector mounting plate intended for deployment on appliances with rigid front panel displays.

4.3 Centrifuge Electronics and Software

The basic design of the centrifuge electronics is illustrated in Figure 43. The abbreviation ASM indicates Animal Support Module. HCM is the Habitat Control Module and LVB refers to the Lighting and Video Board positioned above the ceiling of each habitat. RX/TX refers to the serial receive/transmit lines that together make up the data-carrying element of the RS-232 protocol. The abbreviation DAQ refers to the National Instruments Data Acquisition system that features digital I/O ports for low-level communication.

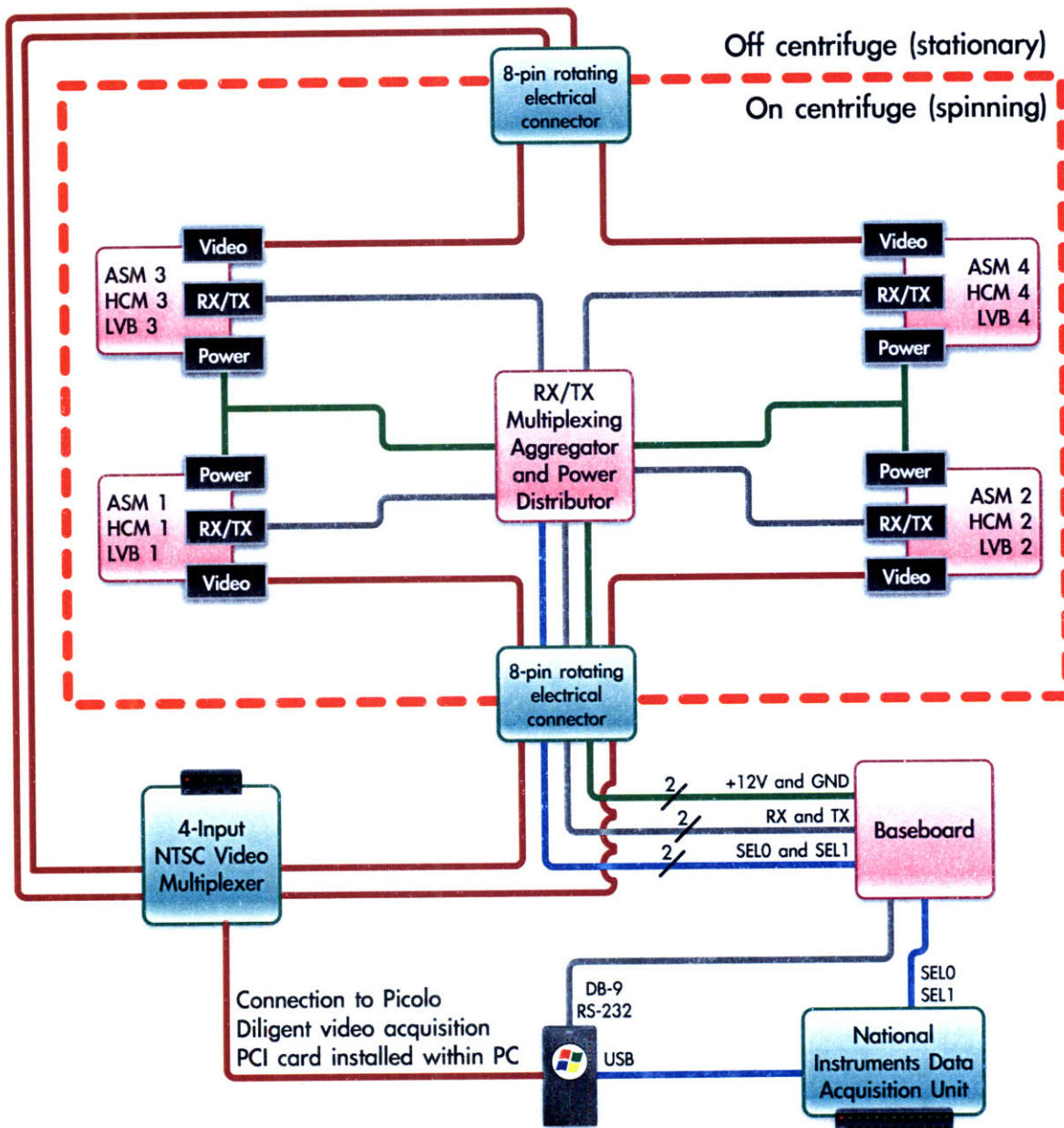


Figure 43: IGTA centrifuge electronics

Each red element in Figure 43 represents a custom-designed circuit board or group of boards that perform a certain set of specialised tasks. These PCBs are discussed in section 4.3.1 onwards. Green rectangles are commercial off-the-shelf components that were purchased from local distributors and integrated into the system without modification.

The 8-pin rotating electrical connector is a replacement for the traditional slip ring that for decades was the standard for this type of application. One rotating electrical connector interfaces with the top of the centrifuge shaft while the other unit interfaces with the bottom. The principle of operation is simple. One side of each connector is secured to the inside of the centrifuge shaft and is allowed to freely rotate with the spinning central tube. The other side is held motionless so that wiring can be routed to stationary external

components. The advanced design of the rotating electrical connector features eight internal circumferential baths of liquid mercury. Each electrical pin is connected to a paddle that is chemically bonded to the appropriate mercury reservoir. The electrical performance for high-speed digital and analogue signals is substantially better than any slip ring design. The unit guarantees exceedingly low signal noise even when rotating at very high rates. Figure 44 shows a product photograph.

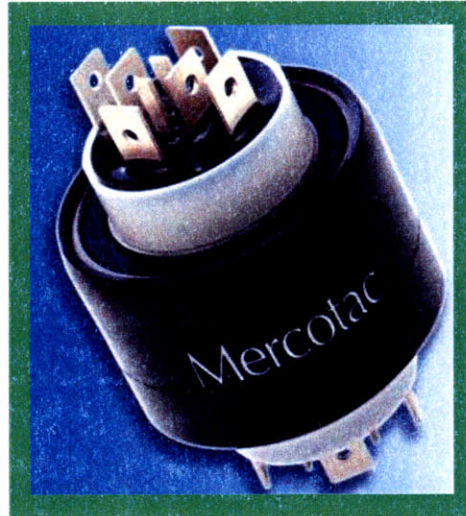


Figure 44: The 8-lead rotating electrical connector (manufacturer image)

The 4-input video multiplexer in Figure 43 is a commercial device approximately the size of a set-top cable TV decoder. It accepts up to four greyscale NTSC video inputs and generates a 4-in-1 live video output feed. The aspect ratio of each video input is preserved, as is the frame rate and image quality. The device is marketed as a solution for multiplexing feeds from multiple CCTV security cameras and accordingly it is designed for high reliability and 100% uptime. It features a built-in audible alarm that sounds the instant a video camera loses power or otherwise fails to generate a valid NTSC signal. The incoming and outgoing signals are carried on industry-standard coaxial cables fitted with BNC connectors. Such a connector on the output port directly interfaces with the chosen Pico Diligent PCI board that performs real-time full-rate video acquisition, digitisation and compression.

National Instruments product USB-6229 is a 16-bit 250 kS/s multifunction data acquisition module. It features 32 analogue inputs, 4 analogue outputs and 48 digital I/O ports. It is externally powered and interfaces with the supervisory PC via a USB 2.0 port. It is fully compatible with LabView and with other National Instruments software products.

4.3.1 Habitat Control Module

The HCM boards installed on the ASMs are identical to the flight-ready version described in section 2.5.8 on page 54. The ASMs within the IGTA are high fidelity prototype models similar to those described previously but without operational body mass sensors (this deficiency was in part due to funding constraints). In addition, the ASMs do not feature inflow/outlet lockoff valves because the need for chamber isolation in the case of an expired rodent is a requirement only for flight operation. None of the ASMs are equipped with the temperature/humidity and ammonia sensors that are baselined for the flight design.

4.3.2 Lighting and Video Board

The lighting board was briefly described in section 2.5.6. The boards used in the IGTA are an implementation of the PDR-level design. For power efficiency, each unit features product AD8845, an LED charge pump driver IC from Analog Devices. This model is an OEM part frequently deployed in mobile electronic devices where it serves to efficiently drive white LED backlights for liquid crystal displays. Further detail is in Appendix H: Circuit Diagrams.

In the centre of the lighting board is seated one unit of a greyscale NTSC (EIA) camera, model STC-H170CS by Sentech America, Inc. This compact uncased board camera features an 8.4 mm CCD with a 2:1 interlaced analogue output. Since observation of the rodents under dim red lighting conditions was desired, this model of camera features excellent low-light performance and high sensitivity. Its video output lines can be readily interfaced with a shielded coaxial cable for transmission through the centrifuge shaft and out of the rotating electrical connector.

4.3.3 Multiplexing Aggregator

The Multiplexing Aggregator printed circuit board is situated within an enclosure on the upper side of one centrifuge arm. It performs the following functions:

- Routing of power from the central supply line that exits the centrifuge shaft to each of the video cameras and to each of the ASMs.
- Routing of power to the circulatory blower that guarantees a minimum of 60 air changes per hour in each ASM.
- Translation of signal voltage levels between CMOS (0 V to 5 V) and RS-232 (± 10 V).
- The provision of DB-9 interfacing connectors to link the aggregator board to each of the HCMs via industry standard premanufactured cables.
- Multiplexing of signals from the ASMs to the single pair of RX/TX lines that are routed out of the base of the centrifuge shaft. The supervisory PC is able to select which of the four ASMs it communicates with by taking control of the SEL0 and SEL1 lines previously shown in Figure 43.

Signal translation and multiplexing is achieved through the use of MAX399, MAX3221 and MAX3223 ICs. Further detail is in Appendix H: Circuit Diagrams and labelled CAD visualisations are in Figure 45 and Figure 46.

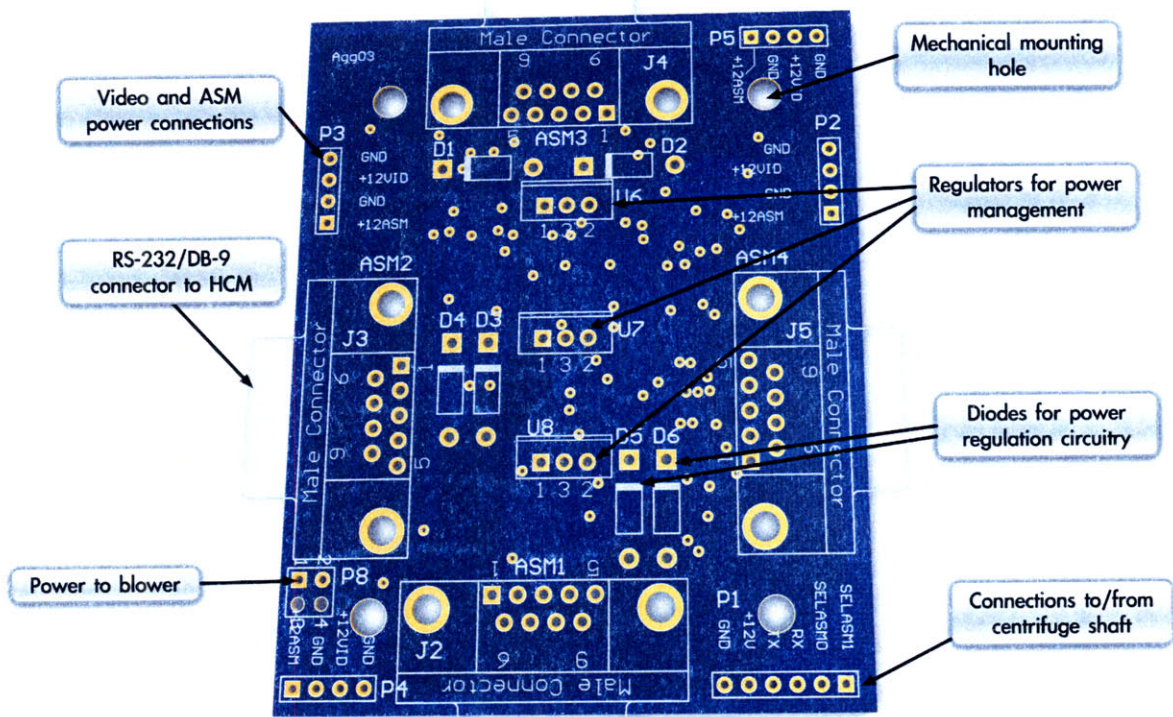


Figure 45: CAD rendering of the Multiplexing Aggregator board (front)

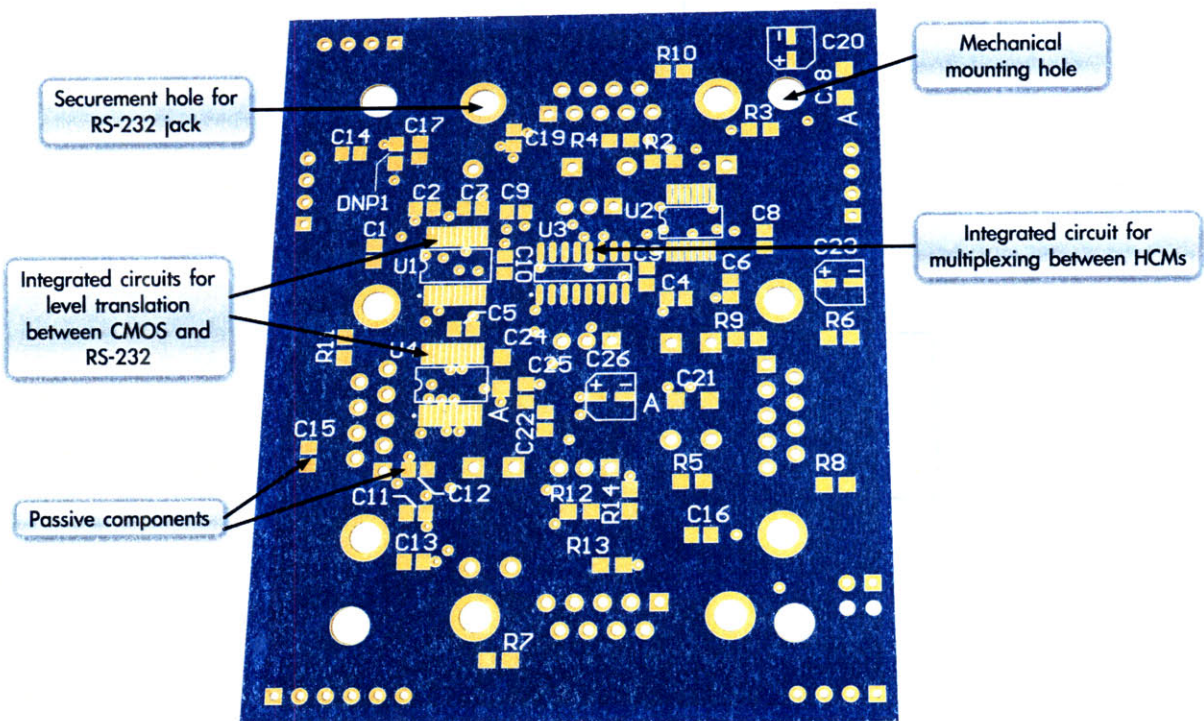


Figure 46: CAD rendering of the Multiplexing Aggregator board (back)

The board is purposely designed to mount within a commercial electronics enclosure that provides protection from dust, debris and incidental fluid droplets. The four mounting holes shown in Figure 45 and Figure 46 are dimensionally accurate and allow the board to be securely seated within the chosen enclosure.

4.3.4 Baseboard

The Baseboard PCB is a very simple interfacing solution designed for installation at the base of the centrifuge. It is sized identical to the Multiplexing Aggregator in order to fit within the same brand of plastic enclosure box. The purpose of the Baseboard is to accept individual multistrand wires from the centrifuge via a screw-in terminal block and to translate this configuration into a DB-9 connector and into single-core wires suitable for interfacing with the DAQ hardware. In addition, the Baseboard features a jack to allow connection to a 12 V DC transformer. This supply powers all centrifuge electronics with the exception of the AC gearmotor that connects separately to a 120 V electrical outlet.

The Baseboard PCB performs no on-board signal processing and the design features no active components.

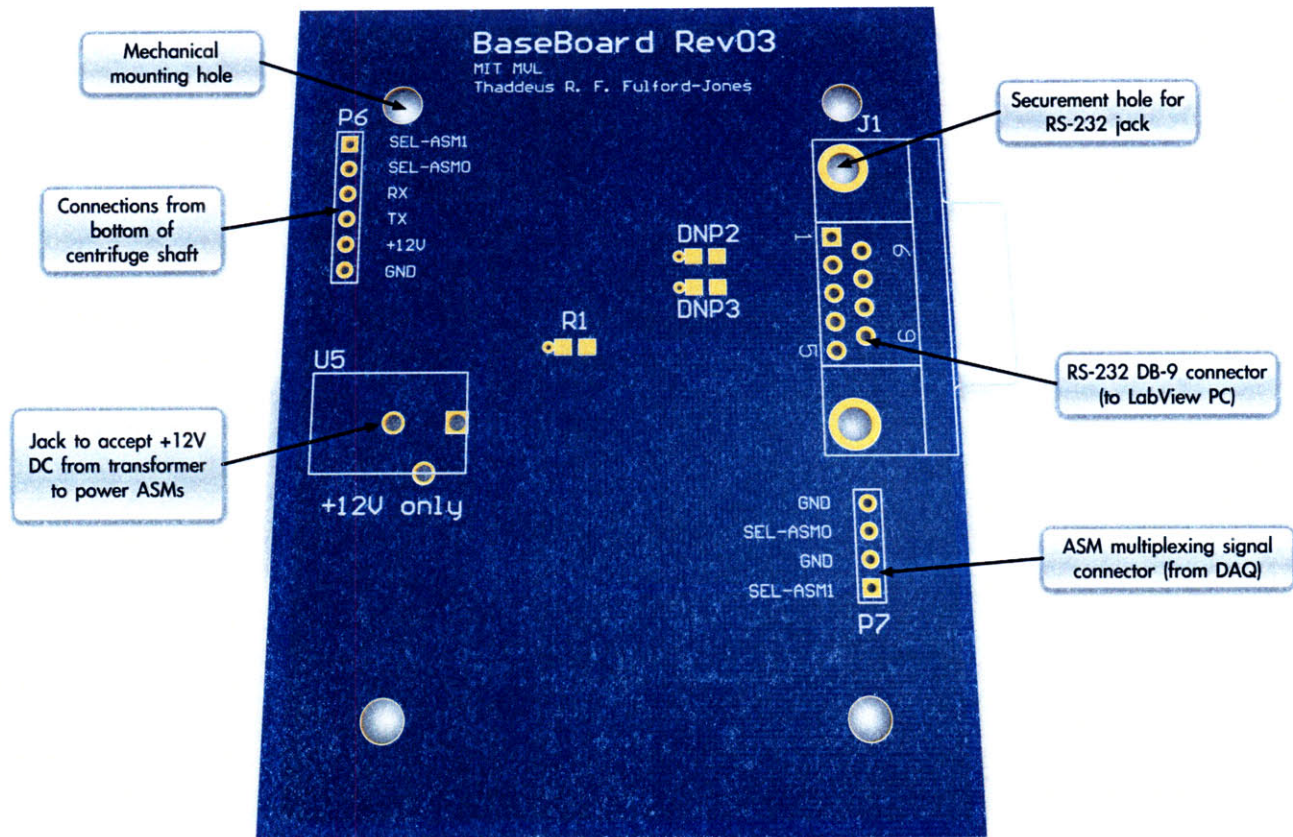


Figure 47: CAD rendering of the Baseboard PCB

4.3.5 Interfaces and Cabling

Because the rotating electrical connector contains liquid mercury, it is not possible to solder wires directly to any of the terminals. Instead, the manufacturer recommends using custom

connectors that can be crimped onto multistrand wires and manually seated onto the eight connection plates. Two of the connectors are designed for smaller 22-18 AWG wires while the remaining six are suitable for 16-14 AWG cabling. Figure 48 shows the design and layout of cabling around the lower of the two rotating electrical connectors. The other connector at the top of the centrifuge shaft is cabled using a similar approach, but as previously illustrated in Figure 43 only a subset of its available leads are used.

To ensure high-fidelity signal transmission, the video feeds within the centrifuge shaft run inside shielded coaxial cables. The outer sheath is grounded and the shielding is maintained the entire distance from the ASM-mounted video camera to the rotating electrical connector. To minimise signal crosstalk, the video signals are routed through the Mercotac unit at the greatest possible distance from one another. One video feed passes through the innermost mercury bath (red connector in Figure 48's photographic view) while the other feed attaches to a paddle in the outermost circumferential mercury channel.

Connections to the Multiplexer Aggregator PCB and NI data acquisition module are via 18AWG cabling interfaced with screw-in terminal blocks. Where necessary, cable ties are used to secure the wiring in place on the centrifuge arms or to the outer frame of the IGTA.

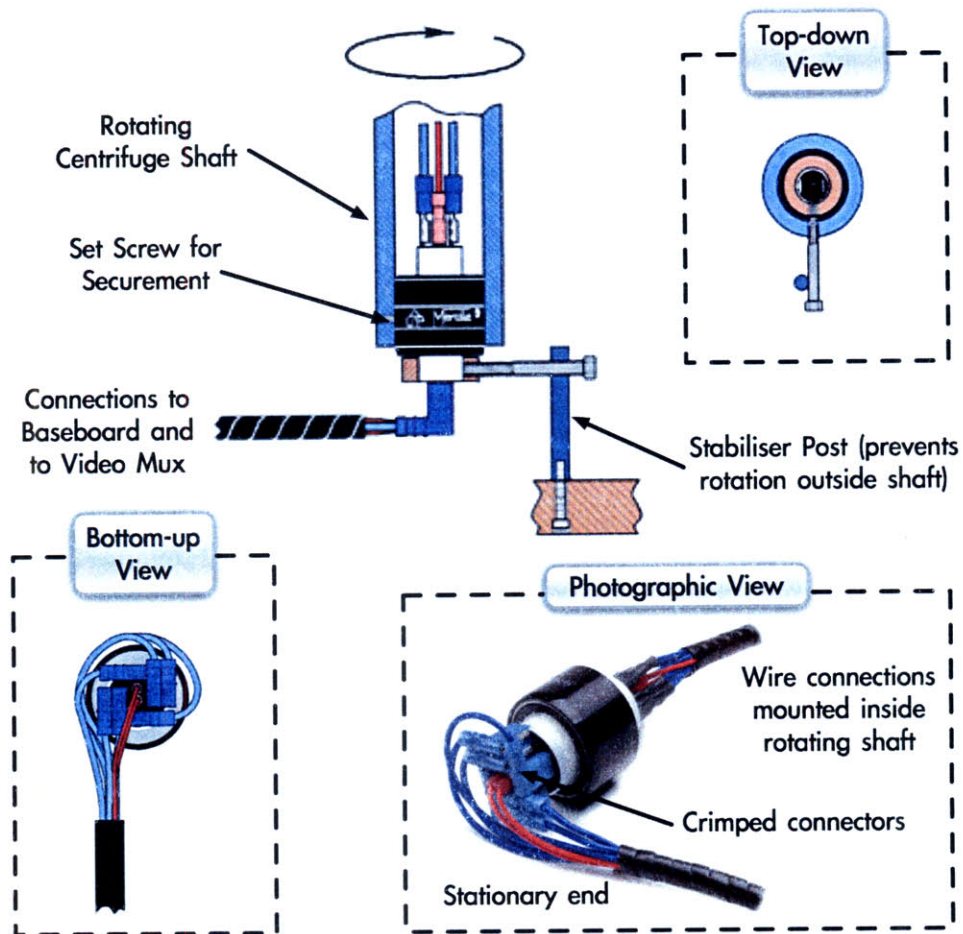


Figure 48: IGTA wiring for lower electrical connector (partial image content from Mercotac.com)

4.4 Environmental Control and Life Support

As previously reported in section 2.7, the baseline Mars Gravity ECLSS design calls for a LiOH canister to remove carbon dioxide, an active carbon bed to eliminate trace gases such as ammonia and methane, and a condensing heat exchanger to control humidity. Lithium hydroxide scrubs carbon dioxide from the air by means of a chemical reaction, while the activated carbon removes gaseous contaminants via adsorption. The condensing heat exchanger entraps and sequesters water vapour via thermodynamic processes.

In Appendix E: Ammonia Production Experiment, data is presented that quantifies the ammonia output of mice housed within high fidelity prototype ASMs. Also demonstrated is an operational validation of the proposed condensing heat exchange units, summarised in Appendix D: Condensing Heat Exchanger Design.

This section details the design and implementation of the ECLSS closed-loop apparatus incorporated within the prototype IGTA. The experimental goal was to build a system to provide life support for two mice over a multi-week period.

4.4.1 Design Overview

The core experimental philosophy was to approximate the Mars Gravity Biosatellite's spaceflight systems to a level sufficient to demonstrate proof-of-concept performance and continuous environmental control. Importantly, control of total pressure and of temperature was outside the scope of this effort. Total pressure was uncontrolled because the IGTA was enclosed within a zero pressure drop barrier membrane. Temperature was maintained at the level of the facility-wide air handling systems.

To ensure system relevance, it was essential to both (a) incorporate realistic contaminant sources, albeit in a scaled-down test scenario, and (b) include flight-equivalent ECLSS processing subassemblies where possible. The resulting system is shown in Figure 49. The design incorporates many of the same elements as the full spacecraft ECLSS layout previously shown in Figure 27 on page 65. Unlike the spacecraft design, the IGTA included no hardware redundancy, in part a consequence of funding constraints. A PC running National Instruments LabView 8.6 took the place of the iNode CPUs and provided supervisory control of all ECLSS operations.

As shown in Figure 49, the sealed ground test module comprises two separate systems, linked by the common air volume. The low pressure loop (top) is driven by fans and performs air distribution, contaminant sensing and oxygen replenishment. The high-pressure loop (bottom) is driven by a compressor; the purpose of this loop is to cleanse the cabin air. All the ECLSS elements shown were enclosed within the sealed zero-pressure barrier membrane previously described. Consequently, total pressure control (and therefore also oxygen partial pressure control) was outside the scope of this effort. Blocks outlined in red are part of the LabView supervisory control loop.

To guarantee the production of realistic contaminants, the IGTA was designed to house live mice of strain and gender identical to the cohort that will fly on board the Mars Gravity Biosatellite. Certain of the ASMs installed within the IGTA had been previously manufactured under NASA SBIR Phase II Grant 6896199, and were on loan to the Mars Gravity Biosatellite from NASA Ames Research Center.

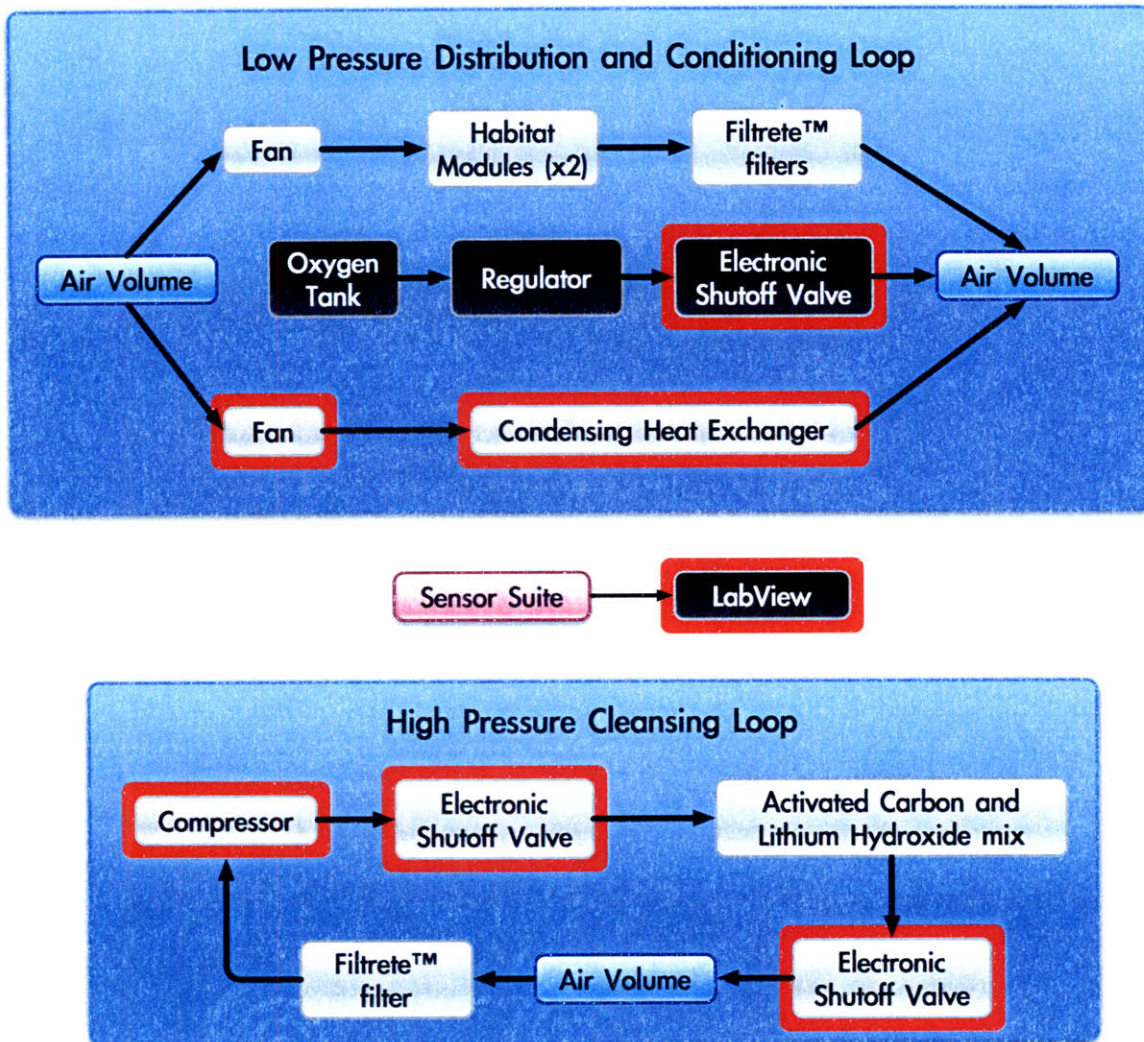


Figure 49: IGTA ECLSS design

4.4.2 Implementation

Design and construction of the ECLSS apparatus for the IGTA took place over the course of several months. First the hardware and mechanical components were designed and selected. Thereafter suitable electronic and software systems were implemented to interface with the ECLSS hardware.

The consumables in the IGTA were the oxygen within the gas cylinder, and the activated carbon/lithium hydroxide within the canister. In every case, the designs were tuned to accommodate substantially greater consumable volumes within the enclosed system than would be necessary to support two mice.

4.4.2.1 Hardware and Mechanicals for the High-Pressure Cleansing Loop

Systematically considering each element of Figure 49, this section begins by addressing the compressor at the leftmost section of the diagram. The compressor selected was the Hargraves Fluidics BTC-II's model D737-23-01 unit baselined for the Mars Gravity

Biosatellite. At its inflow port was a folded segment of Filtrete™ filter substrate, included to prevent dust and particulates from entering the diaphragm chamber of the compressor.

The compressor's outlet was attached via clear flexible polyurethane tubing of 0.48cm inner diameter to a sinusoid-operated valve. Model PV104-5V from Omega Engineering was selected for its low power consumption, 100 millisecond response time, and ability to operate with gauge pressures of up to 2.7 atmospheres. The latter parameter is significantly greater than the maximum possible pressure output of the chosen compressor.



Figure 50: The IGTA ECLSS canister for LiOH and activated carbon

After exiting the valve's 0.2 cm orifice, the air is routed into the LiOH/carbon chemical bed (Figure 50). The canister was created from a COTS equipment box manufactured from ultra high-impact copolymerised plastic for improved strength and durability. Pelican case model 1200 was selected for its favourable dimensions and airtight/watertight certification. Two holes were drilled within the centre of each of the ends in the lower (non-lidded) half of the case, as shown in the lower right of Figure 50. The holes were fitted with white polypropylene push-to-connect tube fitting adapters. They were secured in place and the outer thread was hermetically sealed using silicone caulking.

The Pelican case was fitted with an equipment panel insert, to the underside of which was attached an aluminium sheet sized to seal off the entire lid area (see left column of Figure 50). This aluminium sheet and walls and sides of the Pelican box were lined with Nomex™ fibrous padding similar to that baselined for the spacecraft.

The upper right image in Figure 50 shows a packed canister. The yellow Nomex™ padding is visible at the periphery of the vessel, while the contents includes both LiOH pellets (white) and activated charcoal granules (black).

The exit tube from the ECLSS canister routes to a second Omega PV104-5V valve from where clean air finally remixes with the general IGTA free volume.

4.4.2.2 Hardware and Mechanicals for the Low-Pressure Systems

The hardware selected to distribute air to each of the ASMs was the Comair Rotron Whiffet 12 V DC blower. It was attached to a custom-built cuboidal manifold constructed from aluminium sheet metal (Figure 51).

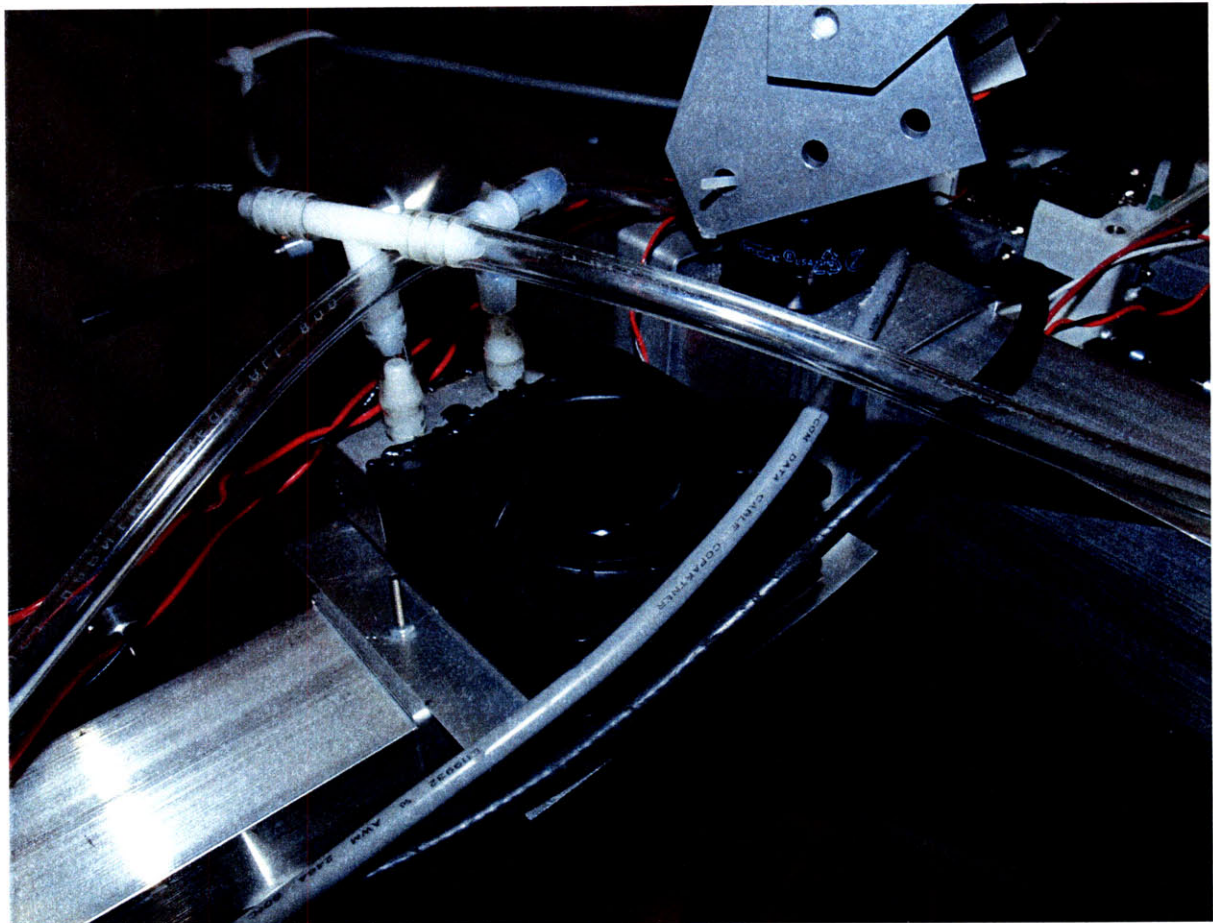


Figure 51: The air distribution manifold (fitted for 4 ASMs)

The manifold features two threaded 0.6 cm holes, into each of which was mounted a nylon barbed tube fitting suitable for interfacing with polyurethane tubing of similar type to that used in the high pressure system. The Whiffet hardware and manifold was mounted to the upper face of one centrifuge arm (Figure 51), and the protruding tubes were routed from this

location to the inflow port of each of the ASMs, secured in place with cable ties. The cable ties were intentionally kept loose to avoid crushing the tubing and restricting air flow. The air outlet of each ASM was fitted with a single wafer of Filtrete™ substrate in order to prevent particulates and dander from exiting the habitat module.

The gas cylinder was supplied and filled by Airgas East, Inc. It is 10 cm in diameter and has a height of slightly over 60 cm. It contains 200 litres of medically-certified 100% USP Oxygen at a pressure of approximately 130 atmospheres. It is fitted with Airgas product WESM1-870-PGB (a rebranded Western Medical Scientific product, model CGA 870). This regulator is appropriate for stepping down the cylinder pressure to a more usable range of 0-3 atm. The attached dial can also be used for flow control.

The outlet of the oxygen regulator attaches via polyurethane tubing to an oxygen-safe Parker Pneutronics flow control valve. The sinusoid-activated model HFPRO7VAF80 operates at pressures of over 3 atm (gauge) and is normally closed when no electrical power is supplied. The effective orifice size is 0.2 cm and the barbed body can mount to any oxygen-safe tubing of 5 mm internal diameter. Figure 52 illustrates the design.



Figure 52: The USP oxygen cylinder, regulator and Parker valve

The final elements of the low-pressure system pertain to humidity control. The fan and condensing heat exchange unit are identical to that described in section 2.7.2. A photograph of the actual fabricated unit is shown in Figure 53. A Teflon tube protrudes into the base of the measuring cylinder. The other end attaches to a fluidic micropump (Bio-Chem Valve model 120SP) that periodically sends water into a sealed condensate reservoir made from a high-durability Tupperware container. The mechanism is described in further detail in section 4.4.2.4.

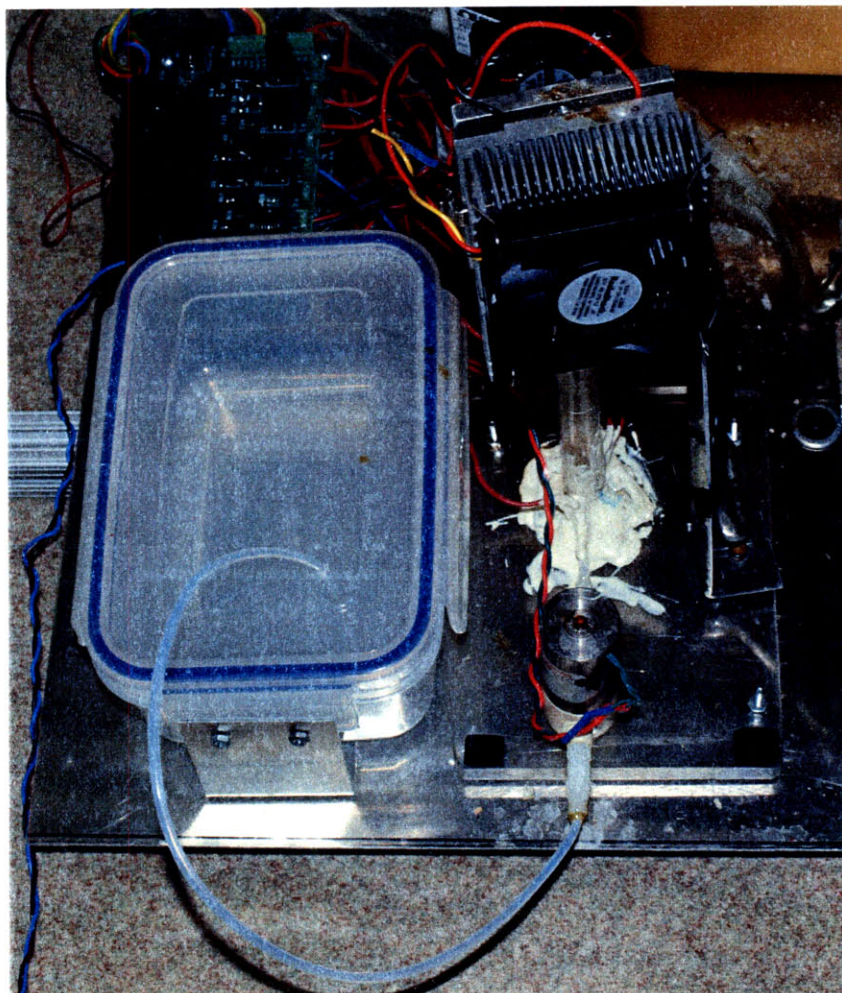


Figure 53: The CHE and pumping system as installed in the IGTA

4.4.2.3 Mounting and Securement of Hardware within the IGTA

With the exception of the ASM circulatory blower that is installed on one arm of the centrifuge, all other ECLSS components are designed to rest on the base of the IGTA. In order to form a secure attachment point, two large pieces of aluminium sheet metal were bolted onto the cross-bars that straddle the IGTA floor. Holes of various sizes were punched in both metal sheets in order to provide both screw-in and cable tie attachment options. One aluminium piece serves as a mounting plate for the oxygen tank while the other sheet secures all remaining ECLSS hardware. This includes the circuit boards, compressor, valves, chemical canister, CHE, condensate collector and condensate reservoir, in addition to assorted tubing and wiring interconnections.

4.4.2.4 Electronics and Software

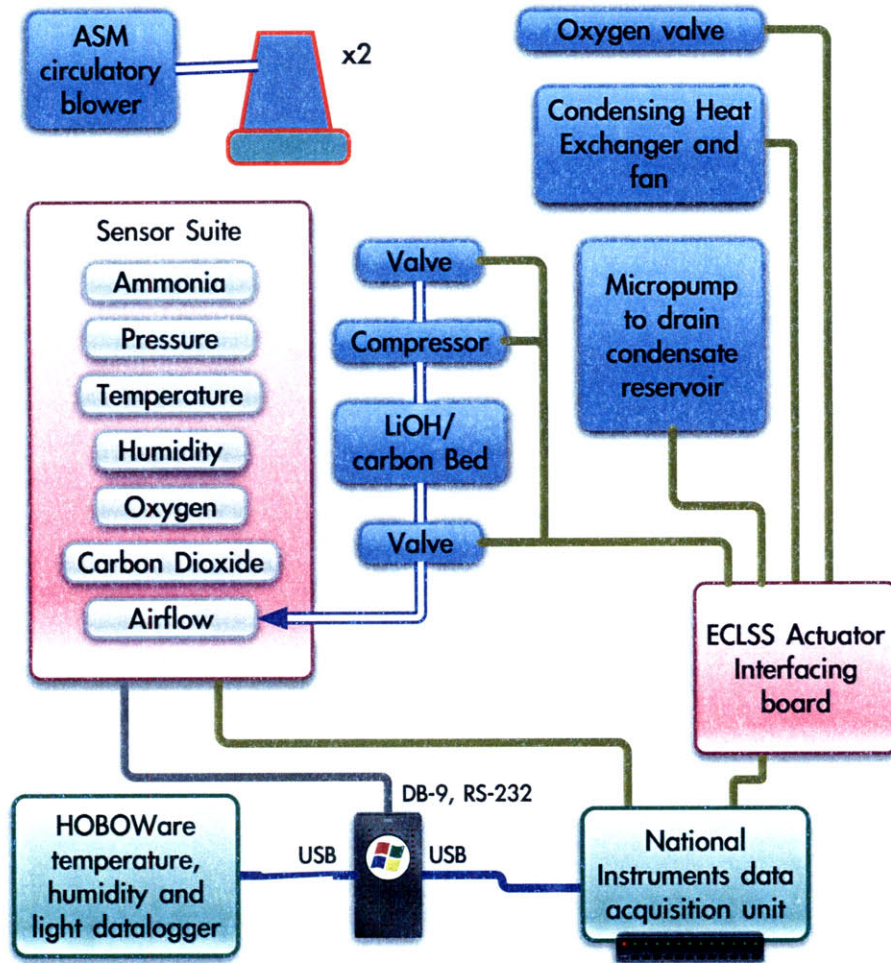


Figure 54: IGTA ECLSS implementation

Figure 54 shows the IGTA ECLSS architecture from the perspective of electronic hardware and computer software. Following the convention of previous illustrations, each red block represents a custom-designed printed circuit board while each green rectangle is a commercial off-the-shelf solution. The design incorporates the same flight-ready multifunction sensor suite previously discussed in section 0. This circuit board has higher voltage requirements than the remainder of the design and accordingly is powered directly from a dedicated 24 V DC transformer. Its data receive/transmit lines connect to the LabView PC via a DB-9/RS-232 connector.

Commercial DC transformers power the entire system. Communication between the computer and ECLSS actuators is made possible by a National Instruments USB-6229 data acquisition and interfacing module. The custom ECLSS Actuator Interfacing Board translates low-current digital signals from the NI DAQ into higher-power signals that can activate valves, compressors and heat exchangers. A CAD illustration is shown in Figure 55 and the schematic for this PCB can be found in Appendix H: Circuit Diagrams. It receives power from a dedicated 12 V DC transformer and features a collection of voltage regulators,

power transistors and signalling switches to activate and deactivate the attached hardware on command:

- The ECLSS PCB interfaces with the compressor and valves associated with the LiOH/carbon bed. Hardware design ensures it is impossible for the compressor to activate with one or both valves closed. This is a safety precaution to guard against compressor blowout or system overpressure conditions.
- The condensing heat exchange unit has high power demands; accordingly, the circuit design features a dedicated relay to transmit power directly from the on-board regulator to the thermoelectric coolers.
- The oxygen valve is enabled by a transistor circuit.
- To activate the fluidic micropump, a timer circuit is included together with an automatic water level detector that senses whether or not the condensate collector needs to be emptied. When the fluid volume in the collection cylinder rises above a certain level, the micropump starts to activate approximately once every 0.7 seconds. Each activation causes the movement of 60 μl from the cylinder to the collection reservoir. Pumping stops automatically once the cylinder has only a few drops of water remaining. This buffer volume is intentionally allowed to remain in order that the pump never has to self-prime after an extended period in the off state.

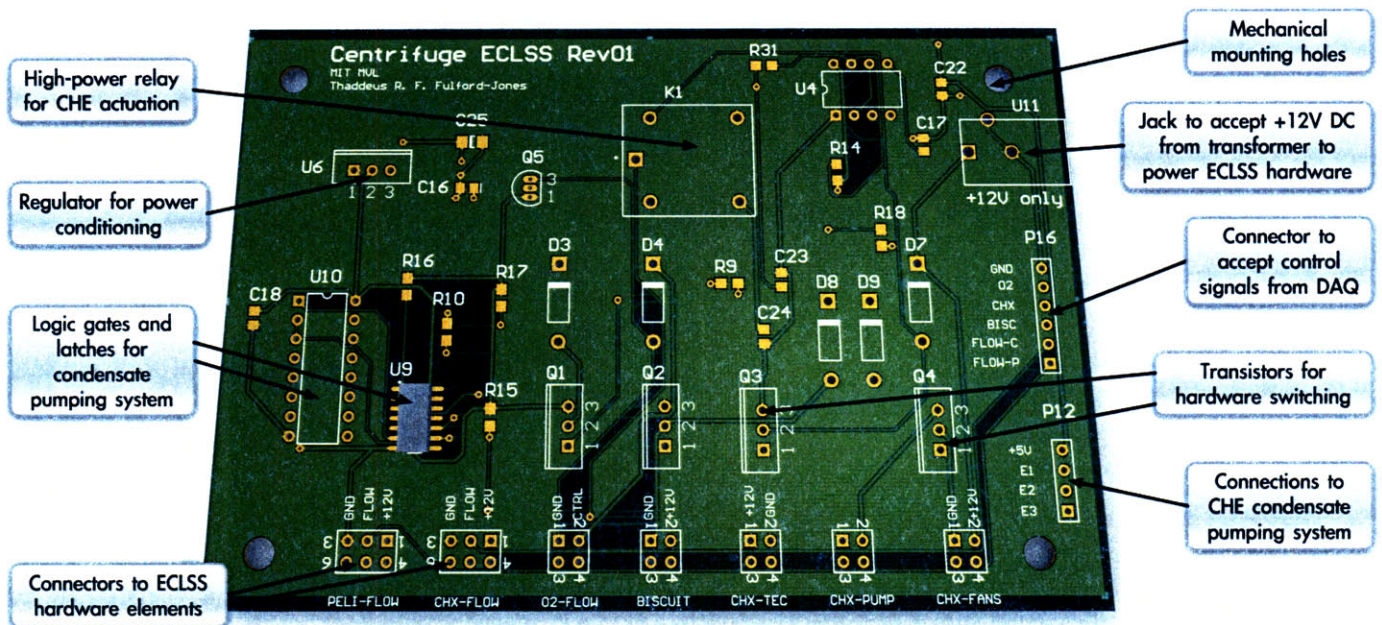


Figure 55: CAD rendering of the ECLSS Actuator Interfacing PCB

The final element of Figure 54 is the HOBO U12-012 digital data logger manufactured by Onset Computer Corporation. This inexpensive COTS component is intended as a backup unit to confirm proper operation of the Sensor Suite. The data logger is installed at the very top of the IGTA, secured to the uppermost bar of the outer framework (Figure 56).

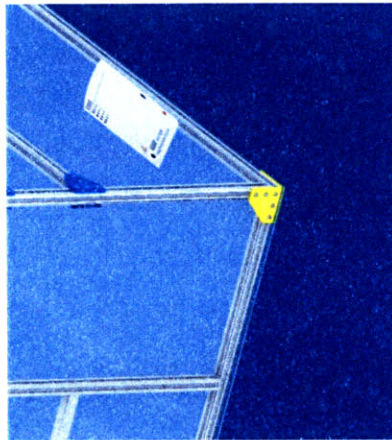


Figure 56: The datalogger within the IGTA (CAD: Kendra Toole)

The PC running custom LabView Virtual Instruments provides autonomous data aggregation and control of all IGTA ECLSS subsystems. LabView polls the sensor suite once every sixty seconds for aggregated atmospheric data. Custom control algorithms determine how the PC commands ECLSS actuators to maintain a comfortable atmospheric environment. These are explained in detail in section 6.1.

4.5 Lessons Learnt from Systems Integration

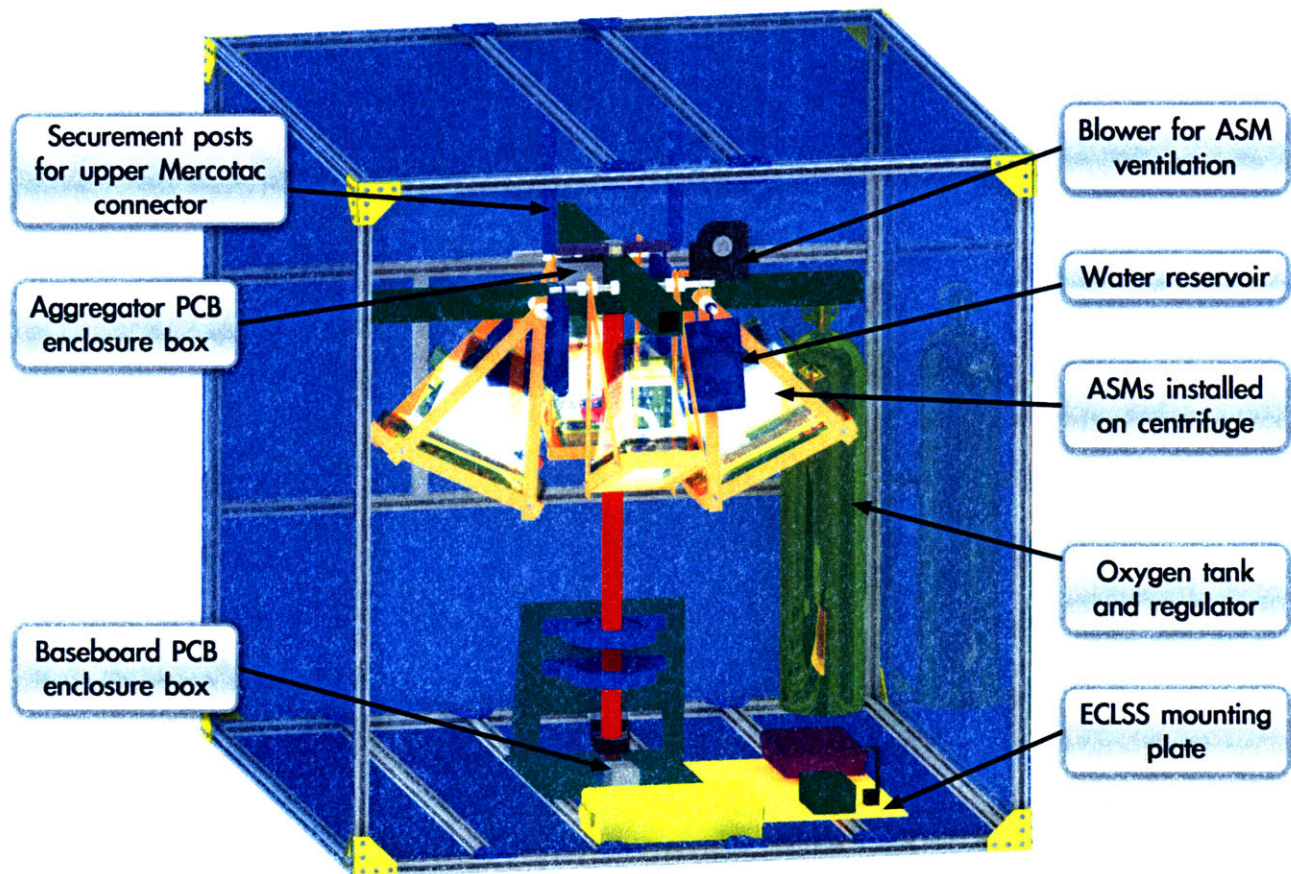


Figure 57: Fully integrated IGTA (CAD: Kendra Toole)

Substantial pilot testing was conducted before the integrated IGTA (Figure 57) could be certified as ready to accommodate live mice during experiments. The final design as described in preceding sections was arrived at only after significant testing, troubleshooting and system rework. Each printed circuit board design underwent multiple revisions as subsystem requirements and design approaches changed. In several cases, subassemblies that had functioned flawlessly during component-level testing failed to operate correctly once integrated into the IGTA. The following are key lessons learnt through the design process:

- *Printed circuit boards should be covered and enclosed whenever possible.* In early testing, a low-risk overnight pilot experiment was conducted with two mice in an open-loop atmosphere (portal door open, centrifuge not spinning). One of the ASMs sprung a leak in the water delivery system, with the result that the base of the habitat flooded and water began to drip out of the module. Unfortunately the ASM in question was positioned directly above the Baseboard PCB, which was seated in its enclosure but without the enclosure lid in place. The dripping fluid caused the board to short out with the result that the power supply transformer entered a safe shutdown mode due to a detected overcurrent situation. However, this did not occur swiftly enough to prevent substantial charring of the Baseboard module and severe component failure. This PCB had to be switched out with a replacement unit. Future protocol checklists included a line item to ensure that operators would check all enclosures before departing from an energised experiment.
- *Thermoelectric coolers draw most power immediately after startup.* The ECLSS Actuator Interfacing PCB was designed from the beginning as a system capable of routing power on the order of several Watts to the various ECLSS components. During testing, the board was observed to function flawlessly except in situations when the condensing heat exchanger was activated. At that point, the on-board low-dropout regulator would generate a severe undervoltage condition and cease to provide the necessary current to any ECLSS systems. Environmental control would fail entirely but, upon system reboot and reactivation without the CHE, operation would return to nominal. This perplexing performance was ultimately determined to be a thermal issue. Spraying the regulator with a cryogenic chemical would allow the system to reanimate, even with the CHE activated. The longer-term solution was to redesign the PCB with a higher-current regulator and a much larger heatsink. The reason for the unexpectedly large power draw was that thermoelectric coolers pull much higher currents when initially activated. Current draw rapidly reduces once the appropriate thermal differential has been established across the device. The first revision of the ECLSS Actuator Interfacing board had been designed only on the basis of observed steady-state CHE current draw.
- *Unexpected mechanical interactions can cause electrical failures.* During an extended test of the ECLSS actuators, the compressor was permitted to run as necessary to control carbon dioxide over a multi-day period. The diaphragm-gasket dual bearing design can cause substantial vibration when active. Since the compressor is secured to the same piece of aluminium as the ECLSS Actuator Interfacing PCB, these vibrations were transmitted to the circuit components via the securement posts that hold the board in place. The design change mentioned in the previous bullet had resulted in the installation of a heavier heatsink onto the regulator. The vibration from the compressor caused the heatsink to hit resonance, resulting in excessive motion of the leads that secured the regulator onto the board. The consequence was joint fatigue and fracture of the lead marked 3 in Figure 58. Note that the fracture

appears above the solder joint and is therefore truly a vibration-induced phenomenon rather than a cold solder issue. In the subsequent board revision, the heatsink posts were seated within custom holes to guard against future resonance events.

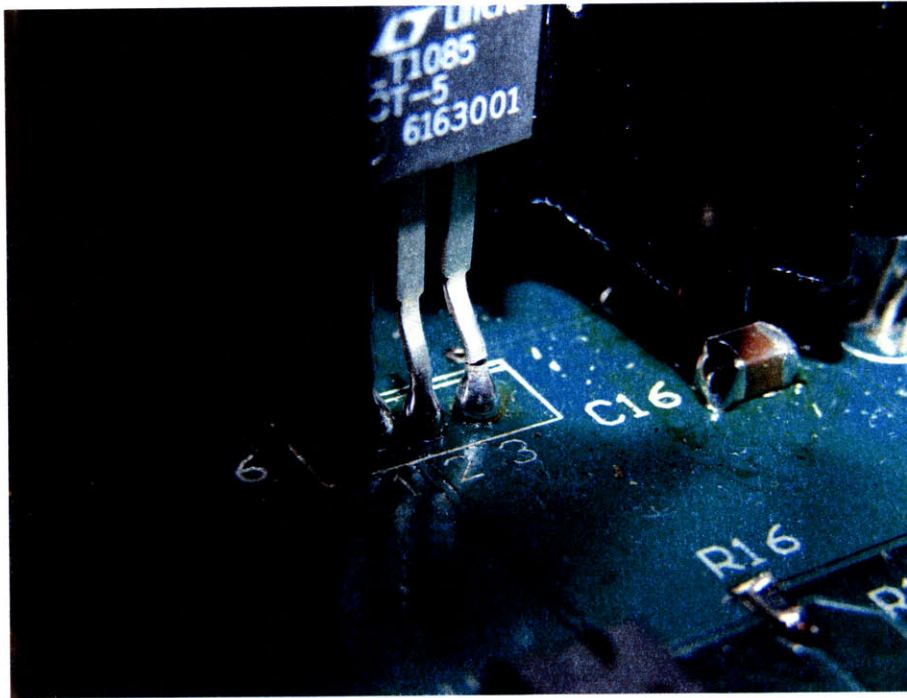


Figure 58: The rightmost lead fractured due to compressor vibration

- *Even the best sensors occasionally glitch.* Sensor Suite data averaging and selective transmission protocols were developed as a result of experimental tracking of output data over extended time periods. It was noted that a sensor would occasionally output a single erroneous datapoint before returning to nominal operation. For example, a temperature sensor might momentarily spike to over 100°C if a byte checking glitch should occur. Alternatively, random noise in low-level signals such as the millivolt readings from the oxygen sensor would occasionally cause jumps of about a percentage point. The solution was for the Sensor Suite microcontroller to be reprogrammed such that it would sample each sensor much more regularly (on average once every few seconds). When queried by the supervisory LabView PC, the Sensor Suite would transmit not only the running average but also an integer to indicate how many readings were being taken into account. By this means, it was possible to gauge the reliability of averaged data and ignore misleading samples.
- *USB 2.0 is a finely-tuned protocol that requires precision signal impedance-matching on the differential D+ and D- lines.* The USB standard began to replace serial modem communication protocols in the 1990s. Since then, subsequent iterations of USB (1.1, 2.0, High-Speed, etc.) have increased the bandwidth and opened new possibilities for high-throughput video and media applications. The original IGTA design specifications called for USB 2.0 cameras to be installed within each ASM. It was considered that the high-speed digital signal would be more robust to noise from the Mercotac rotating electrical connector than the analogue alternative. However, the very act of cabling the USB signal through the Mercotac unit proved highly problematic. Breaking a manufactured USB cable involves removing shielding,

resoldering wire groups and changing impedances – no matter how much caution is employed. Since the high-throughput USB standard is heavily dependent on accurate timing, it proved impossible to ever get a suitable signal lock on the stationary side of the Mercotac connector. Even reworking the system with a USB hub installed on one of the spinning centrifuge arms failed to solve the problem. In a final attempt to resurrect the (already purchased) USB cameras, an effort was made to transition the entire system to the brand new Wireless USB standard that was officially ratified in 2007. This new version of the protocol aims to provide speeds equivalent to USB 2.0 via radio over a distance of several metres. Unfortunately Wireless USB is not guaranteed to be compatible with time-sensitive applications such as web cameras or (as in this case) high-specification scientific digital cameras. Despite repeated attempts, it was impossible to achieve frame rates of better than about 1 fps. Ultimately, the decision was made to purchase a new set of analogue NTSC cameras and to redesign each of the ASM lighting boards in order to accommodate the smaller lens and mounting plate of the new model.

- *Incorrect alignment and insufficient heading space in a rotating system can rapidly lead to metal fatigue and cable failure.* In an early design iteration of the centrifuge hardware, there was minimal space beneath the baseplate. The volume was barely sufficient to route wires from the stationary side of the lower Mercotac connector out toward the NI DAQ, video multiplexer and LabView PC. Because no spinning system can ever be perfectly aligned, it was not unusual for the wires to move back and forth by about 1mm while the centrifuge was powered. Because there was so little space beneath the baseplate, this caused the cables to rub against the floor of the experimental cubicle. It only later became clear that the friction from the continual rubbing was being converted into lateral forces that were transmitted to the protruding metal paddles at the base of the Mercotac connector. After about 24 hours of operation, this continual fatigue caused the two smallest Mercotac paddles to snap, with the result that a video feed was lost together with one grounding connection. The solution was to move the baseplate and entire centrifuge upwards by about 3 centimetres through the use of a spacer stack. The Mercotac connector was replaced and no similar failures were observed thereafter.

Chapter Five: Results of a Chronic 5-Week Rotation Experiment

5.1 Motivation

The goals of this experiment were originally stated in section 1.2 and are reproduced below. The objectives were:

- To scientifically evaluate the effects of chronic centrifugation using habitat modules and instrumentation identical to that proposed for the Mars Gravity Biosatellite.
- To thereby explore the effects of chronic centrifugation (if any) and to confirm that they can be quantified and therefore decoupled from the anticipated effects of chronic hypogravity exposure.

To meet these objectives, an experimental protocol was drawn up and proposed. It was reviewed and approved by the MIT Committee on Animal Care prior to implementation (see Appendix I: CAC Protocols). The protocol proposed the following:

- As a control study, four female BALB/cByJ mice would be placed in the ASMs on the static IGTA for five weeks.
- For the rotational study, the same four mice would subsequently undergo chronic centrifugation at 31.6 rpm on the IGTA.

The mice were to be 14.5-25.5 weeks of age at the start of both the control and the rotational periods. It was hypothesised that the mice would survive while maintaining normal body mass and would exhibit behaviour indicative of vestibular adaptation to this rate of rotation. Specifically, the hypotheses as stated in section 1.2.1 were as follows:

- Hypothesis 1. Body mass at the end of a 5-week period will be no less than at the start of the experiment.
- Hypothesis 2. Mean water consumption will normalise to within 15% of that exhibited by non-rotating animals.
- Hypothesis 3. Video-derived behavioural metrics will normalise to within one standard deviation of those exhibited by non-rotating animals.
- Hypothesis 4. Performance in open field testing, rotarod running, balance beam walking and air-righting will normalise to within one standard deviation of those exhibited by non-rotating animals.

5.1.1 Justification for Choice of Discrete Behavioural Tests

The open field test is a simple type of assessment which is useful in determining general activity levels, gross locomotor activity and exploratory behaviours in mice. A 5-minute session is considered sufficient to detect significant hyperactivity or lethargy (Crawley 2007). Open field testing of longer duration can provide an indication of stress levels and anxiety, in addition to a measure of the time course of habituation. In the IGTA experiments there was a strong incentive to minimise centrifuge stoppage times, and accordingly the 5-minute open field test was considered the maximum acceptable duration.

Motor coordination and balance are measured by performance on the rotarod. Accelerating automated rotarods ramp up from 4 rpm to 40 rpm over a 5-minute period. They offer a more stringent measure of motor coordination since the requirements for running forward are gradually increasing over the course of the trial. One limitation of the rotarod is that the device design prevents observation of gait.

Balance beam walking evaluates the ability of mice to traverse a narrow beam to reach an enclosed safety platform (Crawley 2007). Since cameras can be trained on both sides of the beam, any gait impairment is readily apparent. This test also provides a clear visual indication of balance-related performance anxiety. Mice which are uncertain of their ability to successfully traverse the beam will proceed cautiously with frequent stops.

Air-righting evaluates balance ability while falling. Since this instinctive reaction is largely genetically determined, only a very severe balance impairment would impact results on this type of experiment.

5.1.2 Justification for Use of In-Habitat Video

The Mars Gravity Biosatellite will feature in-habitat video as a primary means of data gathering for the five-week mission. In-habitat video analysis was included in this ground experiment for reasons of test relevance and to explore the capabilities and limitations of extended-duration monitoring.

5.2 Apparatus

The IGTA as described in Chapter 4 was the core apparatus for this study. For the purpose of this experiment, the barrier membrane was detached and removed from the outside of the frame. All environmental control systems were deactivated with the exception of the on-centrifuge blower that operated continuously to move fresh air into each of the specimen chambers. Atmospheric composition and temperature/humidity regulation was managed at the level of the facility-wide air handling systems that guarantee in-cubicle ventilation rates of at least 60 air exchanges per hour.

Prior to the start of both the control and the experimental study, the IGTA was fitted with four clean, reconditioned ASMs. New waste collection media rolls were installed into the WCS and each water reservoir was filled to a volume of 250 ml. Fresh NASA rodent food bars were removed from refrigeration and cut into segments each of approximate dimensions 3.2 cm by 2.3 cm by 10.2 cm. Four such segments were adhered to the wall of each specimen chamber using rodent-safe EP21LV epoxy and following NASA-recommended procedures (Tou, Grindeland *et al.* 2003). To allow time for the epoxy to harden, this operation was completed 24-48 hours prior to the first insertion of mice. The amount of food and water provided was significantly greater than necessary for a five-week period.

5.2.1 Video Analysis of Mouse Behaviour

On board the Mars Gravity Biosatellite, a video acquisition and digitisation system will enhance in-flight collection of data on sensorimotor adaptation. To mirror this capability on the ground, Noldus Ethovision XT 5.0 R2 was installed on the PC that manages IGTA operations. This best-in-class software product is used by researchers across the world for automated animal behavioural analysis. It is specifically designed for compatibility with the Picolo Diligent video acquisition board. The software build used in this experiment was equipped with the Multiple Body Points module and the Multi Arena add-on package. Together, these enabled nose- and tail-detection while also permitting decoding and analysis of the 4-in-1 video picture generated by the multiplexer.

A broad base of research exists using mice with Ethovision XT (Wang, Li *et al.* 2005; Gould, Einat *et al.* 2007). The software is commonly used with transgenic mice to explore anxiety-related behaviour, neural dysfunction, and in various systems biology investigations. Metrics of comparison include data such as total distance moved in a 60-minute period, momentary radial speed (for circular cage designs), median lingering durations (for open field tests) and percentage of time spent moving. Researchers have investigated wall versus centre behaviour as a means of determining anxiety levels (Lipkind, Sakov *et al.* 2004). Statistical methods used to analyse Ethovision output files are experiment-specific but include ANOVA models of various types, direct comparisons of means, General Linear Models, mixed hierarchical regressions, cross-correlations and 2-tailed t-tests.

This experimental proposal called for the use of Ethovision XT to automatically derive a wide range of metrics before focusing in on any that may reflect adaptation and other behavioural changes. The software was programmed to generate day-by-day comparisons between the control and experimental groups. This output format was appropriate for analysing the time-dependent nature of any behavioural adaptation.

5.3 Methods

A group of four mice were first deployed in a five-week control study to ascertain the baseline behaviour. Subsequently, this same group of mice was chronically rotated for five weeks. Continuous 24-hour in-habitat video observation was used in both studies, except for during occasional required maintenance events. Video from the night-time periods 12midnight-6am or 1am-7am was subsequently analysed with Ethovision XT. The switch in timing was due to the annual springtime change to Daylight Saving Time. It was appropriate to analyse night-time footage because mice are nocturnal creatures that normally exhibit higher activity levels in low light conditions. Daytime footage would have been less interesting because the rodents typically spent most of the day sleeping.

The rodents underwent body massing, rotarod, balance beam, video air-righting and video open field testing on days 0, 18, 35 and 36 of each test. Day 0 testing took place within a 90-minute period immediately prior to the start of each study (control and rotational). Day 36 was one day after the end of the five-week study. Efforts were made to conduct scheduled testing between the hours of 15:00 and 19:00 whenever possible.

Table 30 summarises all centrifuge stoppage events. In general, the mice were outside their ASMs and not rotating for the entire duration of each scheduled testing event. As shown in the aforementioned table, scheduled testing events lasted 60-75 minutes in all but two cases:

- On Control Day 0, a misconfigured high-speed video camera contributed additional downtime with the result that the total testing period was 90 minutes.
- On Rotation Day 18, total non-spinning time was 103 minutes. This duration was unusually long because the animals performed certain tests more slowly on this day and this stoppage also included an unscheduled maintenance period.

Table 30: Centrifuge stoppages

Day	Date	Event Description	Start Time	Duration
Control Day 0	16 February 2008	Scheduled Testing	16:15 EST	90 min
Control Day 18	5 March 2008	Scheduled Testing	16:34 EST	75 min
Control Day 35	22 March 2008	Scheduled Testing	11:24 EDT	65 min
Control Day 36	23 March 2008	Scheduled Testing	16:02 EDT	65 min
Rotation Day 0	28 March 2008	Scheduled Testing	17:05 EDT	60 min
Rotation Day 3	31 March 2008	Maintenance Stoppage	18:50 EDT	10 min
Rotation Day 8	5 April 2008	Maintenance Stoppage	15:49 EDT	3 min
Rotation Day 15	12 April 2008	Maintenance Stoppage	13:29 EDT	9 min
Rotation Day 16	13 April 2008	Maintenance Stoppage	09:04 EDT	2 min
Rotation Day 18	15 April 2008	Scheduled Testing and Maintenance Stoppage	17:26 EDT	103 min
Rotation Day 19	16 April 2008	Maintenance Stoppage	23:09 EDT	30 min
Rotation Day 23	20 April 2008	Maintenance Stoppage	18:22 EDT	18 min
Rotation Day 26	23 April 2008	Maintenance Stoppage	17:38 EDT	8 min
Rotation Day 35	02 May 2008	Scheduled Testing	16:32 EDT	69 min
Rotation Day 36	03 May 2008	Scheduled Testing	15:36 EDT	65 min

All seven other maintenance events required stoppages lasting less than 30 minutes, and in all but two cases the stoppage duration was 10 minutes or less. During maintenance, the animals remained in their ASMs but the centrifuge was not spinning. The target stoppage time was intentionally less than 30 minutes. This period was considered reasonable by rodent hypergravity expert Dr. Chuck A. Fuller in a personal communication with the author (Fuller 2007). It is consistent with rat studies in which daily stoppage periods of under 30 minutes were considered to have no adverse impacts on the validity of experimental results (Oyama and Platt 1967; Oyama, Platt *et al.* 1971).

5.3.1 Mouse Ages

The rodents to fly on board the Mars Gravity Biosatellite will be female BALB/cByJ mice of age 14.5-25.5 weeks at launch. The 4 mice used in this ground experiment were female BALB/cByJ specimens, all of which were born on the same date (2nd October, 2007). At the start of the control study on 16th February, 2008, the mice were aged 19 weeks and 4 days. At commencement of the rotational study on 28th March, 2008, the rodents were aged 25 weeks and 3 days. This purposely matched the aforementioned projected flight age requirements. The baseline assumption was that performance on the entire test battery would not be significantly impacted by age-related development during the 20-31 week age window. This is a reasonable assumption because the rodents had already reached reproductive maturity, which occurs no later than 8 weeks of age for this strain.

5.3.2 Atmospheric Environment

The system was continuously exposed to the atmospheric environment provided by the central building air handling systems. Cubicle humidity was measured during both control and rotational studies and was found to be between 30% and 50% RH.

5.3.3 Procedural Details

Tests were conducted in accordance with the directions given in Jacqueline Crawley's highly-regarded text "What's Wrong with My Mouse?" (Crawley 2007).

5.3.3.1 Mouse Acclimation

Prior to the start of the control study, all four mice had been singly-housed in standard laboratory caging for multiple weeks. 48 hours prior to commencement of the experiment, the rodents were transferred to the ASMs that featured fully-operational drinking nozzles and flight-equivalent provision of food. The rodents remained in these habitats for approximately 18 hours before being extracted and restored to standard caging for about 6 hours while final ASM maintenance and electronic checks were completed. Thereafter the mice were reinstalled within the ASMs for a full 24 hours prior to the commencement of "Day 0" testing as further described below.

At the conclusion of the five-week control study, the rodents were transferred to four standard laboratory cages. They remained in these cages until the start of the rotation study six days later. Following "Rotation Day 0" testing, they were installed into the cleaned and reconditioned ASMs and the IGTA centrifuge was activated.

5.3.3.2 Body Mass

The mice were each weighed on a scale with resolution 0.1 g on days 0, 18, 35 and 36.

5.3.3.3 In-Habitat Video

The IGTA's greyscale NTSC video monitoring system together with the 4-input multiplexer and PCI-based video acquisition card was programmed to record continuously to MPEG-4 files. The resulting footage was post-processed by Noldus Ethovision XT. The recording rate of 10 frames per second matched that recommended by Noldus Information Technology for behavioural analysis of mice.

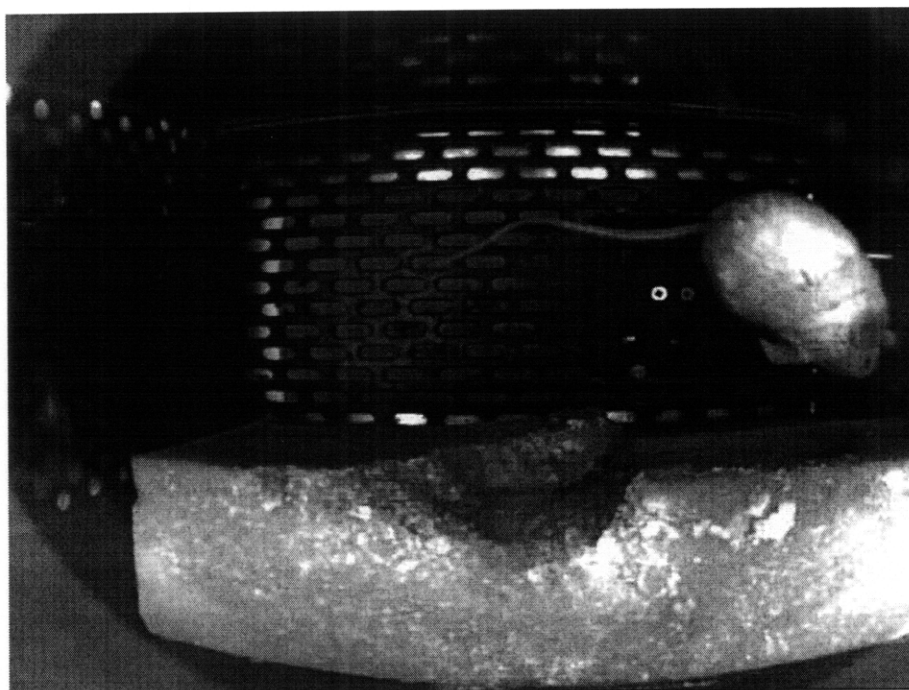


Figure 59: A representative video frame from early pilot studies

5.3.3.4 Video of Open field Test

Four open field enclosures were constructed for the purpose of these experiments. Each enclosure comprised a floor made of rigid 1 cm thick durable plastic together with four walls constructed from aluminium sheet metal. The walls were secured to one another with pop rivets and were approximately 10 cm tall once mounted to the enclosure floor. Each enclosure floor measured 40 cm by 40 cm, in accordance with recommendations by Crawley (2007).

At least 24 hours prior to use, each open field unit was sprayed down with Quatricide – a germicidal detergent, disinfectant and deodorant approved for use in rodent facilities. Once the enclosure was dry, a sheet of black wrapping paper was used to line the base. The black paper provided a uniform background colour to contrast with the white albino mice for optimal video tracking performance. After each usage, the paper was discarded to remove any faecal boli and urine, together with any odours that could potentially have impacted animal behaviour during subsequent sessions.

For the purposes of video analysis, the four enclosures were placed adjacent to one another as shown in Figure 60. A digital video camera was mounted on a tripod directly overhead. The lens angle and tripod extension length were adjusted to create a field of view sufficient to monitor all four enclosures simultaneously. Figure 61 shows a video frame from one open field trial.

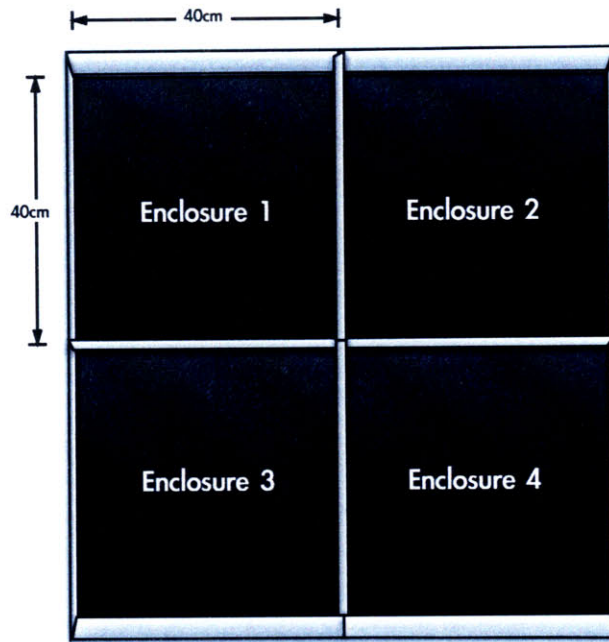


Figure 60: The four open field enclosures configured for video capture

Each open field test episode was of duration four minutes and commenced once all four animals had been placed by the experimenter in the centre of each enclosure. According to Crawley (2007), “a 5-minute test session in a novel open field provides a measure of exploratory locomotion in a novel environment.” She notes that this is substantially shorter than the time required to habituate to the novelty (generally 30 minutes to two hours). The footage was post-processed using Ethovision XT.

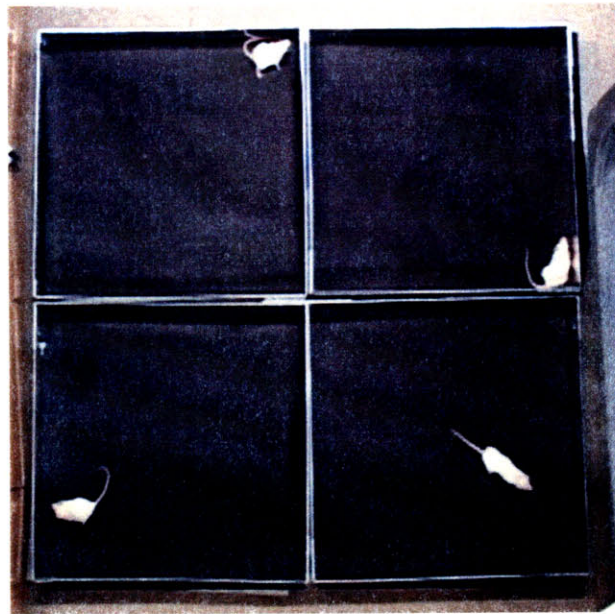


Figure 61: Representative video frame from open field testing

5.3.3.5 Rotarod

Rotarod testing was conducted in accordance with guidelines published in “Methods of Behavior Analysis in Neuroscience” (Buccafusco 2000) and in “What’s Wrong with My Mouse?” (Crawley 2007). All four animals were tested simultaneously using a ramp-up from 4 rpm to 40 rpm over 5 minutes. The mean time until falling was calculated for each animal over three trials (Figure 62). An experimenter was present with a stopwatch as a backup in case a falling mouse failed to trigger the photocell upon landing.

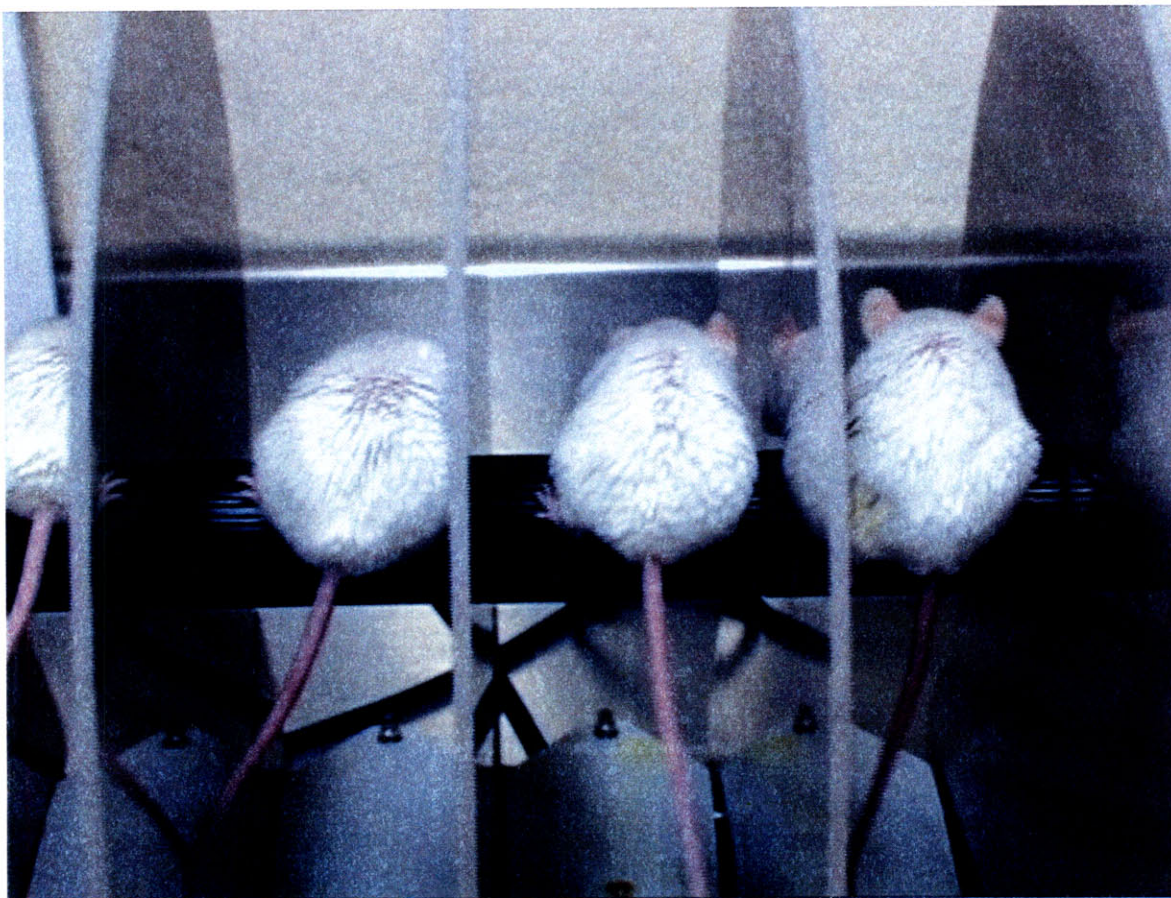


Figure 62: Rotarod testing

The experimenter also noted any cases of mouse non-compliance, which in these trials manifested itself as a mouse clinging and rotating with the rod. This occurred only in rare cases. Without exception, the clinging animal fell off the rod within a few seconds of the first 360° of riding. Accordingly, in these situations the recorded “time-until-fall” was approximated as the instant at which riding around first commenced.

Crawley shows data that suggests mice improve their performance (i.e. they learn to do the rotarod task better) when given three consecutive 5-minute sessions with acceleration from 4 rpm to 40 rpm. Repeating this training regime five or more times prior to a experiment can help ensure there is no learning/habituation effect during the study itself. The schedule shown in Table 31 was used to pretrain the animals and ensure full acclimation to the rotarod prior to the start of the control study. The training regime was never conducted more than twice per day in order to avoid fatiguing the mice.

Table 31: Rotarod pretraining schedule

Detail	Date	Time of Day
Pretrain Session 1	22 January 2008	Morning
Pretrain Session 2	22 January 2008	Evening
Pretrain Session 3	23 January 2008	Morning
Pretrain Session 4	23 January 2008	Afternoon
Pretrain Session 5	26 January 2008	Afternoon
Pretrain Session 6	28 January 2008	Evening
Pretrain Session 7	01 February 2008	Afternoon

5.3.3.6 Beam Balance / Walking

Following guidelines published in Crawley (2007), a beam approximately 6 mm wide and 80 cm in length was suspended approximately 50 cm above a cushioning pad. Each rodent was placed on one end of the beam whereupon they instinctively began to walk toward the opposite end (Figure 63). At the destination end of the beam was positioned a plastic enclosure (retreat). The beam was covered with 240-grade sandpaper for improved rodent paw grip. The trial was considered complete once the rodent reached the retreat. Each trial was repeated three times.

Two video cameras were used to track the left and right sides of the balance beam while the rodent walked from one end to the other. Subsequent visual assessment of the footage generated a count of the number of footfaults, defined as steps for which the forepaws and/or hindpaws slipped from the horizontal surface of the beam. In general, the animal was permitted sufficient time to perform the task. However, in some cases the mouse would freeze in place and fail to move for an extended period. This would occasionally happen when the rodent was very close to the retreat but had no interest in entering the enclosure. If it had still not moved after sixty seconds, the trial was aborted and recorded as incomplete. Percentage footfault data over the distance covered while the animal was moving still provided a meaningful metric for these trials.

To pretrain the animals and ensure full acclimation to the balance beam, it was necessary to perform a set of three balance beam repetitions on each of two days prior to commencement of the control study. Following recommendations in Buccafusco (2000), the animals were given at least 24 hours to recover between these two tests (Table 32).

Table 32: Balance beam pretraining schedule

Detail	Date	Time
Pretrain Session 1	28 January 2008	Evening
Pretrain Session 2	01 February 2008	Afternoon

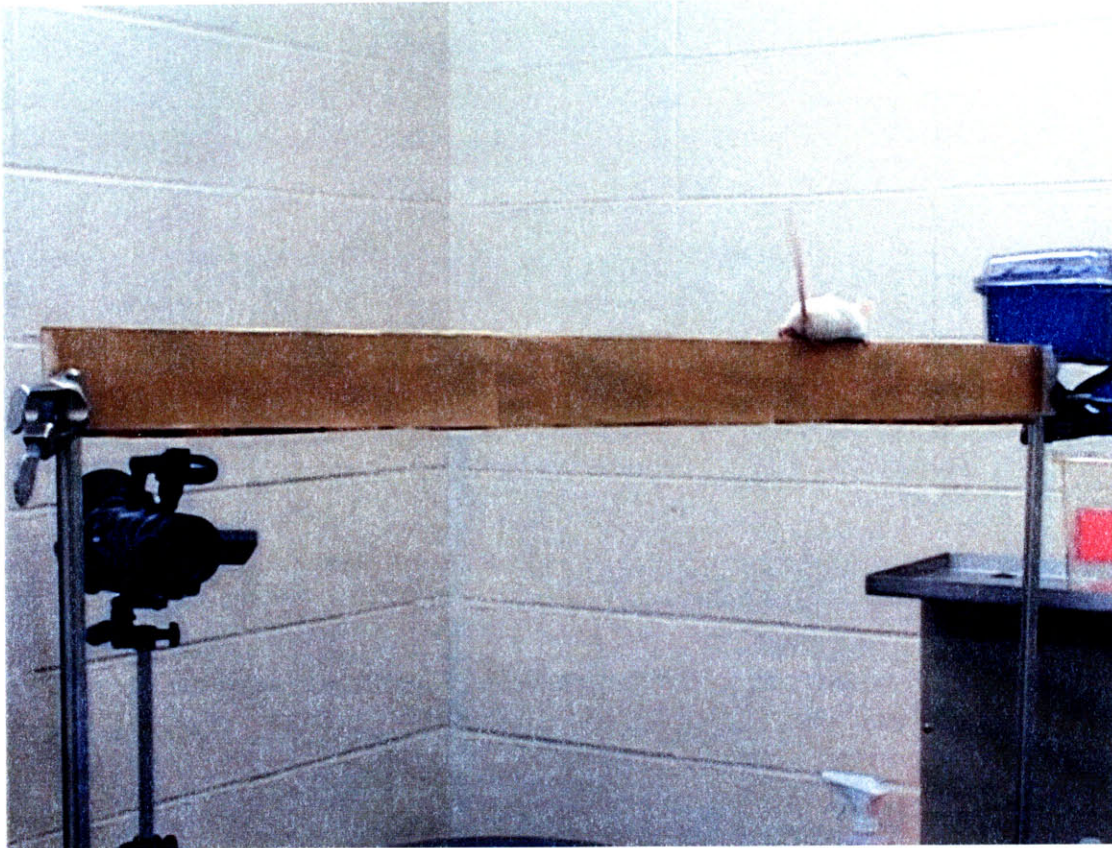


Figure 63: Beam balance / walking

5.3.3.7 Air Righting

Following procedures previously used by the Mars Gravity group, each animal was supinely inverted and held by the scruff of its neck at a height of approximately 50 cm above a soft cushioned pad. A high-speed (125 fps) video camera and infrared light source was used to record the specimen's behaviour while falling. Subsequent frame-by-frame viewing of the video footage permitted an assessment of the amount of time taken for the rodent to reorientate itself such that it was ready to land on its paws. Each air righting trial was repeated three times. Figure 64 shows a sequence of representative video frames during a single drop test. For experimental consistency, the animal was handled and dropped by the same researcher (the author) every session.

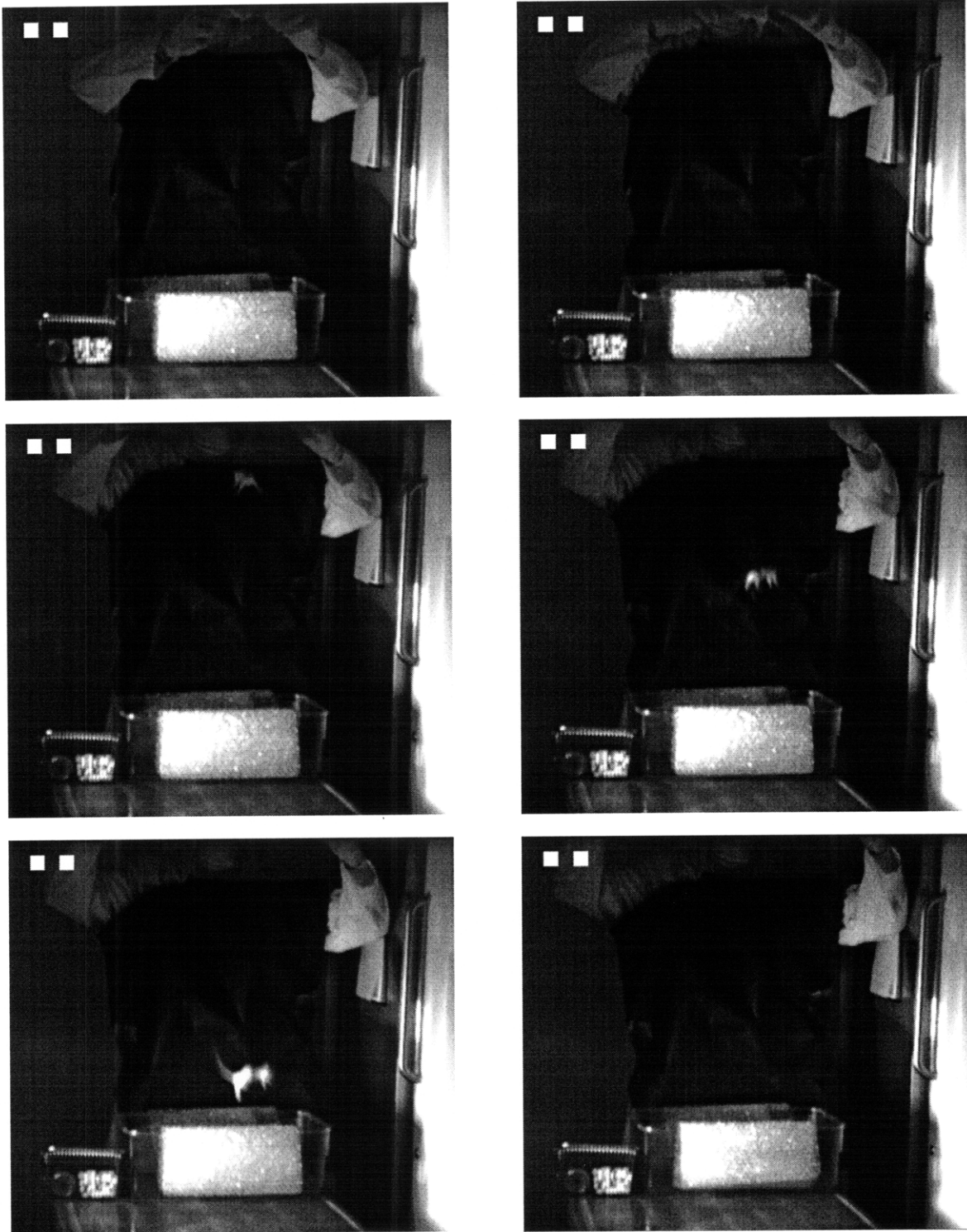


Figure 64: Air righting

5.3.3.8 Cross-Balanced Design

On each test date, the animals were extracted from the ASMs and placed within numbered standard laboratory holding cages (Mouse 1 to Cage 1, Mouse 2 to Cage 2, etc.) on a wheeled cart. Extraction of all animals always took place within 5 minutes, timed from the

moment the first ASM was opened to the instant the fourth mouse was placed in its holding cage.

Once all four mice had been extracted, the holding cages were lidded and the cart was wheeled to the experimental procedure room. Body mass was recorded and each mouse was placed on the rotarod unit for three consecutive trials. Thereafter, all mice underwent open field testing.

Systematic enumeration of testing order applied only to the balance beam and air righting tests that took place after the open field experiment had completed. In contrast with the rotarod and open field tests, only one animal at a time could perform these trials. All the balance beam tests were conducted first, and the air righting drop tests followed immediately thereafter. Air righting was intentionally left to the end because of the potential for animals to become frightened or agitated after being dropped multiple times. Testing was conducted in the order shown in Table 33.

Table 33: Enumeration of test order for air righting and balance beam

Day	Mouse 1	Mouse 2	Mouse 3	Mouse 4
Control Day 0	First	Second	Third	Fourth
Control Day 18	Fourth	First	Second	Third
Control Day 35	Third	Fourth	First	Second
Control Day 36	Second	Third	Fourth	First
Rotation Day 0	First	Second	Third	Fourth
Rotation Day 18	Fourth	First	Second	Third
Rotation Day 35	Third	Fourth	First	Second
Rotation Day 36	Second	Third	Fourth	First

After the end of testing on Rotation Day 35, the animals were returned to the IGTA ASMs. The centrifuge was left inactive so that an additional two nights of video footage could be recorded. These files were analysed to search for evidence of readaptation following withdrawal of the rotational stimulus.

5.4 Results and Discussion

This section discusses in turn results concerning each of the four hypothesis statements outlined in section 5.1.

5.4.1 Body Mass and General Appearance

Hypothesis 1: Body mass at the end of the five-week rotational study would be no less than at the start of that period.

Figure 65 shows that the four rodents exhibited a healthy degree of weight gain during their five weeks in the non-rotating control configuration. It includes readings for “Day Minus-2” that were recorded 48 hours prior to the start of the test in order to confirm the baseline body mass before the animals were installed in the ASMs. All y-axis error bars denote standard error.

The animals were almost 20 weeks of age by the start of the control study. Accordingly, the recorded body mass increase cannot be attributed to development and was instead due to weight gain on account of low stress and sustained normal food and water consumption. The mean body mass increased by 2.7 g, from 23.7 g to 26.4 g, between Day Minus-2 and Day 36.

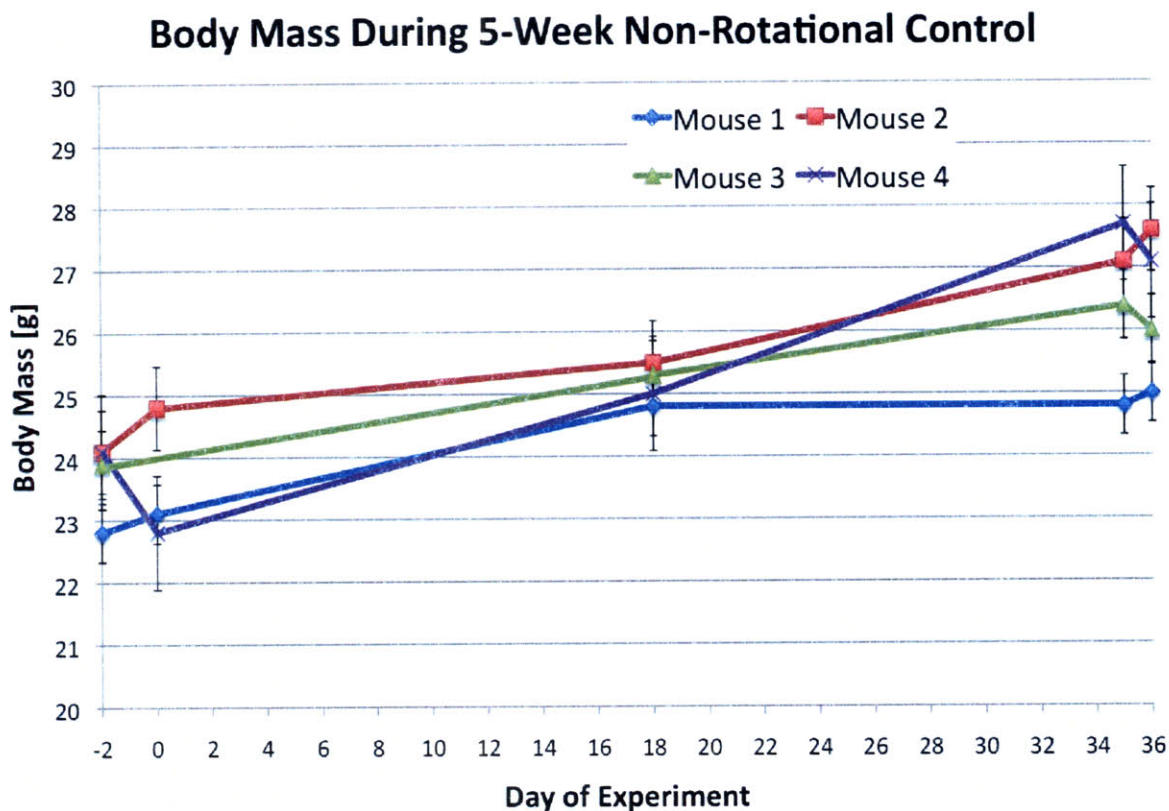


Figure 65: Body mass during non-rotational control experiment

Following extraction from the ASMs at the culmination of the five-week control study, the animals appeared alert, inquisitive and unstressed. A coat pinch test revealed no detectable dehydration and examination of foot pads indicated no abrasion or other cause for concern. No tooth malocclusion was observed. Coat sheen was generally good, and the rodents exhibited only very mild scruffiness consistent with five weeks in a bedding-free habitat module. Hair loss as noted by accumulation within the WCS and on the floor of the specimen chamber was minimal in all cases.

Between the control and the rotational studies, the animals were singly-housed in standard laboratory mouse cages for a period of 6 days. During this time the animals maintained the same body mass, to within error. Figure 66 shows results from the subsequent rotational study. Importantly, body mass at the end of the 5-week period was the same as at the start (means of 25.7 g and 25.5 g respectively). However, the Day 18 reading is of great interest.

By this point in the study, each of the animals had lost an average of 2 g in body mass. On this day, as on every day recorded in Figure 66, the animals did not appear dehydrated and there was no indication of ill health. Vertical error bars indicate standard error.

Following the rotational experiment, all rodents were singly-housed in standard laboratory cages. Periodic observation of the specimens confirmed that all animals remained healthy. They maintained good body mass after their time in the IGTA; the Rotation Day 36 mean of 25.5 g was the same to within error as the 26.1 g average recorded 22 days later.

Body Mass During 5-Week Rotational Study

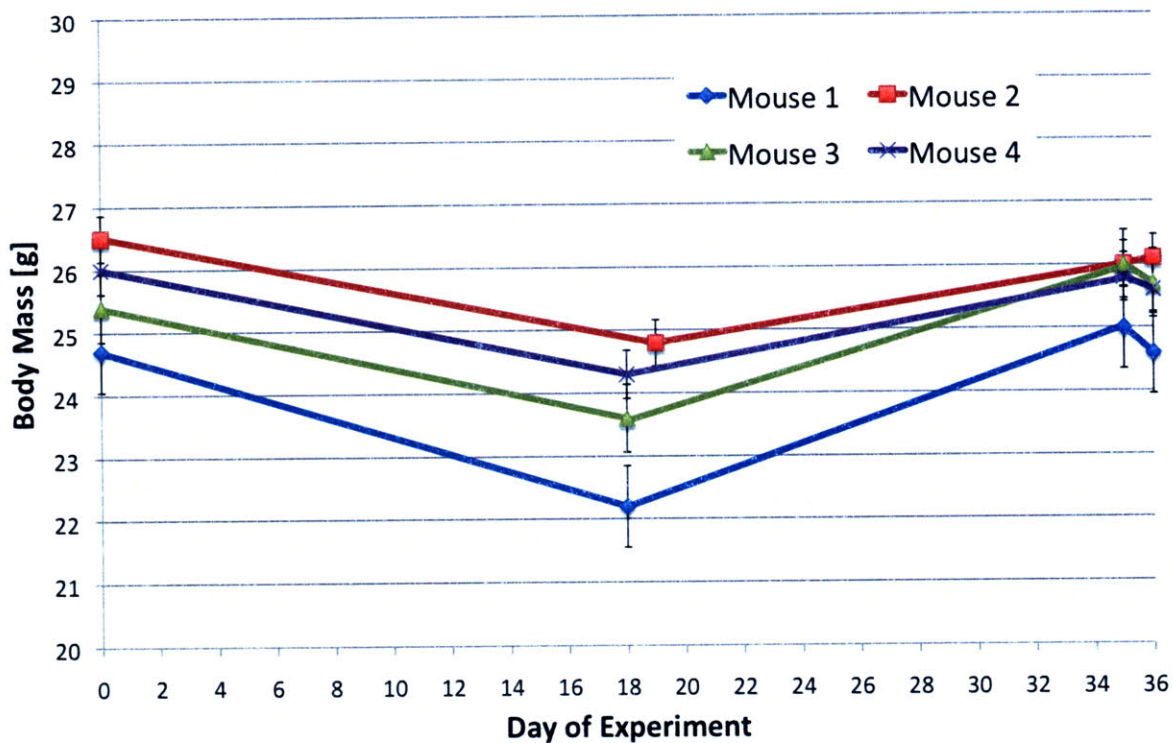


Figure 66: Body mass during rotational experiment

Given that the animals maintained good body mass throughout the rest of the study, the Rotation Day 18 datapoint is of greatest interest. The marked and consistent body mass reduction across all animals between Rotation Day 0 and Rotation Day 18 would suggest a difference between the first half of the study and the second. Critically, the fall in body mass and subsequent recovery in Figure 66 is distinct from 3-G mouse centrifugation results which indicate prolonged body mass reductions of approximately 10% (Frey, vonKanelChristen et al. 1997). Time-dependent mass changes such as those evidenced in the IGTA are possible indicators of adaptation when a specimen acclimates to a new environmental stimulus such as chronic rotation. Questions addressed in subsequent sections seek to understand and contextualise this finding:

- Was there a reduction in water consumed by the animals during the first half of the rotational period that could in part account for the observed loss of body mass? (However, there was no evidence of dehydration when the animals were extracted from the ASMs on Rotation Day 18, so this would seem unlikely.)

- Did the animals exhibit higher or lower activity levels during the first half of the rotation period? Such a response could be indicative of stress and/or an ongoing process of adaptation to the rotational stimulus. A higher activity level that is not accompanied by a commensurate increase in food uptake could in some cases manifest itself as a reduction in body mass. By contrast, a lower activity level may indicate a general stress response or heightened anxiety, consistent with incomplete or ongoing adaptation to the rotating environment. Such states are commonly accompanied by loss of appetite that would explain the recorded body mass data.
- Did any of the other derived metrics provide supporting evidence for the hypothesis that adaptation-related changes were occurring during the first half of the rotational period? Metrics to be discussed include those from nightly in-habitat video tracking and the discrete behavioural testing conducted on Days 0, 18, 35 and 36.
- Are any of the metrics indicative of a “recovery” during the second half of the rotation period? Do parameters normalise during this period and start to resemble data from the control study?
- On Rotation Days 36 and 37 is there any indication of altered behaviour following withdrawal of the chronic rotational stimulus? Such a finding may indicate readaptation and would therefore retroactively confirm that a process of adaptation did occur during the centrifugation period.

5.4.2 Water Consumption

Hypothesis 2: Mean water consumption would normalise to within 15% of that exhibited by non-rotating animals.

It is not unusual for water consumption to vary by as much as 15% among rats that are fed NASA’s rodent food bar (Tou, Grindeland *et al.* 2003). To date, it has not been possible to identify an equivalent dataset for mice in the available literature. Figure 67 shows data from both the control and the rotational experiment, expressed as volumetric totals over each 17-day period. The 15% variations observed in rats are shown as reference extent indicators on each of the bars in the chart.

Unfortunately volumetric data is incomplete for Mouse 2 and for Mouse 3. During the control period, the water monitoring system for Mouse 2 periodically malfunctioned, with the result that water consumption was not reliably aggregated even though the animal was still receiving fluid. During the first half of the rotational study, the diaphragm within the fluidic micropump serving ASM 3 failed. The resulting very slow leak was not detected during maintenance episodes until the second half of the study. This animal was provided with HydroGel rehydration substrate (ClearH2O, Maine) on several occasions during days 0 to 18, and consequently it is not possible to determine the total fluid volume consumed by this specimen.

There is some evidence that Mouse 1 consistently consumed more water during the second half of each study, but this is not true for the rest of the specimens. Mouse 1’s behaviour may in part be explained by food bar moisture loss over time. Dehydration of the food substrate is known to occur during the first two weeks of exposure and has been shown to result in about 10-15% mass loss (Appendix C: Food Bar Experiments). If an animal receives less moisture through food, it is more likely to increase water consumption in order to maintain hydration levels.

Aside from Mouse 1, Figure 67 does not suggest that water consumption was different during the first half of the rotational period than during the second half. This is consistent with the experimental observation that animals were adequately hydrated on every occasion that they were extracted from the IGTA. Considering only water consumption readings from the three animals for which complete data is available, the mean consumed water for the control study is 96.4 ml while the mean for rotation is 110.4 ml. This is within the 15% range stated in the hypothesis.

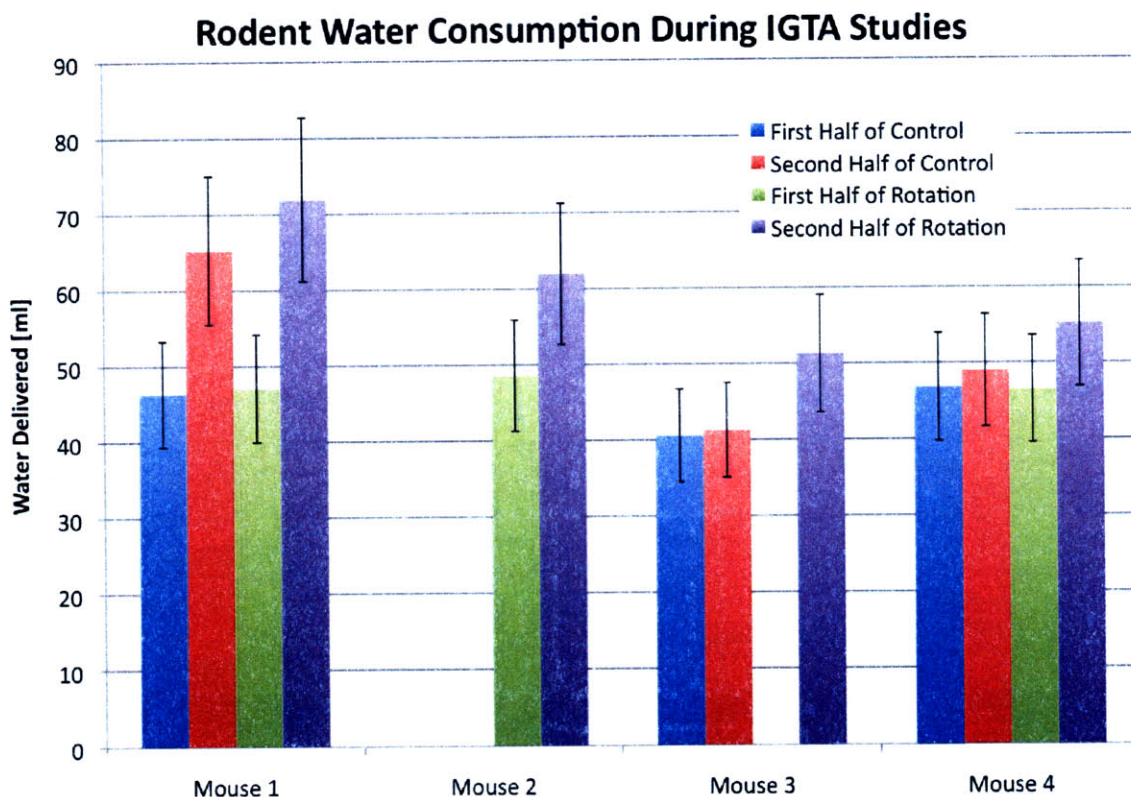


Figure 67: Rodent water consumption in 18-day increments

5.4.3 Nightly Video-Derived Behavioural Metrics

Hypothesis 3: Video-derived behavioural metrics would normalise to within one standard deviation of those exhibited by non-rotating animals.

Ethovision XT analysed six-hour 10 fps video clips from each of the 35 night-time episodes recorded during the control and rotational studies, and from the two nights following centrifuge deactivation. Detection settings were left unchanged for each video file in order to ensure high-contrast pictures so that Ethovision could reliably detect the rodent in each frame.

The following parameters were automatically calculated by the software during post-processing:

Mean angular velocity about the centre point [°/sec]

Angular velocity is calculated by monitoring the change in movement direction of the centre point between two consecutive samples. It is equivalent to the average turn angle over time and can range between -180° and $+180^\circ$.

Assessing angular velocities can be useful in identifying stereotypic movements. For example, large angular velocities can help identify circling behaviours in rodents. The mean angular velocity can be used to assess turn bias or circular tendency.

Total distance moved by the centre point of the animal [cm]

This metric is derived by measuring the distance travelled by the centre of the specimen from one sample to the next, and then summing over all samples in a given period. Distance travelled is generally accurate so long as the animal is on the floor of the specimen chamber. However, when a mouse climbs the food bar wall the metric is necessarily invalid because the animal appears substantially larger in the video camera's field of view. The validity of inter-day comparisons is based on the assumption that each animal spends a roughly consistent percentage of the night-time period on the floor of the specimen chamber.

Distance moved is often used as a measure of general activity and rodent health.

Duration [seconds] and counts of centre point in central zone of ASM

The “in zone” metric is a binary state variable. The state is determined by comparing the location of the mouse centre point at each sample with the predefined coordinate region identified as the central zone of the specimen chamber floor area. Figure 68 shows a four-feed multiplexed video frame acquired during the night-time period by Ethovision XT. Image contrast is artificially enhanced for clarity. The central zones are labelled “Zone 1.”

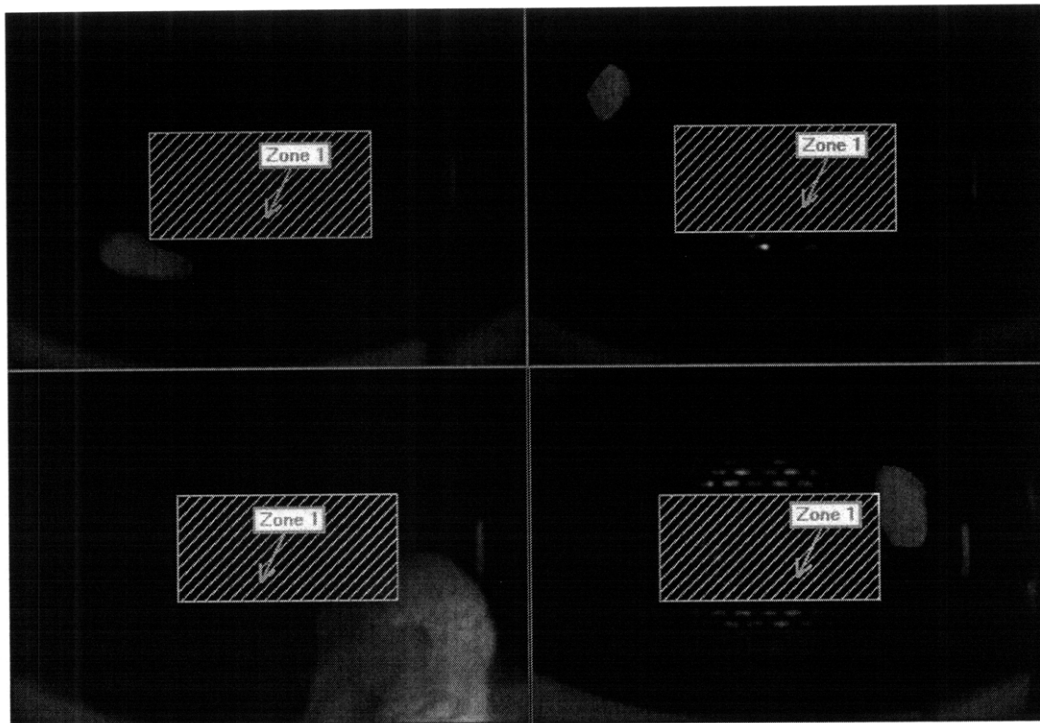


Figure 68: ASM central zones as defined in Ethovision XT

Duration refers to the total time spent by each mouse in the central zone during the 6-hour tracking period. The count indicates the number of transitions from the peripheral zone to the central zone. These metrics are used in larger habitats to determine anxiety levels. Higher anxiety increases a rodent's tendency to remain huddled toward the periphery of the habitat, while more confident mice will readily venture out into the open. Since the Mars Gravity ASM is relatively small, it is unclear whether these parameters have significant meaning in the IGTA studies.

Mean/standard deviation of head direction [degrees], and duration for which head direction was pointing toward central zone [seconds]

The head direction metric ranges from $+180^\circ$ to -180° and is calculated on the basis of the specimen's contour. It is defined as the smallest angle between the instantaneous per-sample head direction line and a line parallel to the long axis (x axis) of the specimen chamber. By default the line points toward the right of the video camera view, and this therefore defines the 0° direction. Positive values indicate head direction pointed toward a location in the upper half of the image, while negative values denote head direction toward the lower half of the frame. Figure 69 illustrates the derivation of this metric with a representative video frame.

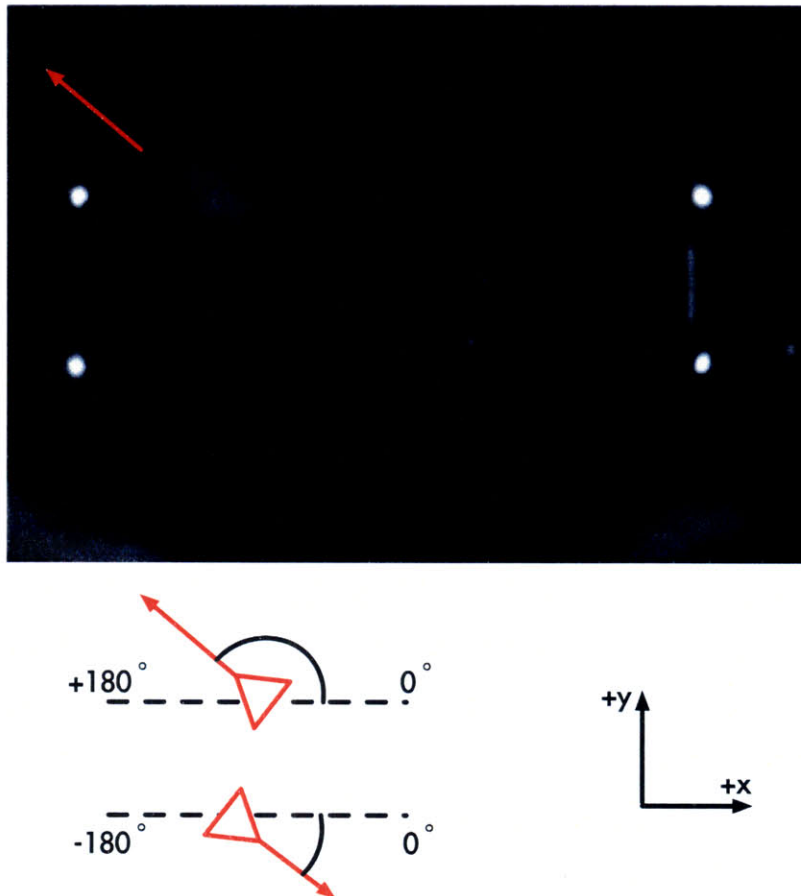


Figure 69: Head direction (adapted from Noldus product manual)

Head direction is considered useful in studies of spatial orientation and searching behaviour. The floor of the ASM is rectangular and disregarding other factors one would therefore expect the modal head direction to be aligned with the long axis of the habitat.

Mean centre point heading [degrees]

The heading in degrees is defined as the direction of movement of the centre point of the animal in a given sample relative to the x-axis line previously described.

Heading is used in studies of spatial orientation. It can help quantify response to Coriolis effects, for example, when a specimen may preferentially move in a direction tangential to the arc of motion. Again, due to geometric considerations one would ordinarily expect the modal centre point heading to align with the longer dimension of the ASM.

Mean and total meander measured with respect to centre point [°/cm]

Meander is expressed as degrees of turn per centimetre of distance travelled. It is the change in direction of movement of a specimen's centre point relative to the total distance moved.

Relative meander is the signed version of the coefficient; it ranges between -180° and +180°. It is of experimental value mainly in conjunction with other turn bias variables, such as relative turn angle, since meander is equivalent to turn bias 'corrected for' the distance moved. For example, if two specimens move at entirely different speeds, the mean turn angle can be very different while the mean relative meander parameter ends up being the same. Absolute meander is the corresponding unsigned variable; it ranges between 0° and 180°. When plotted, it can generate a smoother curve than absolute turn angle. This is because the turn angle tends to be influenced by speed of travel as well as by the pure turning rate.

Duration of movement of centre point [sec]

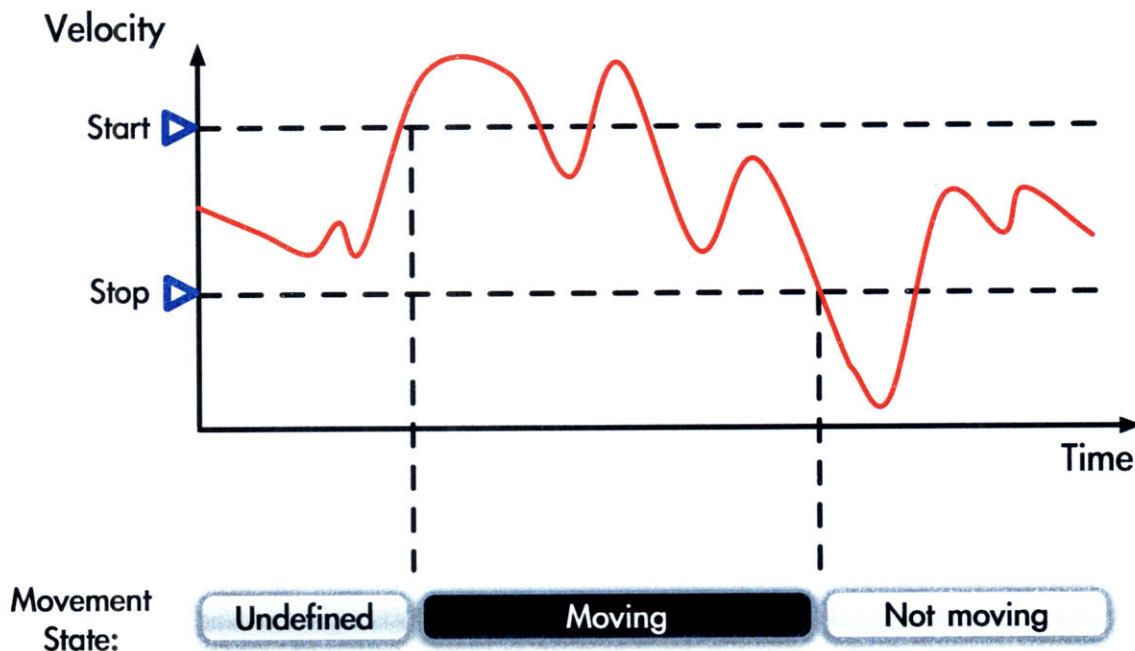


Figure 70: Movement states (adapted from Noldus product manual)

Figure 70 illustrates the derivation of the “duration of movement” parameter. The state variable “movement” is set to “moving” if the running average of velocity exceeds the user-defined start velocity. The state remains “moving” until the velocity drops below the user-defined stop velocity. The state then transitions to “not moving” until triggered again. To reduce the sensitivity of this variable to instantaneous changes in velocity, the window over which average velocity is calculated can be modified by the user.

As with total distance travelled, the movement parameter provides insight into the specimen’s locomotor activity.

Duration spent in each of three elongation states: contracted, normal, stretched [sec]

This discrete variable is calculated through analysis of the running average elongation measure. If it is greater than the “stretched above” user-defined value, the specimen is designated “stretched.” If it is less than the “contracted below” user-defined value, the specimen is “contracted.” In all other cases, the elongation state defaults to “normal.” Elongation is expressed as a percentage, with 0% representing a perfectly circular specimen and 100% indicating that the specimen is indistinguishable from a straight line.

The elongation variable can be used to more objectively assess the number and duration of stretch attend postures, a species-specific behaviour.

Duration [sec] and counts of episodes in each of three mobility states: highly mobile, mobile and immobile

This parameter indicates the extent to which pixels that identify the area of the specimen change between two consecutive video frames. Two user-defined thresholds categorise the mobility level. The value ranges from 0 (the sample is identical to the one preceding) to 100 (zero pixels overlap between the detected specimen in each sample). As with other parameters, an averaging interval is used to increase data reliability.

Mobility is different from movement in that mobility does not require spatial displacement of the animal’s centre point. Thus, the mobility variable can detect activities such as grooming and rearing. Mobility can be useful in assessing general activity, changes in behavioural patterns and freezing episodes (when “immobile threshold” is set to a very low value).

Total number of rotations about the centre point

This variable tracks the cumulative turn angle of consecutive samples and increments by 1 every time the running total reaches a multiple of 360°. Turns can be counted in both clockwise and anticlockwise directions.

This parameter has been found useful in studies of cerebral asymmetry in rats. It is also of relevance in pharmacological studies, including those that explore dopaminergic receptors and the effects of amphetamines. In the IGTA centrifugation experiment, it may indicate degree of spatial disorientation.

5.4.3.1 General Approach for Ethovision-Derived Analyses

The metrics listed in section 5.4.3 were calculated on a night-by-night basis for both the control and the rotational experiment. Track data was smoothed using a 10-frame Lowess

(locally weighted scatterplot smoothing) method to remove the effects of small movements and eliminate variable noise. Data was unusable in the following cases:

- Tracks could not be generated for specimen 2 during the first 6 days of the control experiment because of a video camera failure. This video camera was replaced by the manufacturer and a new model was installed on Control Day 7. It functioned flawlessly thereafter.
- The video file was corrupted and could not be imported by Ethovision on Control Days 7, 8 and 33.
- Video files were not recorded on Rotation Days 7, 10 and 30. This was due to an oversight on the part of personnel conducting daily rodent video monitoring.
- On Rotation Days 11 and 19, a researcher from a different lab accidentally left the cubicle lights on overnight. The added ambient brightness that filtered into each ASM meant Ethovision was unable to track the specimens on these dates.

The graphs were visually inspected in order to identify any obvious trends or features of note. Where meaningful information was apparent, statistical analyses were performed in order to elucidate the significance of apparent trends.

5.4.3.2 Mean Angular Velocity

Figure 71 shows a box plot of the mean angular velocity each night during the experiment. Control days are numbered negatively, commencing at -34 and ending before 0. Days of rotation are numbered positively from 1 to 35. The cameras remained powered and the rodents continued to be housed within their ASMs for two days following the end of the rotational study (Day 36 and Day 37 in Figure 71). This approach was specifically implemented to search for signs of readaptation.

For the purpose of statistical analyses, the dataset was divided into five epochs, delineated by vertical dashed lines in Figure 71. They represent the first and second halves of the control period, first and second halves of the rotation period, and the final two post-rotation days. The data was analysed using a mixed regression and there was a highly significant effect of epoch. During both halves of the rotation period, the mice demonstrated significantly greater angular velocities than the average ($p < 0.0005$). The nightly angular velocity was $29.9^\circ/\text{sec}$ greater than the global mean during the first half and $25.1^\circ/\text{sec}$ greater during the second half. On Rotation Days 36 and 37 there was a significant decrease in angular velocity ($50.3^\circ/\text{sec}$ less than the global mean, $p < 0.0005$). Red arrows in Figure 71 indicate the direction of these statistically significant deviations.

The mean and standard deviation across all days and all animals for the control study was $-7.96 \pm 12.51^\circ/\text{sec}$. The equivalent metric for the rotational study was $2.13 \pm 13.95^\circ/\text{sec}$, while the final two post-rotation days were recorded at $-23.83 \pm 20.84^\circ/\text{sec}$. Positive angular velocities indicate clockwise animal rotations as viewed by the overhead camera. The previous figures therefore suggest that the animals exhibited a tendency to turn anticlockwise during the control study. The centrifuge also rotated in an anticlockwise direction. There was a highly significant tendency for the animals to preferentially turn in a clockwise direction while the centrifuge was rotating. This may have been an attempt to counteract the continuous spinning sensation. Following rotation stoppage, the animals exhibited a highly significant overcompensation in the form of a strong anticlockwise turn

bias. This substantially overshoot their natural but small tendency toward anticlockwise turns as exhibited during the control study.

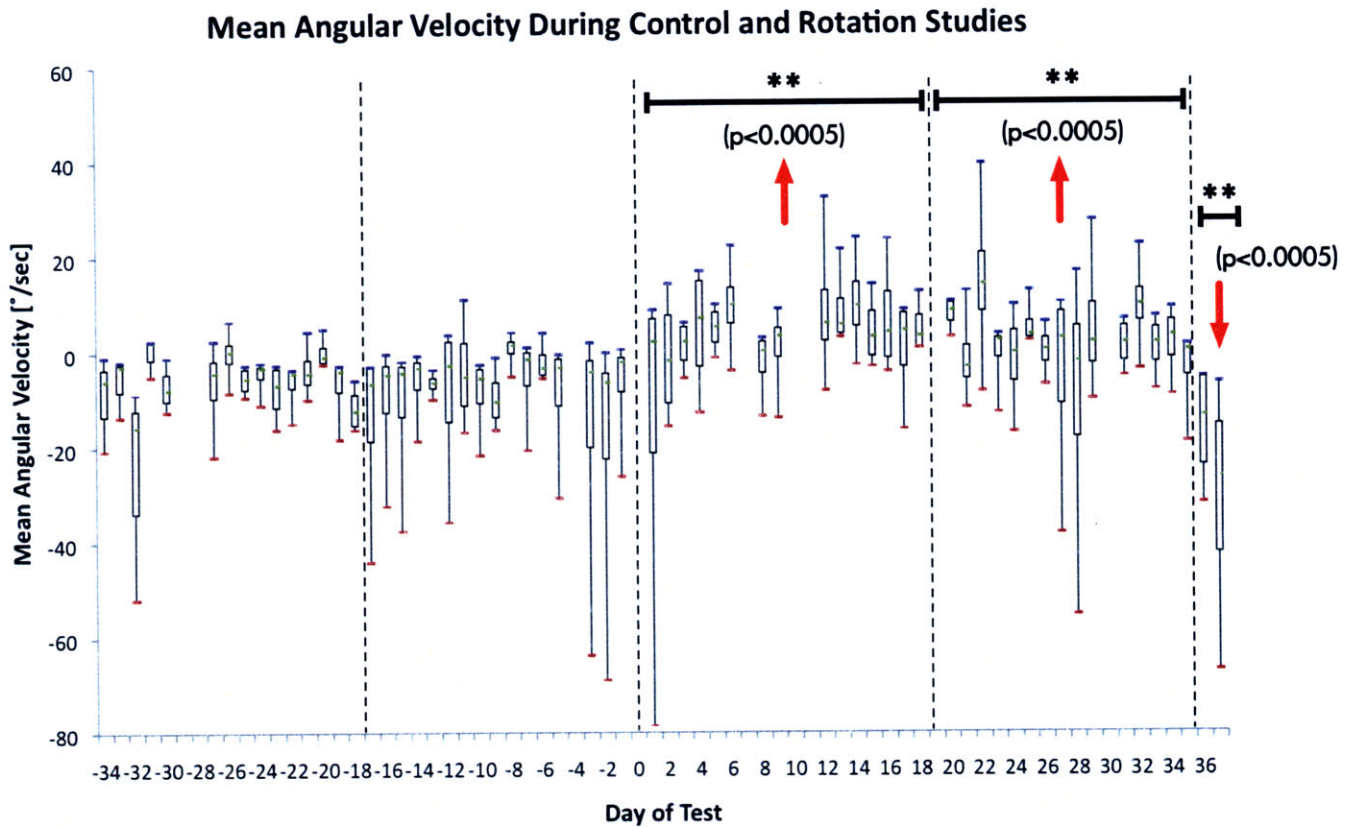


Figure 71: Mean angular velocity per night during entire experiment

5.4.3.3 Mean Meander

In order to elucidate the nature of the changes in mean angular velocity, the meander parameter was also statistically evaluated. The graph of mean meander was very similar in appearance to the angular velocity plot shown in Figure 71. Mixed regression analysis yielded the same conclusions as for angular velocity, with elevated meander coefficients during the rotation tests and substantially reduced values following rotation stoppage (all with $p < 0.0005$). Further detail can be found in Appendix J: Statistical Analyses. Meander is measured as degrees of centrepoint heading turn angle per unit distance, while angular velocity is expressed as degrees per unit time. The correlation of meander and angular velocity results serves simply to reinforce the conclusion that turn bias was significantly impacted by the chronic rotation stimulus.

5.4.3.4 Total Distance Moved

Total distance moved is shown in Figure 72. This data was analysed using a mixed regression and a highly significant effect of epoch was identified. During the first half of the rotation period, the mice demonstrated significantly greater nightly distance coverage than the global average ($p < 0.0005$). However, Figure 72 indicates that this epoch included a remarkably high data point from Mouse 1 on Rotation Day 6. Another similarly high datapoint was recorded from Mouse 3 on Control Day 0. Concerns were raised that these unusual datapoints might be artificially elevating that epoch and generating statistical

significance which was not representative of the entire cohort. Accordingly, these datapoints were reduced to the average of the remaining mice on those days for the purposes of the mixed regression analysis. The statistical significance survived this operation, and Figure 72 shows p-values generated after the normalisation of Mouse 1 on Rotation Day 6 and Mouse 3 on Control Day 0.

The nightly distance moved was 23.1 metres greater than the global mean during the first half of rotation ($p < 0.0005$). On Rotation Days 36 and 37 there was a significant decrease in distance travelled (34.4 metres less, $p < 0.0005$). As before, red arrows in Figure 72 indicate the direction of these statistically significant deviations.

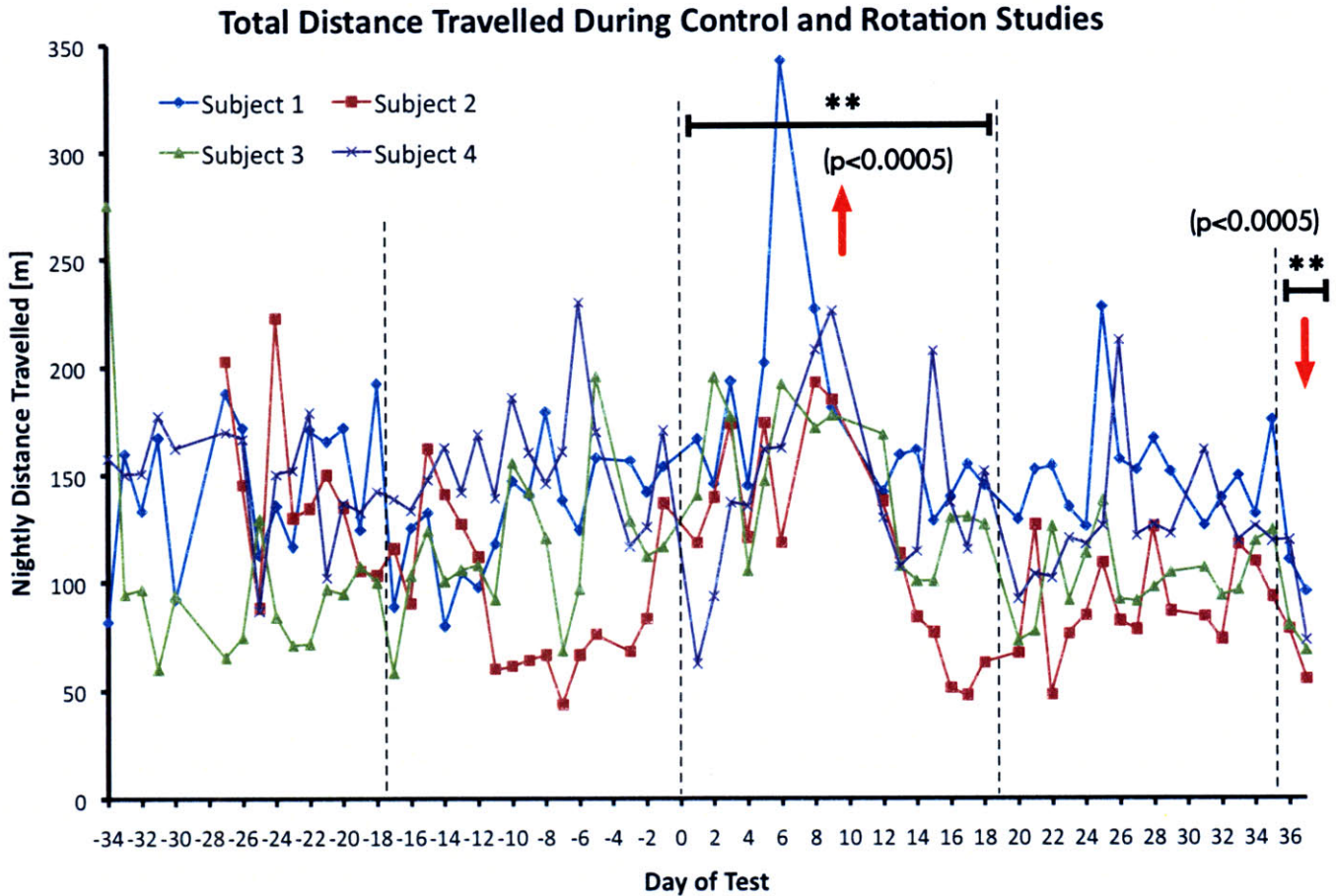


Figure 72: Total distance travelled per night during entire experiment

The higher activity levels evidenced during the first half of the rotation period could be indicative of an ongoing process of adaptation to the rotational stimulus. A higher activity level that is not accompanied by a commensurate increase in food uptake would manifest itself as a reduction in body mass consistent with that observed between Rotation Day 0 and Rotation Day 18.

5.4.3.5 Duration Moving

In order to elucidate the nature of the elevated travel distance, the “duration moving” parameter was calculated using an upper velocity bound of 2 cm/sec and a lower bound of 1.75 cm/sec. These boundary values are the default for Ethovision XT mouse behavioural analysis. The “duration moving” timer would begin counting as soon as the rodent reached 2 cm/sec and would continue until its speed fell below 1.75 cm/sec. Five-sample frame averaging was used for improved data fidelity.

Results from both control and rotational studies are shown in Figure 73. Mixed regression analysis showed a highly significant effect of epoch. During the first half of the rotation period, the mice demonstrated a nightly time spent moving that was 6.59 minutes longer than the global average ($p=0.001$). On Rotation Days 36 and 37 there was a significant decrease in time spent moving, recorded as 13.67 minutes less than the global average ($p<0.001$).

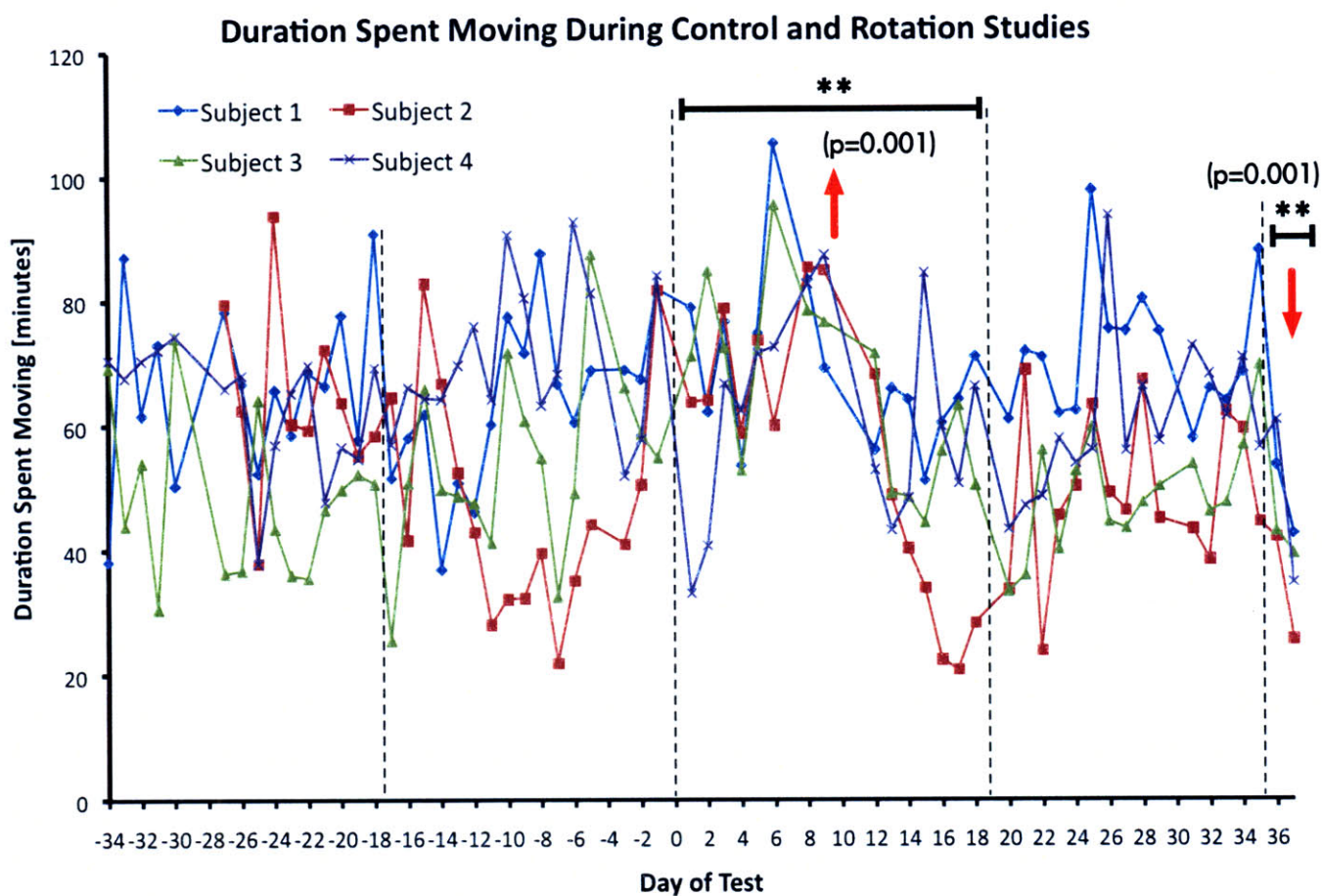


Figure 73: Time spent moving each night during entire experiment

In section 5.4.1, the question was posed “Did the animals exhibit higher or lower activity levels during the first half of the rotational period?”. The duration moving results together with the distance travelled data suggests that the animals did exhibit a higher activity level during this period. Specifically, the results indicate that during the first half of the rotational

study the animals covered approximately 18% more distance than the global mean (23.1 m on a mean of approximately 130 m). This was partially accounted for by an 11% increase in time spent moving (6.59 minutes on a mean of 59.35). The remaining additional distance covered can be attributed to the fact that the average speed during the moving episodes was elevated during the first half of the rotational study.

In section 5.4.1, another question asked was “On Rotation Days 36 and 37 is there any indication of altered behaviour following withdrawal of the chronic rotational stimulus?”. The duration moving parameter together with distance travelled suggests that gross motor activity was suppressed following cessation of centrifugation. The rodents exhibited a 33.9% decline in nightly distance moved which was almost wholly explained by a 28.0% decline in time spent moving. Both percentages are ratios of the respective global means.

5.4.3.6 Time Spent in Central Zone

Ethovision calculated a parameter that described the total time spent per night by each mouse in the central zone of the ASM. The resulting graph is shown in Figure 74.

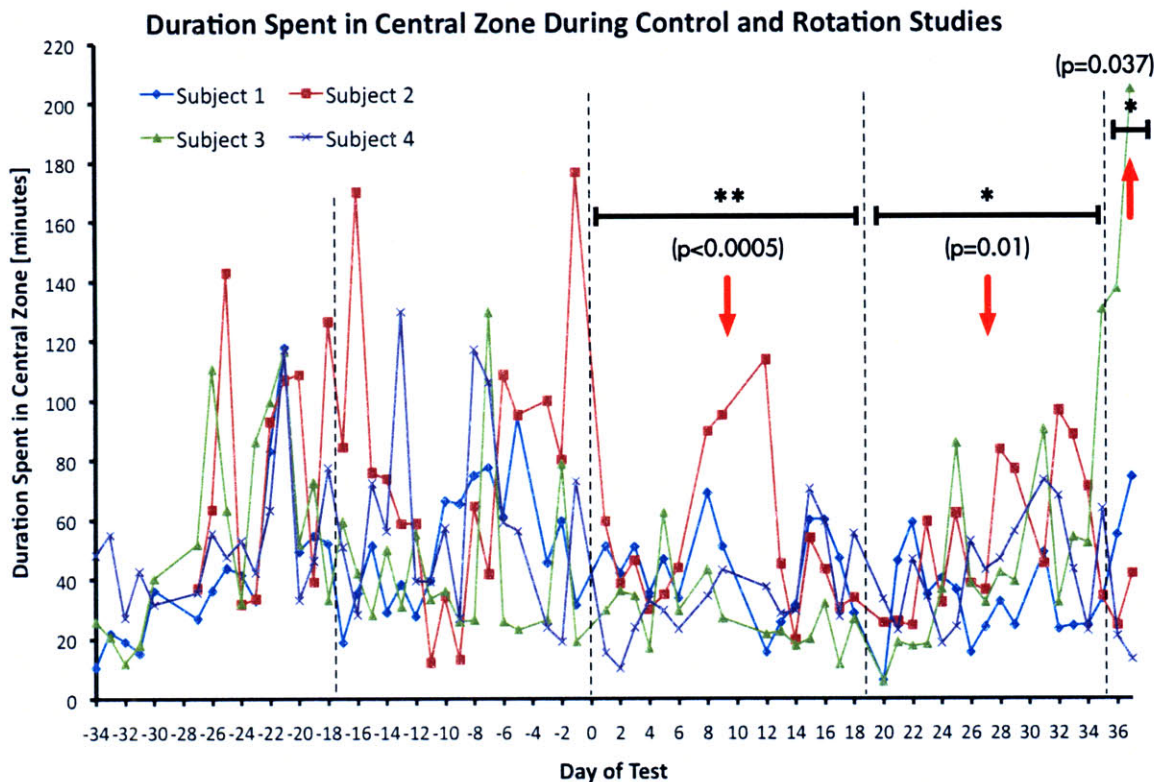


Figure 74: Time spent in central zone during entire experiment

This parameter exhibited higher variation between the different subjects, and the meaning of the data is consequently not entirely clear. In particular, nightly variation during the control study substantially exceeded that recorded during rotation.

The global mean of the data suggested that the average mouse spent 49.8 minutes per night in the central zone of the cage. This is less than one-sixth of the nightly video recording duration. A mixed regression was calculated and the mice were found to preferentially

remain toward the periphery of the ASM, spending an average of 14.2 minutes less in the central zone ($p < 0.0005$). During the second half of the rotational period, the animals spent 10.1 minutes less in the central zone as compared with the global mean but at a slightly less strong significance level ($p = 0.01$). The post-rotation days showed a significant preference for the animals to remain at the centre of the habitat. However, this result is likely not representative of the cohort due to the unusual behaviour exhibited by Mouse 3 on Days 36 and 37. For reasons which are unclear, this animal remained in the centre of the floor for substantially extended time periods as shown in Figure 74.

5.4.3.7 Other Variables

The parameters previously discussed are the most relevant to this type of behavioural study. However, plotting and analyses were also conducted on many of the other Ethovision output variables listed in section 5.4.3. Representative output can be found in Appendix J: Statistical Analyses. For most of these parameters, no statistical differences were identified between the control and the rotational studies. In addition, the autocorrelation was tested and no significant autocorrelation was found at the level of thirty-five days. This suggests no systematic differential effect of day-of-study.

5.4.3.8 Summary

Hypothesis 3 was shown to be incorrect for the important variables of angular velocity, mean meander and time spent at the centre of the habitat. While the animals underwent centrifugation, these variables did not normalise to the setpoint exhibited during the non-rotational period. However, the validity of the centre zone result is questionable due to the significant inter-animal and inter-day variation.

Hypothesis 3 was shown to be correct for the important parameters of total distance travelled and time spent moving. For each of these variables, a highly significant change was evident during the first half of the rotational period. That change subsequently normalised during the second half such that the behaviour became indistinguishable from the control.

Interesting re-adaptation phenomena were observed during the two post-rotation days at the end of the study. The results showed overcompensation responses for all 5 of the aforementioned parameters. In these cases, behaviour shifted back toward the normal pre-rotational setpoint but would overshoot, often by a highly significant amount.

5.4.4 Discrete Behavioural Trials

Hypothesis 4: Performance in open field testing, rotarod running, balance beam walking and air-righting would normalise to within one standard deviation of that exhibited by non-rotating animals.

5.4.4.1 Rotarod

A box plot of rotarod performance over the course of each study is shown in Figure 75. The vertical extent of each box illustrates the span of the second and third quartile performance across all four mice and over all three daily rotarod repetitions. The red and blue whiskers represent the minimum and maximum extent of each recorded performance window.

The box plot illustrates that there is no significant change in rotarod performance during the studies. The median values are slightly higher on Control Day 0 and Rotation Day 18. The elevated Control Day 0 value may suggest that the animals had not yet fully acclimated to the ASMs, a novel and unusual habitat to which they had first been introduced just 48 hours previously. On Rotation Day 18, the elevated median could be explained by the animals not having fully adapted to the rotational stimulus. This would be consistent with the loss of body mass previously discussed in section 5.3.3.2.

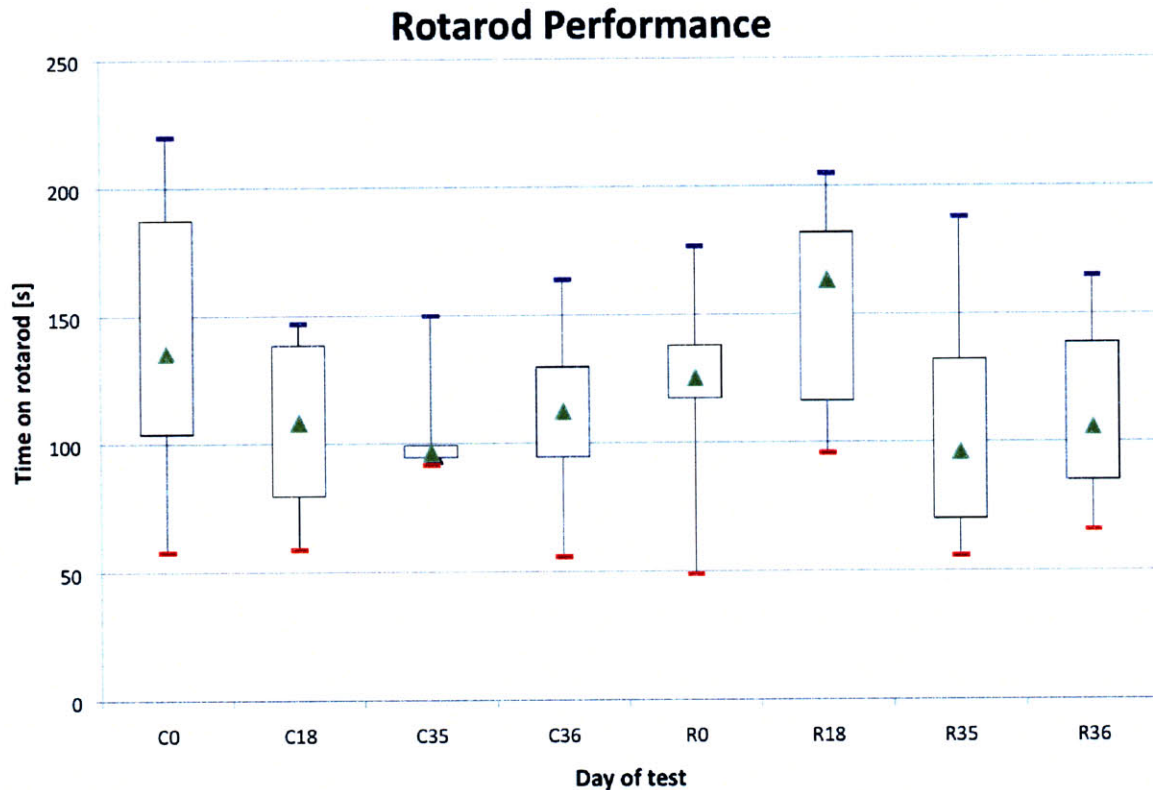


Figure 75: Box plot of rotarod performance over time

The mean and standard deviation before rotating (Control Day 0 to Rotation Day 0 inclusive) was 117 ± 37 seconds. The equivalent value for Rotation Days 18, 35 and 36 was 123 ± 43 seconds. These results are in agreement with Hypothesis 4.

The standard deviation is greatest on Control Day 0 at 56 seconds, followed by Rotation Day 35 at 43 seconds and Rotation Day 18 at 38 seconds. All other days show standard deviations of between 15 and 33 seconds.

5.4.4.2 Open Field Testing

For the 4-minute open field video clips, plotting and analyses were conducted on many of the Ethovision output variables listed in section 5.4.3. Representative output can be found in Appendix J: Statistical Analyses. No statistical differences were found between the control and the rotational studies with respect to any of these parameters.

However, Figure 76 and Figure 77 together show that the rodents' movement was different from other days on Control Day 0 and Rotation Day 18. Specifically, on Rotation Day 18

the animals spent the greatest amount of time in mobility state "mobile" while also exhibiting the greatest number of transitions into an immobile state. In other words, on this day the animals' movement followed a jerky, start-stop pattern with periods of hesitation followed by brief episodes of movement.

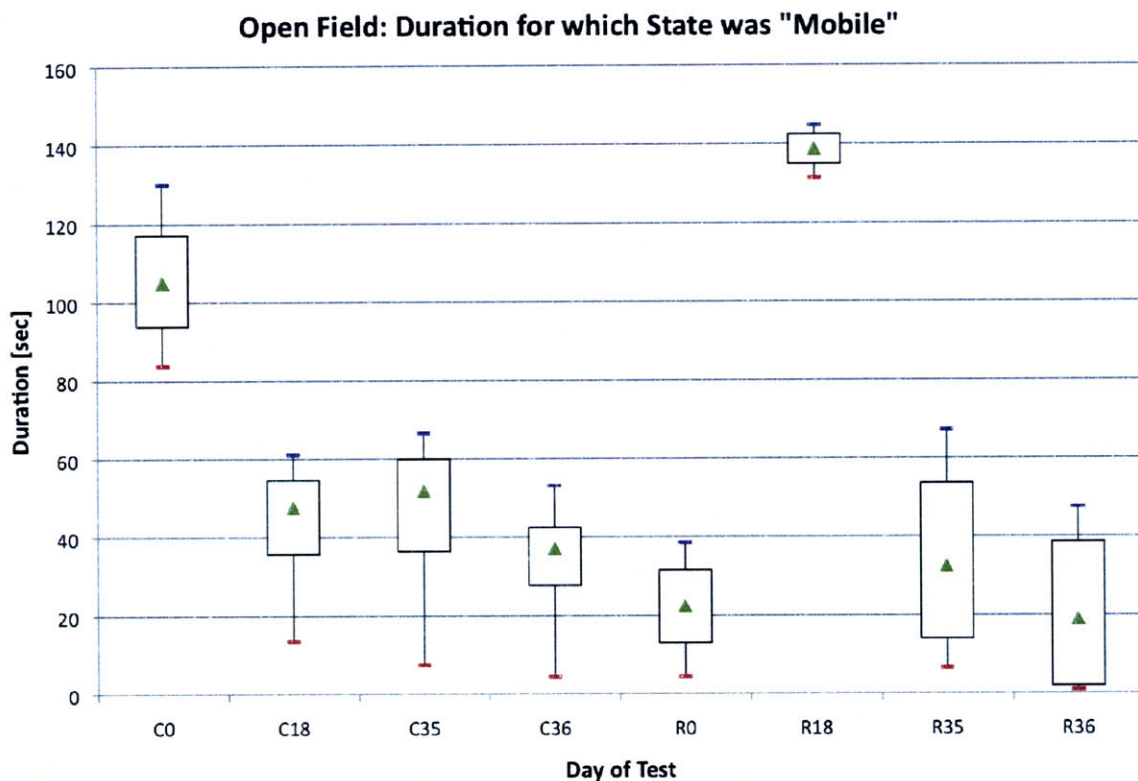


Figure 76: Box plot of mobility duration over time

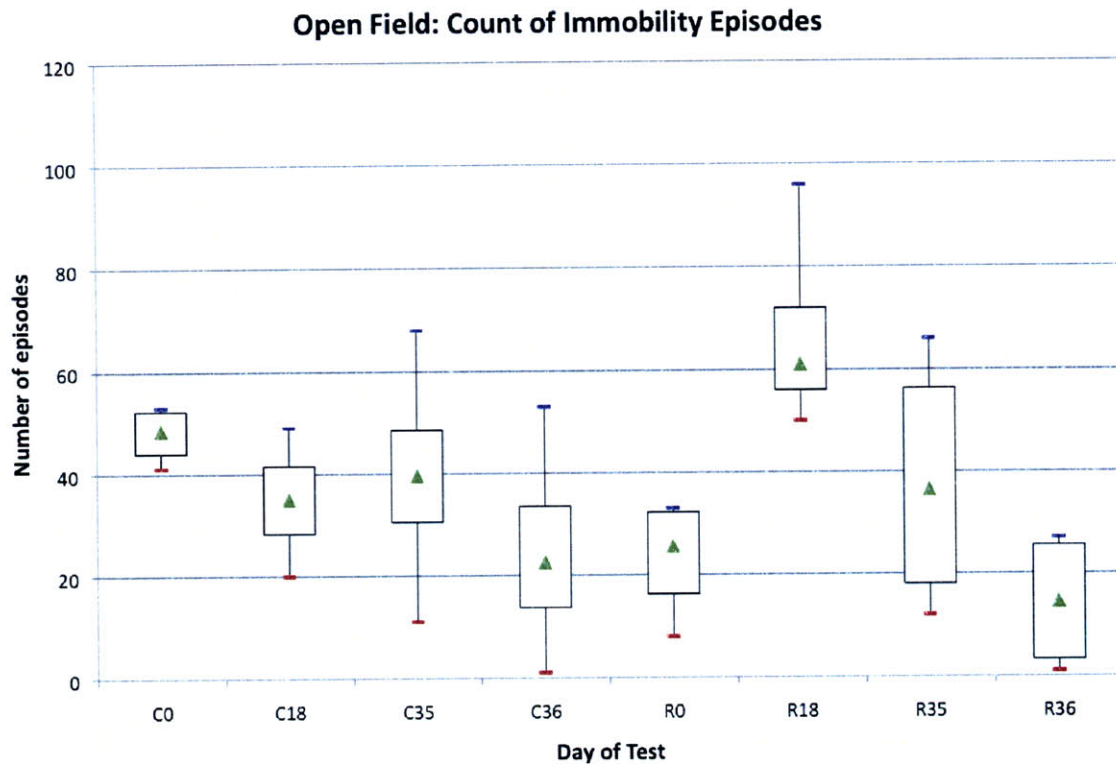


Figure 77: Box plot of number of immobility episodes over time

The phenomena noted for Control Day 0 and Rotation Day 18 are not great enough to be significantly different from the rest of the data. However, these plots do suggest that the degree of agitation exhibited on Rotation Day 18 is comparable to the agitation caused by a rehousing event 48 or 24 hours prior to Control Day 0. The median mouse exhibited a 32% greater mobility duration on Rotation Day 18 than on Control Day 0. Similarly, there was a 26% increase in the median number of immobile episodes across this same interval. Importantly, the variance for Rotation Day 18 in Figure 76 is very small, implying that the animals spent roughly the same amount of time moving during the open field test that day.

The mean and standard deviation in mobility duration before rotating (i.e. Control Day 0 to Rotation Day 0 inclusive) was 50 ± 35 seconds. The equivalent value for Rotation Days 18, 35 and 36 was 65 ± 60 seconds. For the immobile episode count data, the values are 34 ± 17 seconds and 40 ± 30 seconds. These results are all in agreement with Hypothesis 4.

The question arises – to what extent is the Rotation Day 18 result a consequence only of the *transition* from rotating to stationary operation, as opposed to an effect of the preceding *18-day stay* on the centrifuge? The in-habitat video results showed no evidence of different behaviour while spinning during those first 18 days. However, the body mass data suggests that there were longer-term effects of chronic centrifugation over this time period. Subsequent sections examine other types of data in order to elucidate an answer to this question.

5.4.4.3 Air Righting

The data from air righting tests was highly variable and difficult to decipher. In some cases, the animal righted itself successfully while falling but subsequently became unstable and

landed at a 45° angle to the horizontal. On other occasions, the mice would perform a complex double-flip while in the air before landing. Certain air righting trials were challenging to interpret from the black-and-white 2D video picture because part of the rodent would be obscured due to an unusual fall angle.

Sometimes the mouse would attempt to grasp the gloved hand of the experimenter just milliseconds after release, thereby imparting an unusual torque and spinning all the way down to the landing pad. In other trials, a rodent would mostly right itself soon after release but would not become fully pronate until the instant before landing, thereby causing confusion during video assessment and data entry.

Data from the air righting trials is not discussed here because it does not offer any meaningful evidence from which firm conclusions can be drawn.

5.4.4.4 Balance Beam

Both left and right balance beam videos were analysed using slow motion playback. Due to a logistics failure, only one video camera was available on Control Day 0. Accordingly, for that date it was only possible to record the right hand side of each rodent as it traversed the balance beam. It can be argued from subsequent data that footfaulting on the left side of each animal was likely symmetrical to the right on Control Day 0.

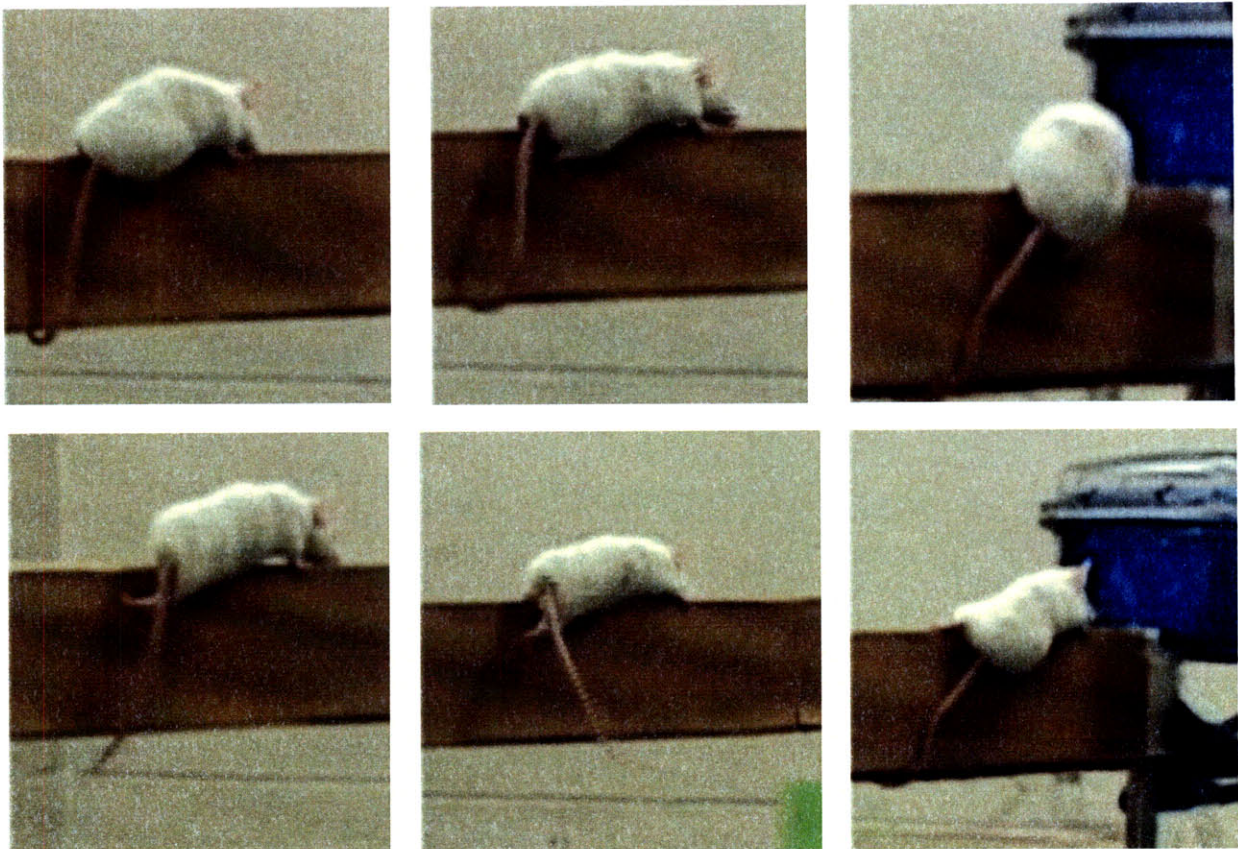


Figure 78: Sample video frames showing footfaults of increasing severity

Videos of all trials were viewed and each step was categorised as shown in Table 34.

The footfault magnitude results were of greatest interest. In general, all animals exhibited near-perfect performance on every test date prior to Rotation Day 18. However, on Rotation Day 18 moderate to severe impairment was noticed in the balance beam tests of almost all the specimens. Subjectively, it appeared that these specimens footfaulted much more often and exhibited a previously unseen asymmetric hindlimb latency (“dragging of rear limb”). This was accompanied by a rear lateral inability to consistently pronate and a noticeable off-medial stance.

Figure 79 to Figure 81 inclusive show quantitative evidence that supports the aforementioned subjective observations. In each case, the datapoints for the box plots were generated by averaging the percentages of each type of footfault across all three balance beam repetition events for each animal on each testing date.

Table 34: Balance beam step categorisation criteria

Data	Detail
Paw ID	Forelimb or hindlimb, left side or right side.
Footfault Magnitude	0: Perfect step 1: Minor footfault (paw contacts but then slips off beam’s horizontal surface) 2: Major footfault (paw misses beam’s horizontal surface) 3: Very major footfault (paw misses beam entirely and slips down beam’s vertical surface)
Nature of Wobble Events	Location of wobble (0%, 25%, 50%, 75% or 100% of beam crossed) Magnitude of wobble: 1: Minor tremor 2: Major unsteadiness 3: Mouse almost falls off beam
Nature of Pausing/Freezing Events	Duration of pause Location of pause (0%, 25%, 50%, 75% or 100% of beam crossed)
Total Time on Beam	Time from start to finish was recorded, as well as the location of the animal at finish (either partway across beam or in the retreat).

Figure 79 reveals that there was a marked change in the percentage of perfect fault-free steps over the course of the study. Almost all the mice exhibited better than 90% performance during the control study, up to and including Rotation Day 0. However, on Rotation Day 18 the median performance fell to below 70%. Although some recovery was made by Rotation Days 35 and 36, the cohort still failed to achieve the performance exhibited during the control study.

One surprising datapoint is from Mouse 2 on Control Day 0. This animal exhibited a remarkably high number of very minor footfaults on the right side of the balance beam (the average for Mouse 2 was as high as 20% that day). Because no left-side video recording was available for Control Day 0, it is impossible to tell whether or not the recorded performance aberrations were representative of both sides of that animal.

The data shown in Figure 79 was transformed using the Arcsin Conversion to map the percentages onto an unbounded data range. The resulting data was analysed by General Linear Model and the H-F corrected difference among days was significant at $p=0.001$. Accordingly, a contrast was calculated and a highly significant difference was found between Rotation Day 18 and the average of the other days at the $p=0.001$ level. In addition, a difference was found between the pre-rotation period (all days up to and including R0) and the set that includes R18, R35 and R36. This was highly significant, with $p=0.006$.

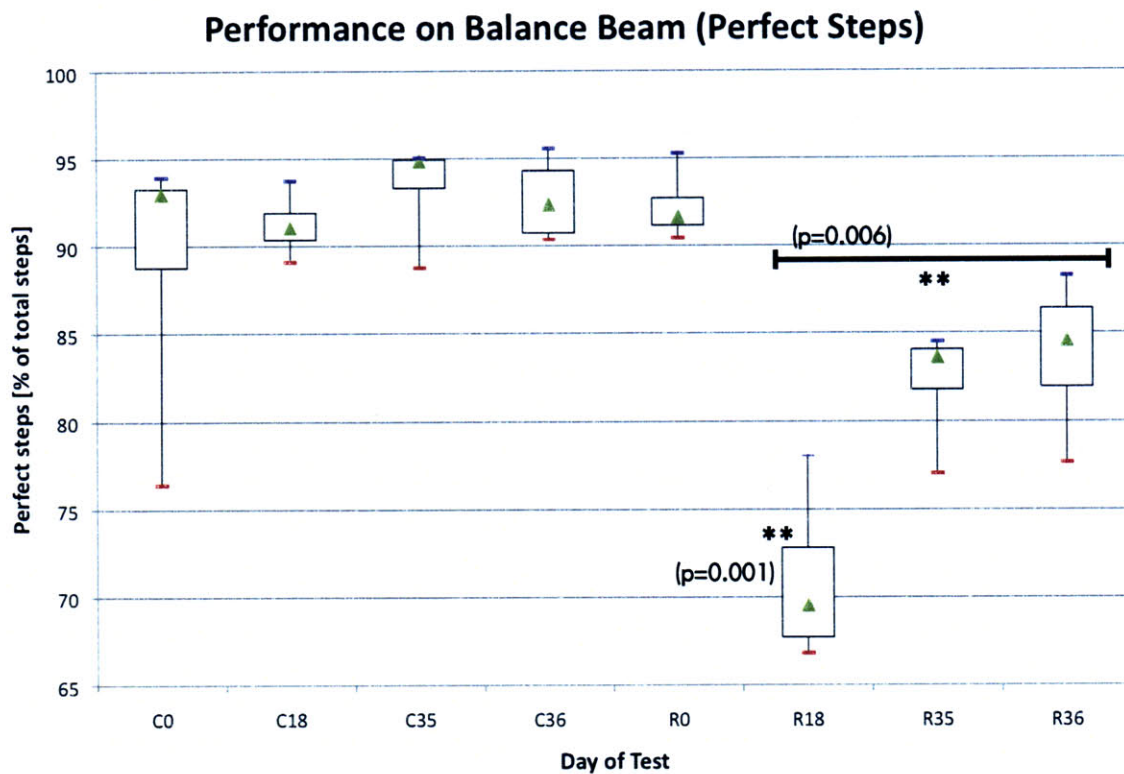


Figure 79: Box plot showing percentage of faultless footsteps

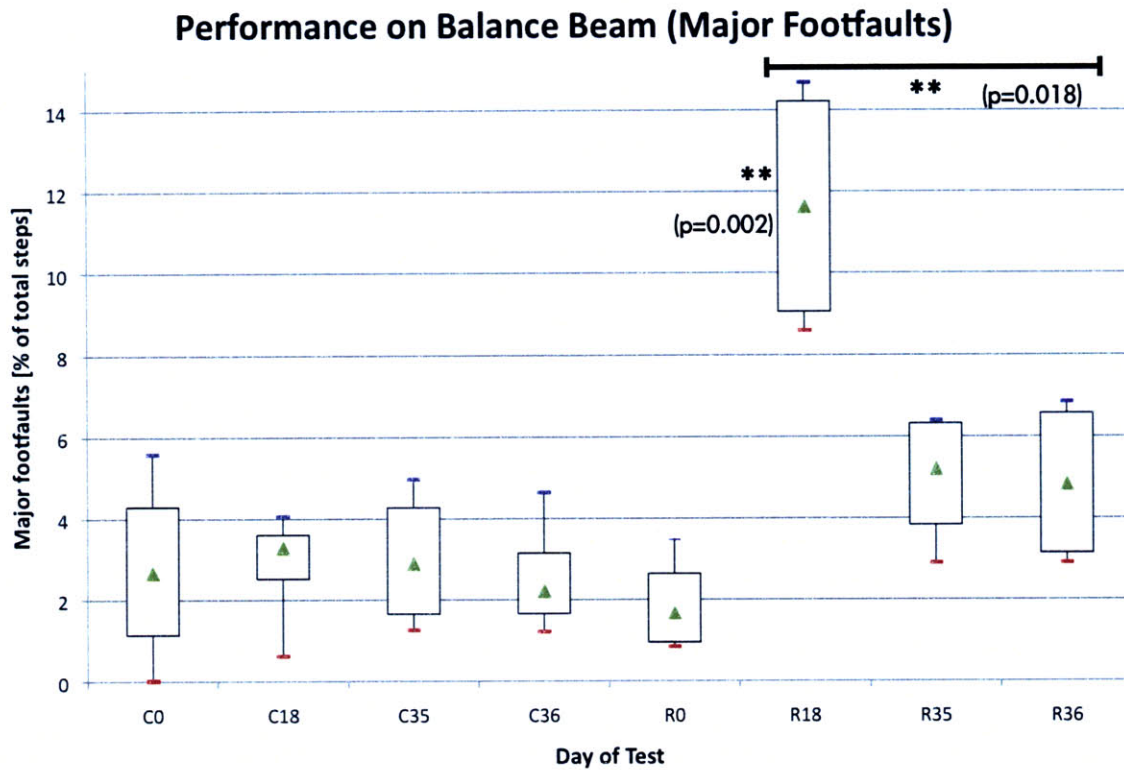


Figure 80: Box plot showing percentage of “major” footfaults

Figure 80 focuses in on those footfaults classified as “major” according to the definition in Table 34. The median percentage during non-rotational test episodes hovers around 3%, but by Rotation Day 18 it almost quadruples, to just under 12%. As with Figure 79, the pre-rotation performance level is never fully regained, with the median value barely dipping below 5% even 24 hours following centrifuge stoppage.

The data shown in Figure 80 was transformed using the Arcsin Conversion and a General Linear Model analysis was performed. A contrast was calculated and a highly significant difference was found between Rotation Day 18 and the average of the other days ($p=0.002$). In addition, a difference was found between all days up to R0 and the set that includes R18, R35 and R36. This was significant with $p=0.018$.

Figure 81 serves to add further weight to this conclusion, with a box plot representation of “very major” footfaults. On Rotation Day 18, Mouse 3 exhibited these severe missteps at an average rate of almost 8% across all three balance beam repetitions. Because there seemed a very real danger that this mouse might fall off the beam entirely, it was deemed exigent to place additional cushioned padding below the test apparatus during these trials.

The statistical approach previously described was applied to the data shown in Figure 81. A highly significant difference was found between Rotation Day 18 and the average of the other days ($p=0.002$). The analysis also identified a significant difference ($p=0.018$) between all control days and R0 and the set that includes R18, R35 and R36.

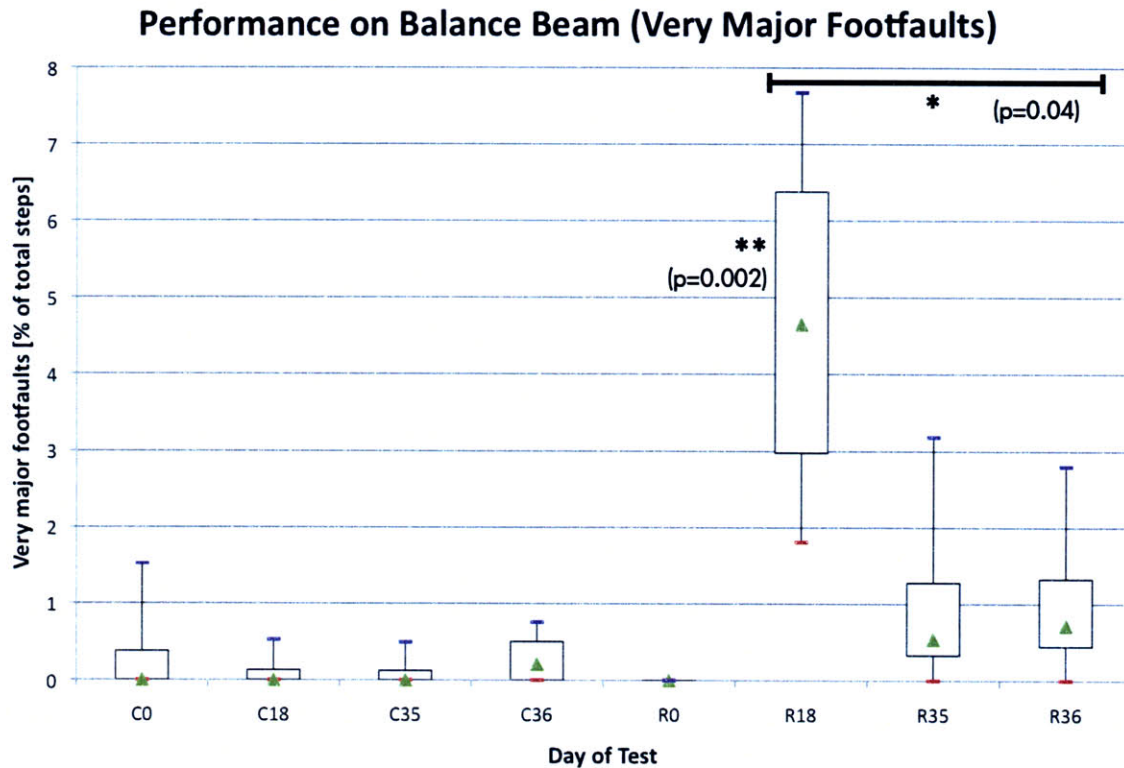


Figure 81: Box plot showing percentage of “very major” footfaults

The balance beam results do not satisfy Hypothesis 4 as summarised in Table 35. With every type of footfault, the observed mean after Rotation Day 0 lies outside the range delineated by the mean and standard deviation of preceding test dates.

The severe gait disturbances exhibited by the rotated animals as they traversed the balance beam are a strong indication of vestibular disorientation following extraction from the centrifuge. To respond to the question posed in section 5.4.4.2, these effects were not transient but persisted for at least 24 hours following stoppage of the centrifuge (data from Rotation Day 36). This would suggest that the global process of adaptation to the rotational stimulus is multi-faceted and may involve multiple neurovestibular and other mechanisms with different time constants.

Table 35: Balance beam performance differences

	Up to and Including Rotation Day 0: Mean±SD	After Rotation Day 0: Mean ±SD
Perfect Footsteps	91.7±4.2%	79.0±7.2%
Minor Footfaults	5.5±4.0%	11.6±2.7%
Major Footfaults	2.6±1.6%	7.1±4.0%
Very Major Footfaults	0.2±0.4%	2.3±2.5%

5.5 Conclusions

“Adaptation” to a stimulus can be thought of as a set of physiological changes sufficient to maximise an organism’s survival chance while exposed to that stimulus. In some cases, these changes may weaken an organism’s survival chance when it is returned to the original pre-stimulus conditions. One example is the loss of plasma volume associated with spaceflight, which requires a period of several hours postflight to return to an Earth-normal hydration setpoint. In other cases, an organism may rapidly re-adapt to the pre-stimulus setpoint with no apparent time delay before it regains the full measure of its original performance. Consider, for example, the synaptic plasticity and subsequent synaptic endurance of a child who learns to ride a bicycle. Even if as an adult that child should go without riding a bicycle for several decades, she will still be able to immediately ride without falling should she wish to do so. In still other cases, the difficulty comes with the transition. A good example is that of astronauts who return from their first extended mission to wrestle with feelings of disorientation, unable to interact effectively with everyday objects (Linenger 2000). Contrast them with the experienced astronauts who function well in both 1-g and 0-g, and make the transition seemingly without any difficulty at all.

The data presented in section 5.4 suggests that the adaptation of mice to chronic centrifugation is multi-layered and features elements of adaptation from several of the above examples. Four key conclusions are drawn from the data.

Centrifugation at 31.6 rpm did not negatively impact mouse health.

Data on body mass and water consumption supported Hypotheses 1 and 2. The mice were healthy and alert on every occasion that they were removed from the centrifuge. Their behaviour when handled was normal and consistent with that shown during the control study.

Anticlockwise centrifugation at 31.6 rpm resulted in a modification to the animals’ circular bias, causing them to preferentially turn in a clockwise direction. This behaviour continued to manifest itself throughout the rotational period. For at least 36 hours following rotation stoppage, the animals overcompensated with a persistent and significant anticlockwise turn bias.

In-habitat video monitoring revealed that the animals were affected by the chronic rotational stimulus. Importantly, the impacts on turn bias did not subside during the centrifugation period. The post-rotational overcompensation serves only to confirm the magnitude of the induced turn tendency.

Centrifugation at 31.6 rpm caused moderate to severe gait disturbance and balance impairment that was improved but not resolved with continued exposure to the chronic rotation stimulus. The mice continued to present these symptoms for at least 24 hours following rotation stoppage.

The balance beam testing revealed that a process of adaptation was occurring, and that this was a persistent process that began at some point during the first half of the centrifugation period and continued at least until Rotation Day 18. One explanation for the improvement in performance is that the mice may have experienced a type of adaptation similar to that of the experienced astronaut. When transitioning the first time from rotating to stationary (for Day 18 testing) they exhibited poor performance. A second transition (on Day 35) was easier. But akin to the astronaut who returns to earth dehydrated, the effects of chronic

centrifugation lingered through to at least Day 36. Accordingly, the results suggest that the adaptation process featured both transient effects (on the order of minutes) and persistent effects (on the order of days).

Importantly, the results of balance beam testing cannot be wholly attributed to stress or other anxiety-related symptoms. Again, it is of interest to distinguish between chronic and acute stress responses. In-habitat video observation showed no evidence that the rodents were unduly stressed or anxious while spinning on the centrifuge (this was in agreement with Hypothesis 3). However, it is very possible that there was marked transient stress associated with the transition from rotating to stationary, in particular on Rotation Day 18 (the first such transition experienced by the rodents). This conclusion is supported by the open field test that suggested – though without statistical significance – that the stress level of this transition was comparable to the stress of having been moved into a new and unfamiliar habitat 24 hours prior to testing on Control Day 0.

A process of adaptation allowed the rodents to acclimate to chronic rotation at 31.6 rpm. This adaptation process was still taking place at least 18 days after the start of centrifugation.

The body mass data for Rotation Day 18 and beyond strongly indicate that the rodents were not fully acclimated to the chronic rotation stimulus until more than halfway through the study. This result is consistent with the data on total distance travelled and time spent moving as recorded by the in-habitat video cameras. The animals covered a significantly greater distance during the first 18 days of rotation. This is attributed in part to an increased total time spent moving and in part to a faster speed of motion during movement episodes. Taken together, these data suggest that the time constant of whole-organism physiological (as opposed to neurovestibular) adaptation is on the order of 2-3 weeks.

5.5.1 Limitations and Future Work

Because some of the post-rotational effects had not fully resolved by two days following rotation stoppage, a further monitoring period would have been desirable. Specifically, the time course of turn bias and activity normalisation would have yielded insights into the readaptation process.

Inferences from this work are necessarily limited by the fact that the cohort of mice used in this study was small. Future investigations should aim to replicate these findings with a larger group of animals. To maintain relevance to the Mars Gravity Biosatellite mission, all tested specimens should be female BALB/cByJ mice of flight-equivalent age. Future studies might also consider discrete testing at other time-points in addition to days 0, 18, 35 and 36. Specifically, it would be advantageous to conduct a non-disruptive partial test battery on days 9 and 27 of the study. This would increase the time resolution at which adaptation can be observed and may yield additional insights into the magnitude of behavioural change.

Finally, it should be noted that the conclusions regarding lack of stress and no observed dehydration were only derived at the gross phenotypic level. Further insights and confirmation of these results would require comprehensive assays to measure faecal and serum corticosterone levels, haematocrit and urine specific gravity.

Chapter Six: Results from a Closed-Loop ECLSS Test

6.1 Motivation

The goals of this experiment were originally stated in section 1.2. The primary objective was “to provide proof of concept validation of the Mars Gravity Biosatellite’s proposed environmental control and life support systems strategy.”

To meet this objective, an experimental protocol was conceived. It was reviewed and approved by the MIT Committee on Animal Care prior to implementation (see Appendix I: CAC Protocols). The protocol proposed the following:

- Two female BALB/cByJ mice would be placed in the ASMs on the IGTA for a multi-week period.
- The centrifuge would not rotate but the IGTA would be environmentally sealed and ECLSS control would be provided by the internal atmospheric reconditioning equipment.
- In order to confirm mouse health status, the live ASM video feeds would be viewable by veterinary personnel at any time via the supervisory PC.

As stated in section 1.2.1, it was hypothesised that this closed-loop life support system comprising humidity control, oxygen replenishment, lithium hydroxide and activated carbon would support female BALB/cByJ mice for a period of several weeks. Specifically, it was hypothesised that body mass at the end of the multi-week period would be consistent with published growth curves for this strain. In addition, eating and drinking behaviours would be consistent with available data on NASA’s Nutrient Upgrade 12D Rodent Food Bar.

6.2 Procedures

The design of the IGTA and associated ECLSS elements were described in chapter 4. Once the integrated system had been assembled, additional procedures were performed to prepare the apparatus for the study. These included restocking of consumables, ensuring that all IGTA components were rodent-safe and met laboratory cleanliness standards, and verifying electrical and computer compliance. Sections 6.2.1 to 6.2.4 inclusive describe each part of the process in detail.

6.2.1 Preparation of ECLSS Consumables

Eleven days prior to commencement of the test, the IGTA ECLSS canister was packed using the following steps:

1. 560 g of 4x8 US mesh activated charcoal treated with 17% phosphoric acid was measured out using a standard laboratory scale. The charcoal product was Ammonasorb II (Barnebey Sutcliffe / Calgon Carbon), an impregnated coconut shell based carbon with a capacity for ammonia adsorption of between 7% and 16% by mass.
2. 700 g of 4x14 mesh lithium hydroxide pellets was measured out using a laboratory scale. The product was stock #13407 or L16190 from Alfa Aesar, Ward Hill, MA.
3. The charcoal and lithium hydroxide pellets were thoroughly mixed within a rolling metal canister. Care was taken to not agitate the mixture, in order to minimise dust creation. The resulting mixture was 44% carbon by mass.
4. The blend was packed into a Nomex-lined rigid plastic canister (Pelican Products, Torrance, CA). A 2 cm depth of blend was poured into the canister and a 500 g weight was placed on top to encourage settling. A vibration apparatus that moved ± 0.5 cm in the horizontal direction was placed against the outside of the canister. The frequency of vibration was 20 Hz, and each vibration episode lasted 30 seconds. The purpose of this procedure was to improve packing and minimise the risk of channelling within the bed.
5. When all chemical had been packed within the canister, it was preloaded using a backing wedge together with the aluminium sheet previously described in section 4.4.2.1. The container was subsequently locked shut and the inflow and outlet ports were sealed until deployment in the IGTA.

The above-listed packing method was consistent with previous Mars Gravity Biosatellite pilot experiments and was in line with recommendations from ECLSS engineers at Hamilton-Sundstrand Space Systems. The volumes of oxygen, LiOH and activated carbon were in all cases substantially greater than necessary to support two mice over a period of up to five weeks.

6.2.2 Installation of ASMs and Rodent Consumables

Prior to the start of the study, the IGTA was fitted with two clean, reconditioned ASMs. New waste collection media rolls were installed into the WCS and each water reservoir was filled to a volume of 250 ml. Fresh NASA rodent food bars were removed from refrigeration and cut into segments each of approximate dimensions 3.2 cm by 2.3 cm by 10.2 cm. Four such segments were adhered to the wall of each specimen chamber using rodent-safe EP21LV epoxy and following NASA-recommended procedures (Tou, Grindeland *et al.* 2003). To allow time for the epoxy to harden, this operation was completed 24-48 hours prior to the first insertion of mice.

6.2.3 Acceptance and Verification Testing

Once integrated, all subsystems were required to individually pass acceptance and verification checks. These were rigorous and detailed, in recognition of the life-critical nature of many of the assemblies. Testing with mice was not permitted to commence until the IGTA had passed 100% of its qualification tests. These are described in sections 6.2.3.1 to 6.2.3.6.

6.2.3.1 Power

Table 36 lists the checklist items that confirmed proper electrical connections to the various subsystems. In general this segment of the checklist was easy to complete. It simply required

that an experimenter enter the IGTA enclosure with a voltmeter and hold the probes to the appropriate terminals on the circuit boards and components.

Table 36: Extract of the verification checklist for power

1.	Power	
✓	1.1.	+24 V to Sensor Suite
✓	1.1.1.	Correct voltage at +5 V rail
✓	1.1.2.	Correct voltage at +10 V rail
✓	1.2.	+12 V to Baseboard
✓	1.3.	+12 V to Aggregator
✓	1.4.	+12 V to cameras
✓	1.5.	+12 V to ASM circulatory blower
✓	1.6.	Both ASMs live

6.2.3.2 Sensors

Table 37 was used to confirm both sensor operation and data accuracy. The operational segments of the checklist were mostly completed via the supervisory LabView PC. Calibration operations were performed either by the manufacturer or at MIT via exposure of the powered sensor to a calibration gas within a sealed enclosure vessel. The resulting calibration parameters were coded as variables into either the sensor suite microcontroller or the LabView Virtual Instrument.

Table 37: Extract of the verification checklist for sensors

2.	Sensors	
✓	2.1.	Correct transmission of RH and temperature data
✓	2.2.	O ₂ sensor
✓	2.2.1.	Calibration (100% O ₂) – give date
✓	2.2.2.	Data acquired, readings stored
✓	2.3.	CO ₂ sensor
✓	2.3.1.	Calibration (manufacturer) – give date
✓	2.3.2.	Data acquired, readings stored
✓	2.4.	Pressure sensor
✓	2.4.1.	Calibration (manufacturer) – give date
✓	2.5.	Ammonia sensor (A7AM)
✓	2.5.1.	Calibration (lab, 8.8ppm NH ₃) – give date
✓	2.5.2.	Data acquired, readings stored
✓	2.6.	Ammonia sensor (ChemKey colourimetry backup device)
✓	2.6.1.	Calibration (manufacturer) – give date
✓	2.6.2.	Readings correctly shown on screen
✓	2.7.	Flow rate sensor
✓	2.7.1.	Calibration (manufacturer) – give date
✓	2.7.2.	Data acquired, readings stored
✓	2.8.	Backup Hobo datalogger functional for temperature, RH and light

6.2.3.3 ECLSS Actuators

Table 38 was used to confirm that all non-sensor ECLSS hardware operated flawlessly. In most cases, these checklist items required highly specific procedures. For example, to address checklist item 3.2.1 it was necessary to temporarily seal the IGTA after placing an open vessel of aqueous ammonia within the chamber. The ECLSS computer was activated and it triggered the compressor once ammonia concentrations had exceeded the setpoint. An experimenter would subsequently watch the on-screen plots of ammonia to verify adsorption. In the case of checklist item 3.2.2, a controlled flame was allowed to burn within the IGTA in order to replace oxygen with carbon dioxide. The checklist item could only be cleared once the ECLSS actuator had been observed to activate and scrub carbon dioxide from the atmosphere. Other line items were simpler to verify. For example, 3.3 was simply a question of activating the oxygen valve via LabView manual override and watching the on-screen plot of oxygen to confirm an increase in concentration.

Table 38: Extract of the verification checklist for actuators

3. ECLSS Actuators and Hardware		
✓	3.1.	Lockoff valves at canister inflow/outflow operational
✓	3.2.	Hargraves air compressor operational, flow rate through bed of above 4.9 SLPM
✓	3.2.1.	Evidence for NH ₃ removal
✓	3.2.2.	Evidence for CO ₂ removal
✓	3.3.	Oxygen flow valve operational
✓	3.4.	Oxygen tank filled to pressure of 130 Bar
✓	3.5.	Condensing heat exchanger operational
✓	3.5.1.	Condenses water
✓	3.5.2.	Micropump removes condensate
✓	3.5.3.	Micropump bactericided with 100% ethanol (give date)
✓	3.5.4.	Reservoir emptied prior to start of test
✓	3.6.	Canister packed with fresh LiOH/AC blend (give date)
✓	3.6.1.	Packed mass of LiOH recorded
✓	3.6.2.	Packed mass of Ammonasorb II activated carbon recorded
✓	3.7.	Interconnection tubes checked
✓	3.8.	Electrical power to environmental control board (+12V)
✓	3.9.	Data fidelity to signal connector block / LabView PC
✓	3.10.	All-operational power performance verified (O ₂ flow, CHX on, canister on)

The other checklist items in Table 38 are mostly self-explanatory. Item 3.10 was added after preliminary pilot studies in order to confirm that the environmental control board voltage regulator was providing sufficient power even under high current draw conditions.

6.2.3.4 Software

Table 39 shows checklist items for software and bit-level hardware operations. The designator ASM-SEL refers to the multiplexer selection line that is used to toggle between the two habitats. VID1 and VID2 are the two video lines, while TX and RX refer to the RS-232 / DB-9 serial communications pathways that permit the LabView VI to communicate with the HCMs attached to each habitat module.

Table 39: Extract of the verification checklist for software

4.	Software
✓	4.1. ASM-SEL operational, as shown by switching between ASMs
✓	4.2. VID1 operational, clear video picture shown in VI
✓	4.3. VID2 operational, clear video picture shown in VI
✓	4.4. TX operational, shown by transmission of lixit clear command
✓	4.5. RX operational, shown by receipt of ASM data
✓	4.6. Water delivery counts recorded
✓	4.6.1. All 4 water nozzles operational
✓	4.6.2. For all 4 water nozzles, manually holding toggle stick to one side results in correct “lixit off” auto-disable
✓	4.7. LabView ECLSS performance
✓	4.7.1. Correct control decisions for O ₂
✓	4.7.2. Correct control decisions for CO ₂
✓	4.7.3. Correct control decisions for NH ₃
✓	4.7.4. Correct control decisions for RH
✓	4.7.5. Video acquisition and storage at pre-defined times, pre-defined settings
✓	4.8. LabView logging performance
✓	4.8.1. Correct saving of data to log files for ASM transmissions
✓	4.8.2. Correct separation of data from ASM1 and ASM2
✓	4.8.3. Correct saving of sensor data to log file
✓	4.9. LabView video performance
✓	4.9.1. File saving correct
✓	4.9.2. Video frame rates correct when opened
✓	4.9.3. Each clip lasts constant 23.55 minutes
✓	4.9.4. Files can be opened by Ethovision
✓	4.10. LabView remote information distribution
✓	4.10.1. Text messaging functionality verified
✓	4.10.2. Web-based VI access
✓	4.11. Other software
✓	4.11.1. Ethernet is operational

Given the life support criticality of this experiment, communications and alerting functionality was designed into the custom LabView Virtual Instruments. This included always-on remote access to permit both live and historical monitoring of IGTA ECLSS status via the internet. In addition, the LabView VI had the capability to send SMS alert messages to the author’s mobile phone. This was used to report events such as an atmospheric parameter entering an off-nominal range and remaining uncontrolled for an extended period.

Checklist item 4.9 refers to video functionality. The LabView Virtual Instrument was programmed to record 24 minutes of full-rate video twice per day, at 8am and at 8pm, in order to provide backup reference footage if rodent health became questionable.

6.2.3.5 Animal Care

Checklist elements for rodent care and pre-experiment cohort preparation are listed in Table 40. Most line items are self-explanatory. Item 5.5 was included to ensure that the water

lines were free from bacteria and other contaminants. This was particularly important if the ASMs had been left unused for multiple weeks prior to an experimental run.

Table 40: Extract of the verification checklist for rodent care

5. Animal care		
✓	5.1.	Animals individually housed in standard laboratory cages prior to test (record date of first individual housing)
✓	5.2.	Fresh food bars installed 24-48 hours prior to experiment start (record date of installation)
✓	5.3.	Animals inserted into IGTA ASMs for start of experiment (record date)
✓	5.3.1.	Record mass of Mouse 1
✓	5.3.2.	Record mass of Mouse 2
✓	5.4.	Air flow lines to ASMs verified
✓	5.5.	Water lines cleaned out with ethanol and washed through with water (record date)
✓	5.6.	Water bags filled with 250ml fresh water from rodent-approved water source (record date)
✓	5.7.	Fresh waste collection media installed in ASM base

6.2.3.6 IGTA Preparation

Table 41 shows checklist elements for preparing the IGTA, installing the mice, sealing the cube and completing required final test paperwork.

Table 41: Extract of the verification checklist for IGTA preparation

6. IGTA Preparation and Environmental Soundness		
✓	6.1.	All cubicle light sources shrouded / deactivated
✓	6.2.	Cube verified leak-free by clean-flame O ₂ reduction procedure measured by MOX-9 sensor on Sensor Suite (record date)
✓	6.2.1.	Record O ₂ level at start
✓	6.2.2.	Confirm O ₂ level still the same after 12 hours
✓	6.3.	Cube verified leak-free by NH ₃ concentration maintenance procedure as measured by ChemKey (record date)
✓	6.3.1.	Record NH ₃ level at start
✓	6.3.2.	Confirm NH ₃ level still the same after 12 hours
✓	6.4.	Support structures locked down, screws tightened, twist ties fastened
✓	6.5.	Test commence: install mice
✓	6.5.1.	All circuit boards powered on
✓	6.5.1.1.	Audible motor augment to start of test
✓	6.5.2.	LabView connection activated, confirmed
✓	6.5.3.	Centrifuge motor confirmed deactivated
✓	6.5.4.	Portal door sealed shut
7. Paperwork		
✓	7.1.	Animal care staff and supervisors informed of test start and date
✓	7.2.	“Experiment in progress” card filled in
✓	7.3.	Daily animal check personnel scheduled for expected test duration

Line item 6.1 was important to ensure that stray night-time light sources did not disturb rodents in adjacent cubicles of the otherwise darkened animal care facility. Elements 6.2 and 6.3 represent two different types of leak test to confirm airtightness with the portal door secured. The motor referenced in 6.5.1.1 is part of the WCS; this line item confirmed that the optical sensor system was properly aligned with the installed waste collection media.

6.2.4 Test Commencement

Two female BALB/cByJ rodents were provided at least 48 hours to acclimate to single-housed standard laboratory cages following shipment from Jackson Laboratories (Bar Harbor, ME). Veterinarians consider this time period appropriate for newly-shipped animals. The specimens were subsequently introduced to the custom Mars Gravity Biosatellite habitat modules for a short period and proper acceptance of the automatic water nozzles and NASA Rodent Food Bar was confirmed. When both mice were aged 10 weeks and 6 days, they were installed into two habitat modules within the IGTA, as per currently baselined pre-flight procedures. These mice were a few weeks younger than the 14.5-week minimum age anticipated for flight.

Daily air sampling with an external chemical colourimetry ammonia sensor was performed to confirm proper operation of the electrochemical ammonia sensor within the IGTA. The amount of air extracted each day was negligible compared with the total volume within the enclosure. Because the ammonia sensor exhibited a longer start-up time than had been originally anticipated, periodic recalibration of this sensor was performed via the supervisory LabView Virtual Instrument during the first few days of the test.

6.3 Control Algorithms

The control software used during this test implemented simplified versions of the flight-ready algorithms previously discussed in section 3.5.1. The boundary-based on/off control philosophy was replicated to the extent possible.

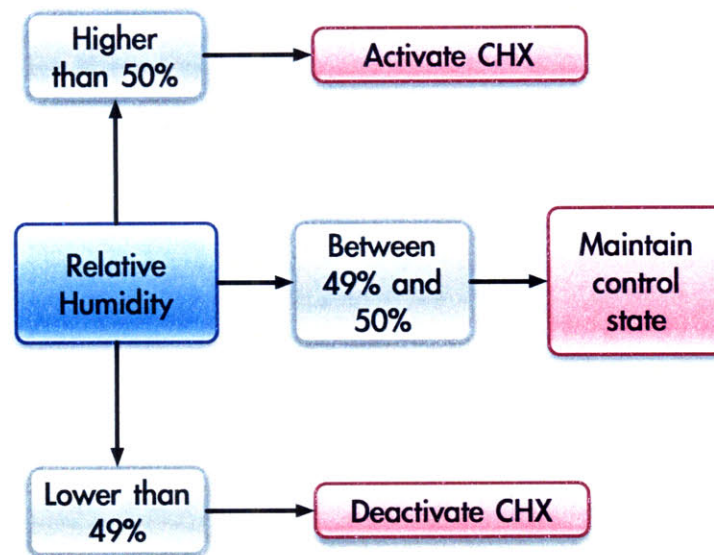


Figure 82: Control algorithm for condensing heat exchangers

The flowchart shown in Figure 82 applies specifically to humidity control. Left unchecked, humidity would rise due to rodent metabolic processes; accordingly, the condensing heat exchanger activates when air moisture content is higher than a certain boundary level.

The approach for oxygen is similar. The algorithm calls for 100% oxygen to be added from the gas cylinder if the sensor readout should become too low. The valve would shut off in the event oxygen level rose above a certain value. The setpoints were altered on three occasions as shown in Table 42 in order to verify proper operation of the control algorithms.

Table 42: Oxygen control algorithms

	Days 1-4	Day 10	Otherwise
Open oxygen valve if below	20.6% or 20.7%	20.6%	20.95%
Close oxygen valve if above	20.9%	20.9°C	21%

The other controlled contaminants were carbon dioxide and ammonia. Since the canister contained a mixture of lithium hydroxide and activated carbon, the control algorithm took into account levels of both contaminants.

As shown in Figure 83, the fundamental approach was to scrub the air until both contaminants had reduced to below the low-level setpoints. This scheme uses more power than alternatives but prioritises animal health by preferentially selecting lower contaminant levels whenever possible.

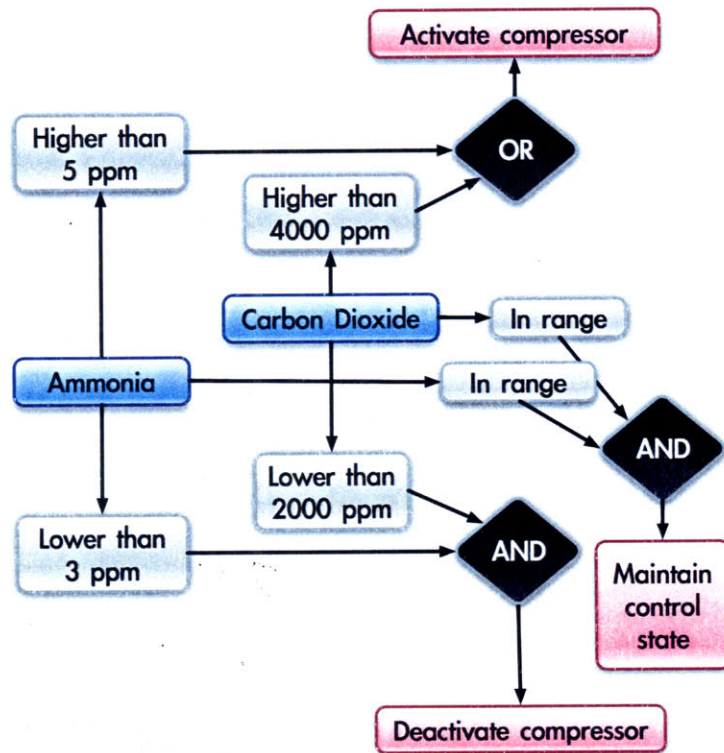


Figure 83: Control of ammonia and carbon dioxide

6.4 Results and Discussion

Table 43 shows that both rodents exhibited normal body mass before and after the 25-day study. The magnitude of weight gain for both test animals was consistent with normal growth curves published by Jackson Laboratory for the BALB/cByJ strain at ages 11 and 14 weeks (shown as mean \pm standard deviation). Mouse 1 was within one standard deviation above the mean both before and after 25 days in the IGTA. Mouse 2 was a smaller specimen that commenced the test presenting a mass two standard deviations below the mean but finished within one standard deviation.

Table 43: Magnitude of weight gain for both test animals

	Day 0, aged ~11 weeks	Day 25, aged ~14 weeks
Mouse 1	23.1 g	24.6 g
Mouse 2	20.6 g	22.3 g
Published data, healthy mice	22.25 \pm 1.41 g	24.03 \pm 2.46 g

Rodent eating patterns were also normal, though the nature of the ASM design made it impossible to determine the exact mass of food consumed over the course of the experiment. Rodent water consumption was generally consistent with previous Mars Gravity studies in which rodents were fed a NASA Food Bar diet for a multi-week period (Figure 84).

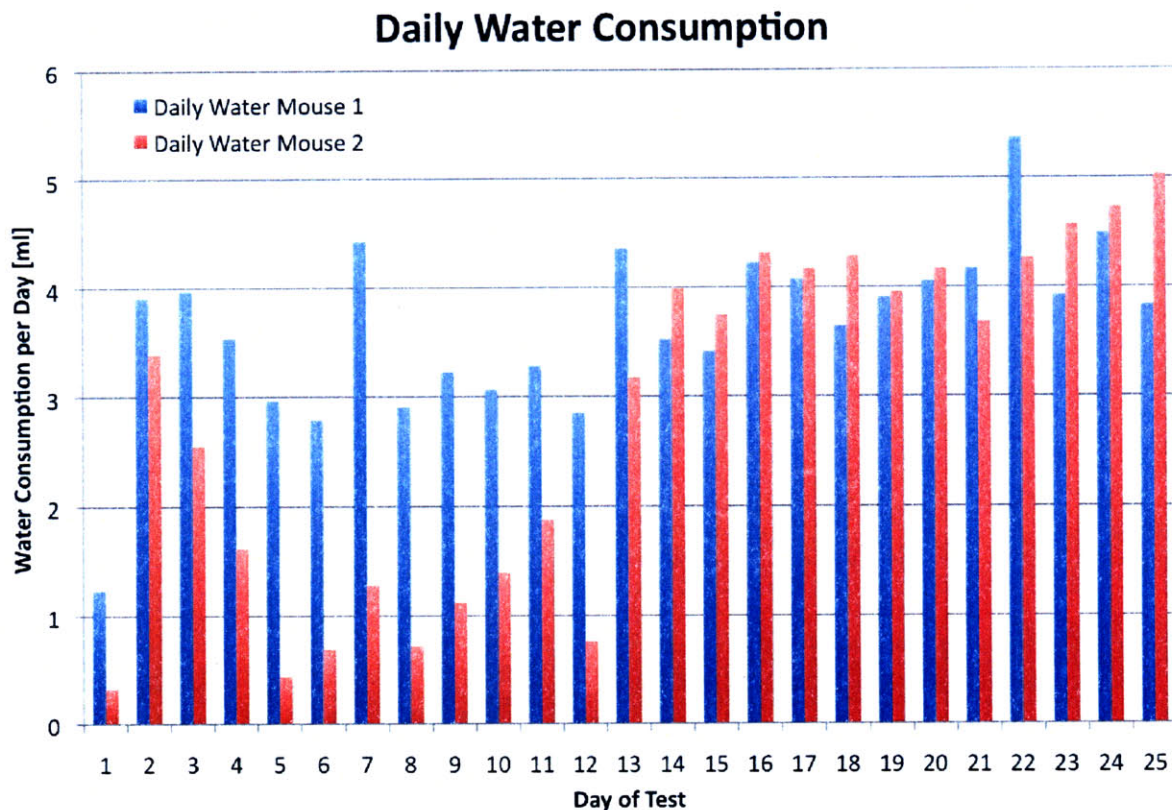


Figure 84: Water consumption data for both rodents

For reasons which are unclear, Mouse 2 consumed less water during the first half of the experiment. Water nozzles in this ASM were functioning normally throughout the study, and there is no evidence that Mouse 2 exhibited a lower metabolic rate during the first twelve days of the experiment. Measurement error alone cannot account for such a marked water consumption difference. However, from day 13 onwards Figure 84 shows that water intake by both animals was closely matched. By the end of the study, Mouse 1 had consumed 91.3 ml of water while Mouse 2 had consumed 70.3 ml. The net difference is consistent with normal inter-specimen variation of $\pm 15\%$ about the mean. This data was reported from a cohort of male Sprague-Dawley rats that consumed food bar over a 20-day period (Tou, Grindeland *et al.* 2003).

Both animals were normal in appearance and a pinch test at the end of the study showed no detectable dehydration. Each of the mice did exhibit a degree of scruffiness and a loss of fur sheen that is to be expected with a bedding-free specimen chamber. Following the study, both specimens were returned to standard laboratory caging. They continued to maintain good body weight and exhibited no ill effects from their multi-week stay in the closed-loop environmental system.

Figure 85 shows that oxygen concentration was controlled within the target range throughout the study. The blue line indicates times at which LabView caused the valve to open, replenishing oxygen from the 137 bar cylinder via a 690 millibar (gauge) regulator. Each upward spike indicates an activation that in most cases lasted approximately one minute. The smaller ripples can be attributed to noise in the system, sensor imprecision of $\pm 0.1\%$ oxygen, natural fluctuations in rodent respiration rates and variations in oxygen concentrations in the immediate vicinity of the sensor. As explained in chapter 4, the sensor suite was placed along the opposite wall of the IGTA from the oxygen cylinder. Accordingly, there was a diffusion distance of approximately 1 metre over which oxygen molecules had to travel to reach the sensor.

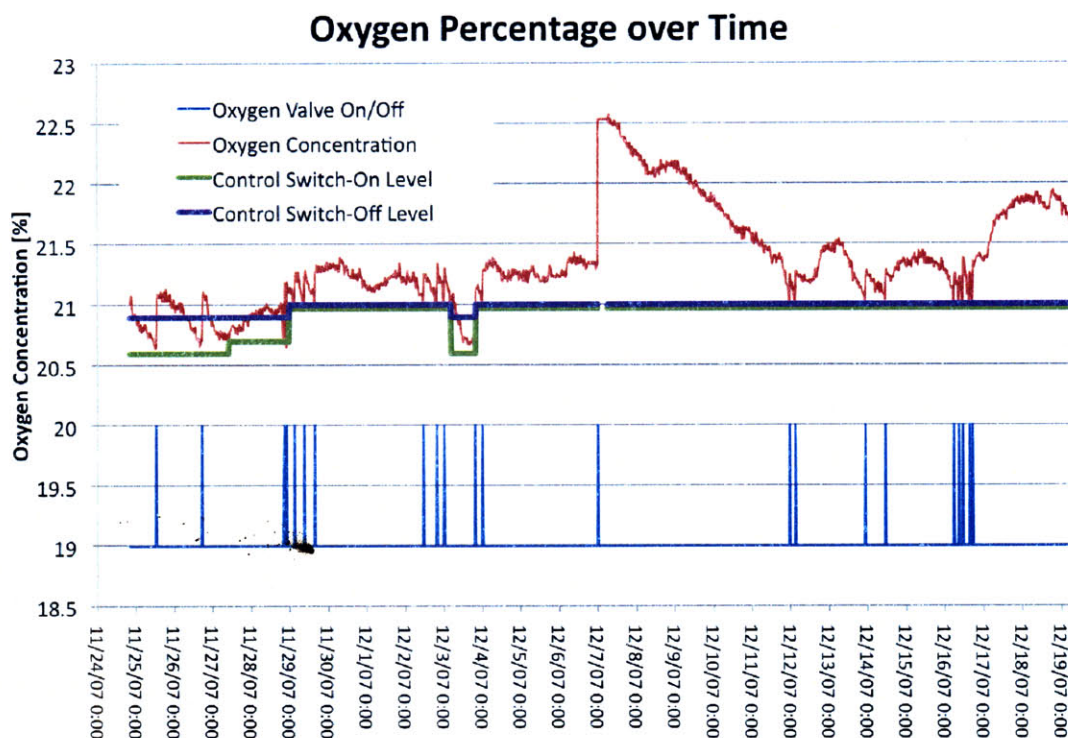


Figure 85: Oxygen concentration

One system glitch occurred early in the morning of 7th December. An operating system failure resulted in an uncommanded computer reboot. Although the software successfully relaunched, an unexpected application startup state resulted in the computer incorrectly detecting the oxygen concentration as 0%. As a consequence, the electronic replenishment valve was activated for an unusually long duration. The result was a rapid spike to slightly over 22.5% at which point the oxygen sensor came back online. This error can be attributed to the fact that commercial rapid prototyping and benchtop development tools were used to write the ground software. The on-orbit software will be designed using strict quality assurance protocols and robust error recovery systems.

Figure 86 shows ammonia concentrations within the IGTA over time. Similar to Figure 85, the overlaid blue trace marked “compressor on/off” is a scale-independent binary indicator. As discussed in chapter 4, the compressor outlet is attached to a canister packed with lithium hydroxide and activated charcoal. Accordingly, activation of the compressor may be triggered by a need either to scrub carbon dioxide or to eliminate ammonia. Even though the rodent health requirement simply calls for ammonia to remain below 10 ppm, the LabView algorithms were written to command compressor activation as soon as the ammonia levels rose above 5 ppm in order to guarantee a tighter level of control authority. In the presence of nominal carbon dioxide levels, compressor deactivation would occur when the ammonia reduced below 3 ppm. Figure 86 demonstrates this performance, and also reveals a phase lag on the order of 30 minutes between compressor activation and the start of detectable ammonia adsorption.

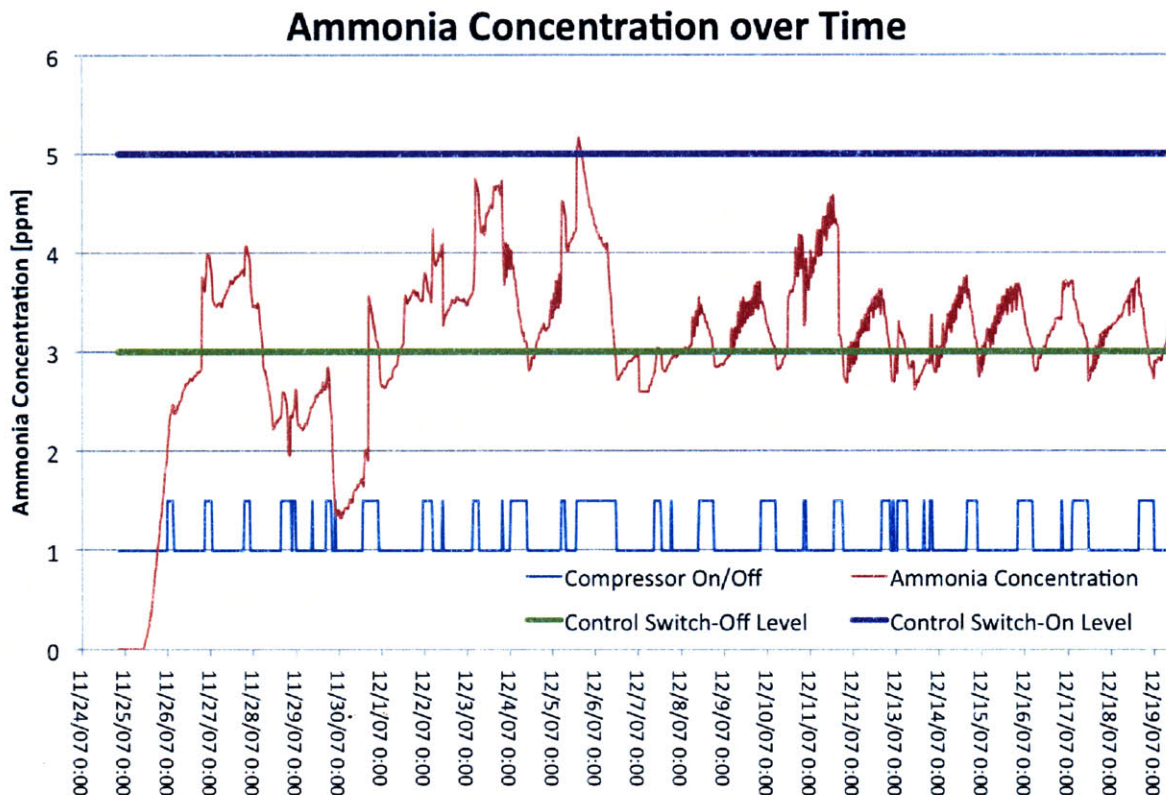


Figure 86: Ammonia concentration

Figure 87 confirms that carbon dioxide levels were well controlled in the IGTA. The science-driven upper limit for carbon dioxide was 7000 ppm, but the LabView algorithms targeted 4000 ppm for improved control authority. Multiple transitions between 4000 ppm and 2000 ppm were observed, indicating good performance of the lithium hydroxide canister and compressor. While the compressor was on, the carbon dioxide trace in Figure 87 sloped steeply downward at a near-constant gradient. Occasions where the carbon dioxide concentration dips below 2000 ppm are attributable to a transient need to reduce ammonia levels.

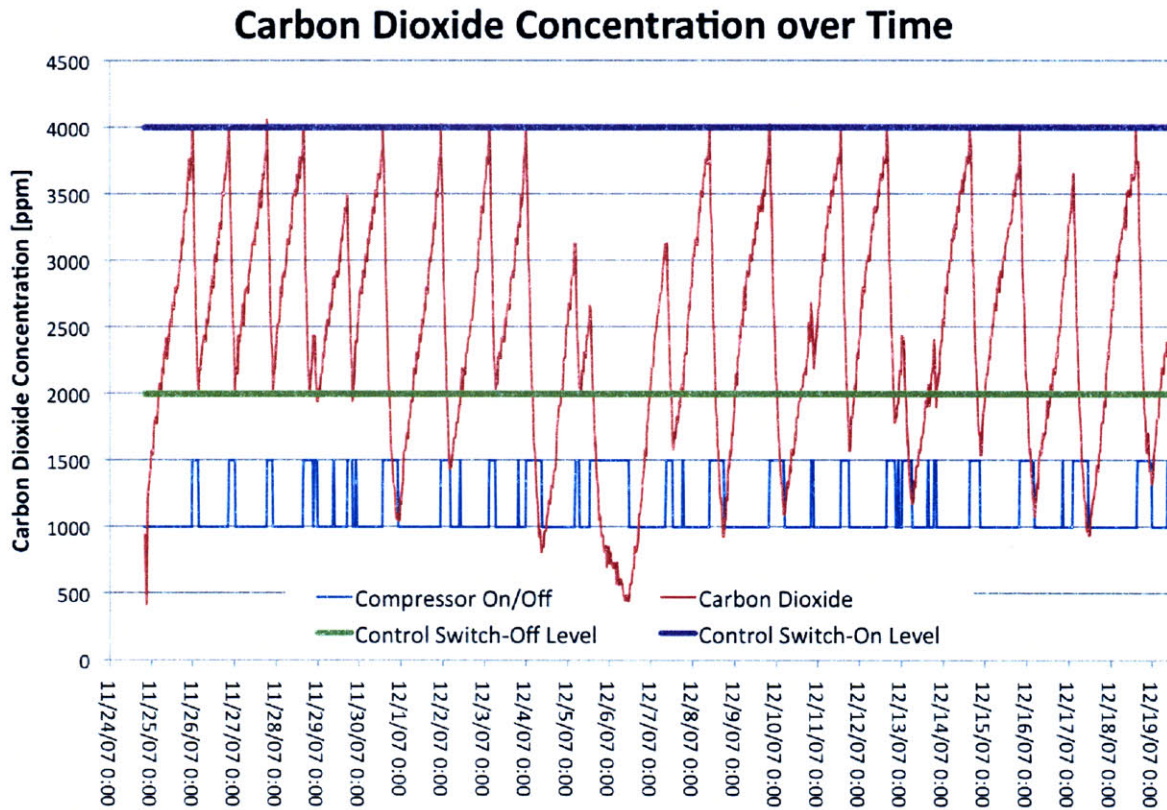


Figure 87: Carbon dioxide concentration

Figure 88 shows relative humidity over time. For optimal rodent health, humidity should remain in the 40%-70% range. Ammonia production is a direct consequence of microbial breakdown of waste products, a process that is accelerated in damp conditions. Accordingly, to minimise ammonia production rates the control algorithms were tuned to favour drier conditions, targeting less than 50% RH.

The importance of the LiOH/carbon bed in relative humidity control is very noticeable. During the first half of the experiment, the condensing heat exchanger activates very rarely. Given the high percentage of activated charcoal in the canister, it is postulated that water was being adsorbed into the micropores of the charcoal pellets and that this was the primary means of dehumidification within the IGTA. In addition, phosphoric acid is known to be highly hygroscopic; chemical interaction between water vapour and the acid-washed carbon pellets may account in part for the observed results. The condensing heat exchanger appears to have been most useful for fine-tuning, maintaining the relative humidity to

within a few percent of the 50% RH upper control limit toward the end of the 25-day experiment.

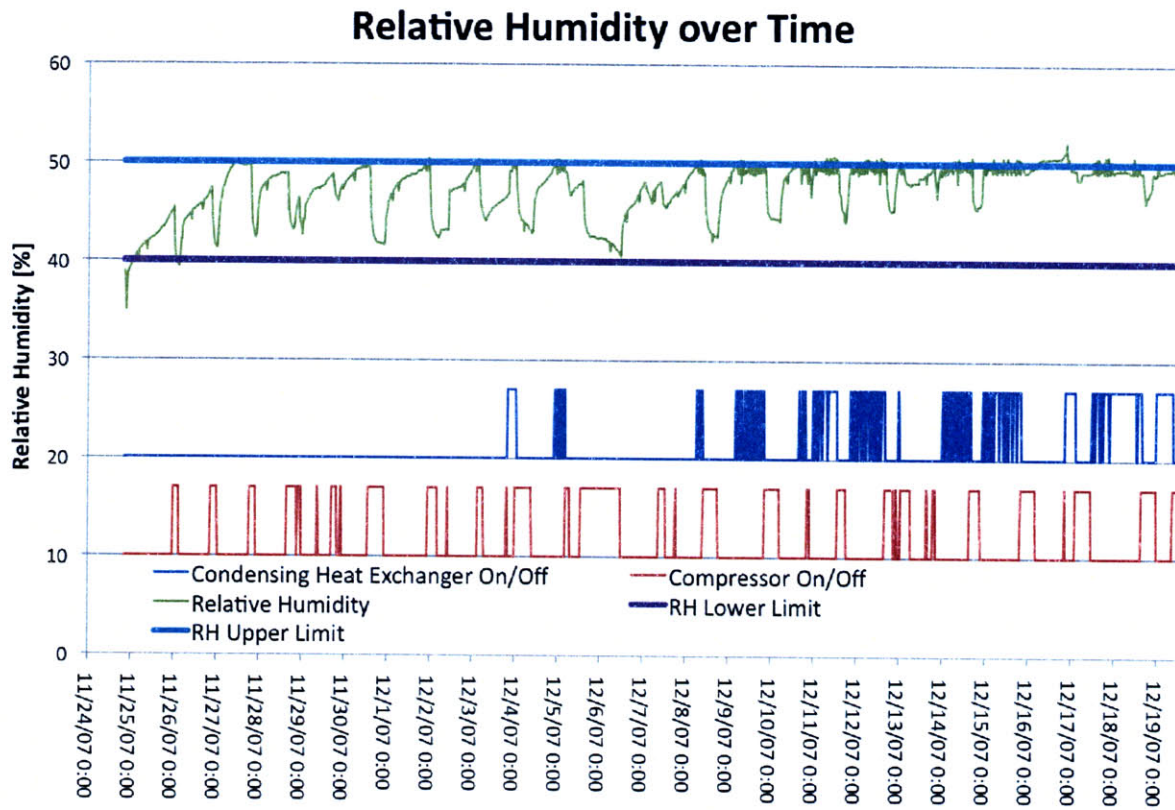


Figure 88: Relative humidity

6.5 Conclusions

This work has demonstrated the preliminary feasibility of the proposed ECLSS concept for the Mars Gravity Biosatellite. Successful control of the key contaminants for two mice within a sealed system confirms the appropriateness of this strategy and suggests future directions for ongoing design refinement.

The experiment demonstrated the operation of the following elements, each of which will be implemented in higher fidelity on board the Mars Gravity Biosatellite:

- Supervisory control software that uses a boundary-based ECLSS activation strategy.
- The flight-ready sensor suite equipped with flight-specified sensors for whole-system atmospheric monitoring.
- Ammonasorb II activated charcoal to remove ammonia from the closed-loop environment.
- Lithium hydroxide to scrub carbon dioxide.
- The flight-like condensing heat exchanger to control relative humidity.

- Use of the flight-specified models of compressor and blower for atmospheric cleansing and air distribution.
- Replenishment of oxygen from a cylinder fitted with a regulator and valve.

Key differences between the ground-based test and the anticipated on-orbit design are as follows:

- The software used in the ground experiment was a first prototype that was developed in an *ad hoc* fashion. The development process did not adhere to standards of quality assurance, testing and verification that are commonly used for spaceflight applications.
- The IGTA did not have rigid walls that would have allowed the enclosure to hold pressure. Consequently, unlike the baseline payload design, it did not feature a nitrogen canister for pressure control.
- The enclosure membrane was not volume-matched to the on-orbit apparatus. To incorporate the centrifuge and for practicality of assembly, the IGTA volume was approximately four times that of the payload module.
- Silica gel desiccant for backup/assistive humidity control was not included in the ground apparatus.
- The volumes of lithium hydroxide, activated carbon and oxygen in the IGTA were substantially greater than the minimum required for a 3.5-week 2-mouse test.
- Thermal control was outside the scope of this ground test.

6.5.1 ECLSS Limitations

No attempt was made in this experiment to quantify levels of offgassing from the plastic enclosure membrane and from equipment within the IGTA. The on-orbit hardware will likewise not feature any trace contaminant sensors; the intention is to select hardware with minimal offgassing characteristics wherever possible. This strategy is yet to be validated in ground-based experiments. It is likely that the activated charcoal bed would adsorb certain volatile contaminants, but this will not be substantial given that the mission will last only 5 weeks.

Although it is generally desirable to minimise methane levels within the ASMs, the IGTA featured no hardware to monitor the concentration of this gas. Most readily available COTS sensors can only detect explosive levels of methane, which would naturally be inappropriate for the biosatellite and for ground-based experiments. Again, the activated charcoal does have some affinity for methane. This is expected to be more than adequate for the chosen mission duration, especially given that mice produce only tiny quantities of the gas.

Overall, there is no reason to believe that the ECLSS apparatus within the IGTA should not have functioned for several more weeks beyond the 25-day cutoff. All systems were operating nominally at the time the experiment came to an end.

6.5.2 Future Recommendations

As the Mars Gravity Biosatellite enters the Critical Design Phase, it will be necessary to construct a fifteen-habitat mockup with higher-fidelity atmospheric systems. This can be achieved by removing the centrifuge from the IGTA entirely and building a set of shelves to support fifteen flight-ready ASMs in ground-normal orientation.

The bullets listed at the end of section 6.5 above should each be addressed as follows:

- Higher-fidelity software development tools and processes should be used, together with more rigorous testing of off-nominal startup condition and reboot scenarios.
- Rigid walls made of aluminium or acrylic should be incorporated. These could potentially be mounted to the outer frame of the IGTA and secured using sealant glue and gaskets.
- Volume-matching could be achieved through the use of rubber inflatables within the IGTA. A number of these could be secured to the framing supports at each of the cube's vertices. Care should be taken to ensure the rubber does not offgas and is compatible with low levels of gaseous ammonia. The inflatables should be filled with a nonflammable inert gas such as nitrogen.
- The silica gel bed can be readily incorporated into the current apparatus. Modifications would be required to include additional valves and to interface these with the ECLSS PCB and with LabView.
- By obtaining various sizes of Pelican case it should be possible to very closely match the volumes of LiOH, activated charcoal and silica gel to the on-orbit parameters. To match the available oxygen volume, the cylinder should be partially depleted prior to installation within the IGTA.
- Incorporating thermal control elements would require installation of a large aluminium baseplate below the IGTA and attachment of an industrial chiller. It may also require the addition of extensive insulation around and outside the IGTA. This major systems-level rework would require substantial resources since it poses several technical challenges.

Chapter Seven: The Biosatellite as a Research Platform

7.1 Motivation

The Mars Gravity Biosatellite payload module is designed to support rodents in a partial gravity environment. It builds on microgravity biological spaceflight heritage from the Cosmos missions and the NASA Animal Enclosure Module (AEM). It takes into account advances showcased in the now superannuated AAH-C blueprints. The design approach is tuned to incorporate best practises from space systems engineering and related disciplines. The resulting system is modular and robust. The habitat modules in particular are now a generation more advanced than any currently manufactured spaceflight design.

This chapter asks how the payload module could be modified or augmented to address other needs of the space life sciences research community. As a starting point for considering this question, reference was made to the December 2003 NASA Free Flyer Workshop held at Ames Research Center under the auspices of the now defunct Office for Biological and Physical Research (Israelsson 2003). At that workshop, participants formulated over a hundred reference experiments and categorised them under three broad goal headings (Carpenter 2004).

Goal A: To learn how life interacts with the physical world using free flyers

Determine the basis of altered immunity, determine responses to galactic cosmic radiation, understand effects of accumulation of volatiles in enclosed spaces, understand biofilms, determine mechanisms underlying physiological adaptation.

Goal B: To expand knowledge of the physical world using free flyers

New physics, conditions beyond the Van Allen belts, testing Einstein's theories, origins of self organisation, models of turbulence and combustion effects.

Goal C: To develop and validate exploration technology using free flyers

Harmful microgravity physiological effects, critical crew life support systems, new radiation shielding, development of nutritional and pharmaceutical countermeasures, validate advanced propulsion systems, advanced sensors and autonomous controls.

Goal A and Goal C are most closely aligned with the nature of the payload module as an integrated system capable of supporting life sciences experiments. Accordingly, sections 7.2 to 7.6 address the design changes that would support these goal areas:

- (Goal A and Goal C) What types of study could be performed with group-housed mice? How might group-housed animals be accommodated within the payload?

- (Goal A and Goal C) Would it be meaningful to provide support for animal models other than mice? Which species would these be, and what modifications to the payload would be necessary to adequately accommodate them?
- (Goal A) The payload ECLSS subassemblies are designed to replicate an Earth-normal atmospheric environment. Would it be meaningful to target other setpoints, including those that model the trace contaminant buildup which is anticipated in closed-loop extended-duration life support systems? If so, which design modifications would be necessary?
- (Goal A) How might the payload module be redesigned to support radiation studies? Such research, with or without partial gravity, would have clear relevance for the exploration agenda and for long-term human spaceflight. As an unmanned craft, the free-flyer has advantages for the exposure of biological specimens to high radiation orbits or on-board radiation sources.
- (Goal C) What modifications would be required to support gravity levels different from 0.38-g, including weightlessness?

7.2 Group Housing Options

The Mars Gravity Biosatellite payload module is designed to support singly-housed rodents, but its modular configuration ensures that group-housed habitats could be readily accommodated. This would enable studies of rodent reproductive success in altered gravity and could provide useful data on interactions among groups of animals during spaceflight. Propagation of disease within group-housed cohorts could shed light on immune system dysfunction in space.

Because the ASMs are arrayed around the central utility truss in blocks of three, it would be simple to replace any block with an ASM three times the current size. Separation of wastes from individual animals would no longer be possible and video cameras would need adjustment to cover all zones of interest. Replacement habitats larger than three times the current ASM volume would pose problems because of the need to maintain cylindrical symmetry around the axis of rotation.

In addition, the shape of the larger ASM would result in the floor no longer being flat. It would need to have a curvature consistent with the outer shell of the life support bucket to ensure all rodents experience the same level of artificial gravity regardless of their location on the floor of each specimen chamber. The result would be a sensory conflict whereby the rodent visual system would (correctly) indicate that the floor is not flat, even though data from vestibular organs would insist that the opposite is true. For certain types of experiment, this may not be problematic. For others, it may be more appropriate to flatten the floor and accept some variation in gravity on account of changing distances between the mouse and the central axis of rotation. This was the chosen approach for the Cosmos-936 centrifuge design previously shown in Figure 7 (Chapter 1). However, the fact that the rat had very limited floor area within its chamber means that design justification cannot be drawn exclusively from that mission. In the current ASM configuration, the long axis of the specimen chamber is purposely aligned perpendicular to the rotation vector in order to avoid this issue altogether.

The enlarged habitat modules could each accommodate up to six mice, making for a total of thirty rodents on board a single spacecraft. The WCS would require a redesign, but since

all waste collection would be group-based it may be possible to substantially simplify the system. Eliminating urinalysis capabilities would be an obvious first step and would reduce complexities associated with manufacturing the waste collection substrate and ensuring reliable conveyor operation. The body mass platforms could continue to be part of the design, but only if animals were individually identifiable from video footage. Possible approaches could include coloured marking dots on the stomach and back of each animal, a feasible option only if full-colour video cameras were installed within each habitat.

Table 44 summarises key anticipated changes to the core payload subassemblies.

Table 44: Modifications for group housing

Subsystem	Modifications Required
Habitat Modules	Replace 15 standard ASMs with 5 triple-sized ASMs with curved and contoured floors. Simplify waste system for group-housed rodents. Alter video camera placement as necessary. Devise an approach for identifying individual animals via the video cameras.
ECLSS	Include greater volumes of consumables in order to accommodate the larger cohort.
Thermal Control	No changes anticipated.
Structures	Strengthen central utilities truss to hold larger ASMs and heavier ECLSS canisters if necessary.
Electrical/Software	Reconfigure behavioural analysis video software for compatibility with groups of animals. Modify HCM code to communicate with video software to identify which animals are drinking or positioned on the body mass sensor at any instant.

7.3 Other Animal Models of Interest

Over 1133 life science experiments were flown by NASA between 1961 and 2007 (NASA 2007). A multitude of different species have been sent into space, many of which are listed in Table 45 (Gray 1998).

Some of the species were chosen for very specific reasons. The bullfrog, for example, was used in a 1970s experiment to study the impacts of microgravity on the otolith. This organism was selected because its vestibular labyrinth exhibits similarities to the corresponding human organ system. Similarly, newts are of great interest in space medicine studies due to their ability to regenerate following injury or surgical resection of tissue.

Other species were selected more for practicality than for science. Many of the early US missions flew monkeys, only for the reason that engineers required a mid-sized mammal to exhibit metabolic processes approximating those of a human. By contrast, early Soviet missions flew dogs since mission managers believed that canines would be calmer than monkeys in the spaceflight environment. The data from these early flights covered a wide variety of parameters, including the physiological effects of space, the effectiveness of ECLSS designs, and spacecraft structural soundness. Introducing still more variety, when France

began its space exploration program their scientists selected the cat as an appropriate species for initial flights.

Many of the species listed in Table 45 flew only once. The most commonly flown specimens in terms of total number of missions are rats, followed closely by mice. “Extensive” spaceflight heritage is used for any non-insect species of which more than 500 specimens have flown. “Moderate” indicates between 50 and 500 specimens, while “Minimal” refers to fewer than 50 individuals or no more than five missions.

Table 45: Animals in space (embryos, eggs and larvae excluded)

Species	Spaceflight	Species	Spaceflight
Ant	Minimal	Mealworm	Minimal
Bee	Minimal	Mouse	Moderate
Beetle	Minimal	Newt	Moderate
Bullfrog	Minimal	Parasitic wasp	Minimal
Cat	Minimal	Rabbit	Minimal
Chimpanzee	Minimal	Rat	Extensive
Cockroach	Minimal	Rhesus monkey	Moderate
Cricket	Minimal	Scorpion	Minimal
Dog	Moderate	Shrimp	Minimal
Earthworm	Minimal	Snail	Minimal
Fish	Minimal	Spider	Minimal
Fruit fly	Moderate	Squirrel monkey	Minimal
Gecko	Minimal	Tortoise	Minimal
Guinea pig	Minimal	Turtle	Minimal
Jellyfish	Minimal	Wine fly	Minimal

The physical dimensions of the Mars Gravity payload module make it impossible to fly species any larger than a guinea pig and still accommodate a statistically meaningful number of specimens. Accordingly, this section focuses on smaller animals that have been used in recent life sciences missions or for which flights are planned in the 2008-2015 timeframe. For maximal scientific relevance, emphasis is placed on species from Table 45 that have “moderate” or better flight history.

7.3.1 Rats

The average laboratory mouse weighs approximately 25g, while an adult rat can weigh ten to twenty times that figure. The rat also presents significantly greater food and water consumption, faecal output and metabolic load requirements. Indeed, one of the primary drivers for choosing mice for the Mars Gravity mission was to maximise the cohort size and statistical power given the available living space and volume for consumables.

To provide appropriate accommodations for rats, it would first be necessary to increase the size of each ASM using a procedure similar to that described in section 7.2. If the mission duration were shortened, it is likely that the volume of consumables could be commensurately reduced and the ASMs could be lengthened toward the nose of the spacecraft. In general, however, it is unlikely that more than ten adult rats could be accommodated even with double-housing.

In order to accommodate the larger rat, it would be necessary to increase the height of the wall-mounted water nozzle. The body massing platform would need substantially greater surface area. Rat faecal pellets are significantly larger than those of the mouse, but the current ASM floor design and hole sizing would still be adequate to permit good clearance of waste into the WCS. A redesign may be necessary regardless if it is observed that the rats are able to chew through the perforated plastic floor. Mice jaws are too small to clamp around the bars that separate one gridline from the next. For rats this may not be an obstacle, and with their sharper, larger teeth they may be able to chew through the cold-poured urethane substrate fairly rapidly. A fail-safe design solution would be to incorporate a steel grid immediately beneath the plastic floor.

The WCS could be used with minor modifications. A larger collection hopper would be required for solids, and more frequent activations of the roller motor may be necessary to prevent underfloor waste buildup. Rat urinary analytes are different in concentration and in chemical composition from those of mice. Accordingly, different biomarkers and preservation schemes may be selected for the absorptive Durapore pads.

Mouse urine is highly concentrated and features both measurable protein content and a high percentage of solids compared with other mammals (Green 1968). Rat urine, with its higher water content, may require faster ASM air flow rates and/or a more absorptive WCS substrate to achieve acceptable dryout performance. Experimental investigations of urine flow patterns would be needed to verify adequate channelling toward the centre of the WCS media.

NASA Rodent Food Bar is approved for use with rats as well as with mice; it could be affixed to one or more ASM walls using the same procedure as is currently baselined for the Mars Gravity mission. However, substantially greater volumes of both food and water should be installed for each ASM. Greater food mass is not problematic, but larger water reservoirs within a spinning satellite pose problems of sloshing and uneven fluid distribution. Such phenomena can offset the vehicle's centre of gravity and cause perturbations to the spin rate and alignment of the rotational axis. Similar issues would arise in the event an animal should die over the course of the mission. Normally there is a mass migration as the animal eats food bar (which is eventually deposited as waste in the WCS) and drinks water (which is ultimately sequestered in the humidity control systems). The non-movement of greater consumable volumes from an ASM in which a heavier rat has died could prove problematic with respect to mass distribution and spacecraft asymmetry.

Anecdotal evidence suggests that rat urine releases smaller volumes of gaseous ammonia during decomposition than does mouse urine under similar conditions. Accordingly, it might be possible to incorporate a lower mass of activated charcoal in the atmospheric reconditioning subassembly. This and other ECLSS system changes will require separate analysis on the basis of specimen size, number of animals and mission duration.

Table 46 summarises required changes. In general, adapting the payload module to support rats would be readily achievable and carries minimal risk.

Table 46: Modifications for rats

Subsystem	Modifications Required
Habitat Modules	Larger ASMs, with body mass platform enlargement and water nozzle height adjustment. Redesign of ASM floors to prevent chewing and ensure good urine channelling. Increased food and water volumes. Possible changes to water reservoir configuration to eliminate problems associated with sloshing.
ECLSS	Greater volumes of consumables consistent with larger animals, although possible lower ammonia production rates and fewer specimens may permit reduction in canister mass.
Thermal Control	No major changes anticipated.
Structures	Strengthen central utilities truss to hold larger ASMs and heavier ECLSS canisters if necessary.
Electrical/Software	No major changes anticipated.

7.3.2 Newts and Geckos

Adult newts are best suited to dark, moist conditions. They should be kept in a carefully-regulated thermal environment since they are cold-blooded. Periodic exposure to a misting spray is recommended to maintain skin moisture. This species is carnivorous and readily eats a wide variety of insects, worms and brine shrimp. Feeding and drinking is infrequent, and the newt is therefore a very attractive species from the perspective of life support systems engineering.

Optimal gecko housing conditions are very similar to those of newts. Again, given an adequate prefeed the animals can survive and remain healthy for upwards of two weeks without on-orbit provision of food. However, geckos do require a supply of drinking water.

Both newts and geckos should reside on a soft, spongy floor substrate. The material should be an active wicking agent to assist with local humidity regulation. Since both newts and geckos are cold-blooded creatures with lower metabolic rates, ECLSS requirements are substantially reduced.

Geckos and newts are species of great scientific interest because of their ability to regenerate tissue following surgical excision or injury. The space medicine research community has a need to develop strategies for surgical procedures and post-operative recovery regimens in microgravity and partial gravity. Newts have been successfully used in spaceflight

experiments to investigate retinal lens regeneration, toe tip regrowth and tail restoration (Domaratskaya, Almeida et al. 2008).

Table 47: Modifications to house newts and geckos

Subsystem	Modifications Required
Habitat Modules	Addition of misting spray instead of / in addition to water nozzles. Removal of food delivery capability (for missions of less than 3 weeks). Addition of spongy floor substrate and removal of underfloor waste system.
ECLSS	Significant reduction of ECLSS consumables volume. Reduced need for dehumidification, almost no requirement for ammonia control.
Thermal Control	Tighter regulation with a possible need for heating elements adjacent to habitat modules.
Structures	No major changes anticipated.
Electrical	No major changes anticipated.

7.4 Alternative Gravity Setpoints

The payload module is designed to support rodents in a Mars-equivalent gravity field of 0.38-g. Other gravity setpoints within the 0-g to 1-g continuum could also yield valuable research data to address the nature of and processes underlying physiological adaptation. Moon-equivalent gravity of 0.16-g is an obvious and exploration-relevant point of interest. 0.5-g is an engineering-relevant setpoint in the context of assessing rotating artificial gravity spacecraft designs. If physiological deconditioning can be mitigated with a gravity setpoint below 0.5-g, this would permit slower rates of rotation and reduced cost and complexity for future human-rated artificial gravity spacecraft.

Almost the entire Mars Gravity Biosatellite payload is designed to operate independent of the specific gravity level. Critically, the air circulation and ECLSS processing apparatus is built to overcome the effects of rotation-induced partial gravity, rather than to depend on them. The only elements of the payload module that require gravity are the condensing heat exchangers, the body mass sensor and the waste collection system:

- The local gravity vector causes water to drip off the CHE and enter the collecting reservoir at the periphery of the spacecraft. The current design would fail in weightlessness or at gravity setpoints that are too low to overcome the surface tension of water. Under these circumstances, a redesign to include CHE-directed air flow and possibly a wicking substrate would ensure channelling of condensate in the appropriate direction. The efficiency of the CHEs would be negatively impacted in gravitational environments of less than 0.38-g. Experimental validation of the redesigned system through parabolic flight testing would be essential.
- The body mass sensor as currently envisioned could not operate in the absence of a gravity vector and should therefore be eliminated from the design.
- The movement of waste from the specimen chamber into the WCS is dependent on artificial gravity. To operate in weightlessness, a much stronger and more diffuse air

flow system would need to be incorporated into the design of the ASM. Additional filters would be necessary to trap floating fluid and particulates and to prevent them from exiting the ASM consistent with the enhanced air flow patterns.

Anecdotal evidence from NASA AEM operations suggests that smaller animals such as mice and rats have difficulty positioning themselves to drink water from recessed nozzles in zero gravity (Steele 2007). Often the very process of opening and closing the jaws around a nozzle will cause the animals to inadvertently propel themselves away from the water source. One of the AEM design features is a grab-bar adjacent to the water spout that the animals can use to maintain stability while drinking. An equivalent solution would need to be implemented within each Mars Gravity ASM in order to support weightless operation.

In a microgravity environment, floating waste, debris and fluid droplets have a much greater chance of adhering to the ASM ceiling and obscuring the camera's field of view. To mitigate this risk, it would be appropriate to include a video camera lens protection system. A design that includes a motorised rotating Mylar disc would ensure that the camera always has a clean field of view through which to image the specimen chamber.

Finally, all components with moving parts would need to be certified for reliable operation in a weightless environment. Such components include motors, fans, compressors and fluidic micropumps. Several of these elements may need to be fitted with guard mesh to prevent small floating hardware from entering the unit and destroying internal mechanisms.

Table 48 summarises the preceding discussion.

Table 48: Modifications for weightlessness

Subsystem	Modifications Required
Habitat Modules	Elimination of body mass sensor, incorporation of grab-bar adjacent to water nozzles. Redesign of WCS. Increased ASM air flow. Inclusion of better filters to trap airborne particulates before they exit the specimen chamber.
ECLSS	Component certification for zero-gravity operation. Guard meshes to protect moving parts from floating debris/hardware.
Thermal Control	CHE redesign for zero-gravity operation. Component certification for zero-gravity operation.
Structures	No major changes anticipated.
Electrical	No major changes anticipated.

7.5 Alternative ECLSS Setpoints

Closed-loop atmospheric control systems are known to risk trace contaminant buildup when operating over extended periods. Of particular concern for future human Mars missions are slow increases in levels of ammonia, airborne alcohols, elastomer residues, volatile organic compounds, and various pollutants from adhesives, insulation and lubricants (Campbell and Marriott 1987).

A modified Mars Gravity payload module may be used to study the physiological impacts of atmospheric contaminant buildup in partial gravity or weightlessness. ECLSS system modifications would require the installation of one or more contaminant cylinders together with electronic release valves and various specialised sensors. The cylinder outlets could be positioned adjacent to one of the many system fans to ensure proper mixing of the chemical with the general cabin airspace. It may be necessary to modify the operation of the activated carbon bed, since this chemical will generically adsorb almost any small-molecule pollutants. In addition, substantial ground testing would be required to ensure that none of the contaminants are chemically absorbed by tubing plastics, gasket seals or rodent food substrates.

Structural changes may be necessary to accommodate the additional cylinders. It is likely that they could be positioned close to the atmospheric reconditioning canisters, toward the nose of the spacecraft. Alternatively, custom-designed miniature cylinders could be placed toward the periphery of the payload module, at a radius that extends beyond the ASMs.

In order to meet mass requirements with the additional contaminant chemicals on board, it may be necessary to reduce cohort size and/or mission duration. Alternatively, it may be possible to lightweight certain subassemblies by reducing the level of redundancy or electing to rely on fewer sensors for data aggregation and analysis.

Table 49 summarises key design changes.

Table 49: Modifications for ECLSS contaminant buildup studies

Subsystem	Modifications Required
Habitat Modules	No major changes anticipated.
ECLSS	Addition of contaminant chemical sources, increase of payload-wide air flow rates, verification of non-absorption by tubing and other payload module hardware.
Thermal Control	No major changes anticipated.
Structures	Support hardware and mounting plates for contaminant chemical vessels.
Electrical	Additional sensors, possible changes in redundancy strategy, power allocations for new contaminant release valves.

7.6 Exploration-Relevant Radiation Studies

The two primary options for satellite radiation sources are decaying radioisotopes and X-ray machines. A Mars Gravity internal trade study conducted in 2005 suggested that an X-ray machine would be preferable from the perspectives of safety, ease of installation/recovery and dosage control (Kamler 2005). The mass and volume of the two options were comparable. However, the proposed 7.3 kg 80 kV X-ray Source manufactured by Oxford Instruments is highly unsuitable for payload integration. This unit requires 15 W for X-ray power and an additional 35 W for cooling. This 50 W total power draw poses a severe thermal dissipation challenge given that the entire payload baseline design nominally requires only 70 W. Of separate concern, air flow of 47 litres per second is required. This is

equivalent to the entire air volume of the payload module passing through the X-ray unit every seven seconds. Such a flow rate is unachievable within the enclosed, heavily obstructed life support bucket.

Accordingly, the only practical option for an on-board radiation study would be a decaying radioisotope similar to those used on the 1967 Biosatellite II or the 1974 Cosmos-690 missions. For these flights, a powdered radioactive chemical was stored in a tungsten source holder. The shielding system included a motorised wheel that could rotate to either block or unblock emitted radiation from reaching the biological specimens.

One possible radiation experiment using the Mars Gravity payload module might simulate a solar proton event. This would require that the mice be exposed to radiation over a period of approximately 24 hours. A design incorporating a motorised wheel and shielding source holder would meet these needs. It may be possible to use water and plastics as less massive alternatives to tungsten shielding. If only a subset of on-board specimens are to receive radiation exposure, this can readily be achieved through the use of directional shielding blocks.

A redesign would first require assessment of the radiation-blocking properties of the Animal Support Modules and other payload hardware. Radiopaque materials may need to be replaced with radiolucent alternatives to ensure the rodents receive predictable dosing. It would be necessary to move the central oxygen and nitrogen tanks further toward the nose of the payload module in order to accommodate the radiation apparatus. The central utilities truss would be modified to provide an additional platform for securement of the new equipment. The total launch mass would likely increase by approximately 10 kg, a reasonable proposition for a spacecraft that weighs at least 520 kg in its baseline configuration.

New electrical and data connections would command the motor for computer-controlled unshielding of the radioisotope. The average power draw would be minimal because the system would only activate for a few seconds at either end of the radiation exposure period. Digital computer hardware may require additional shielding to guard against radiation-induced data corruption.

Table 50: Performance envelopes for each configuration

Subsystem	Modifications Required
Habitat Modules	No major changes anticipated (although check of materials radiation compatibility will be required).
ECLSS	No major changes anticipated.
Thermal Control	No major changes anticipated.
Structures	Additional support plate for radiation source, reconfiguration of nitrogen and oxygen cylinders.
Electrical	Possible shielding of digital computer hardware. Addition of specialised radiation monitors. Power and data to motorised isotope shielding wheel.

It may be necessary to include additional specialised radiation monitors to monitor the total dosage. Separately, the existing on-board badge-style radiation sensors will require partial shielding in order to provide an accurate reading of the space background radiation, independent of any superposed radioisotope effects.

7.7 Summary

This chapter has demonstrated the design feasibility of modifications to the Mars Gravity Biosatellite's payload module in order to meet scientific needs beyond the scope of the proposed first mission. With realistic and achievable design changes, the payload can be reconfigured to meet the research community's need to "learn how life interacts with the physical world and to "develop and validate exploration technology." These are consistent with stated NASA objectives and showcase the payload module's potential as a reconfigurable platform for future space life sciences research.

Chapter Eight: Conclusions

“The Mouse Tronaut” is the first cartoon based on a real space project, designated to bring a hi-tech and adventurous feel to young audiences in China.

-CRI Online China Radio News⁴

8.1 Summary of Major Findings

A flight-tested research platform with capabilities for both life support and sample return can fill a critical niche in enabling reduced gravity science. With a low per-mission cost, regular reflight opportunities could provide investigators the opportunity to fly multiple related experiments. It would allow the research community to swiftly follow up on evidence gathered in earlier flights and explore specific research targets with different mouse strains, genetically modified animals or alternative setpoints along the developmental continuum.

This thesis has generated original research while simultaneously answering outstanding design questions for the Mars Gravity Biosatellite’s payload module. This work has paved the way for the first flight of this innovative university spacecraft and has built a framework for exploring its broader scientific value.

Four unique contributions are offered in the fields of aerospace biomedical engineering and rodent behavioural science:

1. This thesis has showcased the most comprehensive design and operations plans to date for the payload module of the Mars Gravity Biosatellite. Specific elements which the author claims as unique contributions include the electronics, software and systems-level design of the payload module.
2. The centrifugation experiment was the first direct measurement of the influence of chronic rotation on mice in flight-like habitats rotated at 31.6 rpm. It was the first use of video-based behavioural analysis software to monitor specimens undergoing continuous centrifugation.
3. The closed-loop environmental control test characterised the performance of a subset of life support hardware and software proposed for the Mars Gravity mission. It provided proof-of-concept justification for the environmental control and life support systems design strategy.

⁴ *Mouse Tronauts to Land on Mars!* CRI English Language Edition, 19 July 2004.

4. A sophisticated hardware and software platform was conceived, designed, implemented and operated. The integrated Mars Gravity ground test apparatus is the first system to incorporate high-fidelity flight-like habitat modules on a centrifuge matched to on-orbit radius and rate of rotation. It is the first to additionally provide a closed-loop life support test platform for ongoing refinement of environmental management hardware and control algorithms.

8.1.1 Chronic Rotation of Rodents

It is hypothesised that female BALB/cByJ mice will survive when chronically rotated at 31.6 rpm at a radius of 0.34 m. They will maintain normal body mass and will exhibit behaviour that indicates vestibular adaptation to this rate of rotation. Specifically, it is hypothesised that there will be a normalisation of body mass, water consumption, video-derived behavioural metrics and performance in discrete tests.

Chronic rotation did not negatively impact the general health of the four rodents tested. The animals did not suffer from dehydration and showed no signs of chronic stress or anxiety. Their body mass was the same following five weeks of chronic rotation as it had been prior to the stimulus. The recorded water consumption was consistent with published data on rodents fed NASA's Nutrient Upgrade 12D Rodent Food Bar.

Statistically significant differences were found between the control and the rotational studies with respect to several of the most important video-derived behavioural parameters. Firstly, a clockwise turn bias was elicited during the period of chronic anticlockwise rotation. This bias was reversed (and overcompensated) in the 36 hours following rotation stoppage. Secondly, both gross activity and time spent moving increased during the first half of the rotation period. These parameters subsequently normalised to levels identical to the control period. Movement was significantly reduced during the 36 hours following cessation of centrifugation.

Of the discrete tests, balance beam performance provided the most insight into adaptation processes. Results indicated moderate to severe gait disturbance and balance impairment that was improved but not resolved with continued exposure to the chronic rotation stimulus. The mice continued to present these symptoms for at least 24 hours following rotation stoppage.

Open field video testing served to disambiguate the balance beam results and confirmed that the rodents were not subject to severe or unusual levels of stress. Video-derived metrics included total distance travelled and general mobility over the four-minute testing period. The data suggested that the stress level of the Day 18 transition from rotating to non-rotating was not significantly different from the stress of having been moved into a new and unfamiliar habitat 24 hours prior to Day 0 testing.

The body mass data for Rotation Day 18 and beyond strongly indicated that the rodents were not fully acclimated to the chronic rotation stimulus until more than halfway through the study. This data, together with the balance beam results, suggests that the time constant of whole-organism physiological (as opposed to neurovestibular) adaptation is on the order of 2-3 weeks.

8.1.2 ECLSS Performance

It is hypothesised that a closed-loop life support system comprising humidity control, oxygen replenishment, lithium hydroxide and activated carbon can support female BALB/cByJ mice for a period of several weeks. Specifically, it is hypothesised that body mass at the end of this period will be consistent with published growth curves for this strain, and that eating and drinking behaviours will be consistent with available data on NASA's Nutrient Upgrade 12D Rodent Food Bar.

The preliminary feasibility of the proposed ECLSS design for the Mars Gravity Biosatellite was successfully demonstrated. Key contaminants were controlled for two mice within a sealed system for a period of 3.5 weeks. The system operated to maintain all parameters within ranges deemed scientifically acceptable for mice. The activated charcoal bed was found to play a greater role in humidity control than had been initially anticipated.

The mice maintained good body mass consistent with published research. Their food and water consumption was consistent with previous studies and with that specified in available literature.

8.2 Future Work

As part of Critical Phase design efforts, it will be necessary to construct a fifteen-habitat mockup with higher-fidelity atmospheric control systems. The intention is to move toward a more flight-like system in order to better prototype and refine both ECLSS hardware and supervisory software.

Instead of the impermeable plastic membranes used to date, future prototypes should include rigid outer walls that permit interior pressurisation. Such a modification would allow testing of the flight-like nitrogen/oxygen two-gas control system, while also paving the way for incorporation of thermal control hardware. Implementation of flight-prototype software for active regulation of oxygen partial pressure will be critical for design refinement toward Phase C Review. In addition, confirmation of silica gel desiccant performance in concert with the baseline condensing heat exchangers would provide valuable design validation. Verification of the ECLSS algorithms on flight-like embedded computing hardware is also a high priority, together with simulation of certain failure modes.

The observation that activated charcoal may play a non-negligible role in humidity control is worthy of further investigation. It is also necessary to explore whether water adsorption impacts the carbon bed's total capacity for ammonia.

In respect of the chronic centrifugation experiments, future work should attempt to replicate the key findings with an increased cohort size. If possible, discrete testing should be performed more regularly and assays of blood, urine and faecal matter should be used to confirm stress levels and hydration status.

It has been suggested that the Mars Gravity Biosatellite flight specimens should undergo a process similar to astronaut selection, whereby only the most suitable subjects are cleared for flight. To build on the rodent behavioural analysis results presented in this thesis, future work should include derivation of appropriate cohort selection criteria. Although the flight mice will be genetically identical, behavioural differences across specimens are not unusual. It may be appropriate to select animals to match rotarod and balance beam performance, nominal activity levels and exploratory behaviour. In addition, it would be highly

advantageous to select those mice that are “quick learners.” Such specimens would be able to rapidly find and operate the water nozzle when introduced to the ASM for the first time, and would have sufficient resourcefulness to try out the other water nozzle if the first should cease to function. Finally, it may be advisable to select mice that are naturally calm and stress-free and that do not become agitated when installed in the ASM.

Appendix A: Abbreviations

AAH-C	Advanced Animal Habitat-Centrifuge
ACH	Air Changes per Hour
ADC	Analogue to Digital Converter
AEM	Animal Enclosure Module
ASM	Animal Support Module
C&DH	Command and Data Handling
CAD	Computer-Aided Design
CASPER	Continuous Activity Scheduling Planning Execution and Replanning
CCD	Charge Coupled Device
CFU	Colony-Forming Unit
CHE	Condensing Heat Exchanger
CMOS	Complementary Metal Oxide Semiconductor
COTS	Commercial off-the-shelf
CPU	Central Processing Unit
DAQ	Data Acquisition System
DS-1	Deep Space 1
ECLSS	Environmental Control and Life Support Systems
EDL	Entry, Descent and Landing
EEPROM	Electrically Erasable Programmable Read-Only Memory
EO-1	Earth Observation 1
GSE	Ground Support Equipment
HCM	Habitat Control Module
IGTA	Integrated Ground Test Apparatus
ISS	International Space Station
LDPE	Low-Density Polyethylene

LED	Light-Emitting Diode
LV	Launch Vehicle
LVB	Lighting and Video Board
MPEG	Motion Picture Experts Group
NIH	National Institutes of Health
NTSC	National TV Standards Committee
OEM	Original Equipment Manufacturer
PCB	Printed Circuit Board
PCI	Peripheral Component Interconnect
PTFE	Polytetrafluoroethene
PWM	Pulse-Width Modulation
RAX	Remote Agent Experiment
RH	Relative Humidity
RV	Reentry Vehicle
RX/TX	Receive/Transmit
SEL	Single Event Latchup
SEU	Single Event Upset
SLPM	Standard Litres Per Minute
TEC	Thermoelectric Cooler
UART	Universal Asynchronous Receiver/Transmitter
USART	Universal Synchronous and Asynchronous Receiver/Transmitter
USP	United States Pharmacopeia
VI	Virtual Instrument
WCS	Waste Collection System

Appendix B: Payload Autonomy

Overview

An investigation of autonomy options for the payload module was conducted by Burak Akbulut, a Mars Gravity intern during Summer 2005. The following sections amplify and recapitulate some of his key findings.

The Need for Payload Module Autonomy

Resource utilisation within the payload module strongly drives autonomous system design (Akbulut 2005). Power is the primary constrained resource; the spacecraft bus supplies an average of 53.1W and peak of 262W, as previously shown in Table 4. Instantaneous power needs for any given subsystem are unpredictable – for example, a mouse may choose to drink water at any time, thereby causing fluidic micropumps to activate in an unscheduled manner. Similarly, a progressive decline in cabin air quality may necessitate asynchronous activation of various environmental control systems.

A system that permitted power usage to fluctuate randomly could potentially open the door to subsystem failures of varying degrees of severity (Gat and Pell 1998). Excessive current draw could cause a bus undervoltage condition, leading to component-level electrical shutdowns across the payload. In more severe cases, undervoltage of computer nodes could cause the spacecraft to enter a safe mode in which services (potentially including environmental control) would be suspended throughout the vehicle.

One approach would be to deploy a team of ground engineers to perform dynamic operational planning during the mission, uploading command sequences at each communications pass. This strategy is considered “difficult, time consuming and expensive” (Gat and Pell 1998). “Difficult” because such sequences are open-loop and therefore at risk of errorful data entry. “Time consuming and expensive” because of the need to mitigate this risk with manual ground-based error-catching processes.

The preferred approach requires an autonomous planner within the payload module. This software engine would perform dynamic schedule updates based on real-time systems health and performance data. The monitoring capabilities of such an agent would allow functional diagnosis, error flagging, fault finding and subsystem isolation to prevent off-nominal events propagating to other systems. Such a supervisory control module would also attempt recovery and reboot procedures in the event of system failures.

There also exists a need for an autonomous data-flagging agent to evaluate scientific data and modulate downlinking activities accordingly. Accordingly, the autonomous planner would monitor raw data generated by the payload module and identify those data points that are of maximal scientific interest. The result would be a prioritised transmission scheme whereby the most valuable science would reach the ground in the shortest timelines. This agent would also be responsible for dynamically refocusing data gathering activities in order to maximise mission science return.

Spacecraft Autonomy Heritage

A number of scientific missions have successfully used autonomy to enhance scientific return and better meet operational objectives. In arriving at an autonomy specification for the Mars Gravity Biosatellite, reference was made to Deep Space 1 and to Earth Observing 1 (Akbulut 2005).

Deep Space 1

Deep Space 1 was the first mission of the NASA New Millennium Program series, launched on October 24, 1998. The satellite was operated by JPL until its retirement on December 18, 2001. Its focus was advanced technology validation; DS-1 carried twelve modules, including the Remote Agent Experiment (RAX).

RAX operated on board DS-1 for several days, controlling several spacecraft subsystems including the ion propulsion system, attitude control and autonomous navigation. The Remote Agent was highly successful, accomplishing 100% of its flight validation objectives (Rayman, Varghese *et al.* 1999).

The Remote Agent was written entirely in Common LISP and operated under the VxWorks real-time operating system running on a Rad6000 processor (Gat and Pell 1998).

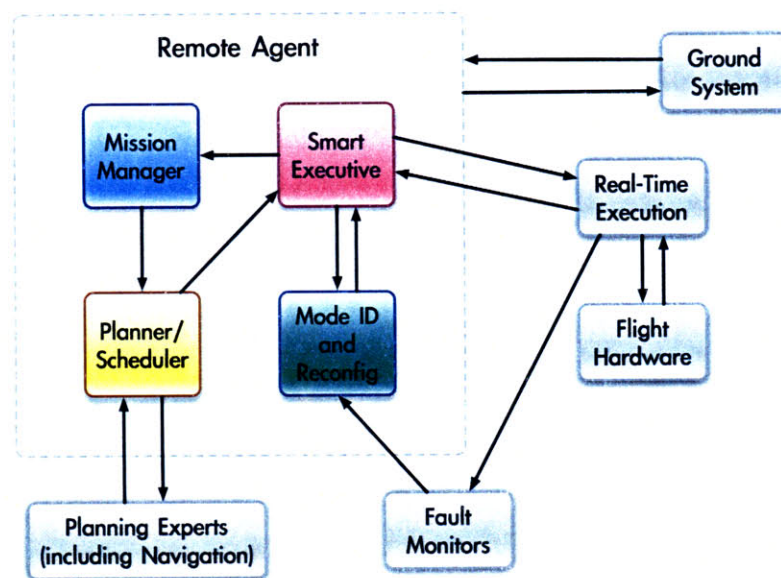


Figure 89: RAX architecture for DS-1 (after Rayman *et al.* 1999)

The Smart Executive (shown in pink in Figure 89) coordinates remote agent activities and interfaces between different software modules. The Mission Manager (blue) can accept a broad set of mission goals from which it maps out a complete mission profile. This output is subsequently converted into a timeline via the Planner/Scheduler (yellow) that tracks spacecraft constraints and allocates system resources over time (Bernard, Gamble Jr. *et al.* 2001). The timeline is a stepwise plan for completing a particular activity or set of activities. A “batch formulation” algorithm is used to create this timeline, which is subsequently transmitted to the Smart Executive for implementation and execution.

“Batch formulation” involves dividing up the available operations time into a number of planning windows, each of which has a predefined duration and is bounded by an endpoint known as a horizon. When the system nears the end of a certain planning window and moves closer to the horizon, the algorithm projects what the system state will be at the end of the planning window. At that time, the planner dynamically generates a timeline for the subsequent window using outstanding goals and a projected initial state.

One disadvantage of batch formulation is that the speed of system reaction is limited by the duration of planning windows. In general, this algorithm lacks responsiveness and is best for slowly-changing systems.

Returning to Figure 89, the only remaining component of the Remote Agent is the green block labelled Mode Identification and Reconfiguration. Mode Identification uses built-in spacecraft models to assess the state of the vehicle and perform fault detection. The algorithm focuses on discrepancies between sensor data and data projected by running the model. If a fault is suspected, Mode Reconfiguration is activated to generate a list of actions that will shift the system back to a desired nominal configuration.

The DS-1 Remote Agent was able to control the spacecraft for several days without any major off-nominal events. The technology validation was deemed a success.

Earth Observing 1

The Earth Observing 1 (EO-1) mission was also part of the New Millennium Program. It launched in November 2000 to visually record transient Earth surface phenomena such as landslides, volcanic eruptions and floods.

EO-1 featured two Mongoose M5 processors, one to act as a mass storage controller and the other to perform command and data handling. Each processor was clocked at 12 MHz for a combined throughput of 8 MIPS. 512 MB of RAM was shared equally between the two processors.

In place of the RAX planner/scheduler, the spacecraft included a new system known as CASPER (Continuous Activity Scheduling Planning Execution and Replanning). EO-1 featured a traditional three-layer autonomy architecture with CASPER at the highest level of abstraction, as shown in Figure 90 (Chien, Sherwood *et al.* 2003).

Requests for observation are generated either by an observation planner on the ground or by the on-board science analysis software that algorithmically detects potential scientific opportunities. These requests are transmitted to the CASPER planner that operates on much shorter timelines than the DS-1 RAX system previously discussed. Critically, CASPER updates system states and goals incrementally, rather than waiting for an arbitrary event planning horizon. Accordingly, it can better respond to situations such as a camera instantaneously drawing more power than expected.

CASPER generates activity plans that are translated into commands via the Spacecraft Command Language block. In this way, the autonomy agent rides on top of traditional reflexive-response flight software, augmenting its capabilities and adding intelligence in order to deal with contingencies. The EO-1 mission was a great success and the CASPER autonomy engine is considered a best-in-class solution.

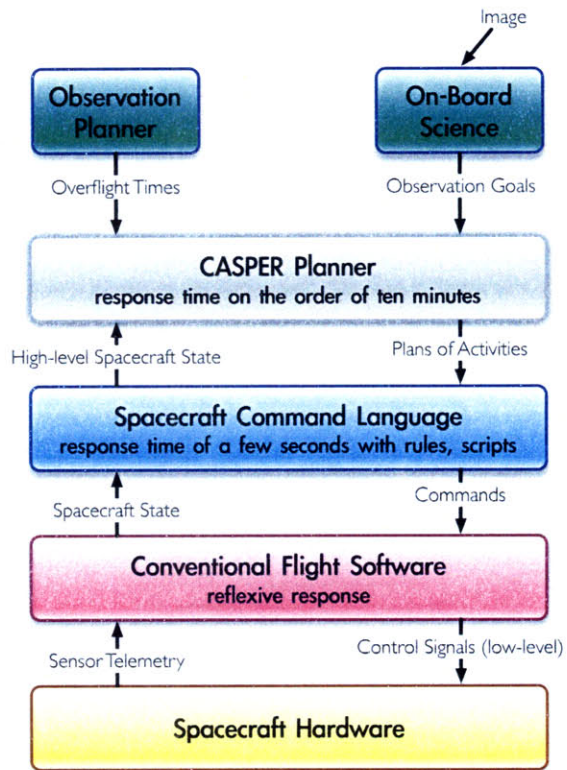


Figure 90: CASPER architecture for EO-1 (after Chien *et al.* 2003)

Appendix C: Food Bar Experiments

Experiments into the long-term durability of NASA's Rodent Food Bar were conducted in Summer 2005 by undergraduate interns Noelle Steber (MIT) and Daniel Blustein (Kalamazoo College). They were supervised by the author.

OVERVIEW

Each of the fifteen mice on board the Mars Gravity Biosatellite will be individually housed with free access to food and water throughout the duration of the flight. NASA's Nutrient Upgrade 12D Rodent Food Bar has been baselined as the preferred substrate for the extended-duration mission. Previous crewed flights have typically required that astronauts provide fresh food bars approximately once every seven days. This section reports on novel approaches to ensure the food bars remain edible and free from pathogenic bacteria for a full five weeks.

TEST OF FOOD BAR DEHYDRATION

An experiment was performed to explore the extent of dehydration of food bars which were coated with edible wax.

Method

Four polycarbonate chambers were constructed, each with volume equal to that of a single Mars Gravity ASM. The chambers were equipped with active humidity control systems: a fluidic microinjector to increase humidity and a silica gel desiccant bed to adsorb excess moisture.

A custom LabView Virtual Instrument provided 24-hour computer control of all humidity chambers. The system maintained each chamber at a preprogrammed relative humidity setpoint, with a variance of $\pm 2\%$. Chamber setpoints were 40%, 50%, 60% and 70% RH. Each chamber held one food bar which was coated with food-grade edible wax and another bar which was wax-free. Both were prototypes of the NASA Nutrient Upgrade 12D Type 1 Rodent Food Bar. Food bar mass was recorded daily over a six week period.

Results and Conclusions

Figure 91 shows the recorded mass data.

The waxed bars showed constant water loss over time and minimal humidity dependence. The gradient of each line is approximately constant, indicating that water loss was continuous and unchanged over the 43-day test. There appears to be no trend in the ordering of the four lines in Figure 91; bars in 70% RH exhibited the most dehydration (5% mass loss) while 50% RH bars exhibited the least.

Uncoated bars dehydrated rapidly during the first 14 days but stabilised thereafter. Wax-free bars were more sensitive to the effects of local humidity. The 40% RH bar lost almost 15% of its original mass. Even the bar in 70% RH showed more than 10% mass loss. Figure 91 shows that after day 14 the gradients begin to match those of the wax-coated bars.

Although wax coating seems in theory to be a very promising approach, testing showed that mice eating habits are not compatible with this technique. During a multi-week test,

the animals were observed to strip off all wax on the food bar within 48 hours of introduction.

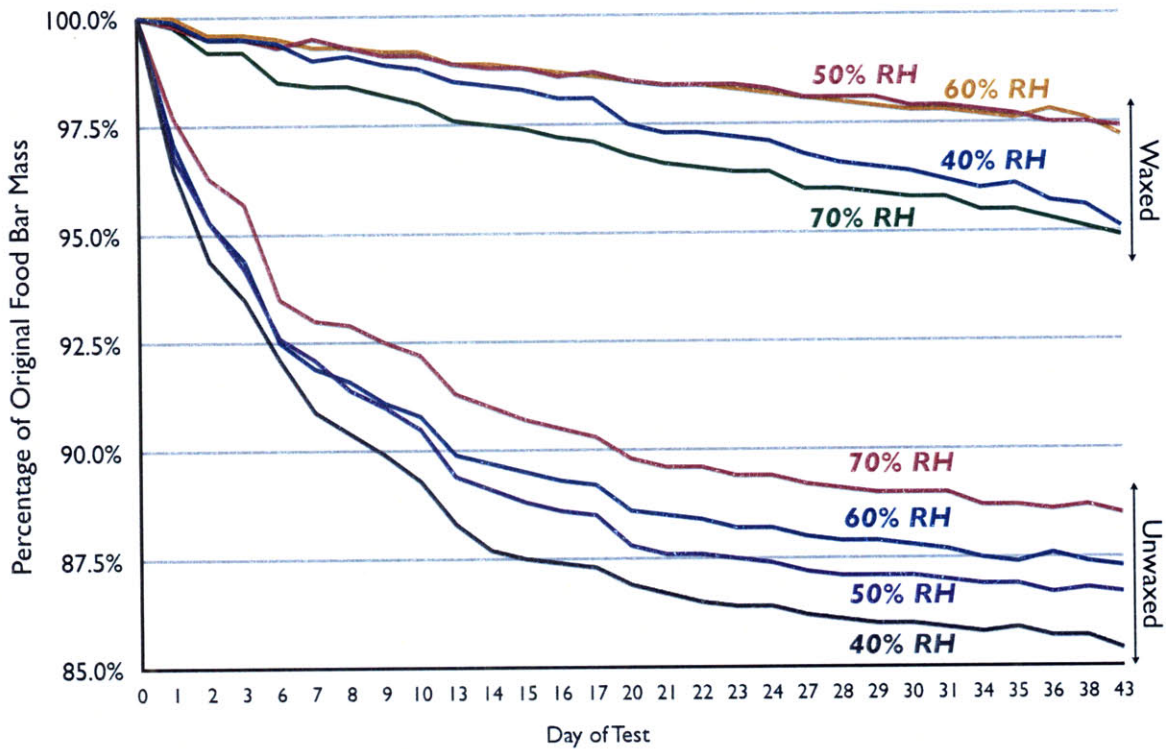


Figure 91: Results of food bar dehydration test

TEST OF PATHOGENIC BACTERIA GROWTH ON FOOD BARS

An experiment was performed to explore the extent of pathogenic bacteria growth on uncoated food bars exposed to mice for a six-week period.

Method

Over a six-week period, bacteria detection testing was performed weekly on uncoated food bars. The bars were freely accessible to individually-housed mice in prototype Mars Gravity ASMs. Aseptic techniques were followed at all times:

- A 2 cm by 2 cm swabbing template was cleansed with alcohol and allowed to dry. The food bar plate was removed from the specimen chamber under test. Suitable swabbing areas were selected to include both eaten and untouched parts of the food bar.
- For bacteriological testing, the samples were plated using agar before incubation at 35°C for 48 hours. Subsequent identification and enumeration of colonies constituted a representative microbiological assessment. In order to assess yeast and mould growth, 3M Petrifilm™ Plates were left for 5 days in a 25°C incubator. Colonies were enumerated and the results recorded.

Results and Conclusions

Prior to animal insertion, all food bar Total Bacteria Counts were lower than 250 Colony-Forming Units (CFU) per sample. Following animal insertion, bacteria levels increased at different rates in each specimen chamber.

One dominant species (gram-positive coccus, white colonies) and one secondary species (gram-negative rod, yellow colonies) were observed throughout testing. The primary species accounted for 99% of total bacteria observed and was likely from the genus *Staphylococcus*, bacteria commonly found in and around mammals. Staining, morphology and appearance confirmed the genus classification and suggested that the observed bacteria was *S. epidermidis*. This most likely originated from the mice themselves. Its presence is to be expected and is not a cause for concern.

No mould or yeast growth was detected over the duration of the test.

Appendix D: Condensing Heat Exchanger Design

Overview

The testing, analysis and conclusions described in this appendix were a joint effort of Andrew Heafitz and the author.

As previously shown in Table 21 on page 64, relative humidity within the payload module must remain between 40% and 70% at all times. Thermal requirements call for the temperature to remain between 18°C and 28°C. For any given combination of temperature and relative humidity, the dewpoint can be readily calculated using basic physics and mathematics. Within the ranges specified above, the dewpoint may be as low as +4°C (for cooler, drier air) or as high as +21°C (for warm, humid conditions).

Method

A condensing heat exchanger was designed and constructed as a ground-based simulation of the intended space-ready design. At its core is a thermo-electric cooler, Marlow Industries model DT12-8, on the cold side of which is mounted a 64 mm thick aluminium plate to serve as a condensing surface. A small brushless fan (RadioShack #273-240, 12 V DC, 0.13 A, 1.56 W, 38 mm diameter) channels air directly onto the cold plate. The hot side of the TEC is attached to a commercially available aluminium heat sink and 2.52 W fan, which was operated from 12 V DC for all the experiments. Baffles were installed to keep warmer air from blowing on the back of the cold plate. It was noted that the spring-loaded clip securing the hot and cold plates and sandwiching the TEC (Figure 92) acts as a thermal short circuit between the hot and cold sides. However, the clip is made of thin steel and its conductivity was found to be negligible. Condensate on the cold plate accumulates at the lowest point, from where it is funnelled into a 10 ml measuring cylinder for collection and volumetric analysis.

The goal was to explore system efficiency within various performance regimes. 35 experimental runs were conducted to test various attributes of the system.

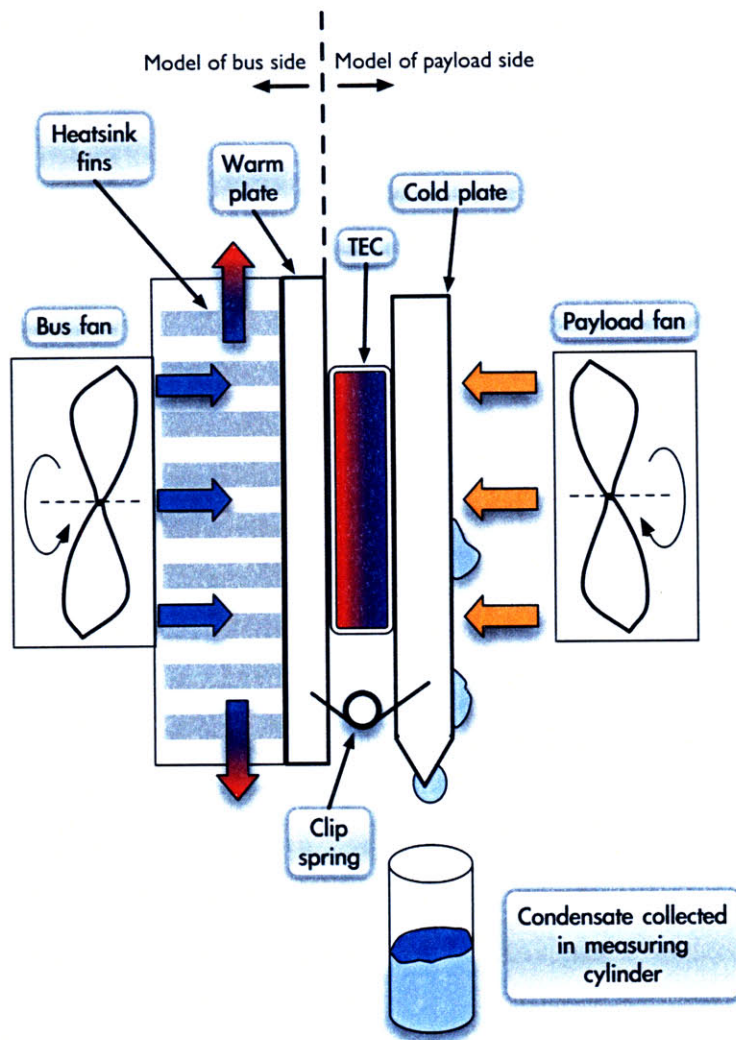


Figure 92: The condensing heat exchanger

The right side of Figure 92 shows equipment within the payload pressure vessel – including a fan, cold plate and thermoelectric cooler. The left side represents the spacecraft bus, with the thermal transfer path to space substituted by a plate, heatsink and fan. Block arrows represent air flow paths, with blue colours indicating cooler zones and red signifying warmer areas.

The controlled independent variables were as follows:

- Ambient relative humidity.
- Temperature of the condensing plate (varied by altering the power supplied to the TEC).
- Speed of payload fan.
- Area of condensing surface and number of condensing heat exchange units.

In all cases, the measured dependent variable was a metric of operational efficiency:

- Condensation rate (ml/hr).

The basic experimental procedure was as follows:

- The system was activated and allowed to equilibrate. As the cold plate reached a steady-state temperature (below the dewpoint) water would start to condense and collect in the measuring cylinder.
- Whole-system equilibration was confirmed when droplet formation and drip down into the cylinder reached a constant rate. There was approximately 1 ml of water adhered to the plate during steady-state operation, and this would generally take 10-15 minutes to build up from a dry start.
- Once steady-state operation was confirmed, the cylinder was emptied and timing of a new accumulation period commenced. Timed periods were generally 30 minutes or longer depending on the objective of each experiment.

Results of Varying TEC Power

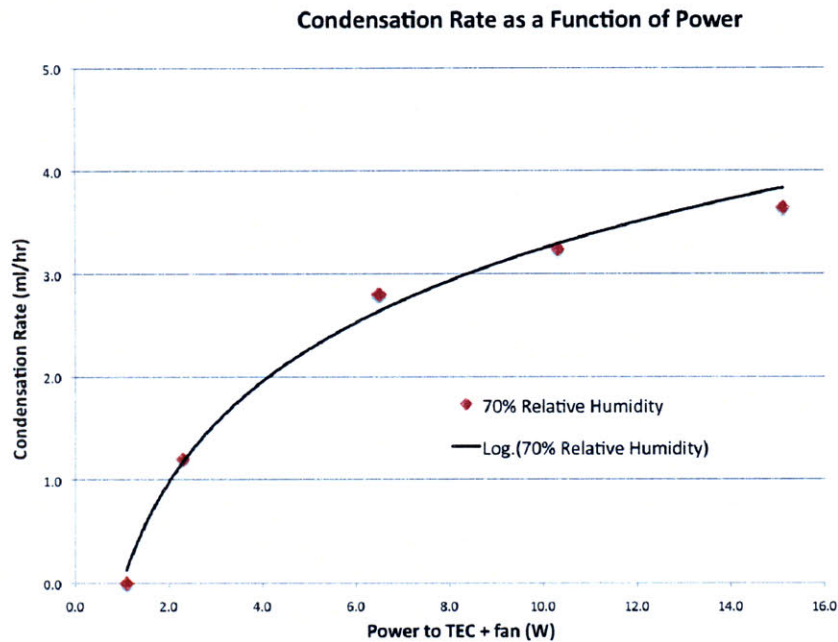


Figure 93: Condensation rate for one CHE unit at 70% RH

With the fan operating at minimum power (0.1 W) and the relative humidity at 70%, the power to the TEC was varied as shown in Figure 93. The trendline strongly indicates a logarithmic relationship.

Condensation Rate as a Function of Temperature and RH

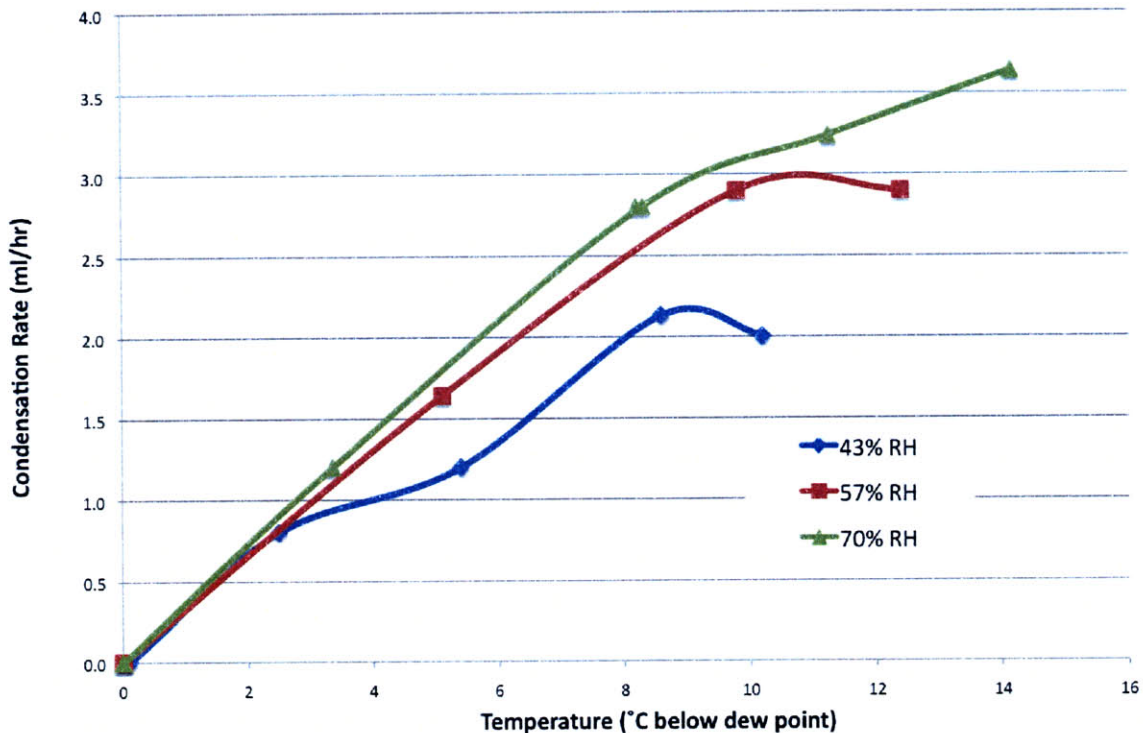


Figure 94: Effects on condensation of temperature and humidity

In order to understand the humidity dependence of this system, the same test was repeated at 43%, 57% and 70% RH. Results are shown in Figure 94. CHE performance is measured in terms of the condensation rate at various plate temperatures and relative humidity environments. Plate temperatures are represented as degrees below dew point. Higher numbers on the y-axis indicate cooler plate temperatures.

Figure 94 confirms that faster condensation occurs at higher humidity levels. There is a reduction in condensation rate beyond a certain temperature for the 43% and 57% cases. This can be explained by the fact that in each case the rightmost datapoint was close to 0°C. It is likely that energy was being used to freeze the condensate in this region.

Results of Varying Fan Power

Increasing the fan speed beyond the 0.1 W setpoint significantly enhanced the condensation rate (data not shown). However, beyond a certain point incremental increases in fan power were not accompanied by similar improvements in dehumidification performance; the curve flattened out rapidly. This can likely be attributed to the fact that when air is moving past the condensing plate at too high of a velocity, there is insufficient local residence time for further condensation to occur. Accordingly, all subsequent experiments in this study were performed with high fan speeds at varying humidity levels.

Full Characterisation of CHE Performance Envelope

Figure 95 shows performance of the CHE at 43% and 66% relative humidity. These RH setpoints were selected because they lie at the extremes of the permissible humidity range for the biosatellite. The TEC voltage was varied while the fan power was kept constant at a

level sufficient to ensure a high flow rate (i.e. performance was not limited by airspeed). Performance between these levels will fall between the two logarithmic trendlines. The frost point is shown by the straight green line. If the CHE operates in a regime to the right of this line, the cold plate will drop below freezing with an accompanying loss of efficiency and possible ice formation. The bold purple line at the bottom of the graph is the dew point. Operating below this line for a given relative humidity will not cool the plate below the dew point and no condensation will occur.

The turquoise line across the top of the graph represents the net 6.7 ml/hr rate of water production that is anticipated with fifteen mice on board the spacecraft. It is clear that the CHE as tested could achieve this performance only by letting the relative humidity rise to over 60% and subsequently consuming more than 30 W of power. This is not an acceptable solution given that the entire payload module has been allocated a total of 70 W for all the systems (atmospheric, thermal, data acquisition, habitat regulation, etc.).

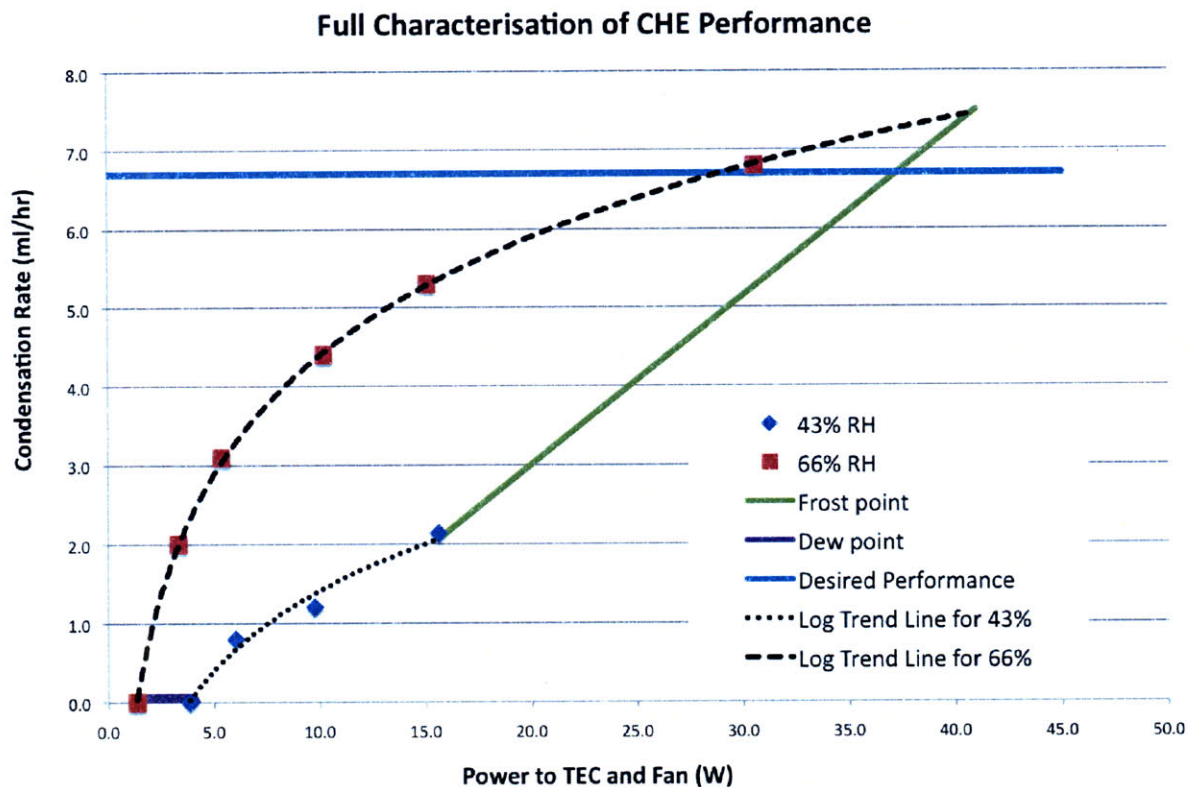


Figure 95: CHE performance characterisation

Projection of Performance in 0.38-g

In the prototype CHE, water drips off the cold plate under the force of Earth's gravity. The droplets increase in size until gravity (acting on the mass, proportional to the volume of the drop) overcomes the surface tension (proportional to the surface area).

In Mars-equivalent gravity, the process of condensate accumulation will necessarily be slower. In order to simulate performance under these conditions, the cold plate was tilted to 23° from the horizontal in order that the component of the gravity vector parallel to the surface of the plate was equal to 0.38-g. This simulation also imparts a force normal to the

surface of the plate; to confirm that this was not a significant factor impacting the rate of condensation, an experiment was conducted as shown in Figure 96.

The rate of condensate production was equal in both cases, despite the fact that the gravity vector normal to the plate was opposite in sign between the experiments. This leads to the conclusion that a plate tilted at 23° to the horizontal is an effective Earth-based simulation of expected performance in the 0.38-g force field. The experiments indicated a 25% reduction in water output compared with the 1-g case.

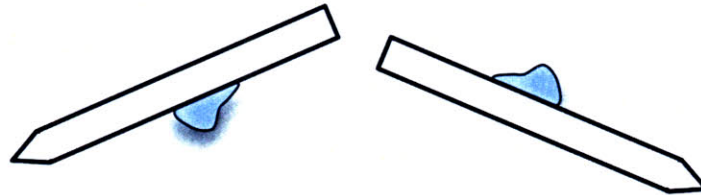


Figure 96: CHE tilt testing to model 0.38-g operation

Optimisation for Power Efficiency

Given the power constraints imposed on the payload module, it is desirable to optimise operational CHE efficiency. Figure 95 demonstrated that the CHE is more efficient at lower power levels. The implication is that two separate CHE units operating at low power would condense more water than a single unit at twice the power. Given the aforementioned 25% reduction in water output for 0.38-g, it can be inferred that the 6.7 ml/hr requirement on board the spacecraft is equivalent to condensing 8.9 ml/hr on Earth. Figure 95 reveals that a set of three CHE units would achieve this performance at a cost of approximately 15 W of power.

Conclusions

The 6.7 ml/hr requirement is only an average; natural variation in water production is to be expected. The control envelope of the CHE is limited as shown in Figure 95. It is clear from this graph that if the instantaneous water production rate should temporarily increase, the power efficiency of the system would be markedly impaired.

Accordingly, it is desirable to have a means of rapidly reducing humidity levels when they increase beyond the preferred operating range of the CHE systems. A small volume of silica gel desiccant can meet this requirement. Silica gel is known to perform more efficiently in humid conditions. Consequently, it is advantageous to switch to using silica gel in place of the CHE units when the relative humidity exceeds a certain level. The exact setpoint at which this switchover would occur will be determined during the Critical Design Phase. It will depend in part on silica gel adsorption efficiency given the power instantaneously available to force air through the silica gel bed. In addition, the merits of a true time-dependent hybrid solution are yet to be explored. Such a system would have the silica gel valves operating at the same time as the CHE for certain control regimes. The baseline algorithmic approach to humidity control is discussed in Chapter 3.

An additional systems engineering concern is the robustness and reliability of the spacecraft life support systems. The use of a hybrid (silica gel with CHE) approach eliminates the possibility of a single-point failure in the dehumidification system. 6 kg of silica gel would be

sufficient to perform all dehumification for a full week, assuming a 50% target humidity. Such a design would be compatible with the scientific requirement that the spacecraft be capable of emergency deorbit and recovery within 7 days in the event of a partial life support failure.

Appendix E: Ammonia Production Experiment

Overview

In order to adequately size the activated charcoal bed, an experiment was performed to measure ammonia production with mice housed in ASMs over a mission-equivalent period.

As discussed in section 2.5.2 on page 42, the ASM features a perforated floor that separates the specimen chamber from the waste collection module beneath. The WCS conveyor system separates solid wastes from liquids and sequesters solids in the hopper at one end of the ASM. This design feature reduces the likelihood of urea breakdown being catalysed by faecal bacteria. The decomposition process is problematic because it results in gaseous ammonia. It proceeds at a faster rate in warmer and more humid conditions. Within the ASM, the forced-convection ventilation system keeps humidity low and ensures that moist waste dries out within a few hours.

Methods

Six BALB/cByJ female mice aged 28 weeks were housed in custom biosatellite habitat modules of the design shown in section 2.5.2. Each module was flight-equivalent but did not include any electronics or telemetry equipment. The total experimental period was 6 weeks and was conducted in a specific pathogen-free facility. During the first 7 days the habitat modules were placed on their ends in order to partially simulate the orientation of certain habitat modules while the satellite waits on the launch pad. Over the subsequent 5 weeks the modules remained in flight orientation.

All animals had uninterrupted access to purified water and to NASA rodent food bar diet equivalent to that baselined for the mission (Tou, Grindeland *et al.* 2003). Because the water nozzle is inaccessible during the launch configuration week, HydroGel hydration substrate (ClearH₂O, Maine) was provided at the start of the study. Forced-air ventilation from a central manifold provided air exchange to each habitat module at a rate consistent with that baselined for flight. The underfloor waste collection assembly was identical to that planned for flight and included an absorptive substrate similar to blotting paper for the purpose of collecting and preserving liquid wastes. The substrate was treated with antimicrobial agents Chlorhexidine and N-Propyl Gallate (Sigma-Aldrich) according to the custom flight-equivalent procedure (Quinlivan, Aull *et al.* 2005). In order to match on-orbit protocol, the conveyor was advanced once per week over the course of the experiment.

Readings of rodent body mass were taken at least once per week using a set of standard metric laboratory scales with a resolution of ± 0.05 g. In-habitat ammonia concentrations were recorded three times per week at intervals of 48-72 hours using an MDA brand ChemKey TLD toxic gas monitor with ammonia Chemcassette from Honeywell Analytics. The monitor is capable of measuring ammonia concentrations with an accuracy of $\pm 25\%$ of the true value, within a range of 2.6 ppm to 75.0 ppm. The repeatability of each reading was $\pm 2.5\%$. In order to assess changing rates of ammonia production within each habitat

module, the following heritage-supported protocol was employed once every 48-72 hours (Fethke, Cook *et al.* 1973):

- The air inflow tube was disconnected from the air inflow port.
- The air outlet port was closed and the ammonia monitor was attached to the inflow port, from which it drew a small volume of air in order to record ammonia concentration. After values had stabilised the displayed reading was recorded.
- The entire habitat module was sealed within a polyethylene enclosure for a period of approximately 20 minutes.
- The enclosure was partially opened and a second series of ammonia readings was taken from within the habitat module.
- The resulting ammonia production rate in $\Delta\text{ppm}/\text{minute}$ was calculated from the two recorded ammonia datapoints.

Temperature and humidity were kept constant in the experimental cubicle that housed the rodents. Less than 5% variation was observed either side of the mean recorded values of $+27.3^{\circ}\text{C}$ and 27.4% relative humidity.

Results

Figure 97 shows that the animals were healthy and maintained or gained body mass across most of the study. The experiment commenced on day 1 and ended on day 43. The transition from launch configuration to orbital configuration occurred on day 8 (see vertical marker bar).

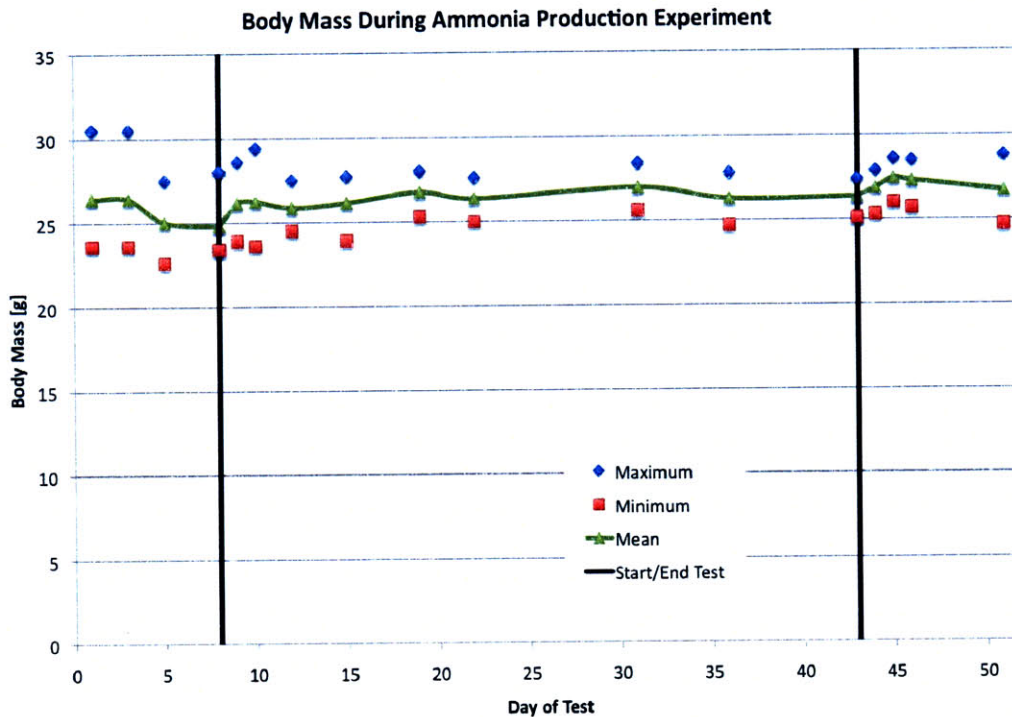


Figure 97: Aggregated rodent body mass from all six specimens

The transition date was accompanied by a notable weight increase in all six specimens. This is to be expected as the animals transition from a smaller floor area to the larger and more comfortable flight configuration. Healthy body mass was maintained at the culmination of the study when animals were transferred into individual standard-issue laboratory cages. These habitats include bedding material and provision for nesting and other species-specific behaviours. Ammonia conditions recorded within the habitat modules are shown in Figure 98. As with Figure 97, vertical marker lines denote the configuration transition and the end of the test. Requirement 2.3.4 in Table 21 mandates that ammonia concentrations should be less than 25 ppm at all times. Figure 98 suggests excellent compliance.

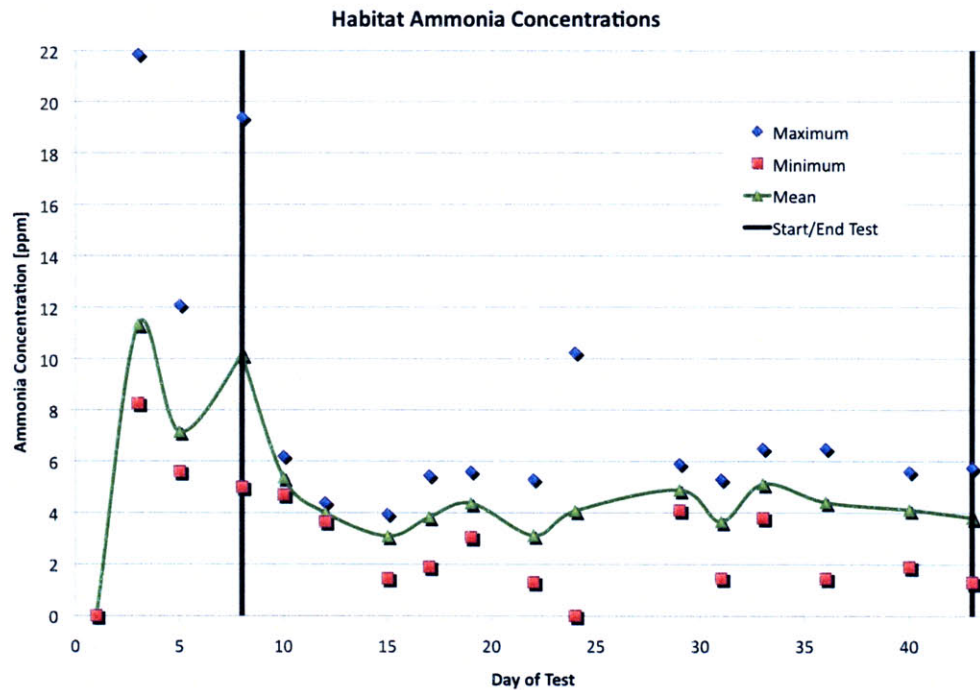


Figure 98: Ammonia production rates from all six specimens

Ammonia levels are elevated during the launch configuration week. This is attributed to the fact that the first week's waste did not enter the WCS and fully dry out until day 8. In addition, the proximity of first week's waste accumulation zone to the air inflow port from which the habitat air was sampled may also have contributed to higher readings. Importantly, the spacecraft will be provided with conditioned external air while on the launch pad. Consequently, the strategy to control ammonia buildup during the pre-launch week will be to simply increase the air exchange rate and thereby flush out all contaminants with greatest efficiency.

ASM 2 exhibited particularly high ammonia readings during the first week and accounted for the one datapoint that approached 25 ppm. This was likely because air flow into this habitat module was partially impaired owing to excess sealant on the air outlet port. Condensation buildup was observed on the inside of the module over the first three days of the test. The condensation dissipated following repositioning of the tubing connector and removal of sealant.

Figure 98 suggests that there was no significant change in ammonia production rates during the five weeks of flight-equivalent configuration. Results shown in Chapter 6 starting on

page 162 confirm this assessment and suggest an maximum rate of ammonia production for the on-orbit payload module of 1.2 g per 24 hours.

Conclusions

These experiments suggest that the ASM/WCS design helps control the amount of ammonia produced within the satellite. It seems likely that the following design elements are of direct benefit:

- The perforated floor ensures minimal contact between waste products and bacteria that are found naturally on and around laboratory rodents.
- The underfloor conveyor system separates solid wastes from liquid waste and sequesters solids in a hopper at one end of the animal support module. This design feature reduces the likelihood of urea breakdown being catalysed by faecal bacteria.
- The forced-convection ventilation system keeps humidity low and ensures that moist waste dries out within hours.
- The antimicrobial properties of urine preservatives N-Propyl Gallate and Chlorhexidine may retard ammonia formation and increase the robustness of the system.
- The absence of bedding material within the custom habitat modules reduces waste buildup and eliminates a key microbial growth substrate.

The open-loop testing described in this appendix quantified the ammonia production rates assuming a constant inflow of clean, ammonia-free air. Accordingly, the results demonstrate that habitat buildup of this contaminant will not be a problem provided ammonia is efficiently controlled at the level of the entire payload module.

Appendix F: Thermal Design

OVERVIEW

The testing, analysis and conclusions described in this appendix were conducted by Andrew Heafitz together with MIT UROPs Arthur Huang, Jerry Richard, Anna Massie, Jesse Marsh and Harvard undergraduate intern Esther Lofgren. As Payload Lead, the author assumed a supervisory role for this work.

Figure 99 is a graphical summary of the thermal control system. Core research questions to be addressed in this appendix include the following:

1. How might air flow patterns in partial gravity impact the efficiency of traditional thermal design strategies? How can experimental and theoretical techniques lead to informed design decisions?
2. What is the preferred design philosophy to ensure efficient thermal transfer between the payload module (a 1-atmosphere pressure vessel) and the spacecraft bus (vacuum)?
3. What is the most effective means of incorporating the condensing heat exchangers, given (1) and (2)?

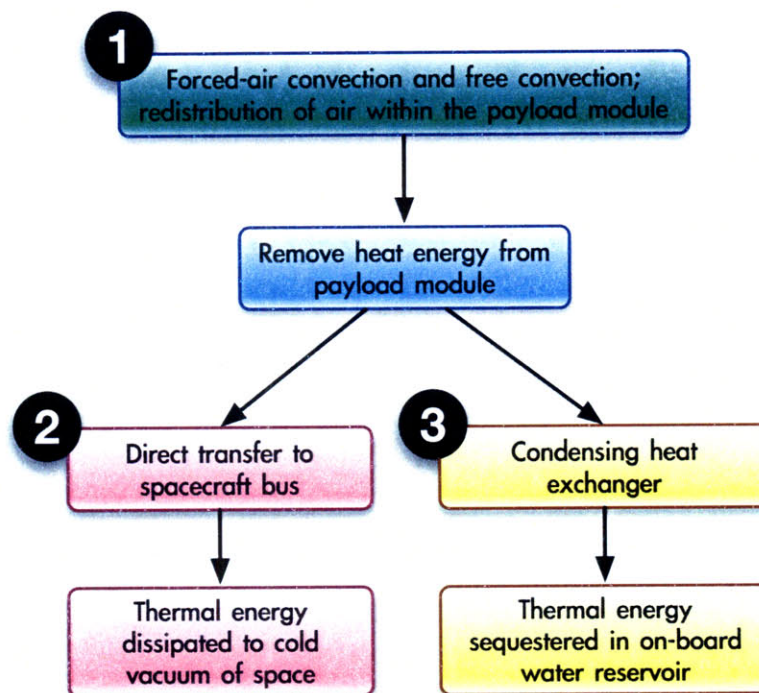


Figure 99: Key elements of the thermal control system

Historical Background

To date there have been remarkably few unmanned vehicles designed to carry biological specimens. The great majority of small research spacecraft have focused on astrophysics, astronomy or fundamental space science. As a consequence, there exists minimal experimental heritage in the realm of vehicles that feature both reentry capability and a sealed atmospheric pressure vessel. Almost all historical examples were part of the successful US-Soviet Cosmos series of missions previously discussed in Chapter 1. As a consequence of the break-up of the Soviet Union, very little engineering performance data survives today. Minimal specific information on thermal control strategies has been unearthed.

ANALYSIS OF STEADY-STATE CONVECTIVE FLOW WITHIN THE PAYLOAD

Free convection is buoyancy-induced movement of a fluid, created by density differences in the fluid itself. The rate of free convection is directly impacted by the local strength of gravity. Much of the available literature on free convection focuses on natural convection under the uniform pull of Earth's gravity. However, within the Mars Gravity Biosatellite the artificial gravity vector G is defined as follows:

$$G = \omega^2 r$$

The angular velocity is represented by ω while r is the radial distance from the longitudinal axis to the test point.

Within the spacecraft, fans and compressors circulate air through the habitat modules, atmospheric reconditioning canisters and heat exchangers. This is known as forced ventilation and operates alongside free convection.

Accordingly, all heated surfaces within the biosatellite will be cooled by mixed convection, the combination of free and forced convection modes. Following traditional methods of analysis, this convective performance can be characterised using the Grashof, Reynolds and Nusselt numbers. These lead to the Richardson number, which can help determine whether a system is dominated by free or forced convection (Incropera and Dewitt 1981). $Ri \ll 1$ indicates forced convection only, while $Ri \gg 1$ represents dominance of free convection.

Figure 100 shows a simplified segmented cross section of the payload module and heatshield. The oxygen tank can be seen at the centre, surrounded by habitat modules and the atmospheric reconditioning canisters toward the nose of the spacecraft. Other subassemblies are not shown since the layout of the payload module is discussed in more detail in section 2.9.1 on page 74.

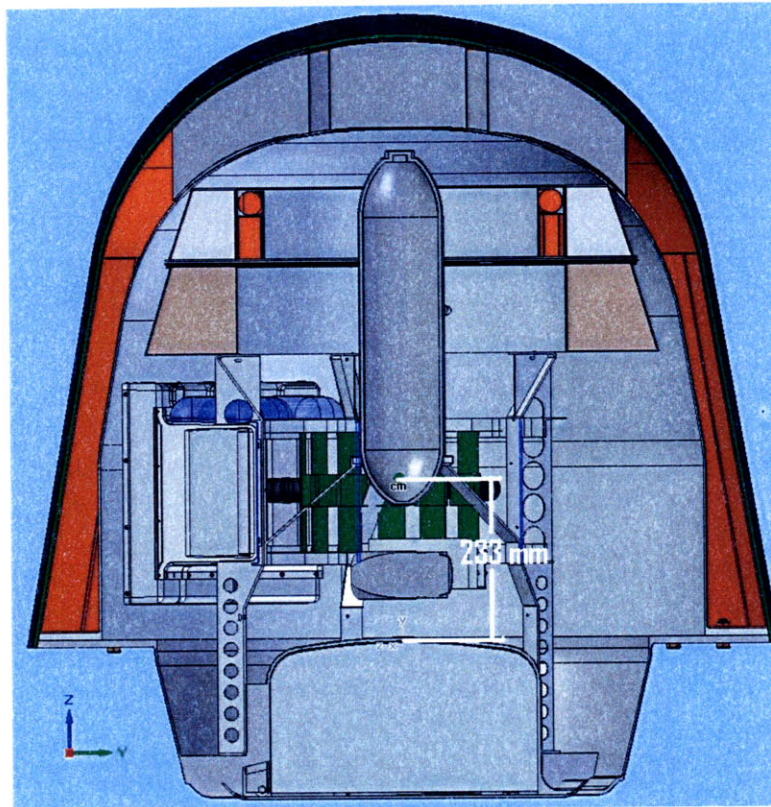


Figure 100: Cross-section of the payload module and heatshield (CAD: David Newell)

Aims

The goal of this work was to determine the expected nature of air flow within the Mars Gravity Biosatellite's payload module. This data is necessary in order to ensure appropriate thermal throughput and sustained cooling of the spacecraft interior. Forced ventilation effects can be experimentally verified in the laboratory through the use of fans. Anticipated free convection in partial gravity must be derived analytically. This section uses a fusion of these two approaches to fully characterise the payload convective environment.

Methods

A full-scale engineering mockup of the payload module was constructed as illustrated in Figure 101. The oxygen tank is in the centre of the diagram. Also shown in outline are the habitat modules and a cross-section of the atmospheric reconditioning canisters toward the nose of the spacecraft. The outer diameter measures approximately 1.16 m and the height is about 1 m. The internal dimensions are slightly larger than that projected for flight, to allow for the installation of test and measurement equipment within the mockup.

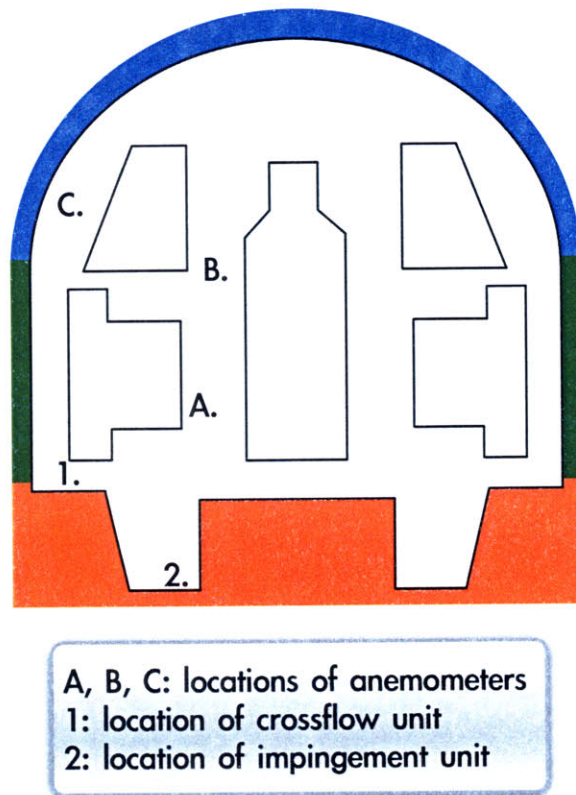


Figure 101: Cross-sectional layout of the air flow testing mockup

The lower segment of the mockup (orange outline in Figure 101) models the area that would ultimately interface with the spacecraft bus. It is constructed from welded aluminium in order to ensure a good thermal pathway for experiments that investigate payload-to-bus heat transfer. The green zone is a cylinder constructed from a single sheet of acrylic. The sheet was mechanically curved to 360° and sealed at the interface. The blue area is also acrylic. This segment was custom-manufactured using the same fabrication techniques as are employed to make bubble canopies for fighter jets. Both acrylic zones are optically transparent to permit viewing of experiments within the mockup.

Lubricated o-rings of 1.27 cm diameter serve as mechanical connections between flanges on the three zones. These airtight interfaces allow the mockup to perform as a pressure vessel. The three-subunit segmentation allows for future reconfiguration if necessary.

For all air flow experiments, foam-core models of the habitats and air tank were used in place of actual prototype hardware. Foam-core exhibits substantially different thermal properties from flight hardware. However, all air flow tests were conducted under isothermal conditions; both foam-core and flight-ready hardware would have generated identical results for these experiments.

The thermal system design baselines 11 cooling units secured to the aluminium bus/payload interface. This experiment assessed the payload module air flow as generated by two different configurations.

The crossflow configuration (Figure 102) is intended for the location marked 1 in Figure 101. Its shorter vertical profile is specifically designed to fit in the volume between the habitat modules and the payload baseplate.

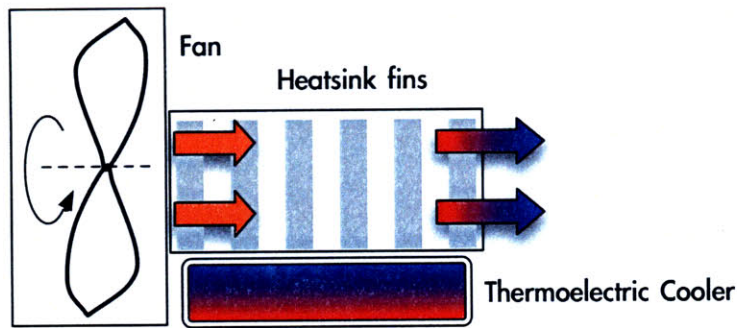


Figure 102: The crossflow configuration of cooling unit

The impingement configuration (Figure 103) has a taller profile and is suitable for the location marked 2 in Figure 101.

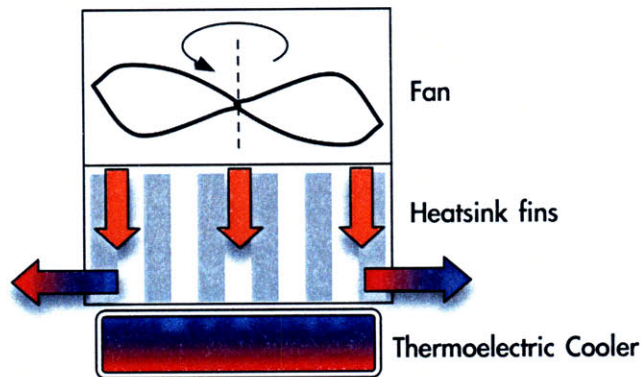


Figure 103: The impingement configuration of cooling unit

In both configurations, the thermo-electric cooler is Marlow Industries model DT12-8. The fan is a small brushless unit (RadioShack #273-240, 12 V DC, 0.13 A, 1.56 W, 38 mm diameter) that channels air directly onto an aluminium heatsink (CoolInnovations Inc. product 2-202014R). High-density polysynthetic thermal compound (product Arctic Silver 5, Arctic Silver Inc.) was used on either side of the thermoelectric cooler to ensure good thermal conductivity.

Air flow was tested for two scenarios (see Figure 101):

- 11 of the crossflow units were installed on the baseplate in the locations marked 1.
- The 11 units were removed and reassembled in the impingement configuration. These were subsequently installed in the locations marked 2.

In both scenarios, the 11 units were equally spaced around the circumference of the mounting area. Figure 104 shows a view looking down into the aluminium baseplate cavity of the thermal engineering mockup that includes a few of these cooling units. The retort stand in the image held an anemometer for preliminary feasibility studies.

11 cooling units were selected because prior experimental results had suggested that this number met requirements for power efficiency and reliable cooling of the payload module

(further detail in Appendix D: Condensing Heat Exchanger Design). Air flow measurements were taken with a commercial hot-film anemometer from locations A, B and C. The anemometer had previously been calibrated with known flow rates through the use of a Pitot tube. Experimental readings were taken over a 30-second period and averaged for improved reliability.



Figure 104: Impingement configuration units installed in the mockup

Results

First, the anemometer was positioned directly above the fan inlet for each configuration (impingement and cross-flow) to determine fan inlet air speeds. The results are recorded in Table 51. Errors in the air flow velocity and computed Reynolds number are propagated from precision uncertainty in the calibration of the anemometer.

Table 51: Fan inlet air flow velocity for fan/TEC/heatsink modules

	Average Velocity	Reynolds Number
Crossflow (Location 1)	0.240 ± 0.142 m/s	553 ± 386
Impingement (Location 2)	0.456 ± 0.084 m/s	2077 ± 657

Anemometer results are recorded in Table 52. In the trials with impingement configuration, the anemometer voltage fluctuated by 0.01 V from the reading with all fans turned off. Since the fluctuation was equal to the resolution of the readout, these measurements were taken to be negligibly small and were recorded as zero. The impingement configuration in location 2 was therefore dismissed as a design option because it could not generate sufficient circulation within the payload module. Accordingly, Table 52 focuses exclusively on the crossflow configuration at location 1.

Table 52: Anemometry for crossflow configuration fans in location 1

	Average Velocity	Reynolds Number
Anemometer Location A	0.240±0.084 m/s	505±353
Anemometer Location B	0.148±0.065 m/s	525±460
Anemometer Location C	0.210±0.078 m/s	344±256

Even though the fan inlet flow rate was nearly halved in the crossflow configuration, it is clear that the advantage of location 1 substantially outweighs any air flow rate inefficiencies. This configuration is the focus of subsequent analysis.

With the knowledge of the radial position at which each forced-convection measurement was taken, a theoretical Grashof number may be computed for each experimental datapoint. The following values are used for an example on-orbit scenario:

- Artificial gravity calculated from centripetal acceleration, given the radial position at which the forced-convection measurement was taken.
- Temperature difference given by a theoretical surface temperature and air temperature. The air temperature within the payload module is assumed to be 22°C, a realistic rodent-safe setpoint. Surfaces are assumed to be 25°C for the habitat module close to anemometers A and B and 30°C for the payload avionics subassembly near location C. This results in a temperature difference of 3°C for the habitat module and 8°C for avionics.
- The volumetric thermal expansion coefficient β given by the approximation $\beta=1/T_{avg}$ where T_{avg} is the boundary-layer temperature. The arithmetic mean of surface and air temperatures are used to compute T_{avg} .
- The kinematic viscosity ν given by standard calculation tables for a certain T_{avg} .
- Length scale taken as the hydraulic diameter of the channel in which the forced-convection measurement was taken.

For each experimental anemometer location shown in Table 53, the Richardson number is computed from the experimentally determined Reynolds number and the theoretical Grashof number.

Table 53: Impacts of artificial gravity on convection

	Temperature Difference	Theoretical Grashof Number	Richardson Number
A	3°C (habitat)	1.02E5	0.37
B	3°C (habitat)	5.53E4	0.22
C	8°C (avionics)	3.84E4	0.32

Table 53 confirms that in orbit the forced convection effects would largely dominate any free convection induced by artificial gravity given the assumptions in the example calculation.

In order to provide a more rigorous engineering analysis, computations were performed to determine the required forced-convective flow velocity at each of the measurement positions given a desired Richardson number for the worst-case temperature difference scenario. Worst-case differentials come from the mission science requirements, which state a minimum air temperature of 18°C and a maximum surface temperature anywhere in the payload module of 37°C. An adequately small Richardson number would be on the order of 0.1, assuming an engineering safety factor of 10 to ensure complete dominance of forced convection.

Table 54 shows the computed minimum air flow velocity given a Richardson number of 0.1. The worst-case temperature difference is calculated by subtracting 18°C from 37°C.

Table 54: Computed required minimum air flow velocities

	Temperature Difference (Worst Case)	Minimum Air flow	Reynolds Number
A	19°C (habitat)	0.358 m/s	2536
B	19°C (habitat)	0.443 m/s	1864
C	19°C (avionics)	0.292 m/s	959

Conclusions

This section has addressed the core research questions identified by block 1 in Figure 99, namely:

- How might air flow patterns in partial gravity impact the efficiency of traditional thermal design strategies?
- How can experimental and theoretical techniques lead to informed design decisions?

The conclusions are as follows:

- Forced-air convection units at the locations marked 1 (see Figure 101) can generate good air flow in a 1-g ground testbed environment.
- Calculations verify that, even under worst-case orbital temperature conditions, the system will be able to overcome any natural convection that occurs as a consequence of artificial gravity.

A limitation of this work is the fact that the steady-state convective flow was derived using a purely experimental method. An alternative approach would incorporate a numerical or hybrid numerical/experimental approach to assess the field velocity and convective heat exchange coefficients. Such an analysis should be conducted during the Critical Design Phase in order to augment and more fully contextualise the results presented to date.

These experiments focus solely on air flow and consequently do not address the possibility of a hybrid approach for fan/TEC placement. While location 1 is a clear best choice for air flow, it is possible that location 2 may provide advantages for thermal transfer. Future experiments should assess the option of fan-only systems beneath each habitat module that transfer air toward combined fan/TEC/heatsink units at the bottom of the baseplate cavity.

VALIDATION OF PAYLOAD-TO-BUS THERMAL TRANSFER STRATEGY

Rodent health requirements mandate that the air temperature remain between 18°C and 28°C within the payload module. Given the air flow environment described in the previous section, further experiments were performed to explore the payload-bus interface and understand the most effective means of transferring energy across this boundary. The impingement-configuration fan/TEC/heatsink modules previously described had initially been baselined because Peltier coolers have strong spaceflight heritage in structures that enclose atmospheric pressure vessels (Kotylarov, de Crom *et al.* 2006). The purpose of the experiments described in this section was to verify that such an apparatus could meet the scientific requirements for temperature control within the payload module. Specifically, this study explored how many thermal control modules would be necessary and which configuration(s) would give the desired performance.

The design of the spacecraft bus thermal subassembly is outside the scope of this work. Ultimately, in order to create a defensible unified CDR-level design it will be necessary to calculate the thermal throughput of the bus and thereby derive the temperature of the payload baseplate. Over a multi-year period, teams based at MIT and at the University of Washington (a former Mars Gravity partner) attempted to create PDR-level bus designs. They provided estimates for an achievable baseplate temperature that variously ranged between 0°C and +15°C. At the time of the experiments described in this section, the best estimate was +15°C.

In 2007, the Mars Gravity Biosatellite program began working with Microsat Systems Inc., an industrial design partner that assumed responsibility for the spacecraft bus design. A PDR-level design was arrived at but design details are not available to the author due to ITAR restrictions and U.S. Export Control laws. At the time of writing, the industrial bus design partner has ceased to work on this project due to a lack of program funding. Accordingly, it is not currently possible to perform calculations that would better estimate the flight-ready thermal performance of the bus/payload system.

Method

A simpler thermal mockup of the payload module was constructed. The payload/bus interface was modelled by a flat aluminium baseplate, to the underside of which were attached 11 aluminium struts of cross-section 2.5 cm by 3.8 cm. A hollow plastic vessel approximately equal to the size of the payload module was installed on top of the baseplate. An 80 W heat source (magnitude selected to match the entire payload module's power budget) was installed within the vessel. The mockup exterior was insulated using thermal construction wrapping. The upper surface of the baseplate was insulated with a compressible open-cell foam lining of thickness 1 cm.

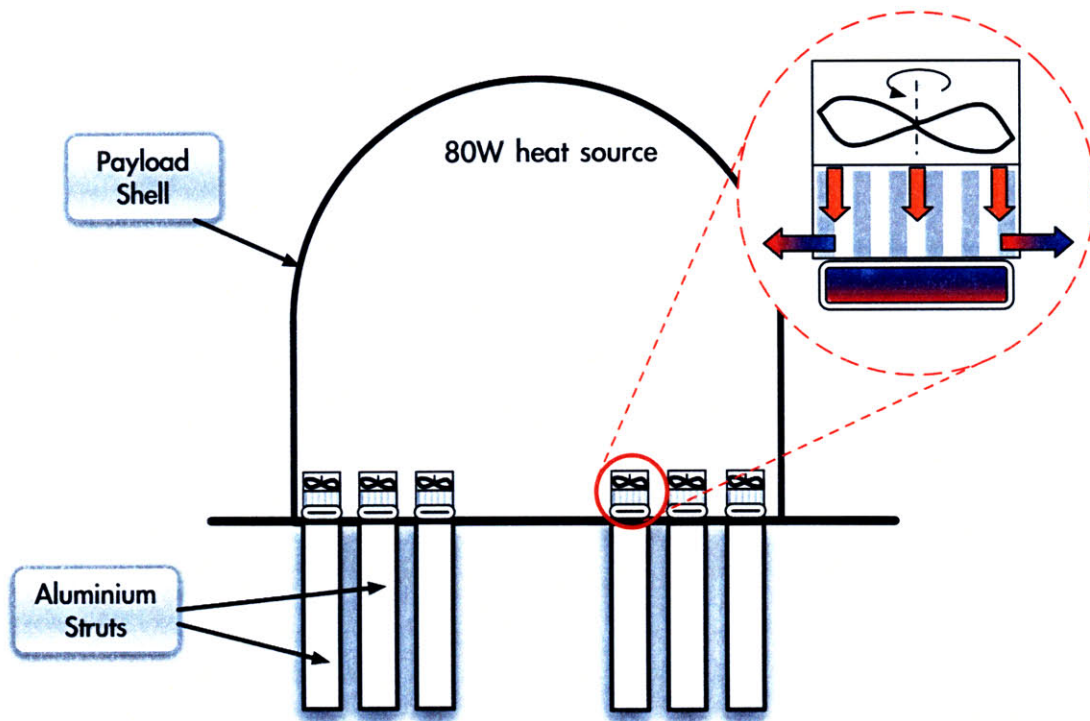


Figure 105: Simplified payload thermal mockup in test configuration

Thermocouples were installed at various locations within the mockup and on the baseplate. Three configurations were tested:

- Configuration A: 11 heatsink/fan/TEC modules.
- Configuration B: 5 heatsink/fan/TEC modules, 6 heatsink/fan modules.
- Configuration C: 11 heatsink/fan modules.

The struts were placed in a constantly recirculating bath of ice water. Varying the depth of the water allowed the baseplate to come to a starting temperature of 15°C for any given experiment.

The goal of this test was to evaluate the relative performance of the various configurations in order to determine which would meet the cooling requirements at the lowest power cost.

Across all experiments, the following were independent variables:

- Choice of configuration (A, B or C).
- Electrical power to fans.
- Electrical power to TECs (if applicable).

The measured dependent variable was as follows:

- Ultimate stabilised delta-T, where delta-T is defined as the steady-state temperature differential between the baseplate (kept as close to 15°C as possible given the

apparatus) and the air within the mockup payload vessel. Steady-state was confirmed when delta-T values were changing by less than 2% over a 5-minute period. Most experimental runs lasted over 60 minutes.

Results

Table 55: Performance envelopes for each configuration

		Maximum Delta-T	Minimum Delta-T
	Science Requirement	13°C	3°C
A	11 heatsink/fan/TEC units	14°C	-3°C
B	5 heatsink/fan/TEC, 6 heatsink/fan units	11°C	6°C
C	11 heatsink/fan units	7°C	3°C

Table 55 illustrates the maximum and minimum steady-state delta-T values that could be sustained by each configuration. In other words, the table shows the performance envelopes for the three design options. The maximum indicates the highest temperature that can be reached when no power is supplied to fans or TECs and the system is in a 100% passive thermal transfer mode. The minimum represents the best cooling capabilities when all thermal systems are fully activated. The science requirement (top row) reflects rodent health needs that require the payload temperature to remain between 18°C and 28°C at all times. A design solution meets requirements if the minimum delta-T value is lower than or equal to that stated in the science requirement. It is also desirable for the maximum delta-T to be lower than that stated in the science requirement.

Figure 106 shows representative performance for configuration A. Increasing TEC power is shown on the horizontal axis, while delta-T is on the vertical. Importantly, fan power greater than 0.5 W does not significantly improve the delta-T. Additionally, any TEC power increases are linear, causing the delta-T to improve by approximately 1.5°C for every additional Watt of power to each TEC.

Figure 107 shows the net recorded performance for all three configurations. An efficiency metric (such as power per degree of delta-T) can readily be mapped from this graph. The data shown comes from many experimental runs; data points of similar total power were averaged where possible.

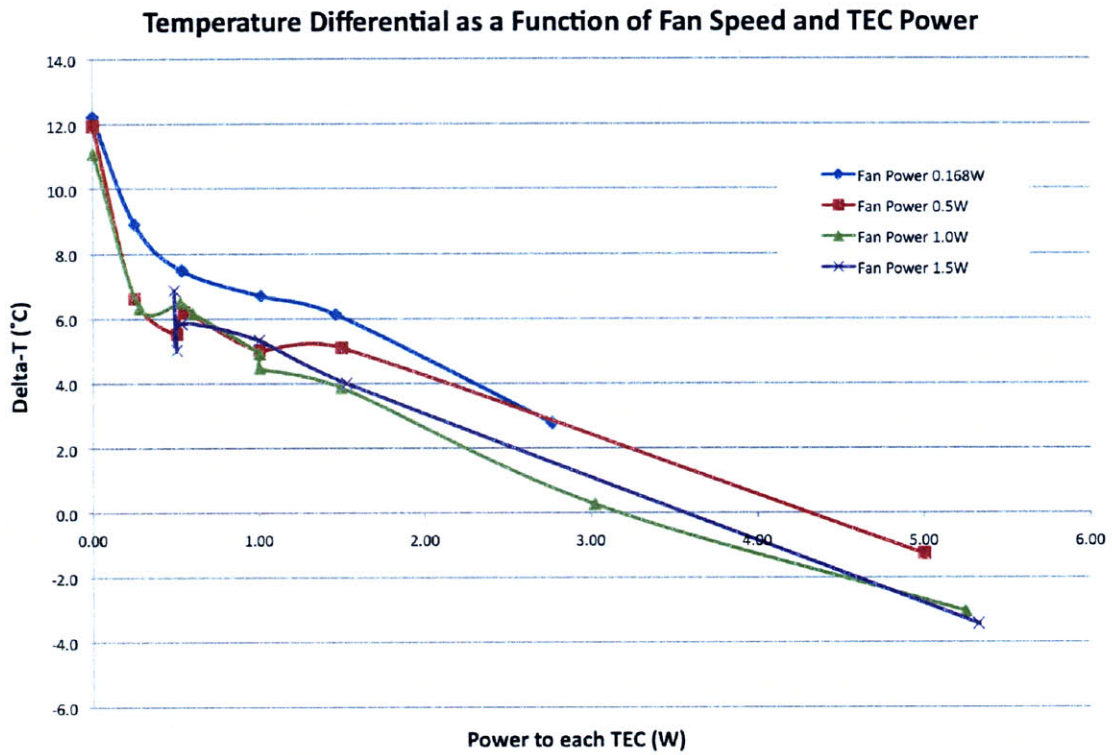


Figure 106: Configuration A at various TEC power levels and four fan speeds

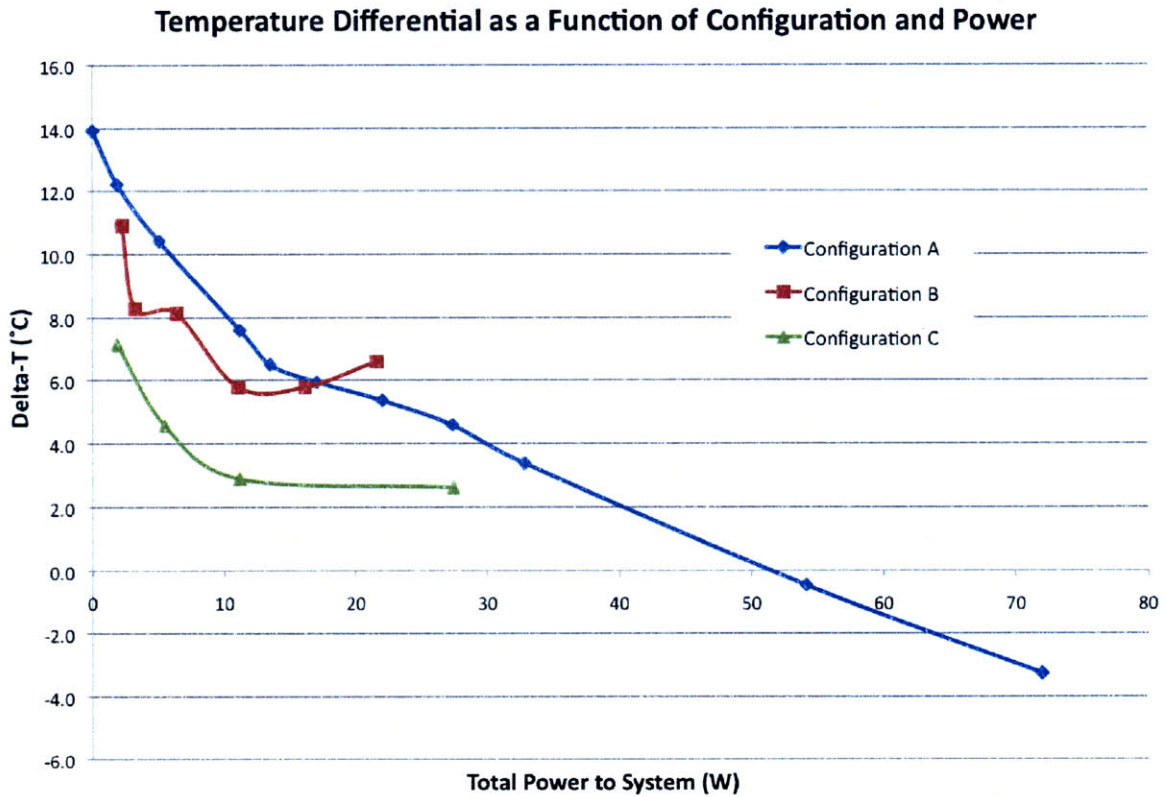


Figure 107: Performance summary for all three configurations at varying power

Table 55 and Figure 107 taken together confirm that all three configurations are able to reach at least part of the desired control envelope. The expected power allocation for the thermal system is 20 W during nominal flight operations. Table 56 shows the results of taking this constraint into account.

From Table 56, it is clear that only configuration C fully complies with the science requirement under nominal power constraints. However, the asymptotic nature of the C line (green) shown in Figure 107 reveals that this configuration will never be able to attain a delta-T lower than 3°C. This is problematic because it suggests the system might be unable to recover from slightly off-nominal conditions. Configuration B appears similarly unable to reach lower delta-T values. However, for slightly reduced power efficiency and more mass, configuration A provides off-nominal control authority.

Table 56: Performance envelopes given Figure 107

		Maximum Delta-T	Minimum Delta-T
A	11 heatsink/fan/TEC units	14°C	6°C
B	5 heatsink/fan/TEC, 6 heatsink/fan units	11°C	5°C
C	11 heatsink/fan units	7°C	3°C

Conclusions

This section has addressed the core research question identified by block 2 in Figure 99, namely:

- What is the preferred design philosophy to ensure efficient thermal transfer between the payload module and the spacecraft bus?

Conclusions are as follows:

- Efficient thermal transfer can be effected through the use of heatsink/fan units and heatsink/fan/TEC units.
- The preferred design solution features 11 heatsink/fan/TEC units distributed evenly around the perimeter of the payload baseplate (configuration A). This option has been selected because it provides excellent control authority in return for small mass and power penalties. Control authority in slightly off-nominal conditions is considered essential as a consequence of the need to pre-cool the payload module prior to reentry into the Earth's atmosphere at the culmination of the mission.

The results of these experiments should be augmented and contextualised for CDR through use of the higher-fidelity new thermal engineering mockup previously described and shown in Figure 101.

One possible source of error in the experiments to date was the fact that the ice water in the cooling bath would occasionally increase in temperature if the ice completely melted over the duration of any one experiment. This happened only in those tests that had the highest heat flux out of the simulated payload module. It could readily have been addressed during

a given trial by draining the water and refilling it with the original depth of fresh ice-water mixture as soon as complete ice melting was observed. In reality, however, this does not negatively impact the quality of the results because experimental readings in previous tables are always expressed in terms of temperature differentials from the baseplate. In other words, if there were deviations in the baseplate temperature from the 15°C target, these are already taken into account in the results.

In addition, the problem of TECs back-warming the baseplate was an issue in a number of tests. During Phase C testing, the new mockup should be attached to an industrial chiller unit capable of cooling the baseplate to a known setpoint. Such a chiller would pass water at a constant flow rate through a series of circular copper tubes attached to the flat underside of the aluminium baseplate. By this means, the mockup would accurately model the on-orbit configuration in which the spacecraft bus will maintain the underside of the payload at a predefined temperature. Results should permit full characterisation of the payload thermal performance envelope.

THE EFFECT OF CHE OPERATION ON THERMAL CONTROL

The condensing heat exchangers were previously discussed at the beginning of this appendix. That section focused exclusively on the ability of the CHE design to remove water from the ambient payload air. In reality, however, CHE operation does significantly impact the thermal environment. This section discusses how the thermal system can work in concert with the CHEs to manage and control payload temperature.

CHE Thermodynamic Theory

The thermodynamic pathway for CHE operation is as follows:

1. Fan pulls in air at a certain ambient temperature and relative humidity.
2. The cold plate causes the air to reduce in temperature until it reaches the dew point, at which time the relative humidity is 100%.
3. As cooling continues, water condenses out while the absolute moisture capacity decreases.
4. Drier air leaves the CHE and its relative humidity decreases as the temperature rises.

Table 57: Thermodynamics of CHE operation

#	Air Temp (°C)	Relative Humidity	Moisture Content (kg H ₂ O/kg air)	Change in air temperature energy from initial (kJ/kg air)	Change in water temperature energy from initial (kJ/kg air)	Change in latent heat of vaporisation energy from initial (kJ/kg air)	Total change in energy (kJ/kg air)
1	20	70%	0.0102	N/A	N/A	N/A	0
2	14.2	100%	0.0102	-5.80	-0.25	0.00	-6.05
3	8.3	100%	0.0063	-11.70	-0.31	-8.81	-20.82
4	20	46%	0.0063				

Reference to a standard psychrometric chart gives the values shown in Table 57 for energy transferred when 1 kg of air moves through the thermodynamic pathway listed previously. The energy calculations show that cooling the air by 11.7°C and removing 24% of the moisture requires 3.4 times as much power as simply cooling the air by 5.8°C to reach the dew point.

Discussion

The CHE is optimised for removal of water, whereas the fan/heatsink/TEC modules are optimised for cooling the payload module with minimal power. From a systems-level engineering perspective, it will ultimately be necessary to conduct combined mass and power optimisation for the thermal and humidity control systems together.

One possible approach for saving power would be to position the CHE so that it receives pre-cooled outflow air from one of the standard TEC cooling units. This would allow the CHE to run at a lower power, which may improve efficiency. It would also eliminate the need for a dedicated CHE fan; in the event that the TEC were not being used for cooling at a given time, its fan could still be activated to send air toward the CHE.

Although the CHE is designed primarily to dehumidify rather than to cool the air, Table 57 verifies that it will provide a certain level of additional cooling performance. Experiments show that the thermal transition from ambient to the dew point is similar in efficiency to the TEC thermal unit performance described earlier in this appendix. In the condensing regime, the CHE takes 3.4 to 5 times the power of a TEC to lower the temperature of the air (calculated and measured values, respectively). The TEC cooling system would accomplish the same reduction in temperature at 20% to 35% the power used by the CHE. Therefore, in a systems-level analysis it would be appropriate to “credit” 20% of the power used by the CHEs to the thermal control system since the TEC units will have 20% less cooling to perform.

Conclusions

This section has addressed the core research question identified by block 3 in Figure 99, namely:

- What is the most effective means of incorporating the condensing heat exchangers, given prior results?

The conclusions are as follows:

- A 20% power credit should be allocated to the thermal control system as a consequence of CHE operation.
- Judicious design decisions that allow the CHEs to work in concert with the thermal and atmospheric control systems have the potential to significantly enhance power and mass efficiency. Such possibilities should be explored during Phase C detailed design efforts.

Appendix G: Payload Structural Design

THE AEROSHELL: LIFE SUPPORT BUCKET AND AFT FAIRING

The main purpose of the aeroshell is to serve as a pressurised container for the payload that interfaces with both the EDL and the Payload. Its two main components include the life support bucket and the aft fairing, which are bolted together to create the aeroshell.

Aeroshell Requirements

The aeroshell must maintain a pressure of approximately one atmosphere throughout the mission. To meet this requirement, the leak rate should not exceed 9 standard cubic centimetres over a 35-day period. It must be structurally sound to withstand both launch and landing accelerations with a safety factor of 1.4. In addition, the aeroshell must be mechanically compatible with interfaces to the heatshield and spacecraft bus. Importantly, this includes attachment to the Lightband™ quick-disconnect separation ring that carries power and data lines and also serves as the thermal transfer pathway to the spacecraft bus. The anticipated vibration environment shall not cause the aeroshell to become unseated or to contact the inner surface of the heatshield.

In compliance with ground support requirements (discussed previously in Chapter 3) the aft fairing must feature air inflow and outlet ports to support a flow rate of up to 22 standard litres per minute.

The design of both life support bucket and aft fairing should be as lightweight as possible. No aerodynamic requirements are imposed because the aeroshell is exposed to the air only when the reentry vehicle is descending at a relatively slow rate. This occurs once the heatshield is jettisoned after the drogue parachute has already been deployed. At this point, the rate of descent is less than 15 m/s and the parachute ensures there is no danger of the vehicle tumbling or spinning.

Design

After multiple iterations, an aft fairing design was completed that meets all requirements. Figure 108 shows finite element analysis output completed by Active Space Technologies, Inc., which confirmed a factor of safety of 1.6. The mass of this welded aluminium design is 26.8kg. The upper half interfaces with the payload module, while the lower part faces the spacecraft bus. The central bubble is the parachute container.

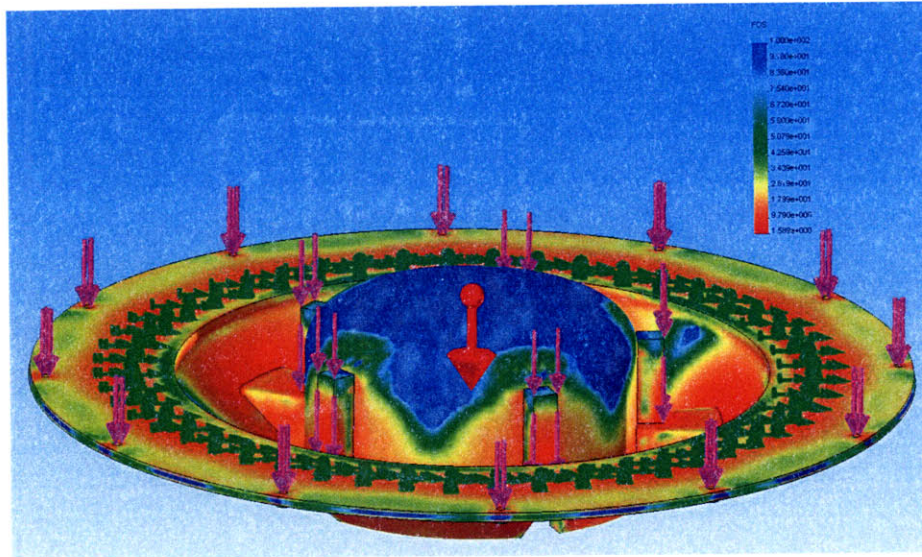


Figure 108: Finite element analysis of aft fairing design (CAD: Joao Ricardo)

The dynamic loading, modal analysis, shock analysis and lateral loading have not yet been fully determined for the whole satellite. These tasks are scheduled for the Phase C design effort, at which point it would be appropriate to consider aft fairing mass reduction techniques in order to bring the factor of safety closer to the required value of 1.4.

Figure 109 shows the outcome of the life support bucket design process. The life support bucket encloses the entire payload module while also interfacing with the heatshield above. Finite element analysis took into account both the 10-G launch loading and the internal atmospheric pressure and showed a maximum anticipated stress of 176 MPa. This is acceptable since the value is substantially less than the 276 MPa yield strength of 6061 T6 aluminium. Manufacturability constraints associated with this design will be further explored as part of Phase C design efforts.



Figure 109: Life support bucket design (CAD: Emily Grosse)

Atmospheric Sealing

Two concentric o-rings will seal the junction between the aft fairing and the life support bucket. Each will be seated within a circular groove on the aft fairing. The o-rings will be manufactured from virgin Teflon® with a cross-sectional diameter of 5.33 mm. Steel M10 bolts will be arrayed around the perimeter of the aft fairing to compress the o-rings and ensure a good seal. Eight permanent bolts will be sufficient to maintain the pressure seal, while an addition four pyrotechnic bolts will secure the heatshield. These four bolts will detonate to jettison the heatshield during descent.

Ground Support Connections

Quick-disconnect air flow ports such as those manufactured by Parker or Souriau have been baselined for installation within the slanted wall of the aft fairing. They will be positioned so as to avoid welded joint-lines and the parachute container. One port will serve as an air inlet while the other will be for outflow. A tube will carry the inlet air directly to the suction port of the habitat circulatory fan.

The design of the selected product is such that the port self-seals when a force is applied to disconnect the bus-side hoses. This would occur a few minutes prior to launch when ground support is no longer required. A hole will remain in the base of the spacecraft bus once the hose is fully extracted, but this is of no consequence since the bus is neither sealed nor internally pressurised.

Figure 110 shows a cross-section of the quick-disconnect mechanism.

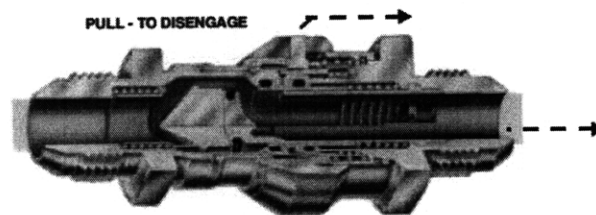


Figure 110: Parker Stratoflex Slide-Lok™ (manufacturer image)

Two Slide-Lok™ connectors manufactured by Parker Stratoflex will serve to pass air into and out of the aeroshell while on the ground. The seal on separation is rated for use in a vacuum, and is therefore suitable for space operations. The diameter of connector required to allow the passage of 22 SLPM of air is 5.7 cm, while the tubing will be 1.27 cm diameter. Each connector has a favourable mass of 64 grams.

Central Utilities Truss

The central utilities truss (Figure 111) provides structural support for the habitat modules, avionics, ECLSS systems and other hardware. It has cylindrical symmetry and is mechanically strong since it is directly welded onto the aft fairing. The base of each of the five spars is welded to one of the parachute attachment points on the aft fairing. It is advantageous to have the payload centre of mass as far toward the nose of the spacecraft as possible in order to promote stable reentry dynamics. Accordingly, the truss extends up the entire length of the payload module and provides a secure attachment point for the heaviest payload subassembly (the ECLSS canisters) toward the nose of the vehicle. The

truss also features mounting brackets for the sensor suite and payload video acquisition computer in addition to a central plate to hold the oxygen and nitrogen gas cylinders.

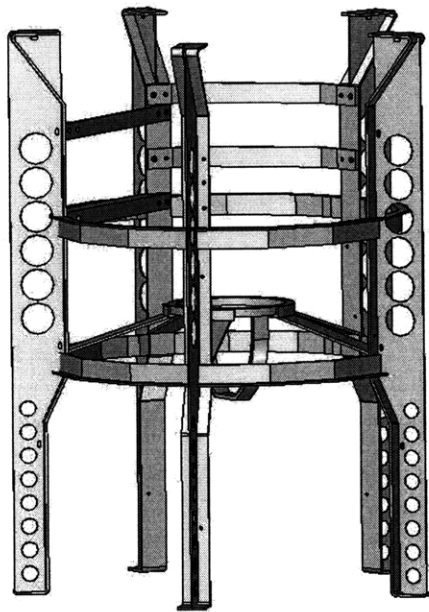


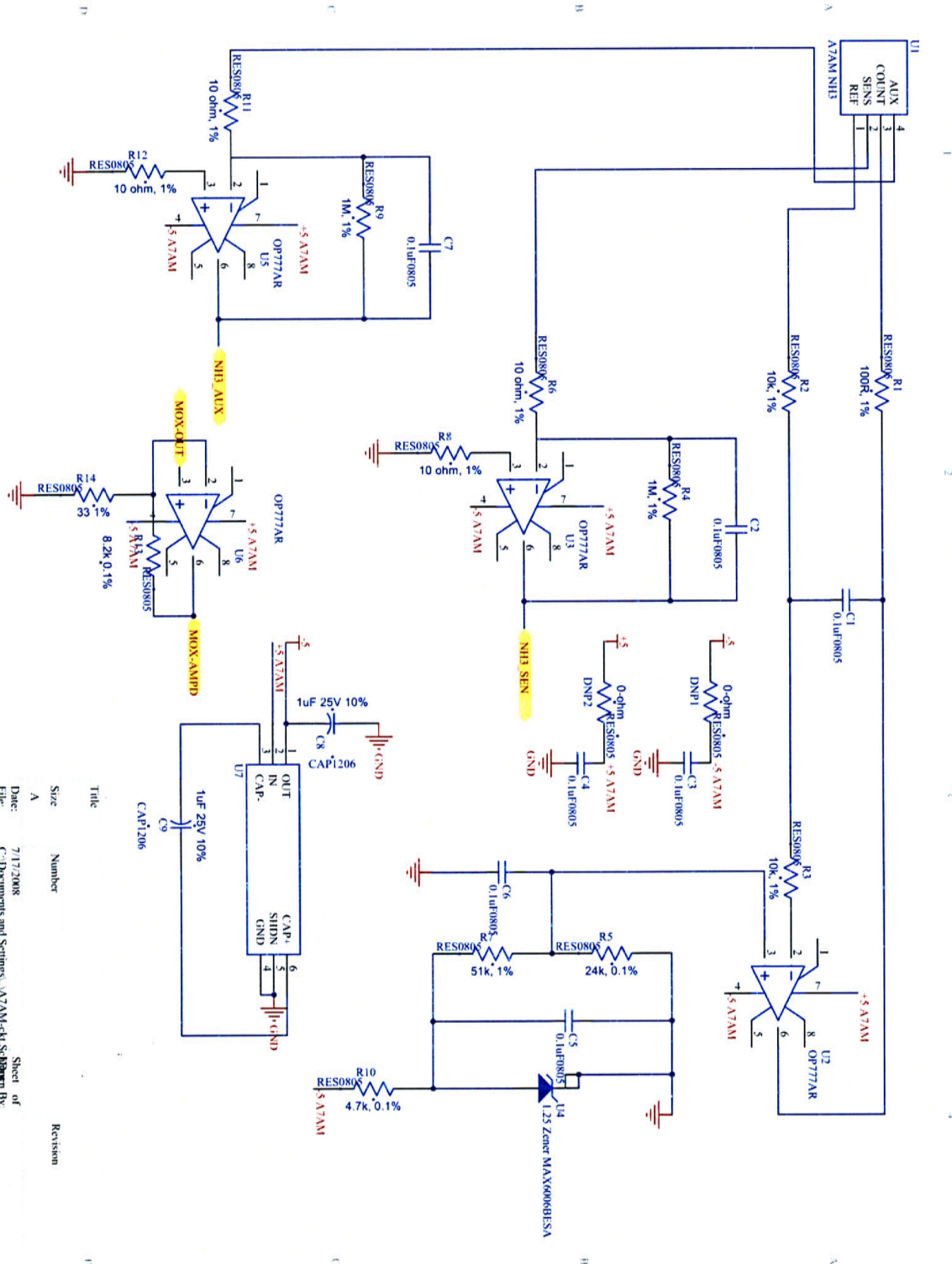
Figure 111: Central Utilities Truss (CAD: Emily Grosse)

Preliminary Finite Element Analysis using 10-G loading conditions and a simplified payload mounting model showed that the truss exceeds the required factor of safety of 1.4. Mass optimisation is incomplete and should be an early focus of Phase C development work.

Appendix H: Circuit Diagrams

SENSOR SUITE

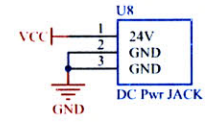
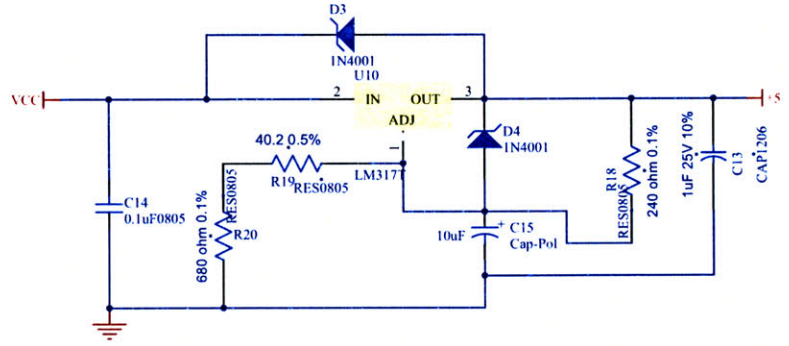
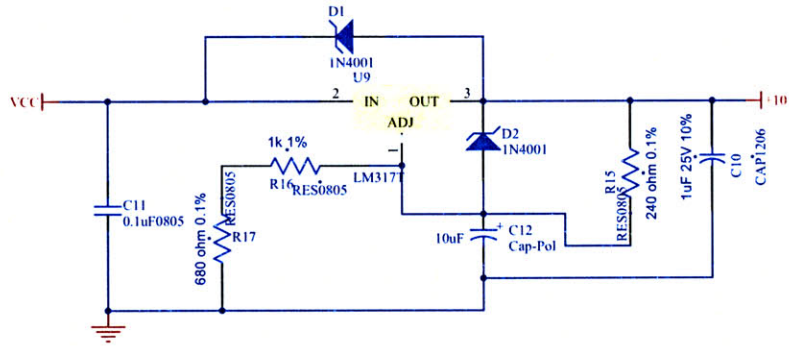
Ammonia Sensor Circuitry



Revision	Number	Title	Size
A	1		

Date: 7/17/2008
 File: C:\Documents and Settings\AV7AM-dk\Schman By: Sheet of

Power Management



Title

Size
A

Date:
File:

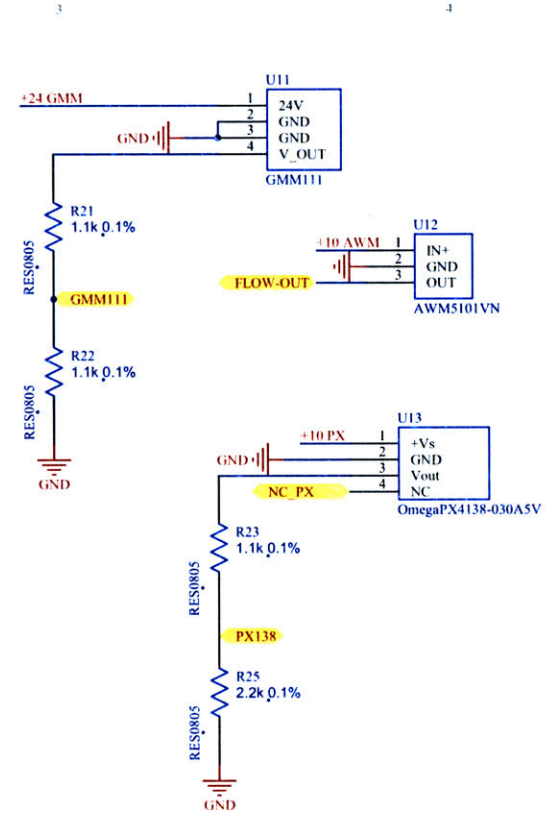
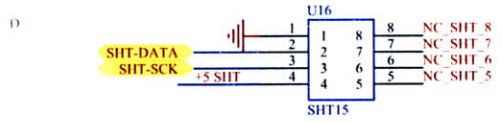
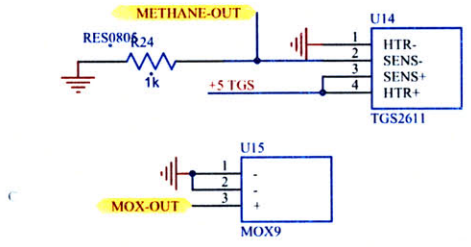
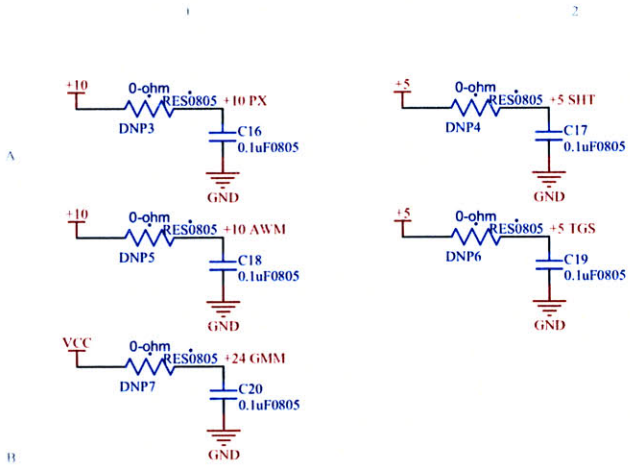
Number

7/17/2008
C:\Documents and Settings\...Power-Conditioning\3141.Dwg

Revision

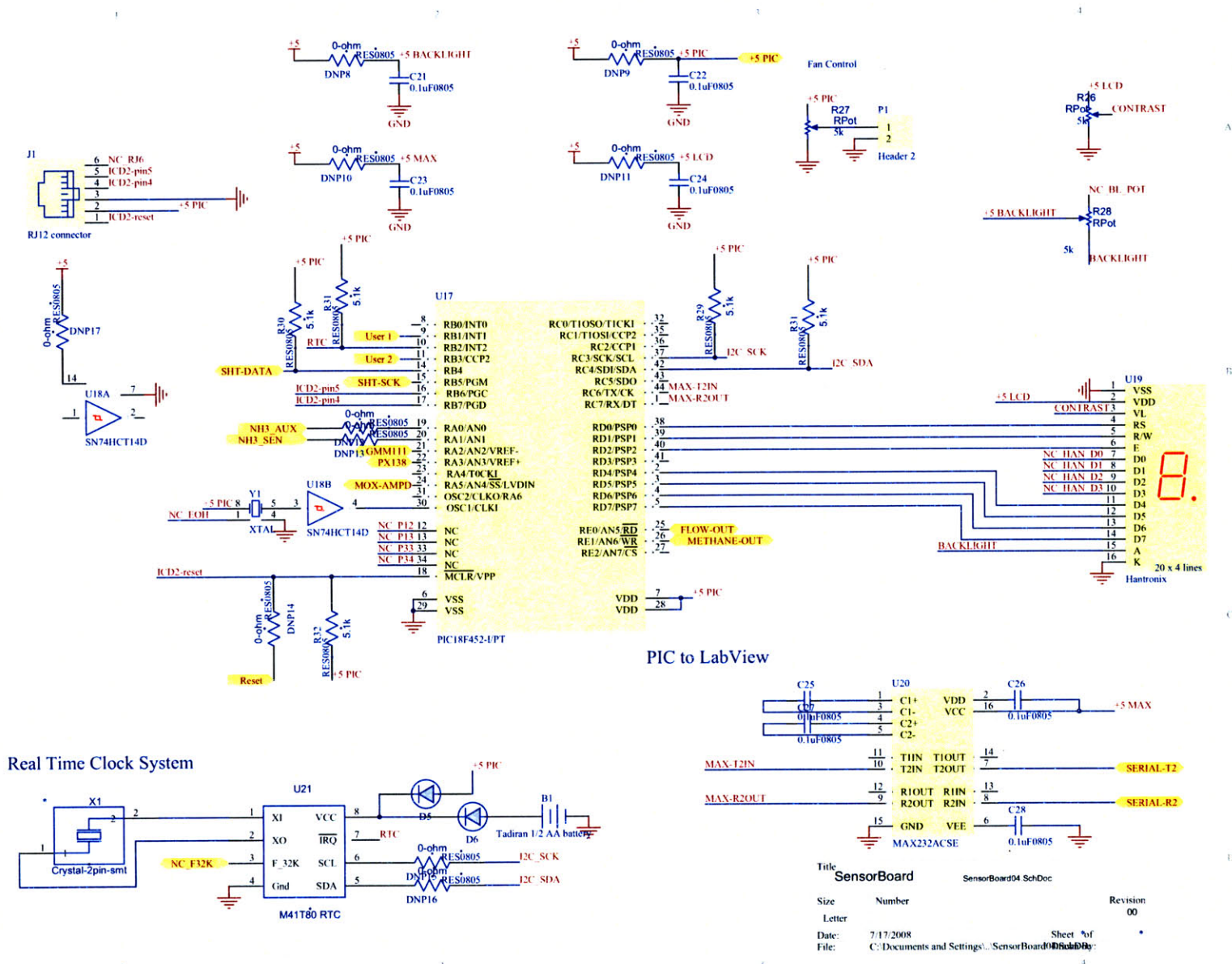
Sheet of
3 of 4

Circuitry for Other Atmospheric Sensors



Title	Number	Revision
A		
Date:	7/17/2008	Sheet of
File:	C:\Documents and Settings\...\Sensor+circuitry\03.01.Doc	23 of 275

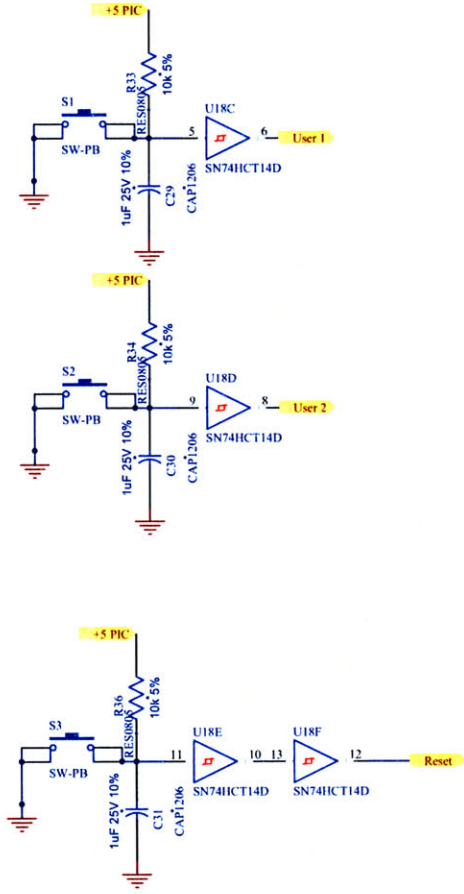
Microcontroller Interfaces



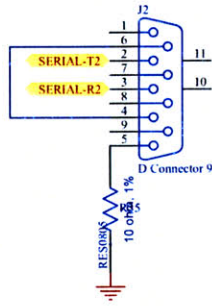
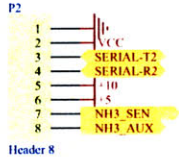
Title: SensorBoard
SensorBoard04 SchDoc

Size	Number	Revision
Letter		00
Date:	7/17/2008	Sheet 4 of 4
File:	C:\Documents and Settings\... \SensorBoard04	Drawn By:

User Interface and Connectors

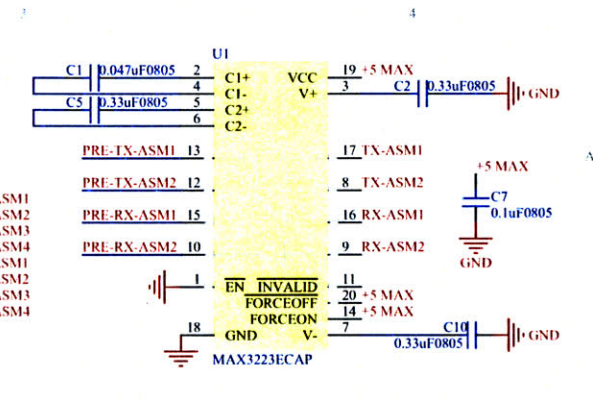
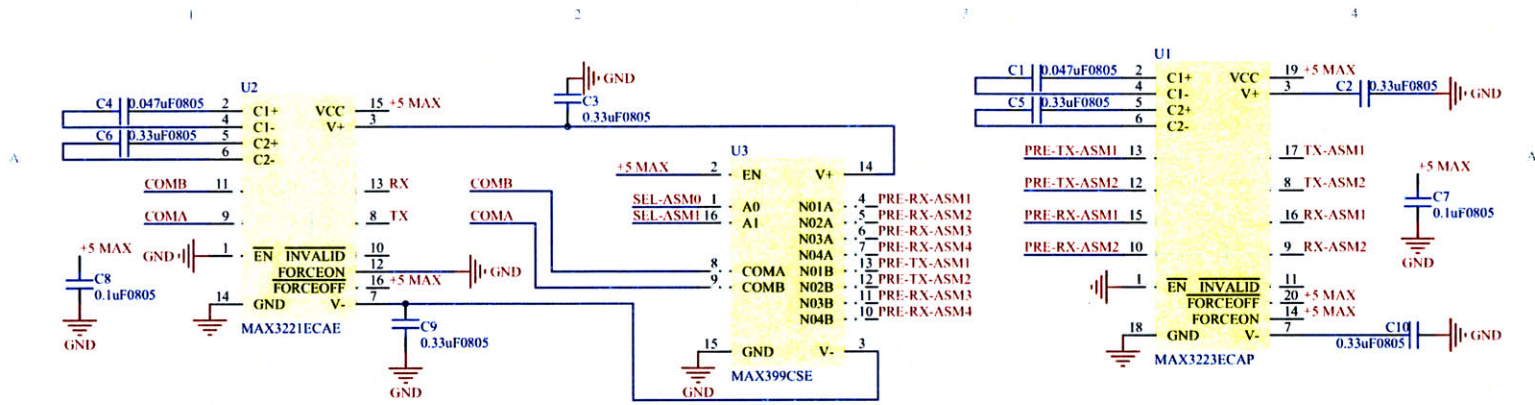


Connector

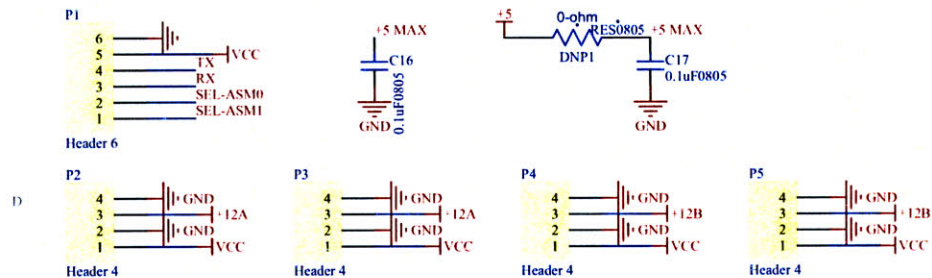


Title		
Size	Number	Revision
Letter		
Date:	7.17.2008	Sheet of
File:	C:\Documents and Settings\...User-switches\...	4

AGGREGATOR Multiplexing Circuitry

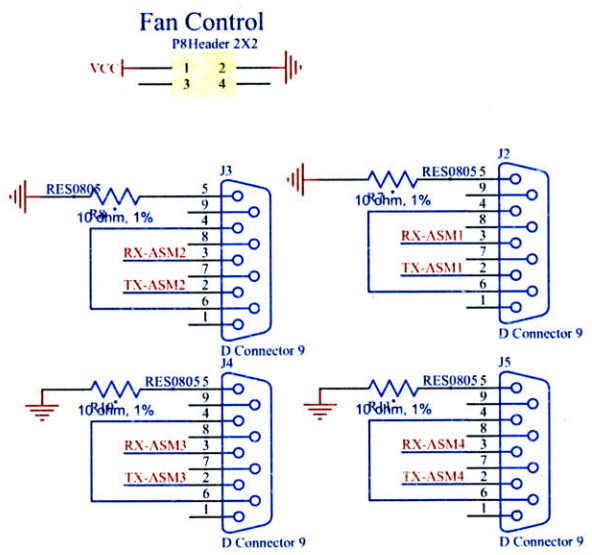
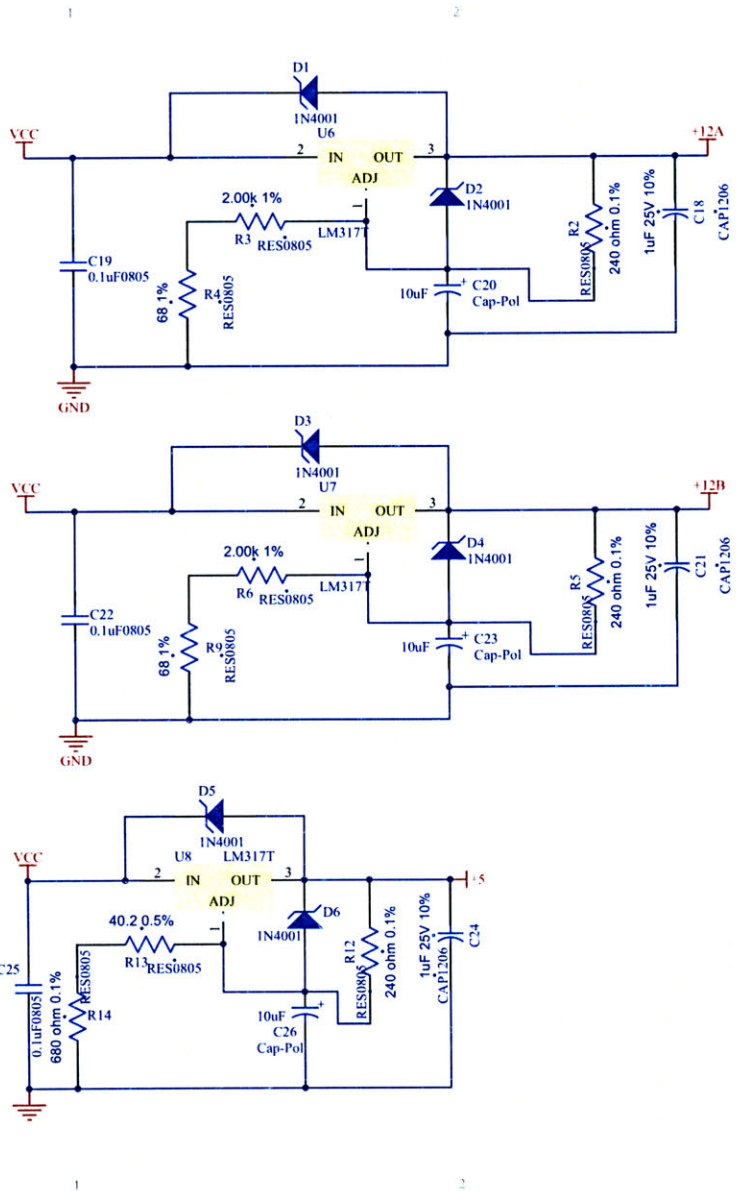


Wires from Spindle and To Cages/Cameras



Title	Number	Revision
Size		
Date:	7/17/2008	Sheet of
File:	C:\Documents and Settings\...\Multiplexing08\...	By:

Power Management and Connectors to HCMs



Title	Number	Revision
A	7/17/2008	Sheet of 1
C:\Documents and Settings\...Multiplexing\...Doc\...		

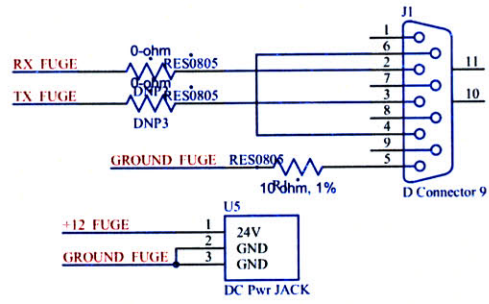
Wires from Spindle



Header 6

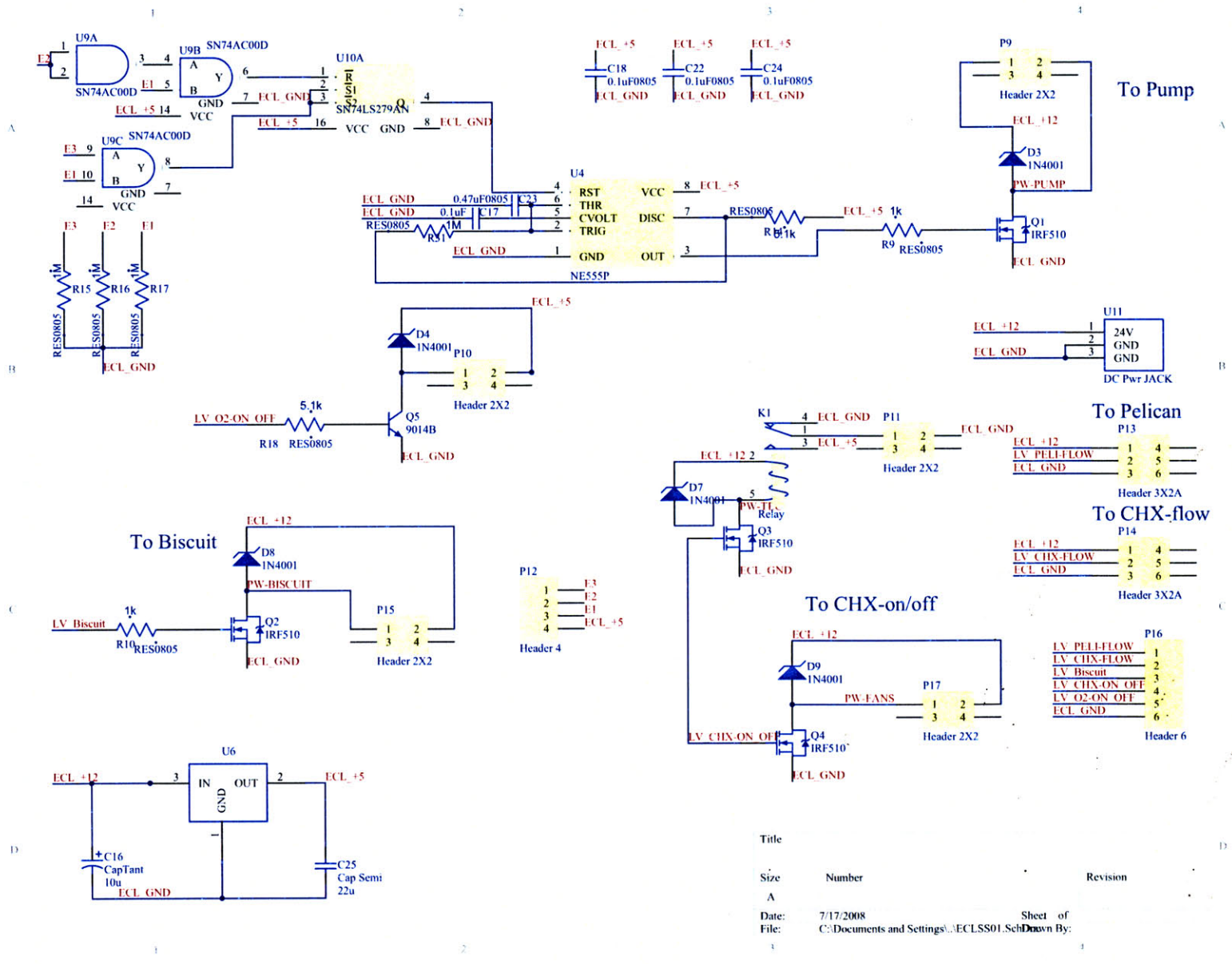


Header 4



Title	Number	Revision
Size		
A		
Date:	7/17/2008	Sheet of
File:	C:\Documents and Settings\...BaseBoard03.Dwg	By:
3		4

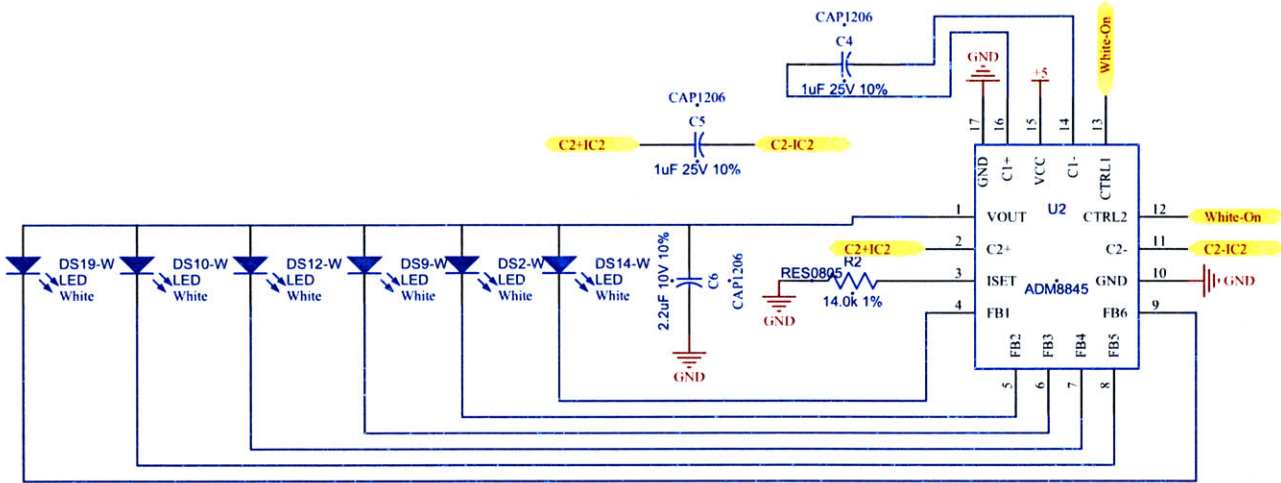
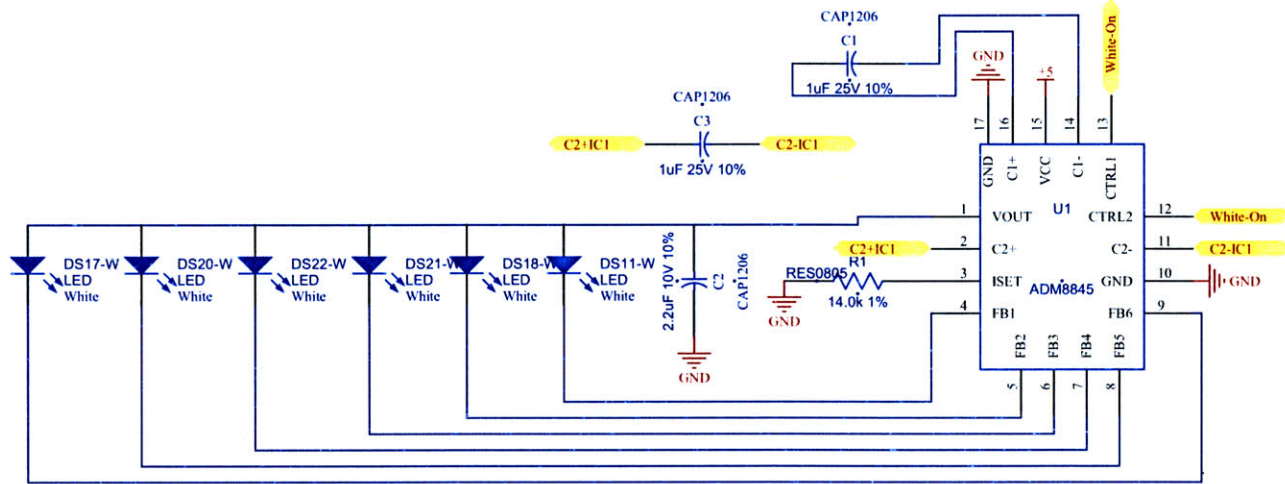
ECLSS BOARD



Title	Size	Number	Revision
	A		
Date:	7/17/2008		Sheet of
File:	C:\Documents and Settings\...ECLSS01.Sch	Down	By:

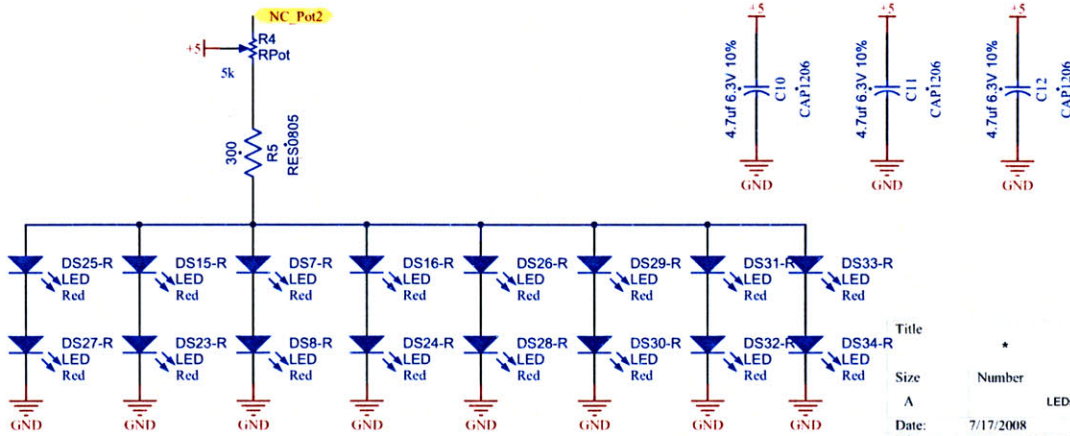
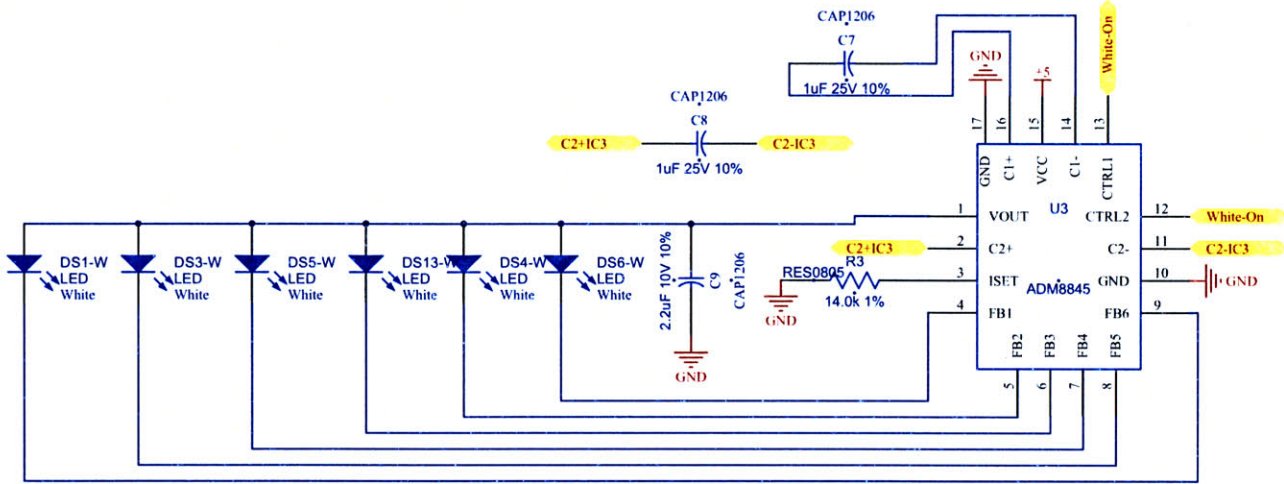
LIGHTING/VIDEO

White LEDs and Driver Circuitry



Title	Number	Revision
A	LEDBoard04.SchDoc	
Date:	7/17/2008	Sheet * of *
File:	C:\Documents and Settings\...LEDBoard04.SchDoc	Drawn by:

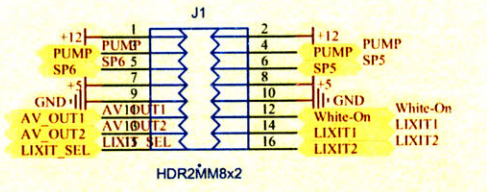
Remaining White LEDs and All Red LEDs



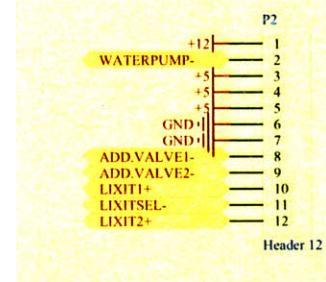
Title	Number	Revision
LEDs04.SchDoc	*	
Size	A	
Date:	7/17/2008	Sheet of
File:	C:\Documents and Settings\...LEDs04.SchDoc	Drawn By:

Connections to HCM and to Water Delivery Hardware

Connection to HCM

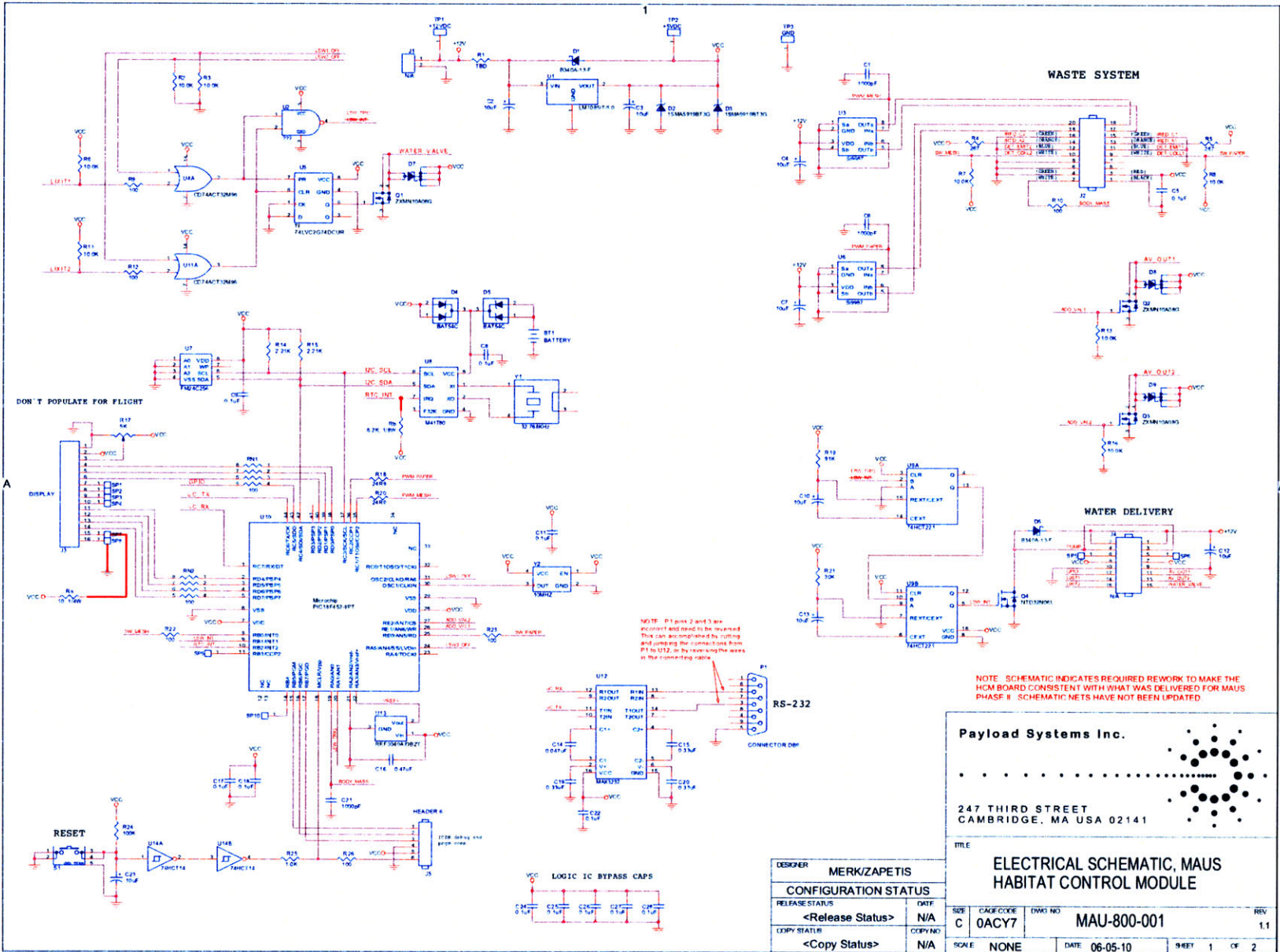


Connection to Water System



Title	Number	Revision
A		
Date:	7/17/2008	Sheet of
File:	C:\Documents and Settings\NewCxr04	Drawn By:

HABITAT CONTROL MODULE Microcontroller and Peripherals



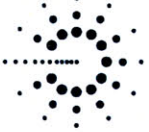
DESIGNER	MERK/ZAPETIS
RELEASE STATUS	<Release Status>
COPY STATUS	<Copy Status>

DATE	06-05-10
SCALE	NONE
DATE	06-05-10
SHEET	1
CF	2

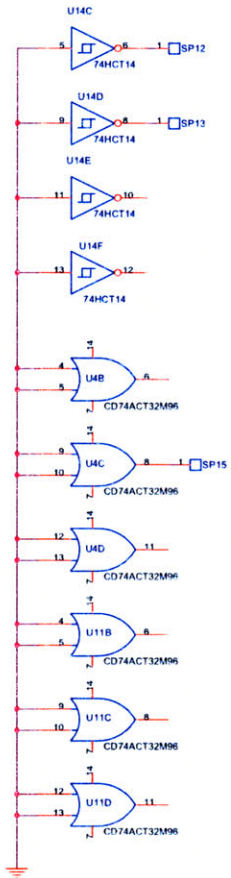
Payload Systems Inc.

247 THIRD STREET
CAMBRIDGE, MA USA 02141

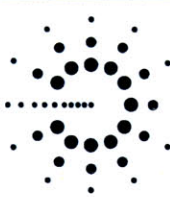
**ELECTRICAL SCHEMATIC, MAUS
HABITAT CONTROL MODULE**



Logic Gates



DESIGNER	MERK/ZAPETIS
CONFIGURATION STATUS	
RELEASE STATUS	DATE
<Release Status>	N/A
COPY STATUS	COPY NO
<Copy Status>	N/A

Payload Systems Inc. 	
247 THIRD STREET CAMBRIDGE, MA USA 02141	
TITLE	
ELECTRICAL SCHEMATIC, MAUS HABITAT CONTROL MODULE	
SIZE	REV
B	1.1
CAGE CODE	DWG NO
0ACY7	MAU-800-001
SCALE	DATE
NONE	06-05-10
SHEET	OF
2	2

Appendix I: CAC Protocols

ANNUAL PROTOCOL RENEWAL JANUARY 2007

For CAC use only

Date received:	Date approved:	
----------------	----------------	--

Last revision date:

8/16/06

CAC Annual Renewal Application for the Use of Animals at MIT/WIBR/Broad Institute

This form is required at the end of the first and second years of an ongoing study. Only the current version of this form will be accepted; it can be downloaded from the CAC website: <https://web.mit.edu/comp-med/Restrict/CAC/forms.htm> (MIT certificates required. WIBR personnel may submit their name, email address, and birthday (mm/dd) to Bruce Brown (bbrown@mit.edu) to request a guest certificate). Animal orders will be held on protocols that are overdue for renewal.

Instructions

1. Complete this form using Word.
2. Do **not** substitute reprints or attach copies of other printed materials in lieu of explanation in each section.
3. Answer all questions or indicate "N/A" where not applicable. Review your original protocol or the last annual renewal, as well as any addenda and CAC correspondence, to be accurate in describing every change. **This annual renewal form must summarise all addenda since the last three-year application and also include any other changes you wish to introduce.**
4. Use supplemental forms (see Section 10) to add appropriate details for specific procedures that have not already been approved under this protocol.
5. Refer to the DCM *Laboratory Animal Users' Handbook* for information on general procedures, drug doses, acceptable methods of euthanasia, etc. This handbook is on the CAC website under "CAC Policies & Resources" and is available in hardcopy from the DCM and CAC offices.
6. When completed, submit a **single-sided** copy of this form to the CAC office (Room 16-408; Fax: 617.258.8257).

Section General Information	1 Principal Investigator: Colonel John E Keesee, jkeese@mit.edu	Department: Aero/Astro
-----------------------------	--	---

(MUST BE CONTACT PERSON (for all protocol-related communications):

COMPLETELY FILLED OUT AS PART OF ANNUAL RENEWAL) Editor Editor and Erika B. Wagner

E-mail address: Fulford-Jones: fulford@mit.edu Wagner: Erika@mit.edu, Keesee: jkeese@mit.edu	MIT mailing address: Building 37 Rm 219
---	---

Office phone: x4-0529	Lab phone: x4-6793	Fax: X8-8111
------------------------------	------------------------------	-----------------

Title of protocol: Mars Gravity Biosatellite Animal Module Development

Current protocol number: **0205-013-08**

Will any aspect of the experimental study, teaching course, or animal husbandry be conducted at another institution?

No

Attach the most recent IACUC approval notification from the second institution.

Section 2 Funding Information	Funding agency	Grant number (or 7-digit MIT Cost Object)	Date grant submitted	Date grant begins	Date grant ends
(FIRST TWO COLUMNS OF TABLE MUST BE FILLED OUT. COMPLETE REMAINDER OF THIS SECTION ONLY IF CHANGES IN FUNDING OR PEER REVIEW. IF NO CHANGES, PI TO INITIAL)	1 NASA SBIR Phase II Grant, Codename "MAUS"	6897356	mid-2004	Jan 05	Mar 07
	2 Mars Gravity Biosatellite Program Office	2734815	N/A	N/A	N/A

If the funding agency requires the MIT Office of Sponsored Programs to verify CAC approval, indicate **name** and **mailing address** of contact person at granting agency: **Ms Kimberly K. Hines, NASA Ames Research Center, MS240A-3, Bldg N240A, Rm 144, Moffett Field, CA 94035**

Does the information in this form agree with the animal use section of the grant application(s)?
Yes

Has this research been subject to peer review (*peer review must be updated every three years*)?

Yes, NASA Ames MAUS CDR, 2006

Section 3
Specific Aims Justifying Animal Use and Updating CAC Progress Since Last Renewal

Enumerate (1, 2, 3...) the specific aims of your research. Concisely explain scientific merit (i.e., why the experiments are important) and justify your choice of animal model. This form is reviewed by both lay readers and scientists--please use language that will be understood by a non-scientific reader.

The Mars Gravity Biosatellite team is developing an autonomous rodent life support system for an Earth-orbiting biosatellite scheduled for launch before 2010. Work projected for 2007 includes the following ongoing developmental items:

1. Final design refinements to our custom integrated caging system which includes autonomous food delivery, a volumetric water monitor, video capability, a body mass

**(MUST BE
COMPLETELY
FILLED
OUT AS
PART OF
ANNUAL
RENEWAL)**

- sensor, automated waste collection and preservation, together with sensors to monitor a wide range of environmental parameters.
2. The construction of centrifuge-mounted ground control units which will rotate at approximately 30rpm
 3. The installation of the centrifuge within an airtight vessel, in order to develop and test closed-loop atmospheric reconditioning systems
 4. Continued consumption tests for the use of fluorescent bone labels to monitor bone growth over the course of the mission
 5. Work on urine preservation and analysis which will yield insights into bone density, muscle atrophy, and other changes during the mission

Our life support system will operate longer than any previous NASA system, will do so without astronaut operation or surrounding environmental control systems, and will meet additional design requirements related to the existence of artificial gravity on board the spacecraft. Due to the novel design parameters of our life support system, no prior research can provide these answers.

Some animals will be rotated on a centrifuge at a rate identical to that which is planned for our biosatellite. This rate has been previously shown by our research group to have no adverse effects on animal health and well-being. Animals under rotation will live in a sealed system and will be regularly viewed by researchers via a video feed. The centrifuge may be stopped if this is necessary to ensure animal well-being.

The animal model chosen for our experiments was determined based on scientific requirements for the experiments that will eventually fly on our spacecraft. These considerations led to the selection of the BALB/cByJ strain from the Jackson Laboratory, based on (a) relatively strong history in the gravitational physiology research community and (b) readily observable skeletal responses to unloading. As we wish to evaluate our life support system specifically with our future experimental animal model, no further considerations were deemed necessary.

No medical procedures will be performed on animals in association with this protocol. Interactions between animals and consumable distribution / waste removal / atmospheric processing / video systems / other sensors will be monitored daily. Any indication of deteriorating health will lead to the reinstatement of afflicted animals within standard laboratory housing, and modification of the experimental hardware based on collected observations.

For each Specific Aim (identified by number above), briefly summarise your progress since the last renewal. Include successful and failed outcomes. For invasive procedures (tumors, surgery, implants, food or water restriction, hazardous materials, etc.) provide a summary of the morbidity encountered, how it was managed and what your plans are for refinement of the model to avoid morbidity.

During 2006, significant progress was made toward a robust final design of the animal support module. Specifically, all-new cage modules were fabricated and underwent extensive rodent testing for periods of up to 6 weeks. Body mass sensing equipment was developed and areas for improvement were identified. Next-generation automated waste collection was demonstrated. Techniques for waste analysis were expanded and enhanced. Software for control of sensor systems was developed. Operational results led to refinement of the electronics and mechanical hardware. None of the procedures used under this protocol are invasive.

Section 4
Search for Alternatives

Investigators are required to annually document their consideration of alternative animal models and methods.

A well-designed literature search strategy should justify:

(MUST BE COMPLETED AS PART OF ANNUAL RENEWAL)

- Choice of animal model: Have non-animal, *in vitro*, or "lower species" models been considered?
- Choice of methods: Ensure you are using procedures that minimise potential pain, discomfort, distress, or morbidity, given the limitations imposed by the objectives of the project. Examples of procedures with the potential to cause pain and distress include, but are not limited to: surgery, water restriction, food restriction, prolonged physical restraint for imaging or behavioral studies, adjuvants, tumor induction, infectious diseases, irradiation, use of paralytics under anesthesia, decapitation without anesthesia, cervical dislocation without anesthesia, neonatal anesthesia using hypothermia, and toxic substance administration. CAC-approved euthanasia methods (see Lab Animal Users' Handbook) and routine handling and injections (other than adjuvants) are not considered to cause pain or distress.

Keywords used in the search for alternatives should be selected based on their potential to identify published work that is similar to that proposed and the availability or lack of alternative models and methods. Keywords should include the species, genetic modifications (transgenic and knockout mice), procedures likely to cause pain and distress (see above for examples) and methods that will minimise pain and distress (drug choices for anesthesia and analgesia, refinements to invasive procedures, use of humane endpoints for euthanasia such as body condition scoring).

The Animal Welfare Information Center of the National Agricultural Library offers assistance and database search services for alternative models and methods (<http://www.nal.usda.gov/awic>).

Name of database(s) searched: PubMed

Date of search (month/day/year): 03 Jan 07

Years covered by search:
1965-2007

Keywords used: "mouse AND bone AND unloading"

"mouse AND gravity"

"mouse AND hindlimb AND suspension"

"mouse AND caging"

"mouse AND urine collection"

"rodent AND centrifuge"

Conclusions from search for alternatives:

Justify the choice of animal model (including any genetic modifications) as the best model available to address the scientific hypothesis. Explain why a lower species (phylogenetically) or non-animal system would not be suitable.

The animal model chosen for our experiments was determined based on scientific requirements for the experiments that will eventually fly on our spacecraft. These considerations led to the selection of the BALB/cByJ strain from the Jackson Laboratory, based on (a) relatively strong history in the gravitational physiology research community and (b) readily observable skeletal responses to unloading. As we wish to evaluate our life support system specifically with our future experimental animal model, no further considerations were deemed necessary.

Explain how use of the proposed animal model will add to work previously reported, particularly if aspects of the study will duplicate previous work by your lab or others.

To our knowledge, no previous work outside our group has been done with this animal in the field of autonomous life support development. However, as described above, our choice of animal model is based on other considerations.

Justify the choice of methods that will minimise potential for pain or distress (examples include surgical approach, choice of anesthetic or analgesic, choice of adjuvant, choice of reward paradigm in behavioral assessments). **Include drug names, doses, and dosing schedule.** (Note: First dose of analgesic should always be before cessation of anesthesia. If drugs cannot be used for scientific reasons, explain the rationale.

No medical procedures will be performed on animals in association with this protocol. Interactions between animals and consumable distribution / waste removal / atmospheric processing / video systems / centrifuge apparatus / other sensors will be monitored daily. Any indication of deteriorating health will lead to the reinstatement of afflicted animals within standard laboratory housing, and modification of the experimental hardware based on collected observations.

Section 5
Rationale for
Species and
Numbers

Animal species, strains, or stocks to be used in the coming year
Estimate required number of **each** species/strain/stock for the **next year** of the project:

	Species/Strain/Stock	Purchase	Breed In-house	Expected Total
(MUST BE COMPLETED Y FILLED OUT AS PART OF ANNUAL RENEWAL)	1 BALB/cByJ	20	Nil	20
	2			
	3			

Provide scientific justification for the number of animals requested, as well as study group sizes. Include a description of statistical analyses used to estimate the number of animals needed (Attention NHP users: Please indicate the current size of your colony, specifying how many animals are in active use and your plans for any inactive animals):

Study groups will consist of four to five animals each, to permit meaningful comparisons with our previous work and to ensure statistical significance. Each animal will be housed in a separate custom specimen chamber as planned for the eventual spacecraft animal module.

How many animals of each species have been used since the last protocol review?

10

Section 6
General Procedures
(Refer to DCM Lab Animal Handbook for guidelines on common procedures)

Summarise sequentially all animal procedures. Describe the techniques used, time intervals between procedures, endpoint of experimental use, and the final disposition of each species. Special husbandry requirements (e.g., diet, housing) and equipment to be used should be included. Specific information is required as to route, dose, and potential morbidity of all chemical, microbial and physical agent administrations. Detailed methods must also be provided on a supplemental form (Section 10) when applicable. If some aspects of your experiments are conducted at other institutions, indicate which procedures using animals occur off-site. **List any addenda approved since last renewal.**

(COMPLETE ONLY IF CHANGES/ADDITIONS IN PROCEDURES. IF NO CHANGES, PI TO INITIAL) *No procedures will be performed on the animals. Our study is primarily behavioral and is designed to generate data that will allow us to further develop and refine animal support systems for the Mars Gravity Biosatellite.*

The following are changes/additions to previous protocol submissions:

1. Most rodents in our study will be fed NASA Rodent Food Bar New

Formulation TD97071; our previous experiments showed that these bars could be used in our custom-designed cages for periods of up to 6 weeks with no detectable mold or fungal growth.

2. ClearH2O 98% pure water substrate (details at www.clearh2o.com) will be used instead of Napa Nectar for short-term rodent hydration lasting less than 10 days.
3. Our custom-designed cage hardware will be attached to a multi-arm centrifuge which will spin the rodents at a rate of approximately 32 rpm. Such chronic centrifugation was previously shown by our research to cause no mouse health problems; however the centrifuge was stopped and restarted on a daily basis in order to assess each animal. In 2007, we anticipate conducting extended duration five-week tests in which the centrifuge will not be stopped unless there is evidence that human intervention is required to ensure animal health.
4. The centrifuge will be enclosed within a sealed environmental chamber which replenishes the atmosphere and recirculates/reconditions the air as necessary to support the rodents.

Which of these procedures have not been performed in this laboratory before? How will personnel be trained in new techniques?

No procedures will be performed on the animals.

If **prolonged restraint** is needed, describe method, frequency and duration of restraint; and how animals will be monitored:

N/A

Is there a potential for the **development of morbidity** (procedures as surgery, ascites production, tumor induction, transgenic experiments, injections of adjuvant, prolonged restraint, water restriction, etc., all have inherent risk of medical problems)?

Not that we are aware of.

Provide specific agents, doses, and route of administration for **euthanasia** of each species:

Carbon dioxide suffocation, administered manually by a trained researcher.

If requesting either cervical dislocation or decapitation without anesthesia as a method of euthanasia, provide scientific justification:

>

Animal identification techniques:

Method used: None

Age of animal at time of procedure:

Type of anesthesia, if indicated:

**Note: Toe-clipping of rodents requires scientific justification; if used, provide rationale that other methods of identification are not adequate. Toe clipping can only be done between 10-15 days of age; anesthesia is not required. As a more humane alternative, toe-tattooing provides permanent ID without amputation; DCM vet staff can provide instruction.*

Will any animal manipulations take place outside of DCM animal facilities?

No

If **yes**, where will they occur (building and room number(s))?

>

If **yes**, what types of procedures will be performed (e.g., behavioral studies, euthanasia, necropsy with tissue collection, terminal surgery, survival surgery, etc.)?

>

Section 7
Hazardous Materials
In Animals

List hazardous agents to be used in animals. All use of hazardous materials must be described in detail on Supplement I, "Use of Hazardous Materials in Animals" (see Section 10). Be sure to indicate in the Personnel Table (Section 8) which personnel will be handling each of these hazards.

**(COMPLETE ONLY IF
CHANGES/ADDITIONS
IN
AGENTS. IF
CHANGES, PI
INITIAL)**

**HAZARDOUS No changes since last protocol; no hazardous agents are to be used in
IF NO animals
PI TO**

Radioactive:	None
Chemical*:	None
Biological**:	None

* *Chemicals are considered hazardous if the MSDS or other sources indicate there is a human health hazard during dosing, husbandry, or necropsy of animals. Novel compounds without established hazard information are considered on a case-by-case basis.*

***Biological hazardous agents include potentially infectious agents, primary human cells or established human cell lines, and recombinant RNA or DNA, including gene transfer vectors.*

Note that use of hazardous agents may not begin until all of the following have occurred (in listed order):

- 1) The CAC has approved this protocol application;
- 2) A specific "Required Protection/Control" form for each particular hazard involved has been generated by DCM and EHS (MIT or WIBR), and the principal investigator has signed and returned the form(s) to DCM (Lucy Wilhelm, 16-825);
- 3) Study personnel have contacted the DCM Hazards Coordinator (Mary Patterson, mmpatt@mit.edu, X4-5403) for consultation, space allocation, and orientation in the animal facility on the use of each particular hazard in animals.

Section 8
Personnel Qualifications

List all personnel to participate in the study. Any personnel working with animals must be CAC-certified in advance. Information on obtaining CAC certification may be found at https://web.mit.edu/comp-med/Restrict/CAC/training_new.htm.

**(MUST BE COMPLETELY
FILLED OUT AS PART
OF ANNUAL RENEWAL)**

Contact the DCM veterinary staff if training is needed for specific animal procedures. It is the principal investigator's responsibility to affirm that all participants understand DCM and CAC policies (see DCM *Lab Animal User's Handbook* and policy section on CAC website) and are adequately trained.

All new protocol participants performing survival surgery (or others desiring additional training) must contact either Kris Hewes (mice only - khewes@mit.edu/X3-9439) or Dr. Robert Marini (all other species - rmarini@mit.edu/X4-3340) for review of MIT guidelines for survival surgery.

Always list Principal Investigator. Describe protocol responsibilities as supervision if PI has no animal contact.

Name:	Year of CAC-certification	Survival surgery ("Y" if YES)	Hazardous materials to be used in animals (Identify the "hazmats")	Protocol responsibilities ("All" or keywords if limited participation)	Summarise prior experience and training beyond CAC-certification
PI (required): John E. Keesee	None	N/A	N/A	General oversight	None
Editor Editor	Approx. 2002/2003	N/A	N/A	Habitat and life support lead	Yes
Erika B. Wagner	2002	N/A	N/A	Manager/trainer /supervisor	Additional CAC training in retro-orbital and pericardial bleeding, CO2 euthanasia, isoflurane anesthesia
Wen Hui Tan	2006	N/A	N/A	Urine collection and basic animal care	Blood-draws, surgery, isoflurane, CO2 euthanasia
Jacob McGrane	2007	N/A	N/A	Urine collection and basic animal care	CO2 euthanasia

Section 9
Occupational Health

All personnel on this protocol with ANY animal contact must have an Animal Handler's Baseline Occupational Health Questionnaire (OHQ) evaluated by an EHS physician or nurse.

(MUST BE COMPLETELY FILLED OUT AS PART OF ANNUAL RENEWAL)

Questionnaires are available at the CAC website: <https://web.mit.edu/comp-med/Restrict/CAC/forms.htm>

(Form #17) and may be submitted:

- 1) Electronically;
- 2) Manually (send directly to MIT Medical Employee and Occupational Health Office (EOHS, E23-180));
- 3) In person: Schedule an appointment with the EOHS (Jackie Sherry, X3-8552, E23-180).

Has everyone listed on this protocol submitted an OHQ?

NO; John E. Keesee has not submitted an OHQ

Are there any occupational health issues that have developed for any protocol participant since a questionnaire was first submitted?

No

For users of materials/substances potentially hazardous to human health, have new personnel been educated about health risks?

Yes

Note that information about safety and health measures (e.g., immunisations, protection against explosion and fire) is available through DCM, EHS, and the MIT Medical Department.

Verification of compliance with DCM requirements for use of appropriate personnel protection equipment (PPE) in the animal facilities: shoe covers, head covers, and lab coats; gloves (when handling animals); masks and face protection (for contact with nonhuman primates):

Initials of principal investigator to verify lab compliance _____ (required for use of any species)

For personnel working with nonhuman primates, list each name with the date of the most recent tuberculosis screen by MIT Medical (must be current within one year). Protocol approval and renewal are contingent on strict compliance by all participants; "pending" is not satisfactory.

> Not applicable

Investigators working with nonhuman primates (including tissue harvest) are advised to obtain exposure control training from EHS at X2-3477.

Section 10
List of
Supplemental
Forms

Supplements must be filled out for the following procedures. **Check all that apply. Examine the CAC website (<https://web.mit.edu/comp-med/Restrict/CAC/forms.htm>) to make sure you are using the most current version of a supplemental form. Supplemental forms should also be used to describe new procedures in support of an addendum to an existing protocol.**

(COMPLETE ONLY IF CHANGES/ADDITIONS IN PROCEDURES. IF NO CHANGES, PI TO INITIAL)

- A. Surgical Procedures
- B. Polyclonal and Monoclonal Antibody Production
- C. Chemical, Microbial, Physical Agent Administration
- D. Use of Human or Rodent Cells or Tissue in Animals
- E. Device Implantation
- F. Transgenic/Knock-out Animals
- G. Behavioral Training Techniques
- H. Teaching Proposal
- I. Use of Hazardous Materials in Animals
- J. Food or Water Restriction Unrelated to Behavioral Motivation
- K. Tumor Induction

Section 11
PI Signature

Principal Investigator

Date

The CAC meets on the first Thursday of every month except August and December.

Submissions received at least two weeks in advance of a CAC meeting will be reviewed at the upcoming meeting; submissions received less than two weeks in advance may be delayed to the following meeting cycle. If expedited review is required, please provide a cover letter justifying the necessity.

Note that a substantial change in protocol, an increase in the number of animals used, a change in the animal species used, or addition of personnel necessitates an addendum to this form. The principal investigator must sign the addendum before it will be reviewed by the committee.

THREE-YEAR PROTOCOL RENEWAL JANUARY 2008

<i>For CAC use only</i>	Date received:	Date approved:	Previous protocol number:
-------------------------	----------------	----------------	---------------------------

Version:
11/07

CAC New/Three-Year Protocol Application for the Use of Animals at MIT/WIBR/Broad Institute

This form is required for all new studies and must be completely updated and resubmitted every three years for ongoing studies. In addition, annual renewals are required using the form entitled "CAC Annual Renewal Application for the Use of Animals at MIT/WIBR/Broad Institute." Only current versions of these forms will be accepted; they may be downloaded from the CAC website: <https://web.mit.edu/comp-med/Restrict/CAC/forms.htm> (MIT certificates required. WIBR personnel may contact their IT Department to request a guest certificate). Animal orders will be held on protocols that are overdue for renewal.

INSTRUCTION S

1. Complete this form using Word.
2. Do **not** substitute reprints or attach copies of other printed materials in lieu of explanation in each section.
3. Answer all questions or indicate "N/A" where not applicable. If this is a three-year renewal, review your original protocol or the last annual renewal, as well as any addenda and CAC correspondence, to be accurate in describing every procedure. **The contents of this document will replace all previously approved procedures under prior versions of this protocol.**
4. Add appropriate details for specific procedures using supplemental forms (Section 10).
5. Refer to the DCM *Laboratory Animal User's Handbook* for information on general procedures, drug doses, acceptable methods of euthanasia, etc. This handbook is on the CAC website and is available in hardcopy from the DCM and CAC offices.
6. When completed, submit a **single-sided, black-ink** copy of this form to the CAC office (Room 16-408; Fax: 617.258.8257).
7. **If all animal work will be taking place at a collaborator's academic institution**, you may submit the following in lieu of this application form:
 - 1) A cover letter that includes the information requested in Sections 1, 2, and 3 of this application and a statement explaining your lab's involvement in the research;
 - 2) A copy of the protocol that was submitted to the other institution's Institutional Animal Care and Use Committee (IACUC);
 - 3) A copy of the most recent IACUC approval notification from the second institution.

Section General Information	¹ Principal Investigator: Col John E. Keesee E-mail address: jkeese@mit.edu	Department (to which CAC should send copy of approval letter): Aeronautics & Astronautics
-----------------------------	--	--

Contact Person (for all protocol-related communications):
Thaddeus R F Fulford-Jones, Lead Payload Engineer for the Mars Gravity Biosatellite Program

E-mail address: fulford@mit.edu		Campus mailing address (Bldg-Room): 37-219
Office phone: 4-0529	Lab phone: 2-3309	Fax: 8-8881

(100-Character Maximum)

Title of protocol:
Mars Gravity Biosatellite Animal Module Development

Current protocol number (if 3-year renewal):

0205-013-08

Will any aspect of animal husbandry, experimentation, or instruction be conducted off-campus?

No

Attach a copy of the most recent IACUC approval notification from the off-campus institution (not necessary for contract facilities).

Section 2
Funding Information

All funding sources for this research must be listed.

Funding agency	Grant number (or 7-digit MIT Cost Object)	Date grant submitted	Date grant begins	Date grant ends
Internal Funds	2734815	N/A	N/A	N/A

The CAC will notify the MIT/WIBR Office of Sponsored Programs (OSP) of protocol approval. If an external funding agency requires the MIT/WIBR Office of Sponsored Programs to contact them to verify CAC approval, indicate **name** and **mailing address** of contact person at funding agency; notification will not be sent if complete details are not provided:

> **N/A**

Does the information in this form agree with the animal use section of the grant application(s)?

N/A (Internal funds only)

Has this research been subject to peer review (*peer review must be updated at each three-year renewal*)?

Yes (Identify source of peer review if not by external funding agency listed above): **Mark Whary, and by scientists at the National Space Biomedical Research Institute to which we have applied for further funding support.**

Section 3
Specific Aims Justifying Animal Use and Updating CAC on Progress Since Last Renewal

Please use language that will be understood by a non-scientific reader; this form is reviewed by both lay readers and scientists.

Enumerate (1, 2, 3...) the specific aims of your research. Concisely explain scientific merit (i.e., why the experiments are important) and justify your choice of animal model.

The Mars Gravity Biosatellite team is developing an autonomous rodent life support system for an Earth-orbiting biosatellite scheduled for launch before 2015. Work projected for 2008 includes the following ongoing developmental items:

- Continued refinement of autonomous closed-loop environmental control systems for atmospheric reconditioning.
- The use of existing centrifugation apparatus (constructed in 2007) spinning at approximately 30rpm to generate video data for analysis of behavioral adaptation to chronic centrifugation.

3. Exploration of the impacts of chronic centrifugation through the use of various behavioral tests, including Roto-Rod, balance beam, open field testing.
4. Continued consumption tests for the use of fluorescent bone labels to monitor bone growth over the course of the mission.
5. Work on urine preservation and analysis which will yield insights into bone density, muscle atrophy, and other changes during the mission.

Animals will be rotated for five weeks on a centrifuge at a rate identical to that which is planned for our biosatellite. Animals under rotation will live in previously-approved flight-ready prototype habitat modules with *ad libitum* access to food and water. A video feed will be available on demand via computer for the purpose of conducting animal status and health checks. The centrifuge may be stopped if this is necessary to ensure animal well-being.

The animal model chosen for our experiments was determined based on scientific requirements for the experiments that will eventually fly on our spacecraft. These considerations led to the selection of the BALB/cByJ strain from the Jackson Laboratory, based on (a) relatively strong history in the gravitational physiology research community and (b) readily observable skeletal responses to unloading. As we wish to evaluate our the impacts of chronic rotation with our specific experimental animal model, no further considerations were deemed necessary.

No medical procedures will be performed on animals in association with this protocol. Interactions between animals and consumable distribution / waste removal / atmospheric processing / video systems / other sensors will be monitored daily. Any indication of deteriorating health will lead to the reinstatement of afflicted animals within standard laboratory housing, and modification of the experimental hardware based on collected observations.

If this is a renewal, briefly summarise your progress for each Specific Aim (identified by number above) since the last renewal. Include successful and failed outcomes. For invasive procedures (tumors, surgery, implants, food or water restriction, hazardous materials, etc.) provide a summary of the morbidity encountered, how it was managed, and what your plans are for refinement of the model to avoid morbidity.

Section 4
General
Procedures
(Refer to
DCM Lab
Animal Users'
Handbook for
guidelines on
common
procedures)

Summarise sequentially all animal procedures. Describe the techniques used, time intervals between procedures, endpoint of experimental use, and the final disposition of each species. If an individual animal will undergo multiple procedures, details must be specified. Special husbandry requirements (e.g., diet, housing) and equipment to be used should be included. Specific information is required as to route, dose, and potential morbidity of all chemical, microbial and physical agent administrations. Detailed methods must also be provided on a supplemental form (see Section 10) when applicable. If some aspects of your experiments are conducted at other institutions, indicate here and in **Section 1** which procedures using animals occur off-site. **The contents of this document will replace all previously approved procedures under prior versions of this protocol; be thorough.**

>

Video Open field Testing for a period of up to 30 minutes, approximately once every 2 weeks.

At least 24 hours prior to commencement of test, each open field enclosure will be sprayed down with Quatricide. Once the enclosure is dry, a sheet of black wrapping paper will be used to line the bottom and will be secured in place with double-sided adhesive tape. After each test the paper will be discarded to remove any fecal boli and urine, together with any odors that might impact the subsequent test specimen. Each open field enclosure will be of floor dimension 40cm by 40cm. A video camera will be mounted on a tripod directly overhead. The video camera will be connected to Ethovision XT and will have a field of view sufficient to monitor all four enclosures simultaneously. The open field test episode will be of duration 5 minutes and will commence once all 4 animals have been placed by the experimenter in the center of each enclosure. According to Crawley (2007), "a 5-minute test session in a novel open field provides a measure of exploratory locomotion in a novel environment." She notes that this is substantially shorter than the time required to habituate to the novelty (generally 30 minutes to 2 hours).

Rota-Rod testing, up to three consecutive trials, approximately every 2 weeks.

Rota-Rod testing will be conducted in accordance with guidelines published in "Methods of Behavior Analysis in Neuroscience" (ed. Buccafusco, 2000) and in "What's Wrong with my mouse" (Crawley, 2007). Four animals will be tested simultaneously using a ramp-up from 4rpm to 40rpm over 5 minutes. The mean of 3 trials will be taken from each animal. An experimenter will be present with a stopwatch as a backup in case a falling mouse should fail to trigger a photocell upon falling. The experimenter will also observe any cases of mouse non-compliance (such as clinging and rotating with the rod). If a mouse is observed to exhibit "riding around" behavior, it will be taken off and the session will be restarted for that animal. Similarly, if a mouse falls off the Rota-Rod immediately it will be given a second chance. Crawley shows data that suggests mice improve performance (i.e. learn the Rota-Rod task) when given three consecutive 5-minute sessions with acceleration from 4rpm to 40rpm. Accordingly, to pretrain the animals and ensure full acclimation to the Rota-Rod I propose performing 6 Rota-Rod repetitions per day (3 consecutive morning tests, 3 consecutive afternoon tests) on two consecutive days prior to commencement of test. With 4 data points per animal, time-to-fall should begin to normalise to a repeatable standard. If individual normalisation has not occurred over this period, a third day (i.e. a further 6 Rota-Rod repetitions) may be added.

Beam balance/walking approximately every 2 weeks.

Following guidelines published in Crawley, a beam approximately 6mm wide and 80cm in length will be suspended about 50cm above a foam pad. Animals will instinctively walk along the beam to reach the opposite end, at which will be positioned a darkened cardboard box (retreat). The beam will be covered with 240-grade sandpaper for improved rodent paw grip. The number of footfaults, defined as the number of times the forepaws and/or hindpaws slip from the horizontal surface of the beam per 50 steps, will be recorded. To do this, a video camera will be used together with a mirror which is positioned on the side of the beam opposite the video camera. The animal is permitted sufficient time (approximately 5 minutes) to perform this task. To pretrain the animals and ensure full acclimation to the balance beam, it will be necessary to perform a balance beam exercise on two consecutive days prior to commencement of test. Following recommendations in Buccafusco, the animals will be given at least 24 hours to recover between these two tests.

Air-righting, up to three consecutive trials, approximately every 2 weeks.

Following procedures previously used by the Mars Gravity lab, each animal will be supinely inverted and held by the scruff of its neck from a height of approximately 50 cm onto a foam pad. A high-speed video camera will be used to record the specimen's behavior while falling. The experimenter will record the amount of time taken for the rodent to orientate itself in an upright position such that it is ready to land on its paws, and successful paws-down landings. This will be repeated three times.

Dosing of tetracycline or calcein via automated water delivery system, approximately once every 20 days

Tetracycline or calcein will be administered in suspension via the automated Mars Gravity water delivery system. Each dose will be given over a period of approximately 24 hours in accordance with the below table:

Cage/mouse #	Fluorescent label	Concentration (mg/ml)
1	Tetracycline	0.25
2	Tetracycline	1
3	Calcein	0.125

These concentrations are based on published literature for treating mice orally with tetracycline as an antibiotic (Burgmann and Percy, 1993) as well as data found for doses of Tetracycline and Calcein necessary to label bones with a fluorescent marker (T. C. Lee, et al. 2002).

Procedures:

1. Most rodents in our study will be housed in the custom spaceflight-ready habitat modules previously developed under a NASA Phase II grant with Aurora Flight Sciences (formerly Payload Systems Incorporated) in collaboration with Ames Research Center. These automated modules provide autonomous lighting, video and data acquisition capabilities.
2. Most rodents in our study will be fed NASA Rodent Food Bar New Formulation TD97071; our previous experiments showed that these bars could be used in our custom-designed cages for periods of up to 6 weeks with no detectable mold or fungal growth.
3. ClearH2O 98% pure water substrate (details at www.clearh2o.com) may be used instead of Napa Nectar for short-term rodent hydration lasting less than 10 days. The Mars Gravity Biosatellite may remain in the launch vehicle awaiting liftoff for up to 7 days. During this period, habitat modules will be on their ends and rodents will not have access to the water via the standard pump-activated nozzles. To provide adequate hydration during this time, ClearH2O supplement will be used. We wish to simulate the launch orientation within Building 68 to ensure that ClearH2O is fully compatible with our habitat modules and has no adverse impacts on the mice.
4. Our custom-designed cage hardware will be attached to a multi-arm centrifuge which will spin the rodents at a rate of approximately 32 rpm. Such chronic centrifugation was previously shown by our lab to cause no mouse health problems; however the centrifuge was stopped and restarted on a daily basis in order to assess each animal. In 2008, we anticipate conducting extended duration five-week tests in which the centrifuge will not be stopped unless there is evidence that human intervention is required to ensure animal health.
5. For certain tests, the centrifuge may be enclosed within a sealed environmental chamber which replenishes the atmosphere and recirculates/reconditions the air as necessary to support the rodents.
6. Non-rotatory control experiments will be conducted. These will be of duration 5 weeks. Mice will be housed in flight-equivalent habitat modules, mounted on the centrifuge. The centrifuge will not be spinning but food, water and air will be provided in a manner identical to that of the rotating experiments. The same mice are expected to be used for both non-rotating control and chronic-rotating experiment.

Schedule for Testing:

A group of 4 mice will first be used in a 5-week control study to ascertain the baseline behavior. Subsequently, the same group of mice will be chronically rotated for 5 weeks. Continuous 24-hour video observation will be used in both studies, with the exception of any required scheduled maintenance events, and all video will be analyzed with Ethovision XT. The rodents will undergo body massing, Rota-Rod, video air-righting and video open field testing on days 0, 17, 35 and 36 of each test. NB: Day 36 is one day after the animals are removed from the experiment caging system.

Which of these procedures have not been performed in this laboratory before? How will personnel be trained in new techniques?

> All techniques have been previously administered by the Mars Gravity group with the exception of beam balance/walking. This technique will be performed in accordance with the directions stated in "What's Wrong With My Mouse" (Crawley, 2007). Further information on each procedure is provided on the previous page.

If **prolonged restraint** is needed, describe method, frequency and duration of restraint; and how animals will be monitored:

> N/A

Is there a potential for the **development of morbidity** (procedures such as surgery, ascites production, tumor induction, transgenic experiments, injections of adjuvant, prolonged restraint, water restriction, etc., all have inherent risk of medical problems)?

Yes

If **yes**, describe the expected nature of the morbidity, the procedures which may be responsible, the frequency and duration of observations, the criteria for appropriate intervention, and the objective criteria for humane endpoints that will result in euthanasia:

> Video monitoring will be used to check for changes in clinical health. Any evidence of unacceptable health deterioration will prompt stoppage of the experiment and will require rodents to be rehoused in standard laboratory caging.

Provide specific agents, doses, and route of administration for **euthanasia** of each species:

> Carbon Dioxide suffocation.

If requesting either cervical dislocation or decapitation without anesthesia as a method of euthanasia, provide scientific justification:

> N/A

Animal identification techniques:

Method used: Cage cards

Age of animal at time of identification procedure: **N/A**

Type of anesthesia, if indicated: **N/A**

**Note: Toe-clipping of rodents requires scientific justification; if used, provide rationale that other methods of identification are not adequate. Toe clipping can only be done between 10-15 days of age; anesthesia is not required. As a more humane alternative, toe-tattooing provides permanent ID without amputation; DCM vet staff can provide instruction.*

Will live animals be removed from DCM animal holding facilities or brought into the lab from off-campus sources?

No

If **yes**, please enter details of what procedures will be done and where into the table below:

Building and Room Number	Type of procedure (e.g., behavioral studies, perfusion, euthanasia, necropsy with tissue collection, terminal surgery, survival surgery, etc.)

Section 5
Search
Alternatives

Investigators are required to annually document their consideration of alternative animal models and methods.

A well-designed literature search strategy should justify:

- Choice of animal model: Have non-animal, *in vitro*, or "lower species" models been considered?
- Choice of methods: Ensure you are using procedures that minimise potential pain, discomfort, distress, or morbidity, given the limitations imposed by the objectives of the project. Examples of procedures with the potential to cause pain and distress include, but are not limited to: surgery, water restriction, food restriction, prolonged physical restraint for imaging or behavioral studies, adjuvants, tumor induction, infectious diseases, irradiation, use of paralytics under anesthesia, decapitation without anesthesia, cervical dislocation without anesthesia, neonatal anesthesia using hypothermia, and toxic substance administration. CAC-approved euthanasia methods (see Lab Animal Users' Handbook) and routine handling and injections (other than adjuvants) are not considered to cause pain or distress.

Keywords used in the search for alternatives should be selected based on their potential to identify published work that is similar to that proposed and the availability or lack of alternative models and methods. Keywords should include the species, genetic modifications (transgenic and knockout mice), procedures likely to cause pain and distress (see above for examples) and methods that will minimise pain and distress (drug choices for anesthesia and analgesia, refinements to invasive procedures, use of humane endpoints for euthanasia such as body condition scoring).

The Animal Welfare Information Center of the National Agricultural Library offers assistance and database search services for alternative models and methods (<http://www.nal.usda.gov/awic>).

Name of database(s) searched: PubMed and ISI Web of Knowledge

Date of search (month/day/year): 14Jan08	Years covered by search: 1965-2008
---	--

Keywords used:

- "mouse AND bone AND unloading"
- "mouse AND gravity"
- "mouse AND hindlimb AND suspension"
- "mouse AND caging"
- "mouse AND urine collection"
- "rodent AND centrifuge"
- "rodent AND ethovision"

CONCLUSIONS FROM SEARCH FOR ALTERNATIVES

Justify the choice of animal model (including any genetic modifications) as the best model available to address the scientific hypothesis. Explain why a lower species (phylogenetically) or non-animal system would not be suitable.

> The animal model chosen for our experiments was determined based on scientific

requirements for the experiments that will eventually fly on our spacecraft. These considerations led to the selection of the BALB/cByJ strain from the Jackson Laboratory, based on (a) relatively strong history in the gravitational physiology research community and (b) readily observable skeletal responses to unloading. As we wish to evaluate our life support system specifically with our future experimental animal model, no further considerations were deemed necessary.

Explain how use of the proposed animal model will add to work previously reported, particularly if aspects of the study will duplicate previous work by your lab or others.

> To our knowledge, no previous work outside our group has been done with this animal in the field of autonomous life support development. However, as described above, our choice of animal model is based on other considerations.

Justify the choice of methods that will minimise potential for pain or distress (examples include surgical approach, choice of anesthetic or analgesic, choice of adjuvant, choice of reward paradigm in behavioral assessments). **Include drug names, doses, and dosing schedule.** (Note: First dose of analgesic should always be before cessation of anesthesia). If drugs cannot be used for scientific reasons, explain the rationale.

> No medical procedures will be performed on animals in association with this protocol. Interactions between animals and consumable distribution / waste removal / atmospheric processing / video systems / centrifuge apparatus / other sensors will be monitored daily. Any indication of deteriorating health will lead to the reinstatement of afflicted animals within standard laboratory housing, and modification of the experimental hardware based on collected observations. The only drug to be dosed is tetracycline for the purpose of bone labeling.

Section 6
Rationale
Species
Numbers

Animal species, strains, or stocks to be used in the coming year

for and Estimate required number of **each** species/strain/stock for the **first year** of the project:

Species/Strain/Stock*	Purchase*	Source**	Breed In-house	Expected Total
1 BALB/cByJ	40	Jackson	Nil	40
2				
3				

*Genetically modified strains should be described on Supplement F: Transgenic/Knock-out Animals

* Animal purchase requests (including those for animals used at contract sites) must be routed through the DCM Animal Purchasing Officer

**List source as name of vendor or PI and institution if another lab

Provide scientific justification for the number of animals requested, as well as study group sizes. Include a description of statistical analyses used to estimate the number of animals needed (Attention NHP users: Please indicate the current size of your colony, specifying how many animals are in active use and your plans for any inactive animals):

> Study groups will consist of 4 to 5 animals each, to permit meaningful comparisons with our previous work and to ensure statistical significance. Each experiment animal will be housed in a separate custom specimen chamber as planned for the spacecraft. In most cases, animals used for non-spin controls will be the same as those used for rotation studies.

If this is a renewal, how many animals of each species have been used since the last protocol review?

> 20

Section 7
Hazardous
Materials
In Animals

List hazardous agents to be used in animals. All use of hazardous materials must be described in detail on a Supplement I, "Use of Hazardous Materials in Animals" (see Section 10). Be sure to indicate in the Personnel Table (Section 8) which personnel will be handling each of these hazards.

Radioactive:	N/A
Chemical*:	N/A
Biological**:	N/A

* Chemicals are considered hazardous if the MSDS or other sources indicate there is a human health hazard during dosing, husbandry, or necropsy of animals. Novel compounds without established hazard information are considered on a case-by-case basis.

**Biological hazardous agents include potentially infectious agents, primary human cells or established human cell lines, and recombinant RNA or DNA, including gene transfer vectors.

Note that use of hazardous agents may not begin until all of the following have occurred (in listed order):

- 1) The CAC has approved this protocol application;
- 2) A specific "Required Protection/Control" form for each particular hazard involved has been generated by DCM and EHS (MIT or WIBR), and the principal investigator has signed and returned the form(s) to DCM (Lucy Wilhelm, 16-825);
- 3) Study personnel have been contacted by the DCM Hazards Coordinator (Mary Patterson, mmpatt@mit.edu, X4-5403) for consultation, space allocation, and orientation in the animal facility on the use of each particular hazard in animals.

Section 8
Personnel
Qualifications

List all personnel to participate in the study. Any personnel working with animals must be CAC-certified in advance. Information on obtaining CAC certification may be found at https://web.mit.edu/comp-med/Restrict/CAC/training_new.htm.

- o Contact the DCM veterinary staff if training is needed for specific animal procedures. It is the principal investigator's responsibility to affirm that all participants understand DCM and CAC policies (see DCM *Lab Animal User's Handbook* and policy section on CAC website) and are adequately trained.
- o All new protocol participants performing survival surgery (or others desiring additional training) must contact either Kris Hewes (mice only - khewes@mit.edu/X3-9439) or Dr. Robert Marini (all other species - rmarini@mit.edu/X4-3340) for review of MIT guidelines for survival surgery.

Always list Principal Investigator. Describe protocol responsibilities as "supervision" if PI has no animal contact.

Name:	Year of CAC-certification	Survival surgery ("Y" if YES)	Hazardous materials to be used in animals (Identify the "hazmats")	Protocol responsibilities ("All" or keywords if limited participation)	Summarise relevant prior experience and training beyond CAC-certification
PI (required): John E. Keesee	None	N/A	N/A	General oversight	None
Editor Editor	Approx. 2002/2003	N/A	N/A	Habitats, life support, behavioral lead	Blood-draws, CO2 euthanasia
Erika B. Wagner	2002	N/A	N/A	Manager/trainer/supervisor	Additional CAC training in retro-orbital and pericardial bleeding, CO2 euthanasia, isoflurane anesthesia

Wen Hui Tan	2006	N/A	N/A	Urine collection and basic animal care	Blood-draws, surgery, isoflurane, CO2 euthanasia
Emily Grosse	2007	N/A	N/A	Basic animal care	None
Megan Pennington-Boggio	Expected 2008	N/A	N/A	Urine collection and basic animal care	Training yet to commence

Section 9 Occupational Health All personnel on this protocol with ANY animal contact must have an Animal Handler's Baseline Occupational Health Questionnaire (OHQ) evaluated by an EHS physician or nurse.

Questionnaires are available at the CAC website: <https://web.mit.edu/comp-med/Restrict/CAC/forms.htm>

and may be submitted:

- 1) Electronically;**
- 2) Manually (send directly to MIT Medical Employee and Occupational Health Office (EOHS, E23-180));**
- 3) In person: Schedule an appointment with the EOHS (Jackie Sherry, X3-8552, E23-180).**

Has everyone listed on this protocol submitted an OHQ?

Yes

Are there any occupational health issues that have developed for any protocol participant since a questionnaire was first submitted?

No

For users of materials/substances potentially hazardous to human health, have new personnel been educated about health risks?

Yes

Note that information about safety and health measures (e.g., immunisations, protection against explosion and fire) is available through DCM, EHS, and the MIT Medical Department.

Have all protocol personnel been instructed on DCM requirements for use of personnel protection equipment in animal facilities (PPE: shoe covers, head covers, and lab coats; gloves when handling animals; masks and face protection for contact with nonhuman primates)?

Yes

In lab animal use areas, PPE (lab coats and gloves when handling animals, plus masks and face protection for contact with nonhuman primates) should also be worn.

For personnel working with nonhuman primates, list each name with the date of the most recent tuberculosis screen by MIT Medical (must be current within one year). Protocol approval and renewal are contingent on strict compliance by all participants; "pending" is not satisfactory.

Name:	Date of most recent TB screen

Investigators working with nonhuman primates (including tissue harvest) are advised to obtain exposure control training from EHS at X2-3477.

Section 10
List of
Supplemental
Forms

Supplements must be filled out for the following procedures, even if they have been approved in prior versions of this protocol. **Check the boxes of all procedures that apply. Download forms from the CAC website (<https://web.mit.edu/comp-med/Restrict/CAC/forms.htm>) to make sure you are using the current version; expired versions are not accepted.**

- A. Surgical Procedures
- B. Polyclonal and Monoclonal Antibody Production
- C. Chemical, Microbial, Physical Agent Administration
- D. Use of Human or Rodent Cells or Tissue in Animals
- E. Device Implantation
- F. Transgenic/Knock-out Animals
- G. Behavioral Training Techniques
- H. Teaching Proposal
- I. Use of Hazardous Materials in Animals
- J. Food or Water Restriction Unrelated to Behavioral Motivation
- K. Tumor Induction

Section 11
PI Signature

Principal Investigator

The CAC meets on the first or second Thursday of every month except August and December. The meeting schedule is posted at the CAC website.

Submissions received at least two weeks in advance of a CAC meeting will be reviewed at the upcoming meeting; submissions received less than two weeks in advance may be delayed to the following meeting cycle. If expedited review is required, please provide a cover letter justifying the necessity.

Note that a substantial change in protocol, an increase in the number of animals used, a change in the animal species used, or addition of personnel necessitates an addendum to this form. The principal investigator must sign the addendum before it will be reviewed by the committee.

References:

Burgmann P and DH Percy, 1993. Antimicrobial drug use in rodents and rabbits. In Antimicrobial Therapy in Veterinary Medicine, 2nd ed., ed. JF Prescott and JD Baggot, pp. 524-541. Ames: Iowa State University Press.

Harkness JE and JE Wagner, 1995. The Biology and Medicine of Rabbits and Rodents, 4th Edition. Media, PA: Williams & Wilkins.

Hrapkiewicz, Karen, Leticia Medina (Contributor), and Donald Holmes (Contributor) Clinical Laboratory Animal Medicine: An Introduction Iowa State University Press; 2nd edition (February 1998)

T. C. Lee, A. Staines and D. Taylor, Bone adaptation to load: microdamage as a stimulus for bone remodelling, Anatomical Society of Great Britain and Ireland, 2002.

Buccafusco, Jerry (ed.). Methods of Behavior Analysis in Neuroscience. 2000.

Fox, J. G. (ed.). The Mouse in Biomedical Research: Normative Biology, Husbandry and Models. 2nd Edition.

Crawley, Jacqueline. What's Wrong With My Mouse? 2007.

Appendix J: Statistical Analyses

This section shows a representative sample of statistical output from a mixed regression analysis performed using Systat 12.

Number of Variables : 29
 Number of Cases : 129

SYSTAT Rectangular file C:\MyFiles\ACTIVE\SYSTAT_data\jah\fulford-jones_thaddeus\rota-data-080711.syz, created Fri Jul 11 16:16:22 2008, contains variables:

ROTADAY	REG_1_10	SUBJECT	ANGVELMEAN	DISTTOTAL	DISTTOZ1MEAN
DISTTOZ1TOTAL	ELONGCONTRADUR	ELONGNORMDUR	ELONGSTRDUR	HEADDRIMEAN	HEADDRSTDEV
HEADDRTOZ1DUR	HDGMEAN	Z1DUR	Z1FREQ	Z1LATENCY	MEANDERMEAN
MEANDERTOTAL	IMMOBILEDUR	IMMOBILEFREQ	MOBILEDUR	MOBILEFREQ	HIMOB DUR\$
HIMOBFREQU	MVG DUR	NOTMVG DUR	ROTACWFREQ	ROTACCWFREQ	

Mixed Regression

Effects coding used for categorical variables in model

One case was excluded because the IDENTIFIER Variable was missing.

Terms in the analysis and names of design matrix columns used for those terms:

REG1_10_35_37

FXD1(1)FXD1(2)FXD1(3)

Perform 10 EM iterations

1 random terms

3 fixed terms

Numbers of Observations

Level 2 observations : 4
 Level 1 observations : 128

Descriptive Statistics for all Variables

Variable	Minimum	Maximum	Mean	Standard Deviation
IMMOBILEFREQ	60.000	2,681.000	823.406	402.924
INTERCEPT	1.000	1.000	1.000	0.000
FXD1(1)	-1.000	1.000	-0.031	0.306
FXD1(2)	-1.000	1.000	0.156	0.509
FXD1(3)	-1.000	1.000	0.625	0.602

Starting Values

Mean:

648.747

Covariates:

-494.997 613.218 101.401

Variance Terms:

18,908.309

Residual:

94,541.546

Final Results - MML Estimates

EM Iterations : 10
 Fisher Iterations : 2
 Total Iterations : 12
 Log Likelihood : -891.747

Variable	Estimate	Standard Error	Z	p-value
INTERCEPT	648.747	97.098	6.681	0.000
FXD1(1)	-494.997	95.487	-5.184	0.000
FXD1(2)	613.218	51.618	11.880	0.000
FXD1(3)	101.401	43.944	2.307	0.021

Residual Variance

Estimate	Standard Error	Z	p-value
60,230.802	7,649.320	7.874	0.000

Random-Effect Variance & Covariance Term(s)

Estimate

	1
	INTERCEPT
1 INTERCEPT	31,356.320

Standard Error

	1
	INTERCEPT
1 INTERCEPT	23,504.407

Z

	1
	INTERCEPT
1 INTERCEPT	1.334

p-value

	1
	INTERCEPT
1 INTERCEPT	0.091

Note: p-values are 2-tailed except for those associated with variances, which are 1-tailed.

Calculation of the Intracluster Correlation

Residual Variance : 60,230.802
 Cluster Variance : 31,356.320
 Intracluster Correlation : $31,356.320 / (31,356.320 + 60,230.802) = 0.342$

Correlation of the MML Estimates of the Fixed Terms

	1	2	3	4
	INTERCEPT	FXD1(1)	FXD1(2)	FXD1(3)
1 INTERCEPT	1.000			
2 FXD1(1)	0.235	1.000		
3 FXD1(2)	-0.210	-0.550	1.000	
4 FXD1(3)	-0.332	-0.559	0.388	1.000

Correlation of the MML Estimates of Variance-Related Terms

	1	2
	VarCov1	Residual
1 VarCov1	1.000	
2 Residual	-0.010	1.000

Appendix K: References

- Aizikov, G. S., A. S. Markin, et al. (1992). "Free fall turn-over reaction in rats after a flight on the biosatellite "Cosmos-936"." Aviakosmicheskaya i Ekologicheskaya Meditsina **26**(1): 62-64.
- Akbulut, B. (2005). Mars Gravity Biosatellite Autonomy Evaluation (internal publication). Cambridge MA, Massachusetts Institute of Technology.
- Balinskas, R. (2007). Email on the Effects of Humidity on LiOH Performance at Scrubbing Carbon Dioxide. C. W. Flugel. Cambridge, MA.
- Bernard, D. E., E. B. Gamble Jr., et al. (2001). Remote Agent Experiment DS1 Technology Validation Report. NASA. Pasadena, CA, NASA.
- Bethke, K., E. B. Wagner, et al. (2008). Mars Gravity Science Requirements Document. Mars Gravity Technical Report. Cambridge, MA, MIT.
- Boryta, D. A. and A. J. Maas (1982). Carbon Dioxide Absorption Characteristics of Lithium Hydroxide. Foote Mineral Company Technical Note. Winter Annual Meeting of the American Society of Mechanical Engineers.
- Broderson, J. R., J. R. Lindsey, et al. (1976). "Role of Environmental Ammonia in Respiratory Mycoplasmosis of Rats." American Journal of Pathology **85**(1): 115-&.
- Brown, E. L., H. Hecht, et al. (2002). "Sensorimotor aspects of high-speed artificial gravity: I. Sensory conflict in vestibular adaptation." Journal of Vestibular Research-Equilibrium & Orientation **12**(5-6): 271-282.
- Buccafusco, J. J. (2000). Methods of Behavior Analysis in Neuroscience. New York, CRC.
- Campbell, W. A. and R. S. Marriott (1987). Outgassing Data for Selecting Spacecraft Materials. N. G. S. F. Center, NASA. **NAS 1.61:1124-Rev; NASA-RP-1124-Rev; Rept-87B0347-Rev**.
- Carpenter, B. M. (2004). Biological and Physical Research Advisory Committee (BPRAC) Meeting Minutes February 12-13, 2004. Washington, D.C., NASA Headquarters.
- Chien, S., R. Sherwood, et al. (2003). Autonomous Science on the EO-1 Mission. International Symposium on Artificial Intelligence Robotics and Automation in Space (i-SAIRAS), Nara, Japan.
- Chung, Y. C., Y. Y. Lin, et al. (2005). "Removal of high concentration of NH₃ and coexistent H₂S by biological activated carbon (BAC) biotrickling filter." Bioresource Technology **96**(16): 1812-1820.

Clement, G. and A. Pavy-Le Traon (2004). "Centrifugation as a countermeasure during actual and simulated microgravity: a review." European Journal of Applied Physiology **92**(3): 235-248.

Convertino, V. A. and W. H. Cooke (2007). "Vascular functions in humans following cardiovascular adaptations to spaceflight." Acta Astronautica **60**(4-7): 259-266.

Costanzo, L. (2006). Physiology Third Edition with StudentConsult.com Access. Richmond, VA, Saunders.

Crawley, J. N. (2007). What's Wrong With My Mouse: Behavioral Phenotyping of Transgenic and Knockout Mice, Wiley-Liss.

Davis, S. H. and L. D. Kissinger (1982). The Characterization of Carbon Dioxide Absorbing Agents for Life Support Equipment. Winter Annual Meeting of the American Society of Mechanical Engineers.

Day, M. (1999). 30 Years of Commercial Components in Space: Selection Techniques Without Formal Qualification. 13th Annual AIAA/USU Conference on Small Satellites. Logan, Utah, USA.

Domaratskaya, E. I., E. A. C. Almeida, et al. (2008). Spaceflight Effects on the Hematopoietic Tissue of Ribbed Newts. Life in Space for Life on Earth ESA ELGRA ISGP ASGSB. Angers, France.

Fast, T., R. Grindeland, et al. (1985). "Rat maintenance in the Research Animal Holding Facility during the flight of Space Lab 3." Physiologist **28**(6 Suppl): S187-8.

Fethke, W., K. M. Cook, et al. (1973). "Oxygen Consumption Measurements During Continual Centrifugation of Mice." Journal of Applied Physiology **35**(4): 572-577.

Flugel, C. W. (2007). Emails concerning Lithium Hydroxide for the Mars Gravity Biosatellite. T. R. F. Fulford-Jones. Cambridge, MA.

Flugel, C. W. (2007-2008). Emails concerning activated charcoal for the Mars Gravity Biosatellite. T. R. F. Fulford-Jones. Cambridge, MA.

Frey, M., R. vonKanelChristen, et al. (1997). "Effects of long-term hypergravity on muscle, heart and lung structure of mice." Journal of Comparative Physiology B-Biochemical Systemic and Environmental Physiology **167**(7): 494-501.

Fulford-Jones, T. R. F., E. B. Grosse, et al. (2007). The Mars Gravity Biosatellite: Atmospheric Reconditioning Strategies for Extended-Duration Rodent Life Support. International Conference on Environmental Systems. Chicago, IL, SAE.

Fulford-Jones, T. R. F., A. M. Heafitz, et al. (2007). The Mars Gravity Biosatellite: Thermal Design Strategies for a Rotating Partial Gravity Spacecraft. International Conference on Environmental Systems. Chicago, IL, SAE.

Fulford-Jones, T. R. F., N. Steber, et al. (2005). Ensuring Long-Term Environmental Stability of Rodent Food Substrates within an Autonomous Life Support Module. American Society for Gravitational and Space Biology, Reno, NV.

Fuller, C. A. (2007). Anecdotal Evidence on the Effects of Periodic Non-Spin Events on Rodents Undergoing Chronic Centrifugation. T. R. F. Fulford-Jones. Mountain View, CA.

Galysh, I., K. Doherty, et al. (2000). CubeSat: Developing a Standard Bus for Picosatellites. Vienna, VA, StenSat.

Gat, E. and B. Pell (1998). "Smart Executives for Autonomous Spacecraft." IEEE Intelligent Systems **13**(5): 56-61.

Gazenko, O. G., B. A. Adamovich, et al. (1978). "Radiobiological Experiment Aboard the Biosatellite Cosmos-690." Aviation Space and Environmental Medicine **49**((1 SECT 1)): 42-46.

Gould, T. D., H. Einat, et al. (2007). "beta-catenin overexpression in the mouse brain phenocopies lithium-sensitive Behaviors." Neuropsychopharmacology **32**: 2173-2183.

Gray, T. (1998). "A Brief History of Animals in Space." Retrieved 1 March, 2008, from <http://history.nasa.gov/printFriendly/animals.html>.

Green, E. L. (1968). Biology of the Laboratory Mouse by the Staff of the Jackson Laboratory. New York, Dover Publications.

Guo, J., W. S. Xu, et al. (2005). "Adsorption of NH₃ onto activated carbon prepared from palm shells impregnated with H₂SO₄." Journal of Colloid and Interface Science **281**(2): 285-290.

Gurovsky, N. and Y. Ilyin (1978). "Soviet Biosatellites in Cosmos Series - Main Results of 8-Year Program." Aviation Space and Environmental Medicine **49**(11): 1355-1356.

Gurovsky, N. N., O. G. Gazenko, et al. (1980). "Study of physiological effects of weightlessness and artificial gravity in the flight of the biosatellite Cosmos-936." Acta Astronautica **7**(1): 113-121.

Heafitz, A. M. (2005). Assessment of Payload Oxygen Canister Choices. Mars Gravity Technical Report. Cambridge, MA, MIT.

Heidt, H., J. Puig-Suari, et al. (2000). CubeSat: A new Generation of Picosatellite for Education and Industry Low-Cost Space Experimentation. 14th Annual AIAA/USU Conference on Small Satellites. Logan, Utah, USA.

Hemmersbach, R., R. Voormanns, et al. (1996). "Graviresponses in Paramecium biaurelia under different accelerations: Studies on the ground and in space." Journal of Experimental Biology **199**(10): 2199-2205.

Hoehn, A., J. Clawson, et al. (2005). Carbon Dioxide Scrubbers for Controlling the Gaseous Composition of Spaceflight Plant Growth Chambers - Design Trades and Test Results. International Conference on Environmental Systems. Rome, Italy, SAE.

Ilyin, E. A., L. V. Serova, et al. (1975). "Preliminary Results of Examinations of Rats After a 22-Day Flight Aboard Cosmos-605 Biosatellite." Aviation Space and Environmental Medicine **46**(3): 319-321.

Incropera, F. P. and D. P. Dewitt (1981). Funamentals of Heat Transfer. New York, Wiley & Sons.

Israelsson, U. (2003). OBPR Free Flyer Draft Roadmap Overview. Moffett Field, CA, NASA.

Johnston, R. S., L. F. Dietlein, et al. (1975). "Biomedical Results of Apollo (SP-368)." National Aeronautics and Space Administration Lyndon B. Johnson Space Center, Houston, TX.

Kamler, J. (2005). Feasibility of a Radiation Study on the Mars Gravity Biosatellite. Cambridge MA, Massachusetts Institute of Technology.

Korzun, A. (2008). Mars Gravity Biosatellite Interface Control for EDL (internal publication). Cambridge MA, Massachusetts Institute of Technology.

Kotylarov, E., P. de Crom, et al. (2006). Some Aspects of Peltier-Cooler Optimization Applied for the Glove Box Air Temperature Control. International Conference on Environmental Systems. Norfolk, VA, SAE.

Kozlovsaya, I. B., A. I. Grigoriev, et al. (1995). "Countermeasure of the negative effects of weightlessness on physical systems in long-term space flights." Acta Astronautica **36**(8-12): 661-668.

Lang, T., A. LeBlanc, et al. (2004). "Cortical and trabecular bone mineral loss from the spine and hip in long-duration spaceflight." Journal of Bone and Mineral Research **19**(6): 1006-1012.

Linenger, J. M. (2000). Off the Planet: Surviving Five Perilous Months Aboard the Space Station Mir, McGraw-Hill.

Lipkind, D., A. Sakov, et al. (2004). "New replicable anxiety-related measures of wall vs. center behavior of mice in the open field." Journal of Applied Physiology **97**(1): 347-359.

Lovellette, M. N., K. S. Wood, et al. (2002). Strategies for Fault-Tolerant, Space-Based Computing: Lessons Learned from the ARGOS Testbed. N. R. L. W. DC, Defense Technical Information Center. **Approved for Public Release**.

Mangun, C. L., R. D. Braatz, et al. (1999). "Fixed Bed Absorption of Acetone and Ammonia onto Oxidized Activated Carbon Filters." Industrial and Engineering Chemistry Research **38**(9): 3499-3504.

McLinko, R. M. (2008). Mars Gravity Biosatellite Interface Control Documents (internal publication). Cambridge MA, Massachusetts Institute of Technology.

NASA. (1990). "Life Into Space: Space Life Sciences Experiments NASA Ames Research Center 1965-1990 (<http://lis.arc.nasa.gov/lis/>)." 2008.

NASA (2007). "Life Sciences Data Archive. Last Updated: 12 Dec 2007 (<http://lsda.jsc.nasa.gov>)."

Nikolaev, S. O. and E. A. Ilyin (1981). "Summary of Experiments On-Board Soviet Biosatellites." Acta Astronautica 8(9-10): 919-926.

Oyama, J. and W. T. Platt (1967). "Reproduction and growth of mice and rats under conditions of simulated increased gravity." Am J Physiol 212(1): 164-6.

Oyama, J., W. T. Platt, et al. (1971). "Deep Body Temperature Changes in Rats Exposed to Chronic Centrifugation." American Journal of Physiology 221(5): 1271-1277.

Pavy-Le Traon, A., M. Heer, et al. (2007). "From space to Earth: advances in human physiology from 20 years of bed rest studies (1986-2006)." Eur J Appl Physiol 101(2): 143-94.

PavyLeTraon, A., A. M. Allevard, et al. (1997). "Cardiovascular and hormonal changes induced by a simulation of a lunar mission." Aviation Space and Environmental Medicine 68(9): 829-837.

Quinlivan, V. H., K. H. Aull, et al. (2005). Murine Automated Urine Sampler: Use of Chlorhexidine/N-Propyl Gallate for Hands-Off Small Animal Urine Preservation. American Society for Gravitational and Space Biology, Reno, NV.

Rambaut, P. C., C. S. Leach, et al. (1975). "Calcium and Phosphorus Change of Apollo-17 Crew Members." Nutrition and Metabolism 18(2): 62-69.

Rayman, M. D., P. Varghese, et al. (1999). "Results from the Deep Space 1 Technology Validation Mission." Acta Astronautica 47: 475.

Riley, D. A. (1998). Review of primary spaceflight-induced and secondary reloading-induced changes in slow antigravity muscles of rats. Life Sciences: Microgravity Research. 21: 1073-1075.

Riskowski, G. L., P. C. Harrison, et al. (2006). "Mass Generation Rates of Ammonia, Moisture, and Heat Production in Mouse Cages with Two Bedding Types, Two Mouse Strains, and Two Room Relative Humidities." ASHRAE Transactions 112(Part 1): 134-144.

Rodrigues, C. C., D. de Moraes, et al. (2007). "Ammonia adsorption in a fixed bed of activated carbon." Bioresource Technology 98(4): 886-891.

Ronca, A. E. and J. R. Alberts (2000). "Effects of prenatal spaceflight on vestibular responses in neonatal rats." Journal of Applied Physiology 89(6): 2318-2324.

- Ross, M. D. (1993). "Morphological changes in rat vestibular system following weightlessness." J Vestib Res **3**(3): 241-51.
- Ross, M. D. (2000). "Changes in ribbon synapses and rough endoplasmic reticulum of rat utricular macular hair cells in weightlessness." Acta Oto-Laryngologica **120**(4): 490-499.
- Scheuring, R. A. (2007). (Personal Conversation) Regarding the Loss of Bone Exhibited by NASA Astronauts Following Spaceflight. T. R. F. Fulford-Jones. Chicago, IL.
- Schultheis, L., C. B. Ruff, et al. (2000). "Disuse bone loss in hindquarter suspended rats: partial weightbearing, exercise and ibandronate treatment as countermeasures." J Gravit Physiol **7**(2): P13-4.
- Shapiro, J., B. Smith, et al. (2007). "Treatment with zoledronic acid ameliorates negative geometric changes in the proximal femur following acute spinal cord injury." Calcified Tissue International **80**(5): 316-322.
- Shipov, A. A. and V. G. Ovechkin (1980). "Function of semicircular canals of rats flown aboard the biosatellite Cosmos-936." Kosmicheskaya Biologiya I Aviakosmicheskaya Meditsina **14**(2): 25-30.
- Sonnenfeld, G., D. A. Koebel, et al. (1995). "Effects of Hypergravity on Immunological Function." Microgravity Science and Technology **7**(4): 323-326.
- Steele, M. K. (2007). Thoughts on the Ability of Rodents to Drink from AEM Water Nozzles in Zero Gravity. T. R. F. Fulford-Jones. Moffett Field, CA.
- Tou, J., R. Grindeland, et al. (2003). "Evaluation of NASA foodbars as a standard diet for use in short-term rodent space flight studies." Nutrition **19**(11-12): 947-954.
- Ushakov, A. S., T. A. Smirnova, et al. (1980). "Body composition of rats flown aboard Cosmos-1129." Physiologist **23**(Suppl 6): S41-4.
- Vico, L., D. Chappard, et al. (1988). "Trabecular Bone Remodelling After 7 Days of Weightlessness Exposure (BioCosmos-1667)." American Journal of Physiology **255**(2): R243-R247.
- Wade, C. E. (2005). "Responses across the gravity continuum: Hypergravity to microgravity." Experimentation with Animal Models in Space **10**: 225-245.
- Wade, C. E., M. M. Miller, et al. (2002). "Body mass, energy intake, and water consumption of rats and humans during space flight." Nutrition **18**(10): 829-836.
- Wade, C. E., R. M. Ortiz, et al. (2000). "Increases in body mass of rats during spaceflight: Models and measurements." Aviation Space and Environmental Medicine **71**(11): 1126-1130.
- Walton, K., C. Heffernan, et al. (1997). "Changes in gravity influence rat postnatal motor system development: from simulation to space flight." Gravit Space Biol Bull **10**(2): 111-8.

Wang, X. Y., Y. J. Li, et al. (2005). "Activity-dependent presynaptic regulation of quantal size at the mammalian neuromuscular junction in vivo." Journal of Neuroscience **25**(2): 343-351.

Whedon, G. D. and P. C. Rambaut (2006). "Effects of long-duration space flight on calcium metabolism: Review of human studies from Skylab to the present." Acta Astronautica **58**(2): 59-81.

Wubbels, R. J. and H. A. A. de Jong (2001). "The horizontal vestibulo-ocular reflex of hypergravity rat at different gravity levels." Neuroscience Letters **303**(1): 5-8.

Young, L. R. (1993). "Space and the vestibular system: what has been learned?" J Vestib Res **3**(3): 203-6.

Young, L. R., K. H. Sienko, et al. (2003). "Adaptation of the vestibulo-ocular reflex, subjective tilt, and motion sickness to head movements during short-radius centrifugation." Journal of Vestibular Research-Equilibrium & Orientation **13**(2-3): 65-77.

Young, L. R. and P. Sinha (1998). "Spaceflight influences on ocular counterrolling and other neurovestibular reactions." Otolaryngology-Head and Neck Surgery **118**(3): S31-S34.